

**INFRARED PHOTODISSOCIATION SPECTROSCOPY
OF MASS-SELECTED CLUSTER IONS
IN THE GAS PHASE**

Habilitationschrift

eingereicht am

Fachbereich Physik
der
Freien Universität Berlin

vorgelegt von

von Knut R. Asmis
aus Berlin

Berlin, im August 2005

The only limits we have are those we give ourselves.

Gordo Byrn

to Catherine Mary Speer

PREFACE

This habilitation thesis describes my research activities at the Institute for Experimental Physics of the Free University Berlin, which I conducted in the group of Prof. Dr. Ludger Wöste in the period from September 1999 until December 2004. These research activities were the central part of, and financed by, the projects Asmis/Wöste of the *Dedicated Research Center „Structure, Dynamics und Reactivity of Transition Metal Oxide Aggregates“* (SFB-546) and the *Graduate School „Hydrogen Bonding and Hydrogen Transfer“* (GK-788) of the German Research Foundation DFG.

The central goal of this work was the development of novel experimental methods to characterize the structure of mass-selected gas phase cluster ions (see Chapter A). Infrared spectroscopy (Chapter B) has been a standard method for structural characterization of condensed phase samples for many decades. Its application to gas phase ions poses mainly two experimental challenges. First, the low number densities of ions attainable in the gas phase, roughly less than one million per cubic centimeter, generally prohibit direct absorption measurements. Second, most of the characteristic infrared transitions lie in the fingerprint region (500 to 2000 cm^{-1}) of the electromagnetic spectrum, a region which cannot be continuously covered with the required intensity using commercially available infrared radiation sources.

To address these problems a novel, mobile tandem mass spectrometer was constructed (Chapter C.1), which allows trapping, cooling, and probing of mass-selected gas phase ions. The infrared photodissociation experiments (Chapter B.1) were performed at the FOM Institute for Plasma Physics Rijnhuizen (Nieuwegein, The Netherlands) using the free electron laser FELIX (Chapter C.2). In these experiments, FELIX is used as a monochromatic “Bunsen burner”, *i.e.*, the ions are irradiated with intense infrared radiation of a specific wavelength. If the wavelength coincides with an infrared transition, the ion is resonantly heated and eventually breaks apart (Chapter B.3). The absorption is detected indirectly by measuring the fragment ion yield, resulting in a high selectivity and sensitivity. The measured infrared spectrum is a “fingerprint” of the molecular structure and its assignment is generally based on a comparison with the simulated spectra of possible candidates.

The developed techniques were applied to two research areas. As part of the SFB-546 we were able to measure the infrared spectra of small vanadium oxide ions for the first time and, based on these, characterize their geometric and electronic structure (Chapter D.1). Unexpectedly, we were able to show a correlation between the spectra of a vanadium oxide surface and cluster ion cages of moderate size (~30 atoms). As part of the GK-788 we measured the first infrared spectra of model systems containing strong hydrogen bonds in the spectral region of the shared proton modes (Chapter D.2). The characterization of the spectral signature of the protonated water dimer H_5O_2^+ , also referred to as the „Zundel cation“, was particularly noteworthy. The failure to accurately model this infrared spectrum impressively demonstrates the difficulties of present day electronic structure theory in describing strongly coupled vibrational modes.

The experimental work described in this thesis was a team effort and only possible as such. Parts of this work constitute the Ph.D. and Diploma theses of Mathias Brümmer, Sara Fontanella, Oliver Gause, Cristina Kaposta, Gabriele Santambrogio, and Carlos Cibrián-Uhalte.

VORWORT

Diese Habilitationsschrift umfaßt meine Forschungstätigkeit am Institut für Experimentalphysik der Freien Universität Berlin, die ich in der Arbeitsgruppe von Prof. Dr. Ludger Wöste im Zeitraum von September 1999 bis Dezember 2004 durchgeführt habe. Die hier beschriebenen Untersuchungen sind zentraler Bestandteil des Teilprojektes Asmis/Wöste des *Sonderforschungsbereiches „Struktur, Dynamik und Reaktivität von Übergangsmetalloxid-Aggregaten“ (SFB-546)* und des *Graduiertenkollegs „Wasserstoffbrücken und Wasserstofftransfer“ (GK-788)* der Deutschen Forschungsgemeinschaft DFG und wurden daraus größtenteils finanziert.

Das Hauptziel dieser Arbeit war die Entwicklung neuer experimenteller Methoden zur Strukturaufklärung massenselektierter Clusterionen in der Gasphase (siehe Kapitel A). Die Anwendung der Infrarot-Schwingungsspektroskopie (Kapitel B), welche für Systeme in kondensierter Phase seit Jahrzehnten zu den Standardmethoden gehört, auf geladene Gasphasenteilchen ist vor allem aus zwei Gründen experimentell anspruchsvoll. Zum einen verhindern die niedrigen erzielbaren Teilchendichten von weniger als einer Million Ionen pro Kubikzentimeter eine direkte Absorptionsmessung. Zum anderen liegen die strukturcharakteristischen Schwingungsübergänge in der sogenannten „Fingerprint“-Region ($500 \text{ to } 2000 \text{ cm}^{-1}$), ein spektraler Bereich der durch kommerziell erhältliche Laser nicht komplett mit ausreichender Intensität abgedeckt werden kann.

Der Lösungsansatz umfaßte den Bau eines maßgeschneiderten, mobilen Tandem-Massenspektrometers (Kapitel C.1), mit dem massenselektierte Gasphasenionen gespeichert, gekühlt und dann untersucht werden konnten. Die Infrarot-Photodissoziationsexperimente (Kapitel B.1) wurden am FOM Institut für Plasmaphysik Rijnhuizen (Nieuwegein, Niederlande) am Freien Elektronenlaser FELIX (Kapitel C.2) durchgeführt. Hierbei dient FELIX als monochromatischer „Bunsenbrenner“, d.h., die gröÑenselektierten Teilchen werden mit intensivem Infrarotlicht einer Wellenlänge bestrahlt. Bei charakteristischen Wellenlängen kommt es zur Infrarot-anregung. Die Strahlung wird resonant absorbiert, das Teilchen wird erhitzt und zerfällt schließlich. Der Absorptionsnachweis geschieht indirekt durch Messung der Zerfallsprodukte, welche mit hoher Selektivität and Empfindlichkeit nachgewiesen werden können. Das gemessene Infrarotspektrum enthält einen „Fingerabdruck“ der

molekularen Struktur und seine Zuordnung geschieht in der Regel durch Vergleich mit simulierten Spektren möglicher Strukturkandidaten.

Die entwickelten Methoden wurden zur Untersuchung von zwei Substanzklassen eingesetzt. Im Rahmen des SFB-546 konnten erstmals die Strukturen kleiner Vanadiumoxidcluster experimentell bestimmt werden (Kapitel D.1). Dabei gelang es, völlig unerwartet, einen direkten Zusammenhang zwischen den Spektren der kleinen Käfigstrukturen (ca. 30 Atome) und denen einer Vanadiumoxid-Oberfläche aufzudecken. Im Rahmen des GK-788 wurden Infrarotspektren von Modellsystemen mit starken Wasserstoffbrückenbindungen erstmalig im gesamten spektralen Bereich der Schwingungen des Brückenprotons gemessen (Kapitel D.2). Besonders erwähnenswert ist die erstmalige experimentelle Charakterisierung dieser charakteristischen Schwingungsmoden im „Zundel-Kation“, dem protonierten Wasserdimer H_5O_2^+ . Die Modellierung dieses Spektrums ist komplex und zeigt eindrucksvoll die Grenzen der gängigen theoretischen Methoden zur Beschreibung stark gekoppelter Schwingungsmoden auf.

Die hier beschriebenen wissenschaftlichen Arbeiten waren nur im Team möglich. Sie sind zum Teil Bestandteil der Doktor- und Diplomarbeiten von Mathias Brümmer, Sara Fontanella, Oliver Gause, Cristina Kaposta, Gabriele Santambrogio und Carlos Cibrián-Uhalte.

ABBREVIATIONS

CW	continuous wave
DFG	Deutsche Forschungsgemeinschaft (German Research Foundation)
DFM	difference frequency mixing
FEL	free electron laser
FELIX	free electron laser for infrared experiments at the FOM Institute Rijnhuizen
FOM	Fundamenteel Onderzoek der Materie (Foundation for Fundamental Research on Matter)
FUB	Freie Universität Berlin
GK	Graduiertenkolleg (research training group)
IR	infrared
IVR	intramolecular vibrational energy redistribution
MATI	mass analyzed threshold ionization
MPD	multiple photon dissociation
OPA	optical parametric amplifier
OPO	optical parametric oscillator
PD	photodissociation
PES	potential energy surface
REMPI	resonance enhanced multiple photon ionization
RF	radio frequency
RRKM	Rice–Ramsperger–Kassel–Marcus
SFB	Sonderforschungsbereich (collaborative research center)
TEA	transversely excited atmospheric pressure
UV	ultraviolet
ZEKE	zero electron kinetic energy

TABLE OF CONTENTS

A	INTRODUCTION	1
	A.1 Identifying Active Sites in Heterogeneous Catalysis	1
	A.2 Understanding Strong Hydrogen Bonding	2
B	VIBRATIONAL SPECTROSCOPY OF GAS PHASE IONS	5
	B.1 Infrared Photodissociation Spectroscopy	5
	B.2 Historical Development	7
	TEA Carbon Dioxide Lasers	7
	Molecular Beams: Infrared Photodissociation of Mass Selected Ions	9
	Free Electron Lasers: Accessing the Fingerprint Region	12
	B.3 The Infrared Multiple Photon Dissociation Mechanism	13
C	EXPERIMENTAL SETUP	17
	C.1 The Tandem Mass Spectrometer	17
	Vacuum System	19
	Ion Sources	20
	RF Ion Guide and Mass Filters	22
	Hexadecapole Ion Trap	23
	C.2 Infrared Light Sources	26
	The Free Electron Laser for Infrared Experiments (FELIX)	26
	Table Top IR lasers: Recent Advances	28
D	RESULTS AND DISCUSSION.....	31
	D.1 Vanadium Oxide Cluster Ions	31
	Mass-selected Infrared Photodissociation Spectroscopy of $V_4O_{10}^+$	32
	Formation and Photodepletion of Cluster Ion-Messenger Atom Complexes in a Cold Ion Trap: Infrared Spectroscopy of VO^+ , VO_2^+ , and VO_3^+	37
	Gas Phase Infrared Spectroscopy of Mono- and Divanadium Oxide Cluster Cations	42
	Polyhedral Vanadium Oxide Cages: Infrared Spectra of Cluster Anions and Size-Induced d Electron Localization	53
	D.2 Vibrational Spectroscopy of Strong Hydrogen Bonds	58
	Gas Phase Infrared Spectroscopy of Cluster Anions as a Function of Size: The Effect of Solvation on Hydrogen-Bonding in $Br^-(HBr)_{1,2,3}$ Clusters	59
	Probing a Strong Hydrogen Bond with Infrared Spectroscopy: Vibrational Predissociation of $BrHBr^- \cdot Ar$	67
	The Gasphase Infrared Spectrum of the Protonated Water Dimer	72
	Experimental and Theoretical Study of the Infrared Spectra of $BrHI^-$ and $BrDI^-$	76
	Gas Phase Vibrational Spectroscopy of Strong Hydrogen Bonds	87

E	ACKNOWLEDGEMENTS	115
F	REFERENCES.....	117
G	APPENDIX.....	121
	G.1 Other Publications	121
	Bausteine des Wassers unter der "Laserlupe"	122
	Vibrational Wave Packet Dynamics in the Silver Tetramer Probed by NeNePo	
	Femtosecond Pump-probe Spectroscopy	131
	G.2 List of Publications	137
	Academic Publications	137
	Peer Reviewed Publications	137
	Other Publications	139
	G.3 List of Invited Talks	140
	G.4 Curriculum Vitae: Knut R. Asmis	142

A INTRODUCTION

The present thesis work deals primarily with the experimental characterization of the geometric and electronic structure of cluster ions in the gas phase. It was motivated by the absence of any generally applicable, sufficiently selective and sensitive method in this research field at the time. To introduce the reader to the subject matter the first chapter discusses the motivation for performing such experiments.

The advantages of performing experiments on isolated particles under collisionless conditions are manifold and three important ones are named here. First, the combination of modern spectroscopic and spectrometric techniques generally allows for a significantly higher degree of control of the experimental parameters compared to experiments on condensed phase probes. Second, the characterization of the cluster properties in the absence of any perturbing interactions with their environment as a function of size is generally straight forward. In addition, the interaction of a particle with its environment, *e.g.*, the solute-solvent interaction, can be studied in a sequential fashion by adding one solvent molecule at a time. Third, the properties of isolated gas phase clusters are simpler to calculate than those of the same species embedded in a complex environment. Consequently, higher level computational approaches can be applied leading to more accurate and reliable results. These results can then be used as benchmarks for testing models aimed at describing the more complex systems.

Spectroscopic studies of isolated clusters and complexes in the gas phase continue to be of central importance to many areas of science today. Next to the “classical” research areas of atmospheric, interstellar, and plasma chemistry, a growing interest is directed towards other fields, for example, towards understanding and tailoring the size-dependent properties of nanoparticles or understanding complex biochemical processing like protein folding and transmembrane ion transport.

A.1 Identifying Active Sites in Heterogeneous Catalysis

The present thesis work evolved as part of the DFG-funded *Dedicated Research Center SFB 546 „Structure, Dynamics und Reactivity of Transition Metal Oxide Aggregates“*, which started its activity in July 1999, nearly concomitant with the beginning of this

thesis work. The central goal of the SFB 546 is to gain a detailed understanding of the relationship between structure and reactivity of transition metal oxide aggregates and focuses primarily on the characterization of vanadium oxides in the form of gas phase and deposited clusters, surfaces, thin films and their use as building blocks in nanostructured materials. While vanadium oxides are important as cathode materials in lithium batteries,^[1] in bolometric detectors^[2] and as ferromagnetic nanotubes,^[3] it is their use in supported catalysts^[4] that makes them most relevant to the SFB 546. Prominent examples are the use of vanadium oxide based catalysts in the synthesis of important chemicals like sulfuric acid, phthalic and maleic anhydride, and in the reduction of environmental pollution, e.g., the selective reduction of nitrogen oxides NO_x in flue gas from power plants.

The advantage of supported vanadium oxides lies in the variability in the geometric and electronic structure of surface vanadium oxides. Moreover, it is now well documented that the activity and selectivity of supported metal oxide catalysts are significantly affected by the properties of the support. Despite their industrial importance, most of the microscopic properties are not well understood, including the origin and mechanism of the metal oxide – support effect. The identification of the active sites in heterogeneous catalysis with current available surface science techniques remains challenging and thus gas phase studies may significantly contribute to unraveling the mechanistic details of the underlying catalytic processes. A promising approach involves performing reactivity measurements on size-selected vanadium oxide clusters in the gas phase under well controlled conditions. In order to extract a relationship between structure and reactivity from these experiments an experimental characterization of the cluster structure is essential. Thus the primary goal of the present thesis work was to develop a generally applicable experimental technique to identify the geometric and electronic structure of gas phase vanadium oxide clusters.

A.2 Understanding Strong Hydrogen Bonding

A second research topic that evolved during this thesis work was the study of strong hydrogen bonds as part of the DFG-funded *Graduate School GK-788 „Hydrogen Bonding and Hydrogen Transfer“*. The hydrogen bond interaction is key to understanding the structure and properties of water, biomolecules, self-assembled nanostructures and molecular crystals. However, much confusion remains about its

electronic nature, a combination of van der Waals, electrostatic and covalent contributions, leading to a wide variety of hydrogen bonds with bond strengths ranging from 2 to 40 kcal/mol. In particular, our understanding of strong, low-barrier hydrogen bonds and their central role in enzyme catalysis^[5], biomolecular recognition^[6], proton transfer across biomembranes^[7] and proton transport in aqueous media^[8] remains sketchy.

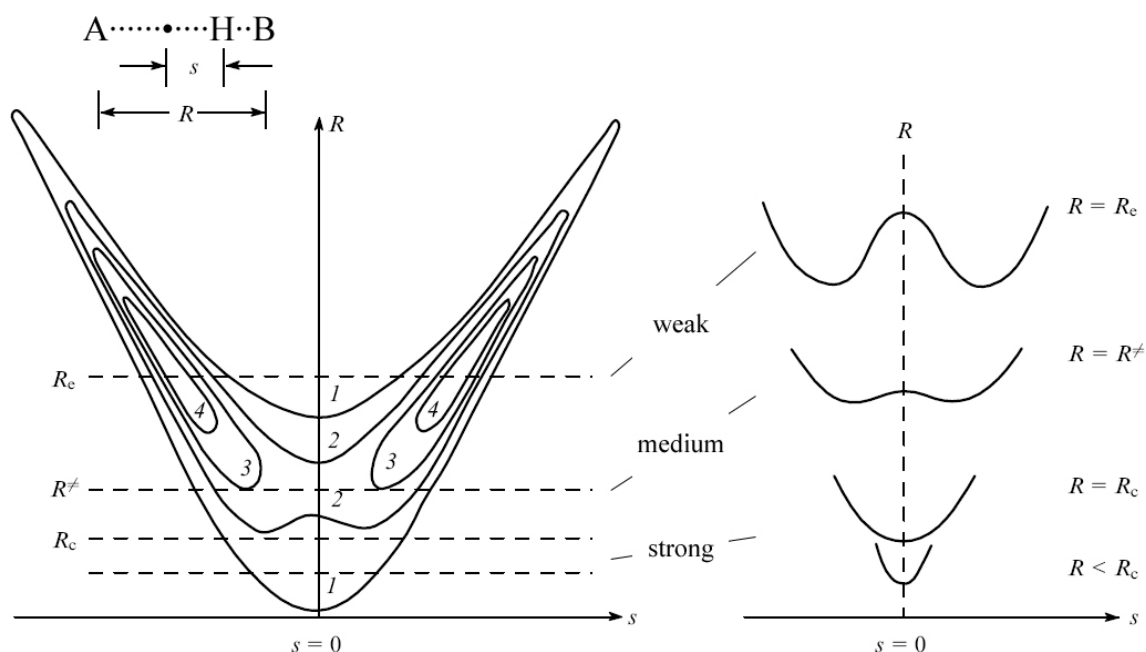


Figure A-1 Typical potential energy surface for a homoconjugated hydrogen bonded system $A\cdots H\cdots A$. As the hydrogen bond strength increases, both, the internuclear distance R between the heavy atoms A and the displacement from the center of mass s , decrease. For strong hydrogen bonds the hydrogen transfer barrier vanishes. Adapted from Vener et al.^[9].

Strong hydrogen bonds ($A\cdots H\cdots B$) are often classified based on their hydrogen bond energy; a typically cited lower limit is >15 kcal/mol.^[10] Their most prominent physical properties are large NMR downfield chemical shifts and considerably red-shifted hydrogen stretch frequencies. Moreover, the H-atom transfer barrier, a characteristic feature of weak hydrogen bonds $A-H\cdots B$, is either absent or very small in these systems at their minimum energy geometry, as illustrated in Figure A-1. Consequently, the H-atom in homoconjugated ($A=B$) strong hydrogen bonds is equally shared by the two heavy atoms forming two identical strong hydrogen bonds. This symmetry is lost in heteroconjugated ($A\neq B$) systems, but the H-atom remains in a more centered position, *i.e.*, the distance between the heavy atoms is smaller than in weaker hydrogen bonded systems.

The protonated water dimer $(\text{H}_2\text{O}\cdots\text{H}\cdots\text{OH}_2)^+$ is, next to $(\text{F}\cdots\text{H}\cdots\text{F})^-$, probably the most widely known model system containing strong hydrogen bonds. It plays a central role in explaining the anomalously high proton mobility in water (Grotthuss mechanism^[11]). The higher than diffusion limited proton mobility is due to structural diffusion, *i.e.*, only the positive charge, and not the much heavier proton, migrates over a large distance via hops along a network of fluctuating hydrogen bonds. This dynamical rearrangement corresponds, in principle, to the interconversion between two limiting structures, the structures of the Zundel^[12] and the Eigen ion^[13]. In the first, the excess proton is equally shared between two water molecules forming $(\text{H}_2\text{O}\cdots\text{H}\cdots\text{OH}_2)^+$. In the latter, the excess proton is primarily bound to a single water molecule forming a hydronium ion H_3O^+ , or more accurately, a solvated hydronium ion $\text{H}_3\text{O}^+(\text{H}_2\text{O})_3$. While these structures are metastable in solution, they can be isolated in the gas phase, where they can be studied in considerable more detail.

The structure of these ions can be characterized by gas phase vibrational spectroscopy. However, the infrared spectrum of H_5O_2^+ had only been measured in the O-H stretching region of the terminal water molecules. The spectral signature of the shared proton modes lies much lower in energy and had not been observed in the gas phase previously. Thus, the second main goal of this thesis was to experimentally characterize the gas phase infrared spectroscopy of strong hydrogen bonds in general and that of the protonated water dimer in particular. The experimental data should then serve as a benchmark for performing higher level computations in order to develop improved methods that accurately describe the properties of strong hydrogen bonds.

B VIBRATIONAL SPECTROSCOPY OF GAS PHASE IONS

This chapter serves as an introduction to the vibrational spectroscopy of gas phase ions. It begins with a description of some general concepts and then leads into historical sketch of the experimental technique of infrared (IR) photodissociation (PD) spectroscopy, which is used in this present work. As the chapter progresses the focus is narrowed and eventually restricted to IR studies of mass-selected ions. The last part qualitatively describes the now widely accepted mechanism of incoherent infrared multiple photon photodissociation (IRMPD). For a more in-depth description the interested reader is referred to the excellent book by Bagratashvili *et al.* “Multiple Photon Infrared Laser Photophysics and Photochemistry” and the articles in “Multiple-Photon Excitation and Dissociation of Polyatomic Molecules” edited by Cantrell.^[14]

B.1 Infrared Photodissociation Spectroscopy

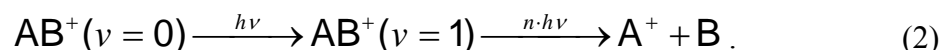
Vibrational spectroscopy paired with quantum chemistry currently offers the most direct and generally applicable experimental approach to structural investigation of neutral and charged cluster in the gas phase.^[15,16] Direct absorption measurements based on discharge modulation methods^[17] can yield high resolution spectra of small and light molecular ions. Problems associated with high discharge temperatures can nowadays be overcome by using pulsed-slit supersonic expansions.^[18] However, these types of experiments become increasingly difficult for larger and heavier molecular ions, particularly ion clusters, owing to spectral congestion, lower gas phase number densities and presence of other absorbing species. Therefore alternative techniques have been developed in which the absorption of photons can be measured indirectly (action spectroscopy), *e.g.*, by way of resonance enhanced PD spectroscopy. PD techniques have the advantage that fragment ions can be detected background-free and with nearly 100% detection efficiency. A high selectivity can be achieved through mass selection of parent and fragment ions using appropriate mass filters.

An IR-PD spectrum is measured by irradiating ions with IR radiation and monitoring the yield of parent and/or fragment ions as a function of the irradiation wavelength. In order to induce fragmentation the parent ion AB^+ (the same line of argumentation holds

for negative ions) is required to absorb sufficient energy to overcome the (lowest) dissociation threshold. Once a metastable ro-vibronic state is reached, intramolecular energy redistribution will eventually lead to dissociation, producing a charged and a neutral fragment:

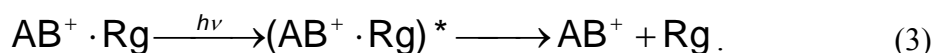


Typical dissociation energies of covalently bound ions are at least 1 eV or higher, while their fundamental vibrational transitions are found well below this limit. Process (1) therefore requires the absorption of multiple IR photons. The coherent stepwise multiple photon excitation, where all photons are absorbed in one vibrational ladder, is unfavorable and becomes unrealistic for higher dissociation thresholds, because the laser runs out of resonance, due to the anharmonicity of vibrational potentials. The excitation process is better viewed as a sequential absorption of photons enhanced by rapid intramolecular vibrational energy redistribution at higher excitation (see Chapter B.3).^[19] Only the first few photons are resonantly absorbed in the “discrete” regime. Higher excitation accesses the “quasi-continuum”, in which the density of states is sufficiently high that the vibrational energy is rapidly randomized among all vibrational modes of the molecular ion, effectively de-exciting the absorbing transition. The ion continues to absorb photons until it has enough energy to dissociate. The transition between the two regimes depends on the vibrational density of states and the strengths of the interactions between vibrational modes. For larger molecular systems this transition occurs already after the absorption of a few photons or even a single photon and the IR-PD spectrum in this case often resembles the linear absorption spectrum.^[20] For smaller systems with less internal degrees of freedom more photons are required and the relative intensities of the bands in the IR-PD spectrum may differ from those in the linear spectrum. However, if the laser fluence is kept at a moderate level, signal is only detected, if the laser wavelength is resonant with a fundamental transition, that is,



At high laser fluence the probability of directly exciting overtones is enhanced, complicating the interpretation of the IR-PD spectrum.^[21]

A useful method to measure IR-PD spectra in the linear regime is the messenger atom technique^[22]:



By forming ion-rare gas atom (Rg) complexes the dissociation threshold of the system is lowered, generally below the photon energy and these predissociation spectra directly reflect the linear absorption spectrum. This technique has also been used to great effect in anion spectroscopy experiments.^[23] The multiple photon dissociation approach remains attractive for systems, in which the perturbation of the messenger atom cannot be neglected or in instruments where rare gas attachment is difficult.

B.2 Historical Development

The development of the optical laser around 1960 concurrently by Gordon Gould and Theodore Maiman^[24] started a new age in molecular spectroscopy, as this introduced the tool to finally observe and study many of the nonlinear effects of the interaction between intense radiation fields and matter that previously had been predicted. Several years later, in 1963, the carbon dioxide gas laser was invented by Kumar Patel at the Bell Laboratories. It was the first gas laser to produce high power radiation continuously. In 1966 Bordé *et al.* used the 10.6 μm radiation from such a continuous wave (CW) CO_2 laser ($< 150 \text{ W}$), which coincides with a vibration-rotation absorption line in ammonia, to irradiate gaseous NH_3 and surprisingly observed the visible luminescence of its decomposition products.^[25] The notion of bond-selective chemistry, *i.e.*, to selectively control bond breaking and forming, was quickly dismissed, however, because it was realized that the main role in this experiment was played by molecular collisions, which transferred the vibrational energy from one molecule to another, effectively heating the ammonia gas to very high temperatures.

TEA Carbon Dioxide Lasers

That bright IR lasers can indeed *directly* (non-thermally) dissociate molecules was demonstrated by Isenor and Richardson^[26] shortly after the development of *transversely excited atmospheric pressure (TEA) CO_2 lasers* in 1970, which delivered orders of magnitude higher peak powers than the CW systems.^[27] Similar to Bordé *et al.*, they observed luminescence from electronically excited dissociation products, the α bands of NH_2 and SiF , upon irradiation of gaseous ammonia and SiF_4 , respectively, with focused TEA- CO_2 laser pulses ($0.5 \cdot 10^6 \text{ W}$). However, time-resolved experiments with nanosecond resolution proved that the luminescence occurred during the duration of the

200 ns laser pulse, ~ 100 ns before optical breakdown of the gas, and well before sufficient collisions could occur to induce thermal dissociation. This discovery of *collisionless* IR molecular multiple photon excitation and dissociation marked the birth of a new research field.

The energetics of the process were quite astounding, requiring the absorption of approximately 40 photons per molecule to break the N-H bond in NH_3 . The direct radiative excitation of high vibrational levels with no collisions can, in principle, provide the observed dissociation rates but encounters an evident problem, that of vibrational anharmonicity. Anharmonic detuning of vibrations requires orders of magnitude higher powers ($>10^{12}$ W/cm²) than used in these experiments. Important insight into the mechanism of collisionless IRMPD came from observations that the dissociation of molecules, like SiF_4 , BCl_3 , and SF_6 , upon irradiation with intense CO_2 laser pulses was isotope selective.^[28] It was soon realized that this effect was of more general character and could be observed in other polyatomic molecules. In particular the enrichment of heavy isotopes, such as osmium from OsO_4 ^[29], stimulated further research with the aim to produce ²³⁵U enriched uranium from UF_6 for nuclear fuel reactors. The new era of IRMPD was born, leading to the rapid growth of disciplines like laser isotope separation and laser induced chemistry. The most striking observations during this time were that both the number of photons absorbed per molecule and the dissociation yield depend only weakly on the laser intensity in contrast to atomic multiphoton ionization, where rates proportional up to $\sim I^{15}$, had been reported. Interestingly, the laser fluence, *i.e.*, the time integral over the intensity, and not the peak intensity determined the dissociation yield.

All these observations lead to the notion of a *vibrational quasi-continuum* in which the density of states is sufficiently high that Fermi's "Golden Rule" becomes valid. Here the full Schrödinger equation reduces to a set of rate equations. To reach this vibrational quasi-continuum of states the first few photons need to be absorbed resonantly between *discrete* rovibrational states of the polyatomic molecule. The anharmonicity of the vibrational potential is compensated by a corresponding change in rotational quantum number (rotational compensation). This first step is highly selective and the origin of the observed isotope selectivity. Once the internal excitation reaches a level in which the rovibrational density of states is high enough, ~ 100 states/cm⁻¹, these levels start forming a quasi-continuum of states far below the dissociation limit.

Absorption in this region allows the polyatomic molecule to reach the dissociation limit within the electronic ground state.

Molecular Beams: Infrared Photodissociation of Mass Selected Ions

The combination of the molecular beam technique with intense IR laser radiation in 1976 by Y.T. Lee and coworkers^[30] represented an important progress in the field, because it provided the most direct evidence (compared to the early gas cell experiments) that the laser-induced MPD process is indeed a collisionless unimolecular process. Detailed information on the identity of the fragments along with their angular and velocity distributions was gained from such experiments. A simple picture emerged from these studies. The multiple photon process excites the molecules through the quasi-continuum to and beyond the dissociation energy level. The level of excitation is eventually limited by molecular dissociation, which can be accurately described by the statistical theory of dissociation.^[31]

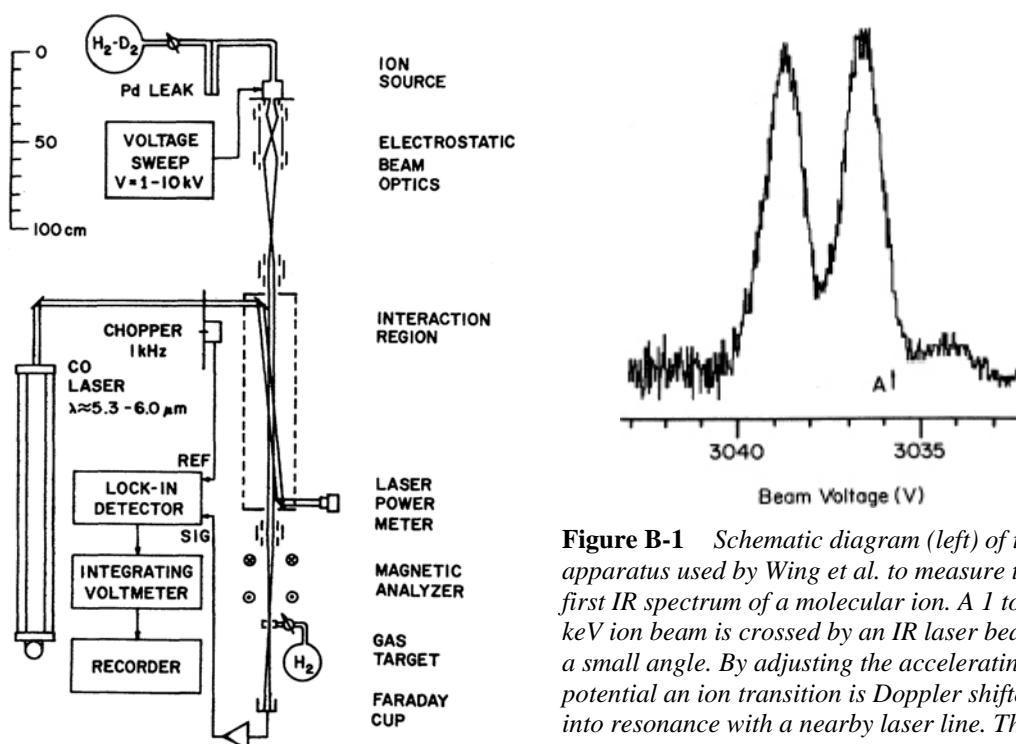


Figure B-1 Schematic diagram (left) of the apparatus used by Wing et al. to measure the first IR spectrum of a molecular ion. A 1 to 10 keV ion beam is crossed by an IR laser beam at a small angle. By adjusting the accelerating potential an ion transition is Doppler shifted into resonance with a nearby laser line. The ions then pass through a gas target where they are partially neutralized by charge exchange. Resonant absorption changes the beam charge survival and, hence, the current into the Faraday cup. The trace of the $(1,1) \leftarrow (0,2)$ transition in HD^+ is shown (right) revealing two hyperfine features. Figures adapted from Wing et al.^[32]

The development of the vibrational spectroscopy of molecular ions during this time proceeded along two paths. These paths differed in the way the absorption of the IR photons was detected. A landmark in the vibrational spectroscopy of molecular ions was the first laboratory observation of the IR spectrum of an ion by Wing and coworkers in 1976.^[32] The IR spectrum of HD^+ was measured in the 1600-1900 cm^{-1} region using a CO laser. The absorption of photons was detected *indirectly* by exploiting a variation in charge exchange cross sections (see Figure B-1). Subsequently, other elegant indirect methods were developed for visible and UV radiation by the Carrington and Lineberger groups based on photodissociation^[33] and photodetachment^[34] in fast ion beams, respectively. In parallel direct absorption techniques were developed by Schwarz^[35], Oka^[36], Dymanus^[37] and Saykally.^[38] These powerful methods were able to deliver vibration-rotation spectra with sub-Doppler resolution, but required extremely high ion densities ($>10^{10}$ ions/ cm^3), prohibiting their application to a wide group of molecular and cluster ions. In order to achieve these high ion yields, the ions were typically prepared in plasma discharges, in which often multiple absorbing species were present and elevated internal temperatures of the ions were common. Subsequent improvements included the velocity modulation technique^[38] as well as the combination of fast ion beams with direct absorption techniques. However, these direct methods remain limited to relatively small ions that can be rather cleanly produced with very high yields.

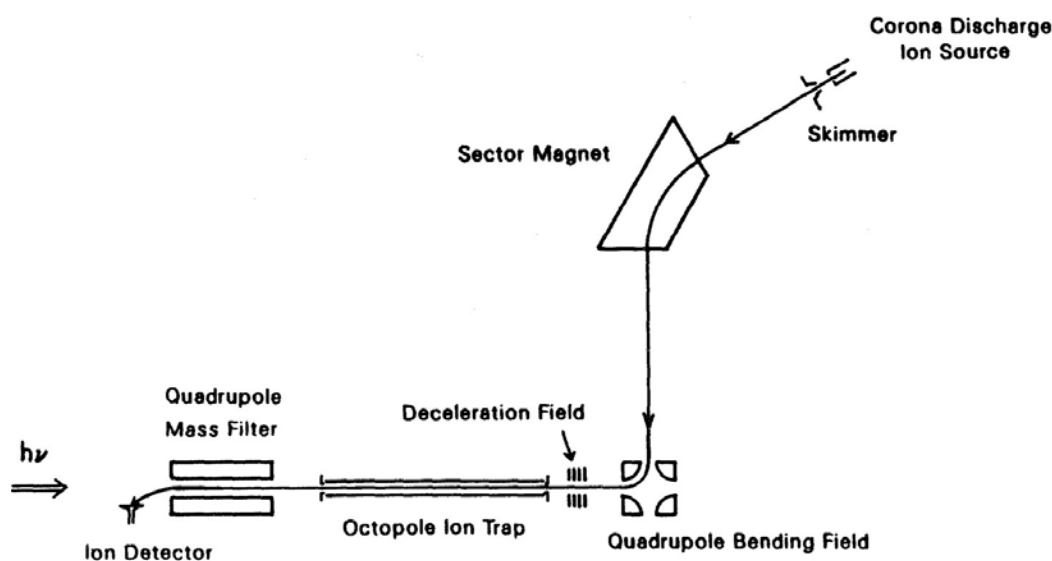


Figure B-2 Schematic diagram of the original ion trap apparatus developed at the University of California Berkeley.^[39]

The indirect detection scheme proved to be of more general applicability. In particular the pioneering vibrational predissociation experiments by Y.T. Lee and coworkers at Berkeley, starting in 1985, on $\text{H}_3^+(\text{H}_2)_x$,^[22,40] $\text{H}_3\text{O}^+(\text{H}_2\text{O})_x(\text{H}_2)_y$,^[39,41] $\text{NH}_4^+(\text{NH}_3)_x$,^[42] and C_2H_7^+ ^[43] marked the beginning of a new era in ion cluster vibrational spectroscopy. Their experimental approach (Figure B-2) involved initial mass selection, the use of an ion trap for IR irradiation and mass-selective detection of fragment ions, an approach still commonly used today and the basis for the experiments described in this thesis. Tunable IR radiation in the 2200-6500 cm^{-1} region was generated by various methods. Low resolution, higher intensity IR pulses were generated in a Nd:YAG pumped optical parametric oscillator (LiNbO₃ crystal). Moderate resolution laser pulses were obtained by difference frequency mixing (in a LiNbO₃ crystal) of the pulsed, near infrared dye laser output with the Nd:YAG fundamental. Higher resolution experiments were performed with a cw F-center laser. In cases where a single photon was insufficient to induce dissociation, either a second photon from the tunable source or an additional cw CO₂ laser was used to provide the additional energy.

Lisy and coworkers extended IR photodissociation studies to mass-selected metal ion – methanol complexes, first in the 9.6 μm range, later in the 3 μm range.^[44] In the mid 90's the groups of Maier and Okumura were among the first to record high-resolution IR spectra for positive^[16,45] and negative^[46] ion-molecule complexes in the 3 μm range, followed by others (see for example the excellent reviews by Duncan; Bieske and Dopfer^[15,16]).

An alternate and completely different approach to the high resolution vibrational spectroscopy of positive ions developed in the 1980's by the Schlag group is zero-kinetic-electron-energy (ZEKE) photoelectron spectroscopy.^[47] Recent advances in synchrotron technology have made the method accessible also to species with higher ionization energies and can in favourable cases yield rovibrational information on molecular cations.^[48] The lack of explicit mass-selection in the ZEKE method is overcome in the closely related mass-analyzed-threshold-ionization or MATI spectroscopy, where the yield of positive ions is measured mass-selectively instead of the yield of slow photoelectrons.^[49] However, the lack of mass-selection prior to photoionization makes studies on clusters and cluster ions, which are generally produced with large mass distributions, challenging.

Free Electron Lasers: Accessing the Fingerprint Region

Until the middle of the 1990's the vibrational spectroscopy of mass-selected cluster ions was restricted to the region below 5 μm , namely the region of O-H stretches, overtone and combination bands, as well as narrow parts of the spectrum around 6 and 10 μm , accessible using CO and CO₂ laser radiation. This dramatically changed with the introduction of free electron lasers (FELs) operating in the IR to molecular spectroscopy by Meijer, von Helden and coworkers in 1996.^[50] The FEL used in these experiments generated intense (typically 20 mJ per 5 μs macro pulse) and continuously tuneable IR radiation from 5 to 250 μm (2000 to 40 cm^{-1}).^[51] This finally opened the door to study the vibrational spectroscopy of molecular and cluster ions in the fingerprint region of the electromagnetic spectrum. While their initial FEL experiments employed a two-color IR/VUV double resonance technique to measure the IR absorption spectrum of para amino benzoic acid in the 700 to 1500 cm^{-1} range^[50], it soon became apparent that the achievable macro pulse fluences were sufficient to perform single-color, IR resonance enhanced multiple photon ionization (IR-REMPI). The pioneering experiments on the gas phase vibrational spectroscopy of the fullerenes C₆₀, C₇₀ and C₈₄ demonstrated the unique sensitivity of this technique when combined with mass-selective ion detection.^[52] Ionization of C₆₀ with IR photons requires the absorption of hundreds of photons; the more interesting is the observation that the IR-REMPI spectrum reveals surprisingly narrow bands related in position to those observed in the emission spectrum of hot C₆₀, confirming that the efficient absorption of IR photons proceeds via a stepwise, incoherent absorption mechanism.^[53] This work was followed by landmark experiments on aromatic hydrocarbons^[54], neutral metal-carbide^[55], as well as metal-oxide^[56] clusters. More recent work includes experiments on metal-ligand complexes^[57], pure metal clusters^[58], amino acids^[59] and the protein cytochrome-c^[60].

In the last couple of years several new groups have exploited the possibility to perform IR-PD experiments on mass selected cluster ions using FEL radiation. Our group was the first to couple a tandem-mass spectrometer including a temperature variable RF-ion to a FEL^[61], ensuring that the "internal" temperature and identity of the signal carrier in mass-selected studies on cluster ions is well defined. In collaboration with the Neumark group at Berkeley we measured the first IR spectrum of a negative ion at a FEL (BrHBr⁻)^[62]. Thereafter, FT-ICR mass spectrometers were coupled

successfully to the FEL CLIO (Orsay, France) by Maitre and coworkers^[63] and to FELIX by von Helden and coworkers^[64].

B.3 The Infrared Multiple Photon Dissociation Mechanism

The mechanism of (collisionless) IRMPD can be conceptually divided into three (overlapping) regions (see *Figure B-3*).^[65]

- (i) The polyatomic molecule is excited resonantly over discrete states into the quasi-continuum region.
- (ii) The molecule continues to absorb photons resonantly, but this energy is quickly randomized among all vibrational degrees of freedom.
- (iii) Once the internal energy reaches the dissociation limit the molecule dissociates according to the statistical model of unimolecular reactions.

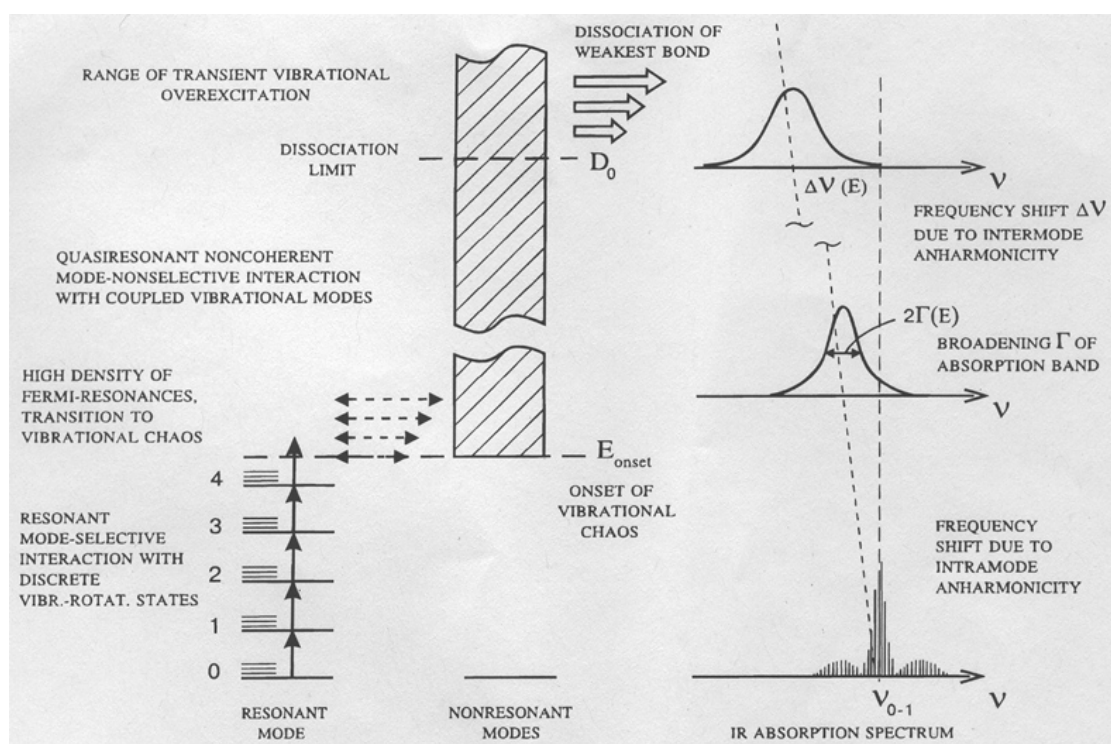


Figure B-3 Main features of the mechanism underlying IR multiple photon excitation and dissociation. Adapted from Makarov et al.^[66].

Region (i) is characterized by the coherent interaction of the radiation field with the discrete energy levels within a vibrational ladder. This resonantly enhanced multiple photon process is governed by selection rules for photoabsorption, which represent the origin of the observed isotope selectivity. The overall cross section for excitation into

the quasi-continuum depends on the laser frequency, the initial vibrational and rotational temperature of the molecule and the laser peak intensity (in contrast to laser fluence). In the discrete region small anharmonic shifts of successive vibrational transitions within a single mode (“anharmonic bottleneck”) can be compensated by changes in rotational quantum number, anharmonic splitting of excited degenerate vibrational states and other effects. In the absence of such effects, in particular in a triatomic system, two- and three-photon vibrational transitions, and thus higher peak intensities, may be necessary to reach the quasi-continuum. Under collisionless conditions de-excitation of the vibrational levels can be neglected, because the time scale, on which the multiple photon photodissociation process proceeds (< 100 ns), is much shorter compared to the typical lifetimes derived from spontaneous emission rates in the IR ($\sim 10^2$ - 10^3 s $^{-1}$). With increasing internal energy E_i the density of rovibrational states $\sigma(E_i)$ increases very rapidly, roughly with E_i^N , where N is the number of vibrational degrees of freedom. Therefore only a few photons are needed to reach the quasi-continuum region, *e.g.*, four photons in the case of SF₆ as illustrated in Figure B-3.

The energy deposition in the quasi-continuum region is mainly through stepwise incoherent one-photon transitions. The absorption properties of the quasi-continuum remain related to those of the discrete region. The absorption bands are generally red-shifted, due to cross-anharmonicities, and lifetime broadened (see right side of Figure B-3). The latter is a direct consequence of the efficient intermode coupling in the quasi-continuum especially at higher energies, which results in rapid IVR. Typical timescales for intramolecular relaxation of highly excited polyatomic molecules are 10^{-11} - 10^{-12} s, much faster than average dissociation lifetimes of several ns.^[67] Thus photoabsorption in this region is always accompanied by randomization of the absorbed energy over the internal degrees of freedom and effective de-excitation of the absorbing transition, making it available for the absorption of another photon. Therefore, the absorption in the quasi-continuum region is, in contrast to the discrete region, dependent on the energy fluence (time-integrated intensity) and not on the peak intensity and is rate-limiting for the entire photodissociation process.

Once the internal energy of the molecule rises over the dissociation limit the (true) continuum of levels is reached and a dissociative channel opens up. The originally bound states become metastable now and can be described in terms of decaying

resonances due to coupling to the continuum states. The resonant excitation to higher levels is then always in competition with dissociation. As the dissociation rate is expected to increase rapidly with increasing internal energy, the up-excitation is quickly balanced by dissociation depleting the population. The distribution is thus different from a thermal distribution. The laser-excited population is narrower and asymmetric, because the high-energy tail is heavily depleted by dissociation.^[68]

A simple phenomenological model^[31,68] based on rate equations can be set up to describe the time-dependent excitation of the excited molecules to and beyond the dissociation limit. It rests on several assumptions:

- (i) The multiple photon excitation proceeds by stepwise incoherent one-photon transitions among a set of equally spaced energy levels.
- (ii) The degeneracy of each level is given by the corresponding molecular density of states.
- (iii) Spontaneous emission is neglected and the ratio between emission and absorption cross section is given by the ratio of the level degeneracies.
- (iv) The dissociation rates of molecules from levels above the dissociation threshold are given by RRKM theory.

The rate equations can then be written as

$$\frac{dN_m}{dt} = \frac{I(t)}{h\nu} \left[\sigma_{m-1} N_{m-1} + \frac{g_m}{g_{m+1}} \sigma_m N_{m+1} - \left(\frac{g_{m-1}}{g_m} \sigma_{m-1} + \sigma_m \right) N_m \right] - k_m N_m, \quad (4)$$

where N_m is the normalized population in level m with energy $m \cdot h\nu$, $I(t)$ is the laser intensity, g_m is the density of states of level m , σ_m is the cross section for absorption from level m to $m+1$, and k_m is the RRKM dissociation rate constant for level m .

For a given molecule with σ_m and $I(t)$ specified, the set of rate equations in Eq. (1) can be easily computed. The density of states g_m in Eq. 1 is generally approximated by the vibrational density of states, which can be determined from the harmonic (or anharmonic) frequencies using the Beyer-Swinehart algorithm.^[69] The absorption cross section and in particular its dependence on excitation energy is generally not experimentally known and is difficult to estimate from *ab initio* calculations. Generally, it is assumed that σ_m decreases exponentially with increasing m . The microscopic rate constant k_m is given by the ratio

$$k_m(E^*) = \frac{\sum_0^{E-E_0} N(E)\Delta E}{N^*(E^*)}, \quad (5)$$

corresponding to the sum of all vibrational and rotational quantum states available to the activated complex with vibrational energy in the range from 0 to E^*-E_{diss} , divided by the density of states in the energized molecule at energy $E^*=m\cdot h\nu$. Based on this model several important and general conclusions can be drawn:

- (i) If the laser pulse duration is too short, no dissociation will be observed, independent of peak intensity.
- (ii) The dissociation rate constant increases more slowly with increasing energy as the degrees of freedom and the number of low-frequency modes are increased.
- (iii) The RRKM dissociation rate constant increases more rapidly with excess energy if the dissociation energy is lowered.
- (iv) Most of the excess energy should remain as internal energy in the emerging fragments, leading to secondary dissociation, if the fragments have strong absorption band coinciding with the laser frequency.
- (v) For heavier, more complex molecules, competing dissociation channels may open up, provided their dissociation energies are not too far above the lowest-energy channel.

C EXPERIMENTAL SETUP

This chapter describes various aspects of the experimental setup and is divided into two parts. It begins with an overview of the tandem mass spectrometer, briefly covering the vacuum system, ion sources, RF ion guides and mass filters. The instrument was designed and constructed at the beginning of this thesis period and delivered its first mass-selected ion signal in June 2001, roughly 18 months after the first rough sketch was drawn up, and its first IRMPD spectrum of cooled and trapped ions in November 2001. The IR experiments were performed at the free electron laser facility FELIX. FEL basics and FELIX details are briefly described in the second part of the chapter, which ends with a summary of currently available table-top mid-IR laser systems.

C.1 The Tandem Mass Spectrometer

The design of the new spectrometer is based on a triple quadrupole instrument constructed by Wöste and coworkers in 1993 and modified thereafter.^[70,71] The original setup was used to perform laser experiments on mass-selected, cooled metal cluster ions. The metal ions were produced in a sputtering source, collimated and compressed in phase space in a He-filled quadrupole ion guide and mass-selected in a quadrupole mass filter. Mass-selected ions were trapped in a 8 cm long RF octopole ion trap. The interaction products were mass-selectively detected using a second quadrupole mass-filter followed by a channeltron detector. The instrument was constructed to produce high currents (\sim nA) of mass-selected cluster ions and is restricted to studying small metal and metal oxide ions.

The goal of the new design was to build a more compact instrument, which would improve on the older design with respect to versatility in ion production, detection sensitivity and mass selectivity. Major improvements compared to the original version in the current “second generation” instrument are:

- (i) Modularly constructed source region,
- (ii) non-linear arrangement of the RF-devices,
- (iii) improved mass resolution ($\Delta m=1$ amu up to 1000 amu),

- (iv) high transmission design of all RF-devices,
- (v) temperature adjustable (15 to 350 K) 16-pole ion trap with axial focusing ring,
- (vi) complete computer control of all electrostatic potentials, RF amplitudes, as well as other parameters, and
- (vii) compact and portable design.

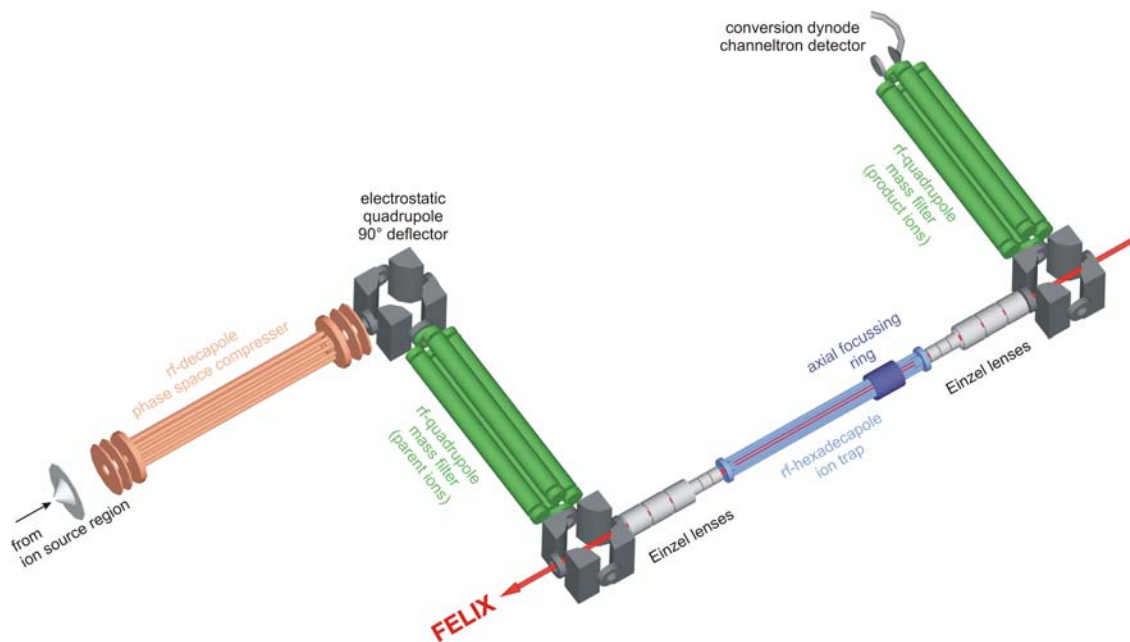


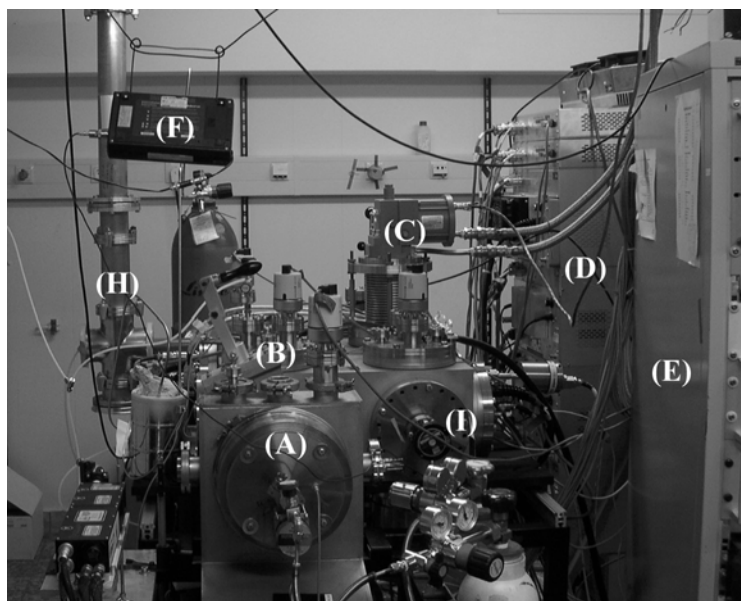
Figure C-1 Schematic 3D-view of the guided ion beam tandem mass spectrometer.

A schematic of the instrument is shown in Figure C-1. The beam of ions formed in the ion source region is skimmed and fed into a RF-decapole ion guide. The decapole device can be filled with a buffer gas in order to collimate and compress the ion beam in phase space.^[72] The ion beam is cleared from any remaining neutral particles in a 90° electrostatic quadrupole deflector and then enters the first quadrupole mass filter. Mass-selected ions exit the mass filter, pass another 90° deflector and are focused into the ion trap using two Einzel lens arrangements. The ion trap consists of an entrance and exit lens, a 16-pole RF-ion guide, and an axial focusing ring. The complete assembly is connected to a closed-cycle He cryostat. The laser beam is applied coaxially to the ion trap. Ions extracted from the ion trap are focused by another two sets of Einzel lenses, pass a third 90° deflector and are finally mass-selectively detected using a second quadrupole mass filter combined with a conversion dynode channeltron detector. The complete instrument is housed in a tailor-made vacuum chamber equipped with ultra-high vacuum flanges.



Figure C-2 Tandem mass spectrometer in the FUB lab without any cables connected. From left to right one can see the source chamber (A), bellow (B), high vacuum chamber (C), cryostat (D), detector region (E), and foreline pumps (F).

Figure C-3 The tandem mass spectrometer in user station 9 at the FELIX facility from a slightly different angle: source chamber (A), gate valve (B), cryostat (C), electronics racks (D+E), power meter and display (F+I) and FELIX beamline (H).



Vacuum System

The vacuum chamber (see Figure C-2) was constructed in the workshop of the Physics Department at the FUB and consists of two regions, the source and the high-vacuum region, separated by a $\varnothing 90$ mm gate valve (Balzers). This allows venting the source region exclusively, which is usually done on a daily basis. The high-vacuum chamber is mounted on a Lintec rail system and can be displaced mechanically relative to the source chamber in the horizontal direction by a spindle / worm-gear / motor assembly. This mechanism allows moving the first ion guide past the gate valve into the source chamber in order to guide the ions as soon as possible. The source chamber is equipped

with a special adapter flange for the source modules and otherwise KF flanges. It is pumped by a 1600 l/s turbo molecular pump (Pfeiffer Vacuum TMH-1601) backed by a 65 m³/h double-stage rotary pump (Pfeiffer Vacuum Duo 65), yielding a background pressures of $<1 \cdot 10^{-6}$ mbar. Typical operating pressures lie in the 10^{-4} - 10^{-2} mbar range.

The high-vacuum chamber is completely equipped with CF flanges and is UHV compatible. It consists of three compact, stainless steel rectangular blocks (see Figure C-2), which are connected via CF flanges and can therefore be configured to either house the RF devices in a bent (presently used) or linear arrangement. A flexible bellow connects this chamber to the source region. The four differential regions Q0 (decapole ion guide), Q1 (first quadrupole mass filter), Q2 (ion trap region) and Q3 (second quadrupole mass filter and ion detector), are each pumped by a 520 l/s turbo molecular pump (Pfeiffer Vacuum TMU 521), which are backed by a second 65 m³/h rotary pump. The high-vacuum chamber houses the main part of the instrument shown in Figure C-1. The background pressure is $<2 \cdot 10^{-8}$ mbar (without baking). Typical operating pressures, when using buffer gases in the ion guide and trap regions Q0 and Q2, in the differentially-pumped regions are $9 \cdot 10^{-5}$ mbar (Q0), $5 \cdot 10^{-6}$ mbar (Q1), $5 \cdot 10^{-6}$ mbar (Q2) and $1 \cdot 10^{-7}$ mbar (Q3).

Ion Sources

Three ion sources are currently in use:

- (i) a 100 Hz rotating-rod laser vaporization source,
- (ii) a continuous ion spray source, and
- (iii) a continuous or pulsed expansion crossed 1 kV e⁻-beam source.

The laser vaporization source is a home-built, Smalley-type^[73] rotating rod source that is useful to produce wide size distributions of pure metal and metal-containing cluster ions. Its details are described in the diploma thesis of G. Santambrogio^[74] and only the salient features are summarized here. A nanosecond laser pulse, usually the second harmonic of a Q-switched Nd:YAG laser, impinges on a metallic target and the metal vapor produced by the early portion of the laser pulse forms a dense cloud near the metal surface. This cloud is quickly ionized and the resulting plasma is entrained in a buffer gas pulse and allowed to thermalize through collisions with the source walls in the expansion channel. Cluster formation occurs here through three-body-collisions.

Adding small amounts of a reactive gas to the buffer gas allows tailoring the cluster composition. The gas pulse then expands into the vacuum cooling mainly the rotational and translational degrees of freedom. The vibrational temperature of the ions is determined mainly by the temperature of the source chamber. The source has recently been upgraded and now operates at a repetition rate of up to 100 Hz (*Big Sky Laser CFR-200*, <12 ns, 20 mJ @ 532 nm and 100 Hz).

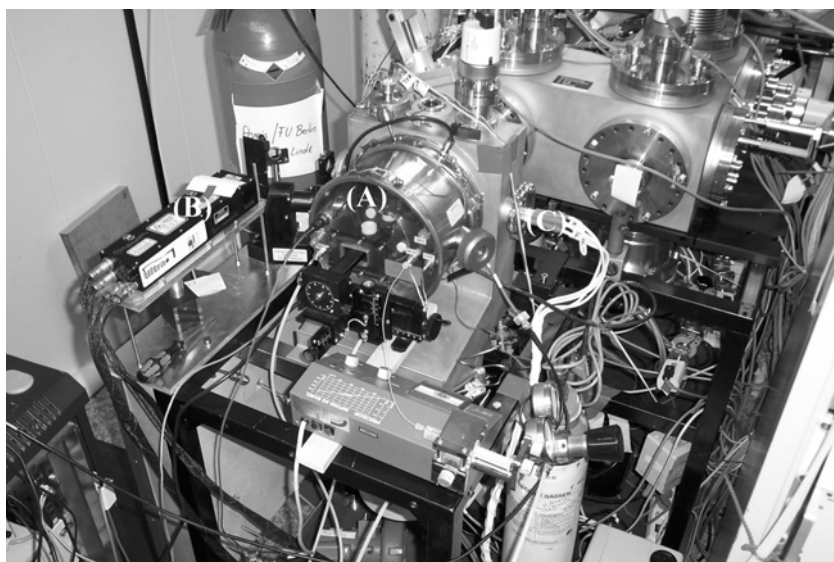


Figure C-4 Picture of the source region with the ion spray source (A) installed. The ablation laser (B) and the feedthrough for the electron gun (C) can also be seen.

The ion-spray source (Figure C-4) was taken from a commercial SCIEX API III triple quadrupole mass spectrometer and adapted accordingly. It allows to introduce polar and thermally labile compounds into a mass spectrometer without fragmentation, thermal degradation and free of solvent molecules.^[75] This method involves spraying a polar liquid containing preformed ions through a charged tip forming charged droplets and subsequent emission of the ions from the droplet into the gas phase. Depending on the way the droplets are formed one refers to ion-spray (pneumatic sprayer), electro-spray (high electric field without gas jet) and thermo-spray (heated tip sprayer). Ion evaporation from the droplet is a complex sequential process, in which solvent evaporation leads to an increase of electrical charges on the droplet surface eventually leading to one or more Coulomb explosions, producing the bare ion.

The crossed electron beam source^[76] consists of a pulsed (or continuous) expansion, which is crossed by a continuous beam of 1 kV electrons from an e-gun (Figure C-5) and is an efficient source to produce molecular anions. Collisions with the fast electrons ionize the buffer gas producing many secondary electrons. These slow electrons can be temporarily captured by neutral molecules forming short-lived anions (

resonances). These species are either stabilized by three body collisions or decay via electron emission or dissociative attachment forming a stable negative ion and neutral molecule. Stable anions are cooled in the supersonic expansion and may react further with other neutral molecules in the gas pulse.

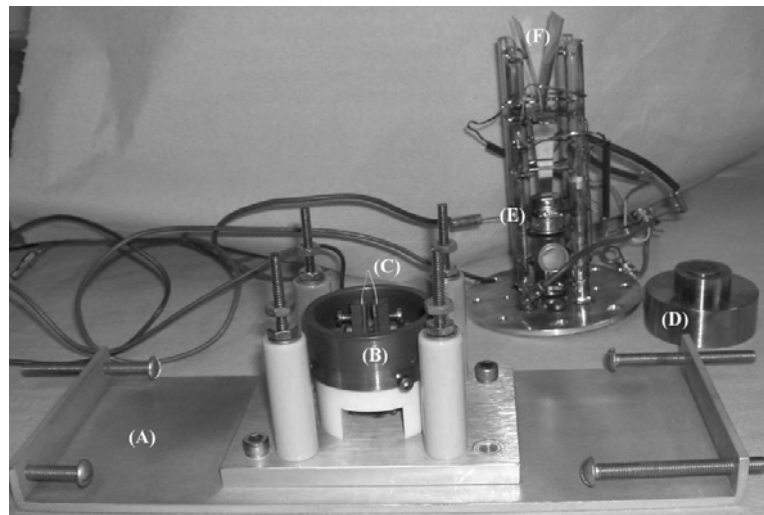


Figure C-5 Picture of the 1 kV electron gun. The electron gun mount (A) is used to secure the e-gun inside the source chamber. The thorium-coated iridium filament (C) is held in position by two screws. A voltage can be applied to the anode (D) in order to extract electrons from the filament region (B) into the focusing and steering optics assembly, consisting of an Einzel lens (E) and two pair of deflectors (F).

RF Ion Guide and Mass Filters

A home-built RF decapole ion guide (5 mm stainless steel rod diameter) operated at 1.2 MHz (Extrel QC150 power supply) is used to guide the ions from the source region into the high-vacuum chamber. The ion guide can be filled with a buffer gas (generally argon) and used as a phase-space compressor, *i.e.*, through multiple collisions with the buffer gas atoms the initially broad ion velocity distribution is narrowed. The reduction of the velocity component perpendicular to the decapole axis leads to a collimation of the ion beam in the RF ion guide.

Mass-selectivity is achieved by two quadrupole mass filters (ABB Extrel CMS Tri-Filter) with $\frac{3}{4}$ inch rods and running at 880 kHz, yielding a mass resolution $m/\Delta m = 1000$. In addition to the high precision main quadrupole rods, the mass filters also have RF-only pre- and post-filters. These are short stub rods before and after the main rods that help to collimate the ions coming into and exiting the main section rods and which increase the ion transmission through the mass filter by shielding the ions from the RF and DC fringing fields present at the end of the main rods. Ions exiting the second mass filter are detected using standard ion counting techniques.

Hexadecapole Ion Trap

The principle of ion trapping in a gas-filled linear RF ion guide was first described by Dolnikowski *et al.*^[77] Exactly as in the gas-free version (see also Figure B-2) the ions are confined in the two dimensions perpendicular to the guide axis by the RF field of appropriate amplitude. Confinement in the third dimension (parallel to the guide axis) is achieved by applying appropriate electrostatic potentials to the entrance and exit lens. While the lens potentials need to be pulsed in the gas-free version, the gas-filled ion trap can be filled continuously. This is done by choosing an ion energy, which allows the ions to barely pass the potential barrier at the ion trap entrance. The ions then traverse the ion trap, are reflected at the exit lens and return to the entrance lens region. At this point the ions have lost sufficient kinetic energy through many collisions with the buffer gas, generally helium, such that they cannot pass the potential barrier at the entrance lens anymore and are thus confined to the region within the ion guide. Another important advantage of the gas-filled version is that the trapped ions are collisionally thermalized to the ambient temperature, generally within less than a millisecond under typical operating conditions.

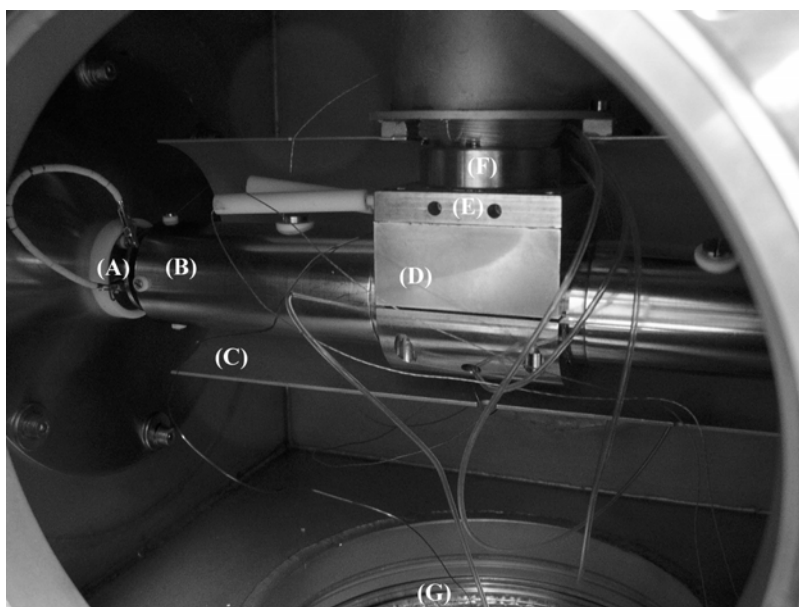


Figure C-6 Picture of the ion trap (B) mounted on the cold head (F) in-between the Einzel lens arrangements (A). The cold shield (C) is connected to the first stage (70 K) of the cryostat. The copper interface plate (E) is connected to the ion trap holder (D) and contains the heater cartridge. The protective grid (G) above the turbo molecular pump is also seen.

The temperature-controllable 16-pole ion trap used in the present instrument was designed considering the basic principles of RF multipoles described in detail by Gerlich^[78] and discussed with respect to the present ion trap by Santambrogio.^[74] Its trapping properties were also modeled using the SIMION 6.0 program. The incorporation of a helium cryostat in the current design was copied from a similar ion trap designed by Hess^[71]. The number of rods was chosen to be as large as possible

without introducing significant mechanical constraints, in order to optimize ion transmission, reduce ion heating and minimize the heat capacity of the ion trap.

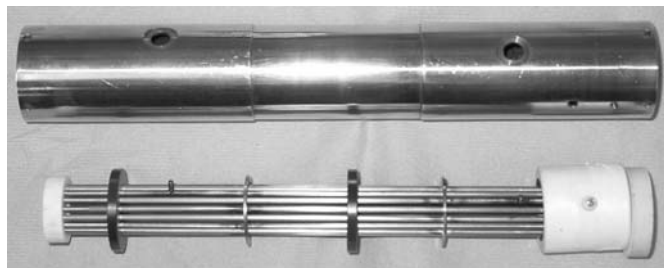


Figure C-7 Photograph of the ion trap housing (gold-coated copper cylinder) and the linear hexadecapole ion guide, consisting of sixteen 2mm diameter, 224 mm long stainless steel rods. The (teflon-coated) stainless steel cylindrical “focusing” electrode is seen on the right end of the rod assembly.

The home-built 16-pole RF ion trap (see Figure C-7) consists of sixteen 2 mm diameter 224 mm long stainless steel rods held equidistantly on a 16 mm diameter circumference by two Macor rings at each end and two additional Vespel spacers. Like the ion guide it is operated at 1.2 MHz using an Extrel QC150 power supply. An additional cylindrical electrode was installed recently to generate a potential well along the axis of the ion trap in order to confine the (slow) ions to a narrower region inside the ion trap. The ion trap is housed in a gold-coated copper cylinder, which also holds the stainless steel entrance and exit lenses (6 or 10 mm aperture diameter). The ion trap is connected to the cold head of a two stage, closed-cycle helium refrigeration system based on the Gifford-McMahon thermodynamic cycle (CTI/Cryogenics, CT-8 cryo pump with SC8300 compressor unit). The cryo pump delivers 5 W at 20 K, and allows cooling the ion trap down to 15 K. The temperature is measured at two points, at the cold head and at the exit lens by Lake Shore DT-670B silicone diode sensors and read out using the Lake Shore 331S temperature controller. The temperature difference between the two measurement points is less than 1 K, assuring a nearly homogeneous temperature across the ion trap. The ion trap can be heated by a Lake Shore HTR-50 heater cartridge (50 Ohms / 50 W), which is mounted into the copper interface plate between the ion trap holder and cold head. This allows continuously adjusting of the ion trap temperature between 15 K and 350 K.

Two separate Teflon tubes allow admitting different gases to the ion trap region. One is generally used for the helium supply (Linde, He 6.0), the other for the admission of reactive gases. The gas flow is regulated by two MKS gas flow controllers with maximum flows of up to 10 and 50 sccm, respectively. The absolute pressure inside the helium trap is measured by a MKS baratron model 627B (0.1 to $1 \cdot 10^{-5}$ mbar) using a

third teflon tube. The absolute pressure measurement (p_m) is corrected for differences in temperature between the manometer (T_m) and the trap (T_{trap}) using the relationship:

$$p_{\text{trap}} = p_m \sqrt{\frac{T_{\text{trap}}}{T_m}}. \quad (6)$$

C.2 Infrared Light Sources

Of central importance to the present work is the possibility to study the vibrational spectroscopy of gas phase ions in the mid-IR, or so-called fingerprint region, which extends roughly from 500 to 2000 cm^{-1} . The low number densities attainable in the gas phase ($< 10^8$ ions/ cm^{-3}) in general prohibit direct absorption measurements and indirect techniques, generally referred to as action spectroscopy, need to be used. These techniques require intense and tunable IR light sources. Even though considerable progress has been made in the field of table-top IR lasers that are widely tunable in the mid-IR region (see final paragraph of this chapter), these systems still lack the pulse energies to induce multiple photon absorption processes. Therefore free electron lasers operating in the IR remain the only available sources to date to perform multiple photon absorption studies throughout the complete fingerprint region.

The Free Electron Laser for Infrared Experiments (FELIX)

A free electron laser (FEL) is a device which generates coherent radiation from a beam of relativistic electrons. The central part of an FEL is the undulator (Figure C-8), a periodically alternating static magnetic field. The peak emission wavelength λ depends on the undulator period L , the strength of the magnetic field, expressed by a dimensionless parameter K , and the electron energy:

$$\lambda \propto \frac{L}{2\gamma^2}(1+K^2). \quad (1)$$

$\gamma = mc^2/m_0c^2$ is the relativistic factor and corresponds to the kinetic energy of the electrons along the axis of the FEL in units of the electron rest energy m_0c^2 . In the moving electron frame the electrons see not only an oscillating magnetic field, but also an oscillating electric field in the perpendicular direction - in short, they see an electromagnetic wave with wavelength L/γ . Upon interaction with this wave the electron emits (first-harmonic) light of the same wavelength. The corresponding wavelength in the laboratory frame is subject to the Doppler effect. Thus, for MeV electrons the macroscopic undulator period ($L \approx 1\text{cm}$) is shortened by the Lorentz contraction ($1/\gamma$) and the Doppler shift ($1/2\gamma$) into the μm wavelength region.

The amount of power radiated spontaneously by a very energetic beam of electrons is not large. Indeed if the electrons were spaced uniformly along the beam,

there would be no power emitted at all due to destructive interference. Only the fluctuations in particle current lead to a net radiation, which scales linearly with n , the number of electrons. The spectrum of the spontaneous radiation is determined by the finite undulator length $l = N \cdot L$, resulting in a finite transit time and a fractional width of the spontaneous or noise radiation of $1/N$.

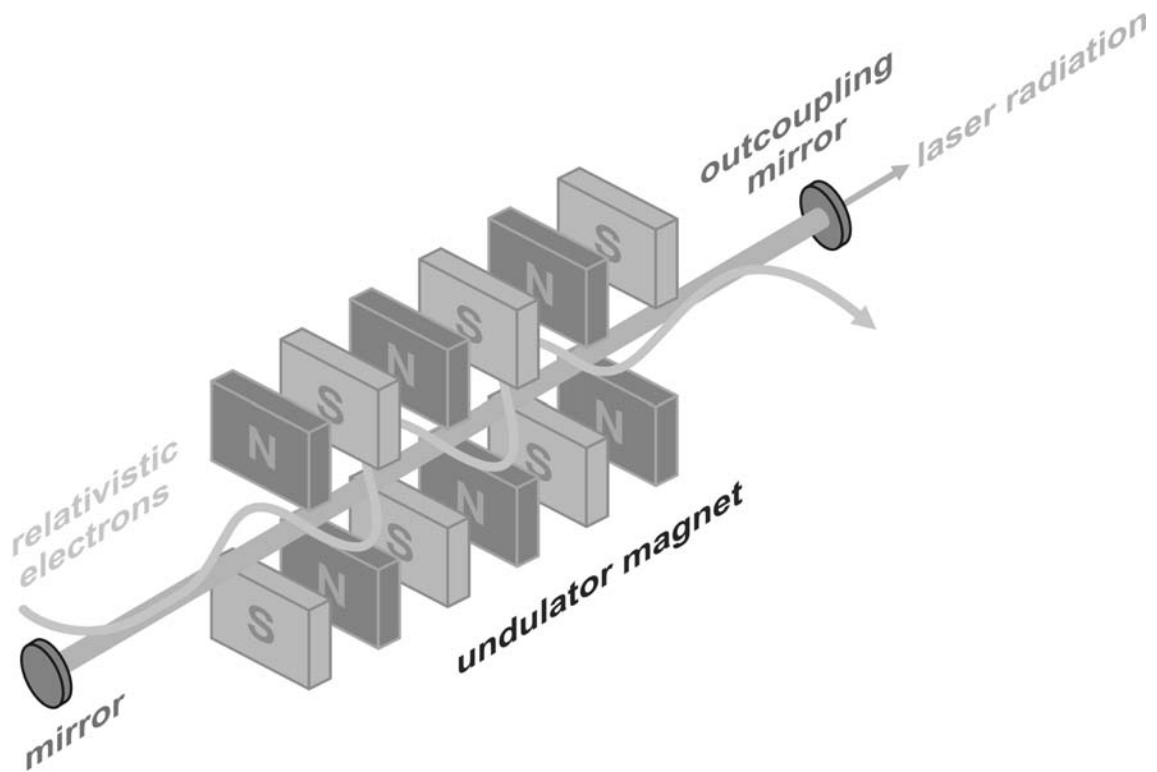


Figure C-8 Schematic of the optical cavity of a free electron laser.

The ponderomotive force acting between the axial electron velocity and the magnetic component of the electromagnetic wave is the origin of the stimulated emission of (highly coherent) photons. It couples the electron motion to the electromagnetic field and is phase dependent. Electrons that are in phase with the electromagnetic wave are retarded while the ones with opposite phase gain energy. Through this exchange of energy a longitudinal density modulation on the scale of the wavelength is created, the so called micro-bunching. More and more electrons begin to radiate in phase, which results in an increasingly coherent superposition of the radiation emitted from the micro-bunched electrons. The more intense the electromagnetic field gets, the more pronounced the longitudinal density modulation of the electron bunch and vice versa (gain mechanism). With complete micro-bunching, all electrons radiate almost in phase and this leads to a radiation power, which is proportional to N^2 and thus

an amplification of many orders of magnitude with respect to the spontaneous emission of the undulator.

For IR, visible and UV FELs, light amplification can be reached in a multi-pass setup, *i.e.* by using an optical cavity with mirrors on both sides and the electrons passing the undulator as the gain medium in between. Saturation will occur when the field gets so strong and therefore the energy loss by the electrons along the undulator is so large, that at the end of the undulator the radiation that was red-shifted at the undulator entrance, appears blue-shifted to the electrons at the end of the undulator, where hence the energy will start to flow back to the electrons. Exactly at resonance, the radiation produced by the density modulation is 90-degrees out of phase with the radiation driving the modulation, meaning that an oscillator will not start up under this condition. Slightly off-resonance, both amplitude and phase of the density modulation evolve along the undulator and a net energy transfer will occur: from electrons to the field for radiation that is somewhat red-shifted and vice versa for radiation that is blue-shifted.

The temporal structure of the optical output pulse is determined by the incoming electron beam. The linear RF accelerators of FELIX typically generate 7 μs long pulse trains of 1 ps long electron bunches at a repetition rate of up to 10 Hz. The micropulse repetition rate is either 25 MHz or 1 GHz, the latter corresponding to 40 optical pulses circulating in the 6m long cavity. The micropulse duration of the optical pulses can be varied in-between 300 fs to several ps and their bandwidth is near-transform limited, ranging from less than 0.5% to several percent full width at half maximum of the central wavelength.

The output wavelength of FELIX depends on the electron beam energy and the magnetic field strength. Generally, the wavelength is scanned by mechanically adjusting the distance of the undulator magnetic poles for fixed beam energy. A factor of three in wavelength can be covered using a single electron beam setting. Typically, macropulse energies at narrow bandwidth and 1 GHz micropulse repetition rate are 30 to 50 mJ. The IR radiation is guided via an evacuated transport system to a user station (roughly 30 m away).

Table Top IR lasers: Recent Advances

The generation of intense and tunable laser pulses in the mid IR region using table top lasers is an active research area. One promising approach is based on difference

frequency mixing in an AgGaSe₂ crystal, pioneered by Raffy *et al.*^[79] and considerably improved and first applied to gas phase spectroscopy by Gerhards and co-workers^[80]. The three stage system consists of a tunable near IR laser (3650-4000 cm⁻¹, bandwidth 0.04 cm⁻¹), whose output is amplified in an LiNbO₃ based OPA. Signal and idler of the OPA process are then used for DFM in an AgGaSe₂ crystal, leading to tuneable radiation from 2100 to 1400 cm⁻¹ with a pulse energy of ~1 mJ at 1645 cm⁻¹ and a bandwidth of 0.1 cm⁻¹. Bosenberg and Guyer have used the same type of crystal, but a more complex OPO/OPA setup, to achieve similar specs.^[81] Johnson and co-workers have recently used a Laser Vision KTP/KTA/AgGaSe₂ optical parametric oscillator/amplifier system to measure IR spectra in the range from 600 to 1900 cm⁻¹.^[82], convincingly demonstrating that the fingerprint region is now accessible for IR-PD experiments of weakly bound species.

An alternate continuously tunable, narrow bandwidth (0.4 cm⁻¹) laboratory laser source for the mid-IR spectral range of 1250 to 2270 cm⁻¹ has been developed by Vilesov and coworkers.^[83] The device is based on the stimulated backward Raman scattering in solid para-hydrogen at 4 Kelvin. The crystal is pumped by a focused beam obtained from a commercial near-IR OPO. Output energies range from 1.7 mJ at 2270 cm⁻¹ to 120 μJ at 1250 cm⁻¹.

D RESULTS AND DISCUSSION

D.1 Vanadium Oxide Cluster Ions

Mass-selected Infrared Photodissociation Spectroscopy of $V_4O_{10}^+$

Knut R. Asmis, Mathias Brümmer, Cristina Kaposta, Gabriele Santambrogio, and
Ludger Wöste

Institut für Experimentalphysik, Freie Universität Berlin, Arnimallee 14, D 14195 Berlin, Germany

Gert von Helden and Gerard Meijer

FOM Institute for Plasmaphysics Rijnhuizen, Edisonbaan 14, NL-3439 MN, Nieuwegein, The Netherlands and Department of Molecular and Laser Physics, University of Nijmegen, Toernooiveld, NL-6525 ED, Nijmegen, The Netherlands

Klaus Rademann

Institut für Chemie, Humboldt Universität Berlin, Bunsenstrasse 1, D 14195 Berlin, Germany

Communication in *Physical Chemistry Chemical Physics* **4(7)** 1101-4 (2002).

Mass-selected infrared photodissociation spectroscopy of $V_4O_{10}^+$ K. R. Asmis,^{*a} M. Brümmer,^a C. Kaposta,^a G. Santambrogio,^a G. von Helden,^b G. Meijer,^{bc} K. Rademann^d and L. Wöste^a^a Institut für Experimentalphysik, Freie Universität Berlin, Arnimallee 14, D 14195 Berlin, Germany. E-mail: asmis@physik.fu-berlin.de; Fax: +49 30 83855567; Tel: +49 30 83856120^b FOM Institute for Plasma Physics Rijnhuizen, Edisonbaan 14, NL-3430 BE Nieuwegein, The Netherlands^c Department of Molecular and Laser Physics, University of Nijmegen, Toernooiveld, NL-6525 ED Nijmegen, The Netherlands^d Institut für Chemie, Humboldt Universität Berlin, Bunsenstrasse 1, D 14195 Berlin, Germany

Received 6th December 2001, Accepted 6th February 2002

First published as an Advance Article on the web 27th February 2002

The gas-phase infrared spectroscopy of $V_4O_{10}^+$ produced by laser vaporization has been studied in the spectral region from 7 to 16 μm . Mass-selected $V_4O_{10}^+$ cations were stored in a helium filled radio frequency hexadecapole ion trap and excited using tunable infrared radiation from a free electron laser. The photodissociation spectrum was recorded by monitoring the $V_4O_8^+$ yield (O_2 loss) as a function of the excitation wavelength. Two absorption bands at 842 and 1032 cm^{-1} are observed, which are assigned to resonant excitation of the antisymmetric V–O–V stretching and V=O stretching vibrations, respectively. Comparison to recent theoretical and experimental studies indicate that the absorbing species consists of a $V_4O_8^+$ ionic core weakly bound to an oxygen molecule.

Vanadium oxides are becoming increasingly important in technological applications, e.g., as catalysts for oxidation–reduction reactions, semiconductors, optical devices and coatings.^{1–3} Despite the importance of bulk V_2O_5 as a catalyst many microscopic details of its catalytic behavior remain under debate.³ Understanding the nature of the reactive sites in heterogeneous catalysis can be aided by gas-phase studies of isolated neutral and ionic clusters. However, only scarce experimental information on the spectroscopy and structure of vanadium oxide clusters is available,^{4–7} complicating the interpretation of the gas-phase reactivity studies.^{8–17}

Studies of the mass spectral distributions and cluster growth dynamics of vanadium oxide clusters^{18,19} and cluster ions^{8,12} show that VO_2 , VO_3 , and V_2O_5 units are the main building blocks for $V_xO_y^{-/0/+}$ clusters. Oxygen-rich cluster ions can also contain a weakly bound O_2 species, as was shown in recent collision induced dissociation (CID) and 532 nm photo-fragmentation studies.^{7,8} Gas phase reactivity studies indicate that the reactivity of vanadium oxide cluster anions and cations depends on cluster stoichiometry and generally decreases with cluster size.^{10,13} However, with the exception of the diatomic VO (see ref. 20 and references therein), which has been found in the spectra of metal-rich M-type stars,²¹ very few spectroscopic studies have been carried out on larger vanadium oxide clusters. Wu *et al.* have measured the photoelectron spectra of the vanadium oxide anions VO_x^- ($x = 1–4$).⁴ Matrix ESR⁵ and FTIR⁶ studies have also been reported for monovanadium oxides and V_2O_2 . Comprehensive theoretical studies on the structure, energetics and bonding of vanadium oxide clusters and cluster ions have recently been reported.^{22–24}

Vibrational spectroscopy of gas phase clusters and cluster ions is a straightforward approach to probe the structure of these species. However, conventional absorption measurements, a standard tool for the characterization of liquid and solid samples, lack the sensitivity and selectivity required for studying isolated gas phase species, due mainly to the low number densities compared to the condensed systems. Therefore in recent years much effort has been put into the development of experimental methods to study the infrared (IR) spectroscopy of gas phase ions.^{25,26} However, most of these studies have been limited to the wavelength region below 3 μm , i.e., the spectral region of hydrogen-stretching motions and of the IR-active combination bands, due to the lack of widely tunable IR light sources. The application of a free-electron laser, which emits widely tunable light from the near to the far IR-region, to molecular spectroscopy by Meijer and coworkers has bridged this gap.^{27–29}

In the present study we combine for the first time, to the best of our knowledge, tandem mass spectroscopy with a free-electron laser to study the vibrational spectroscopy of mass-selected vanadium oxide cluster ions by mass-selected IR photodissociation spectroscopy. After a brief description of the novel experimental apparatus, we present the gas phase IR photodissociation spectrum of the $V_4O_{10}^+$ cation. The results are compared to calculated IR spectra²³ of various neutral V_4O_{10} isomers and discussed with respect to structure and dissociation mechanism.

IR photodissociation spectra were obtained by photoexcitation of mass selected $V_4O_{10}^+$ and subsequent monitoring of the $V_4O_8^+$ fragment ion yield as a function of the excitation wavelength. The experiments were carried out in a novel guided ion beam tandem mass spectrometer, schematically depicted in Fig. 1, and using a widely tunable IR free electron laser.

IR excitation is performed with the “Free Electron Laser for Infrared eXperiments” (FELIX).³⁰ The laser output consists of a macropulse of 5 μs duration at 5 Hz. The macro pulse is composed of a series of ~ 1 picosecond duration micro pulses spaced by one nanosecond. The wavelength is continuously tunable between 5 and 250 μm . The bandwidth is nearly transform limited and depends on the micro pulse duration. In the present experiments the wavelength was scanned from 7.0 to 16 μm , the scanning range determined by the transmission function of the ZnSe optics used in the present experiment, in steps of 0.10 μm . Higher resolution spectra were measured with a step size of 0.02 μm in selected spectral regions. The

macro pulse energy was 50–60 mJ, while the bandwidth was less than 1%. The IR beam was focused through a 2 mm thick zinc selenide window into the center of the ion trap with a 60 cm focal length zinc selenide lens.

Vanadium oxide clusters are prepared by pulsed laser vaporization with the second harmonic (532 nm, 8 ns, ~ 10 mJ pulse $^{-1}$ at 20 Hz) of a Nd : YAG laser focused onto a rotating and translating 6 mm diameter solid vanadium rod (Alfa Aesar, 99.5% purity). The resulting plasma is entrained in a pulse of 1% O₂ seeded in He carrier gas, expanded through a clustering channel and passed through a 2 mm skimmer.

Positive ions are focused into a radio frequency (RF) quadrupole ion guide (Q₀ in Fig. 1), which collimates the ion beam, then deflected by 90° by the quadrupole ion deflector D₀ into the first RF quadrupole mass filter Q₁, which is typically operated at unit resolution. Mass-selected ions are guided via the second 90° deflector D₁ and two sets of einzel lenses (E₁ and E₂) into a temperature-adjustable, He filled RF hexadecapole ion guide (H). The arrangement of a gas-filled RF ion guide in-between two electrostatic lenses can be used as an efficient ion trap.³¹ Ions entering the trap, which is connected to a helium cryostat and kept at a constant temperature of < 70 K, lose both kinetic and internal energy due to inelastic collisions with the cooled He buffer gas (~ 0.08 mbar). Applying appropriate electrostatic potentials to the entrance lens, ion guide pole bias voltage and exit lens of the trap allows ions to be trapped over a period of seconds, effectively increasing the ion density inside the trap and thermalizing the trapped ions to the ambient temperature on a timescale of roughly 10⁻⁴ s.³²

Trapping conditions were optimized on the ion signal and with respect to signal-to-background considerations. In the present experiment the ion trap is continuously filled for a period of 1 s. During this time on average five FELIX macro pulses, which are applied collinearly to the trap axis, pass through the ion trap. When FELIX is tuned in resonance with an allowed IR transition, cluster ions may absorb one or more photons (provided that internal relaxation occurs rapidly compared to the FELIX micro pulse spacing of 1 ns). If the internal energy has risen sufficiently, the ion will dissociate. The fragment ion will remain confined in the trap. To extract ions a 5 ms extraction pulse is applied to the ion trap exit lens. Extracted ions are guided into the second RF quadrupole mass filter Q₂. The yield of mass-selected product ions is monitored by a subsequent off-axis conversion dynode channeltron detector (Det) operated in the pulse counting mode.

At each wavelength 10 fill/extraction cycles (15 for the higher resolution spectra) are performed and the total frag-

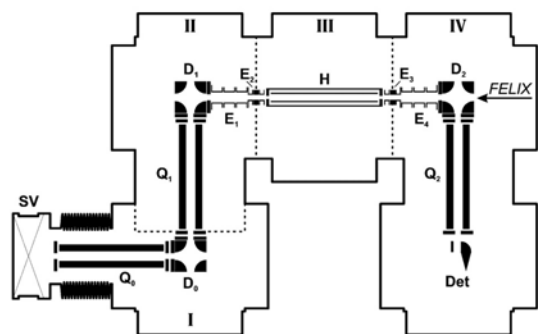


Fig. 1 Schematic of the guided ion beam tandem mass spectrometer (see text for details). D₀₋₂: electrostatic 90° quadrupole deflectors; Det: conversion dynode channeltron detector; E₁₋₄: einzel lenses; GV: gate valve; H: RF hexadecapole ion trap; Q₀: RF quadrupole ion guide; Q_{1,3}: RF quadrupole mass filters.

1102 *Phys. Chem. Chem. Phys.*, 2002, 4, 1101–1104

ment ion count is saved. Before and after detection of the fragment ion signal, the intensity of the parent ion signal is monitored. The yield of fragment ions as a function of FELIX wavelength then yields the photodissociation spectrum.

A typical mass spectrum of vanadium oxide cluster cations produced by laser vaporization with 1% O₂ seeded in He carrier gas is shown in Fig. 2. Vanadium oxide clusters ranging from V₂O₄⁺ to V₈O₂₀⁺ are observed. With the exception of V₅O₁₄⁺, which is produced with a much lower yield than expected, the intensity distribution within each V_xO_y⁺, V_xO_{y+1}⁺, ... series varies smoothly with cluster size. The present source conditions favor the generation of oxygen-rich V_xO_y⁺ clusters. For a given number of vanadium atoms the most intense peak in the mass spectrum is found at a vanadium to oxygen ratio of roughly 1 : 2.4. The mass spectrum is in

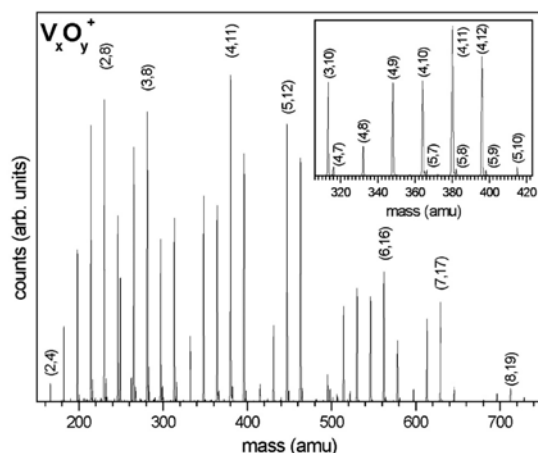


Fig. 2 Mass spectrum of vanadium oxide cluster cations V_xO_y⁺ produced by pulsed laser vaporization using a gas mixture of 1% O₂ seeded in helium carrier gas. Selected peaks are labeled with numbers in parentheses, (x,y), denoting the cluster composition. The mass region from 310 to 425 amu is shown enlarged in the top right corner.

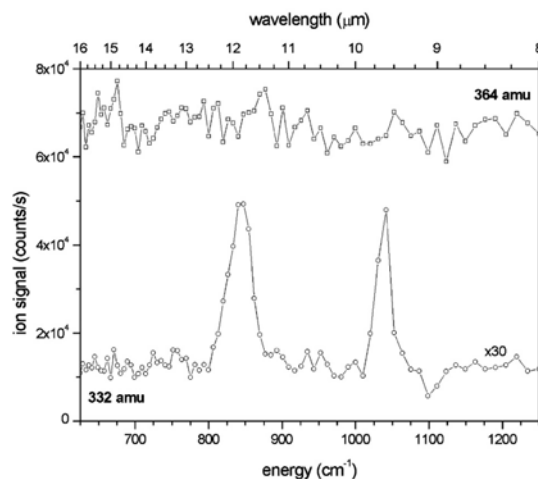


Fig. 3 Gas-phase IR photodissociation spectra of V₄O₁₀⁺ in the spectral region from 8 to 16 μm (1250 to 625 cm⁻¹) scanned in steps of 0.1 μm. Parent ion spectrum (364 amu, top trace) and V₄O₈⁺ fragment ion spectrum (332 amu, bottom trace), corresponding to loss of O₂, are plotted as a function of FELIX wavelength (top axis) and energy (bottom axis).

good agreement with recently published mass spectra, which were measured using a similar cluster ion source, but with a ten times higher O_2 content in the carrier gas.⁸

The IR photodissociation spectrum of mass selected $V_4O_{10}^+$ (364 amu) in the range from 625 to 1250 cm^{-1} is shown in Fig. 3 (bottom trace). It was measured by mass selectively monitoring the $V_4O_8^+$ (332 amu) fragment ion yield as a function of FELIX wavelength, after irradiating $V_4O_{10}^+$ ions confined in the ion trap. The signal of unfragmented parent ions is also shown (top trace). It varies by roughly $\pm 10\%$ over a time of 30 min, the acquisition time of the depicted spectra, and reflects minor changes in the source conditions as a function of time. Depletion of the parent ion signal, which is on the order of 3% at the maximum fragment ion signal, is masked by these variations. The fragment ion signal is comprised of two parts. The constant background signal results from dissociation induced by collisions with the He atoms as the ions enter the trap. Superimposed on this constant background signal due to photoinduced dissociation is observed. The spectrum shows two peaks at 9.6 and 11.8 μm . Tuning FELIX to these resonant frequencies and scanning the second mass filter revealed no fragmentation channels other than the loss of O_2 (or loss of two O atoms, which cannot be discerned using the present experimental setup).

Higher resolution spectra measured with smaller wavelength step size, longer dwell times and in a narrower wavelength region are shown in Fig. 4. These spectra were corrected for variations in the parent ion signal, by scaling the parent ion spectrum by a factor of 0.03 and subtracting it from the corresponding fragment ion signal. The two observed peaks have nearly Lorentzian shapes and an appropriate least square fit yields peak maxima and peak widths (full width at half maximum) of 842 cm^{-1} (32 cm^{-1}) and 1032 cm^{-1} (9 cm^{-1}). The width of the first peak is substantially larger than the bandwidth of FELIX, which was roughly $< 1\%$ in the present study. Based on calculations of Vyboishchikov *et al.*²³ on the IR spectroscopy of neutral V_4O_{10} isomers we assign the 842 cm^{-1} and 1032 cm^{-1} features to the antisymmetric V–O–V stretching and the V=O stretching vibrations, respectively.

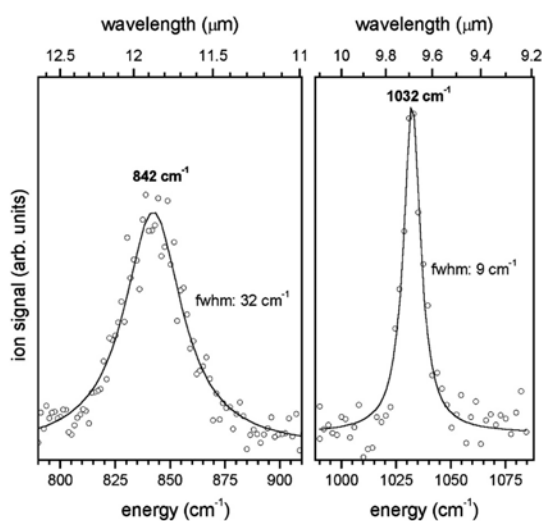


Fig. 4 Gas-phase IR photodissociation spectra (solid dots) of $V_4O_{10}^+$ measured by monitoring the $V_4O_8^+$ fragment ion signal (O_2 loss). The spectra were measured in steps of 0.02 μm and corrected for fluctuations in the parent ion signal (see text). Peak maxima and widths were determined by fitting a Lorentz function to the experimental data (solid line).

For various neutral isomers these are calculated to lie in-between 800–925 cm^{-1} (V–O–V stretch) and 1040–1080 cm^{-1} (V=O stretch).

We first address the observed fragmentation behavior with respect to the photofragmentation mechanism and then discuss the structure of the $V_4O_{10}^+$ cation. Fragmentation of $V_4O_{10}^+$ has previously been studied by CID and photofragmentation using 532 nm radiation.^{7,8} Single collisions with Xenon atoms lead to O_2 loss already at thermal energies, while other fragmentation channels are only observed at collision energies above 3 eV. Similarly, absorption of a single 532 nm (2.128 eV) photon leads exclusively to O_2 loss, while other fragmentation channels are only observed at higher laser fluences, *i.e.*, under multi-photon absorption conditions. Based on these results it is inferred that $V_4O_{10}^+$ is composed of an O_2 molecule weakly attached to a strongly bound $V_4O_8^+$ ion core. It is difficult to estimate an upper limit for the dissociation energy of the O_2 loss channel from these experiments, as the cluster internal temperature is not known.

Evidence for a weakly bound $V_4O_8^+ \cdot O_2$ complex is also found in the present study. Cluster ions formed by standard laser vaporization sources are generally “hot” and their internal temperature is often controlled by an evaporative cooling mechanism, *i.e.*, the internal energy is close to but less than the energy required to break the weakest bond in the system. Such internally “hot” clusters can dissociate upon entering the He filled ion trap. The initial collisions with the He atoms determine the fate of these cluster ions. Either they dissociate within the first few collisions or they are cooled down to the ambient temperature (< 70 K), at which point fragmentation by collisions with He atoms has been effectively quenched. This accounts for the constant background signal observed.

Because the (lowest) dissociation energy of $V_4O_{10}^+$ is unknown, it is difficult to estimate the minimum number of absorbed photons required to induce photofragmentation. For the single photon absorption case, fragmentation occurs at the fundamental vibrational frequencies of the parent ion. Under the present power and fluence conditions also multiple photons can be absorbed. A *coherent stepwise* multiphoton absorption mechanism is, however, unrealistic, due to the “anharmonic bottleneck” of a vibrational potential.²⁹ Resonant excitation by multiple photons rather proceeds *via* a *sequential incoherent* absorption mechanism particular to the pulse structure of free electron lasers. After absorption of a single photon (or a few photons) rapid intramolecular vibrational energy redistribution (IVR) efficiently de-excites the absorbing vibrational state within less than ~ 1 ns, allowing subsequent photons to be absorbed. Note, quenching of the absorption due to collisions with the He buffer gas is negligible in the present experiment, due to the considerably larger time scale for thermalization (to the ambient temperature) compared to IVR. With an increasing number of absorbed photons this mechanism will lead to a distortion and a red shift of the spectral features.³³ Taking into account the symmetric band shapes and the absence of any other fragmentation products we assume that not more than a few photons are required to induce fragmentation of $V_4O_{10}^+$, which supports the proposed, weakly-bound $V_4O_8^+ \cdot O_2$ structure. The width of the 1032 cm^{-1} band is on the order of the laser bandwidth. The three times larger width of the 842 cm^{-1} band is surprising. It could in principle result from lifetime broadening ($\tau \approx 170$ fs) and indicate a mode dependent, efficient vibrational predissociation mechanism or simply be the result of multiple overlapping bands. This aspect warrants further study in the future.

Determination of the structure of $V_4O_{10}^+$ can also be aided by comparison of the present data with the results from a recent density functional theory study on the IR spectroscopy of various isomers of neutral V_4O_{10} .²³ On the basis of these results we have already assigned the observed peaks to the

antisymmetric V–O–V stretching and terminal V=O stretching vibrations. All calculated isomers show absorption in this spectral region. Best agreement between calculated and experimental spectra is found for the highly symmetric cage structure (labeled TETRA in ref. 23), namely due to the absence of strong absorption at longer wavelengths for this isomer. The other three isomers, which were derived from bulk-like crystalline structures of V_2O_5 , show additional absorption features of similar intensity at energies below 800 cm^{-1} , characteristic for V–(O)₂–V double bridges. No fragmentation is detected in the $625\text{--}800\text{ cm}^{-1}$ region in the present study. The calculated cage-like structure is the lowest energy structure of all four isomers considered. It, however, lacks a weakly bound O₂ unit and therefore it is not straightforward to account for the observed fragmentation behavior assuming such a structure. We tentatively conclude that the absorbing species consists of a $V_4O_8^+$ ionic core, which lacks any V–(O)₂–V double bridges, and is weakly bound to an oxygen molecule.

It might be possible that other more strongly bound isomers of $V_4O_{10}^+$ are present in the ion trap, but do not dissociate under the present experimental conditions and thus are not detected. We presently have no means to check this, nor do the theoretical studies treat the energetics of the weakly bound complex. Assuming only a weak perturbation of the $V_4O_8^+$ structure by the presence of O₂, it may, however, be more reasonable to state that we are probing the most stable $V_4O_8^+$ (rather than $V_4O_{10}^+$) isomer, since this $V_4O_8^+$ isomer should intuitively also lead to the most abundant formation of $V_4O_8^+\cdot O_2$. We are currently improving the experimental setup to generate a larger flux of photons at the interaction region in order to reach energetically higher lying fragmentation channels. This is in principle possible, as the recent study on cationic polyaromatic hydrocarbons has shown, where dissociation energies of more than 6 eV were overcome.²⁹

We conclude by highlighting several aspects of the presented experimental technique, which we believe, make it generally applicable. (a) The technique is not limited to the study of a particular species, but may be applied to a wide variety of ions that can be generated with various cluster ion sources available today. (b) Presently, the technique is limited to ions with moderately low dissociation energies (smaller $\sim 1\text{--}2\text{ eV}$), but more strongly bound clusters can be studied, by adding a weakly bound “spectator” atom or molecule to the cluster ion. (c) It yields IR spectra of cooled, mass-selected cluster ions in a spectral region, which should allow for a unique structural characterization of many cluster ions of interest based on the comparison between experimentally and theoretically determined vibrational frequencies.

This work is part of the Sonderforschungsbereich 546 of the Deutsche Forschungsgemeinschaft. We would like to thank J. Sauer for helpful conversations regarding the calculated IR spectra, J. Bakker, J. Oomens, B. Redlich, R. Satink and D. van Heijnsbergen for their help at the FELIX facility and access to various equipment and M. Duncan and P. Milani for help on the construction of the laser vaporization source. We gratefully acknowledge the support by the *Stichting voor Fundamenteel Onderzoek der Materie* (FOM) in providing the required beam time on FELIX and highly appreciate the skillful assistance by the FELIX staff. This work was supported in part under the ‘Access to research infrastructure

action of the Improving Human Potential Programme’ of the European Community.

References

- 1 C. N. R. Rao and B. Raven, *Transition Metal Oxides*, VCH Press, New York, 1995.
- 2 D. Yin, N. Xu, J. Zhang and X. Zheng, *J. Phys. D*, 1996, **29**, 1051.
- 3 B. Grzybowska-Swierkosz, *Appl. Catal. A*, 1997, **157**, 263.
- 4 H. Wu and L.-S. Wang, *J. Chem. Phys.*, 1998, **108**, 5310.
- 5 L. B. Knight Jr., R. Babb, M. Ray, T. J. Banisaukas III, L. Russon, R. S. Dailey and E. R. Davidson, *J. Chem. Phys.*, 1996, **105**, 10237.
- 6 G. V. Chertihin, W. D. Bare and L. Andrews, *J. Phys. Chem. A*, 1997, **101**, 5090.
- 7 S. E. Kooi and A. W. Castleman Jr., *J. Phys. Chem. A*, 1999, **103**, 5671.
- 8 R. C. Bell, K. A. Zemski, K. P. Kerns, H. T. Deng and A. W. Castleman Jr., *J. Phys. Chem. A*, 1998, **102**, 1733.
- 9 R. C. Bell, K. A. Zemski and A. W. Castleman Jr., *J. Phys. Chem. A*, 1998, **102**, 8293.
- 10 R. C. Bell, K. A. Zemski and A. W. Castleman Jr., *J. Phys. Chem. A*, 1999, **103**, 2992.
- 11 R. C. Bell, K. A. Zemski and A. W. Castleman Jr., *J. Phys. Chem. A*, 1999, **103**, 1585.
- 12 R. C. Bell, K. A. Zemski, D. R. Justes and A. W. Castleman Jr., *J. Chem. Phys.*, 2001, **114**, 798.
- 13 A. Dinca, T. P. Davis, K. J. Fisher, D. R. Smith and G. D. Willott, *Int. J. Mass Spectrom. Ion Processes*, 1999, **182/183**, 73.
- 14 J. N. Harvey, M. Diefenbach, D. Schröder and H. Schwarz, *Int. J. Mass Spectrom. Ion Processes*, 1999, **182/183**, 85.
- 15 E. B. Rudnyi, E. A. Kaibicheva and L. N. Sidorov, *J. Chem. Thermodyn.*, 1993, **25**, 929.
- 16 A. Fielicke and K. Rademann, *Phys. Chem. Chem. Phys.*, 2001, submitted (B108046F).
- 17 K. A. Zemski, D. R. Justes and A. W. Castleman Jr., *J. Phys. Chem. A*, 2001, **105**, 10237.
- 18 G. C. Nieman, E. K. Parks, S. C. Richtmeier, K. Liu, L. G. Pobo and S. J. Riley, *High. Temp. Sci.*, 1986, **22**, 115.
- 19 M. Foltin, G. J. Stueber and E. R. Bernstein, *J. Chem. Phys.*, 1999, **111**, 9577.
- 20 L. Karlsson, B. Lindgren, C. Lundevall and U. Sassenberg, *J. Mol. Spectrom.*, 1997, **181**, 274.
- 21 J. Brett, *Astron. Astrophys.*, 1990, **231**, 440.
- 22 S. F. Vyboishchikov and J. Sauer, *J. Phys. Chem. A*, 2000, **104**, 10913.
- 23 S. F. Vyboishchikov and J. Sauer, *J. Phys. Chem. A*, 2001, **105**, 8588.
- 24 M. Calatayud, B. Silvi, J. Andrés and A. Beltrán, *Chem. Phys. Lett.*, 2001, **333**, 493.
- 25 H. D. Babcock and L. Herzberg, *Astrophys. J.*, 1948, **108**, 167.
- 26 M. A. Duncan, *Int. J. Mass Spectrom.*, 2000, **200**, 545.
- 27 G. von Helden, I. Holleman, G. M. H. Knippels, A. F. G. van der Meer and G. Meijer, *Phys. Rev. Lett.*, 1997, **79**, 5234.
- 28 H. Piest, G. von Helden and G. Meijer, *J. Chem. Phys.*, 1999, **110**, 2010.
- 29 J. Oomens, A. J. A. van Rooij, G. Meijer and G. von Helden, *Astrophys. J.*, 2000, **542**, 404.
- 30 D. Oepts, A. F. G. van der Meer and P. W. van Amersfoort, *Infrared Phys. Technol.*, 1995, **36**, 297.
- 31 G. G. Dolnikowski, M. J. Kristo, C. G. Enke and J. T. Watson, *Int. J. Mass Spectrom. Ion Processes*, 1988, **82**, 1.
- 32 J. Westergren, H. Grönbeck, S.-G. Kim and D. Tománek, *J. Chem. Phys.*, 1997, **107**, 3071.
- 33 G. von Helden, I. Holleman, G. Meijer and B. Sartakov, *Opt. Express*, 1999, **4**, 46.

**Formation and Photodepletion of Cluster Ion-Messenger Atom
Complexes in a Cold Ion Trap: Infrared Spectroscopy of VO^+ , VO_2^+ ,
and VO_3^+**

Mathias Brümmer, Cristina Kaposta, and Gabriele Santambrogio

Institut für Experimentalphysik, Freie Universität Berlin, Arnimallee 14, D 14195 Berlin, Germany.

Knut R. Asmis

Fritz-Haber-Institut der Max-Planck-Gesellschaft, Faradayweg 4-6, D 14195 Berlin, Germany.

Communication in *Journal of Chemical Physics* **119**(24) 3122-5 (2005).

Formation and photodepletion of cluster ion–messenger atom complexes in a cold ion trap: Infrared spectroscopy of VO^+ , VO_2^+ , and VO_3^+

Mathias Brümmer, Cristina Kaposta, and Gabriele Santambrogio
Institut für Experimentalphysik, Freie Universität Berlin, Arnimallee 14, D 14195 Berlin, Germany

Knut R. Asmis^{a)}
Fritz-Haber-Institut der Max-Planck-Gesellschaft, Faradayweg 4-6, D 14195 Berlin, Germany

(Received 1 October 2003; accepted 27 October 2003)

A novel experimental technique is described in which radiation from a free electron laser is used to measure infrared spectra of gas-phase cluster ions via vibrational predissociation of the corresponding ion–messenger atom complexes. The weakly bound complexes are formed in a temperature-controllable, radio frequency ion trap. This technique is applied to the study of the vibrational spectroscopy of the monovanadium oxide cluster cations VO^+ , VO_2^+ , and VO_3^+ .

© 2003 American Institute of Physics. [DOI: 10.1063/1.1634254]

Vibrational spectroscopy is a straightforward approach to probe the structure of gas-phase cluster ions. However, conventional absorption measurements, a standard tool for the characterization of liquid and solid samples, lack the sensitivity and selectivity required for studying isolated gas phase species, due mainly to the low number densities compared to the condensed systems. Therefore in recent years much effort has been put into the development of experimental methods to study the infrared (IR) spectroscopy of gas phase ions. Even though accurate information on the vibrational frequencies can in principle be extracted from pulsed field ionization experiments on neutral species, namely using zero kinetic energy electron (ZEKE) spectroscopy¹ and mass-analyzed threshold ionization (MATI) spectroscopy,² it is generally advantageous to detect the IR absorption spectrum of the ion directly. Several methods have been developed in this direction, from which infrared photodissociation (IR-PD) spectroscopy has emerged as the most frequently applied spectroscopic approach.³

In an IR-PD experiment the absorption of IR photons by the target ions yields charged fragments that can be mass-selectively detected with high efficiency. IR-PD spectroscopy generally requires a tunable and intense infrared light source. Continuously tunable tabletop lasers do not have sufficient intensity below 2200 cm^{-1} and consequently the majority of IR-PD studies have been limited to the spectral region of the hydrogen stretching motions, the antisymmetric stretch of CO_2 , as well as IR-active combination bands. Meijer and co-workers⁴ have pioneered the field of molecular spectroscopy with radiation from IR free electron lasers (FELs), which can generate intense and tunable radiation also below 2000 cm^{-1} . They have shown that for larger molecular and cluster ions IR-PD is rather efficient when using radiation from an IR-FEL, because the transition between the discrete and the quasi-continuum region is reached after the absorption of just a few IR photons.⁵ This transition strongly

depends on the density of vibrational states and it is shifted to higher energies for smaller clusters. For this reason it remains challenging to measure higher-resolution IR spectra of smaller, more strongly bound cluster ions, because one runs out of resonance before reaching the quasi-continuum and the IR-PD mechanism becomes inefficient.

This bottleneck can be circumvented if one succeeds in adding a messenger atom to the cluster ion, forming a cluster ion–messenger atom complex.⁶ The absorption of a single IR photon by the cluster ion complex, e.g., $X^+ \cdot \text{He}$, is then signaled via vibrational predissociation,

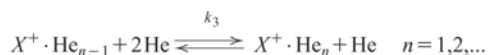


if the photon energy exceeds the binding energy of the complex. While this method has been successfully applied to studies on many atomic and molecular ions, its extension to polyatomic cluster ions formed by association reactions, for example, in standard laser ablation sources, remains non-trivial. Such cluster ions form in the (pulsed) expansion following the generation of an electrical neutral plasma and often remain too hot to bind a rare gas atom, in particular a He atom, because the internal degrees of freedom are not sufficiently cooled.

Here, we address this problem and describe a novel and generally applicable technique to measure IR-PD spectra of small polyatomic cluster ions in the region below 2000 cm^{-1} via photodepletion of their “cluster ion–He atom” complexes by tunable IR-FEL radiation. The weakly bound complexes are not formed in the source region, but in a cooled two-dimensional radio frequency (RF) ion trap by collisions with the He buffer gas. The formation of such complexes under very similar conditions has been previously observed in drift tube experiments reported by Kobayashi and co-workers.⁷ They describe the formation of $X^+ \cdot \text{He}_n$ complexes between diatomic molecular ions ($X^+ = \text{N}_2^+, \text{CO}^+, \text{O}_2^+$) and helium atoms up to $n=13$ at a drift tube temperature of 4.4 K and a He gas pressure of 0.02

^{a)}Author to whom correspondence should be addressed. Electronic mail: asmis@fhi-berlin.mpg.de

mbar. The complexes are formed by the three-body association reaction



and they can break apart by the reverse reaction, namely collision induced dissociation. The equilibrium ion concentrations are determined by the rates for the forward and backward reaction. Resonant absorption of IR radiation by the ion complex leads to vibrational predissociation and consequently to a temporary change in ion concentrations, until the bare ion is able to dissipate the excess energy, reform a complex and return to equilibrium. Therefore, the infrared spectroscopy of the parent ions X^+ can be studied by mass-selectively monitoring changes in the $X^+ \cdot \text{He}_n$ ion yield as a function of photon wavelength directly after irradiation with a tunable IR source.

Here we apply this method to study monovanadium oxide cluster cations VO_x^+ ($x = 1, 2, 3$), which, in a more general sense, also act as prototypes for small cluster ions, whose infrared spectrum is difficult to measure by multiphoton IR-PD spectroscopy of the bare parent ion. Our interest in transition metal oxides, and in particular vanadium oxides, originates from their importance as industrial catalysts for oxidation–reduction reactions.⁸ Recent gas-phase reactivity studies on vanadium oxide cluster ions were aimed at understanding the nature of the reactive sites in heterogeneous catalysis (see Ref. 9 and references therein). The interpretation of the reactivity data requires information on the cluster ion structure. While the spectroscopy of neutral vanadium oxide clusters is accessible via photoelectron spectroscopy of mass-selected vanadium oxide cluster anions,¹⁰ spectroscopic information on vanadium oxide cluster ions remains scarce.^{11–13} For the monovanadium oxide cations, infrared data is only available for the diatomic VO^+ ($1060 \pm 40 \text{ cm}^{-1}$).¹³

The present experiments were carried out on a previously described tandem mass spectrometer–ion trap system.¹² Briefly, vanadium oxide cations are prepared by pulsed laser vaporization. Mass-selected ions are guided into a cooled, He-filled, RF hexadecapole ion trap. The trap is connected to a closed-cycle He-cryostat and kept at a temperature of $\sim 20 \text{ K}$ for the present experiments. Ions entering the trap lose both kinetic and internal energy due to inelastic collisions with the cooled He buffer gas ($\sim 0.015 \text{ mbar}$). By applying appropriate electrostatic potentials to the entrance lens, pole bias and exit lens of the trap the ions can be captured and then thermalized to the ambient temperature.¹⁴

IR photodissociation spectra were obtained by photoexcitation of the trapped ions with radiation from the “Free Electron Laser for Infrared Experiments” FELIX.¹⁵ The ion trap was filled continuously for 600 ms. During this time, FELIX, which was operated at 5 Hz, fired three times. Directly after the last FELIX pulse, all ions were extracted and the mass-selected ion yield was monitored as a function of the excitation wavelength. Overview spectra were measured in the region from 6 to 16 μm with a step size of 0.1 μm . Spectra with smaller step sizes and longer accumulation times were then measured in those spectral regions where

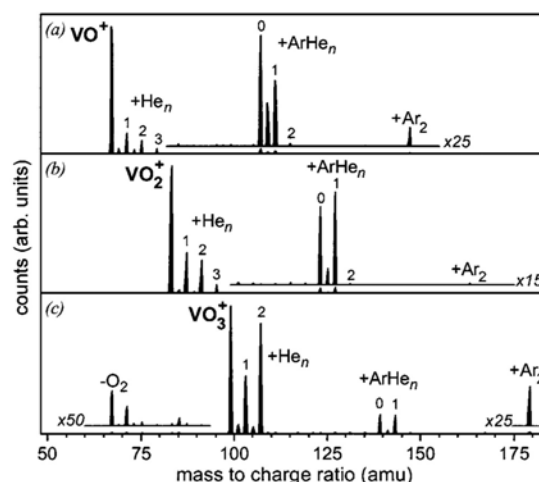


FIG. 1. Mass spectra of trapped VO_x^+ ion–atom/molecule complexes, measured by setting the first mass filter to the parent ion mass of (a) 67 amu, (b) 83 amu and (c) 99 amu and scanning the second mass filter. The ion trap was cooled to $\sim 20 \text{ K}$.

photodissociation signal was observed. For the present experiments the FEL macro pulse energy was 40–50 mJ, while the bandwidth was less than 1% of the central frequency.

The formation of weakly-bound VO_x^+ –neutral atom/molecule complexes ($x = 1, 2, 3$) is observed, when mass-selected, vibrationally “warm” VO_x^+ cluster ions are allowed to be collisionally cooled to sufficiently low internal temperatures. Representative mass spectra are shown in Fig. 1 for VO^+ (a), VO_2^+ (b) and VO_3^+ (c). The mass spectra were measured by mass-selecting bare VO_x^+ ions (parent ions), trapping them for 500 ms, and then extracting all ions (parent and product ions) from the ion trap and mass-selectively detecting them. The spectra of the parent ions VO^+ and VO_2^+ are qualitatively similar. Peaks at +4, +8 and +12 amu relative to the parent ion comprise the main progression with $\Delta m = +4 \text{ amu}$. Additional weaker features are observed at multiples of $\Delta m = +2 \text{ amu}$ and $\Delta m = +40 \text{ amu}$ and combinations of these values. We assign the $\Delta m = +4 \text{ amu}$ series to the formation of $\text{VO}_x^+ \cdot \text{He}_n$ complexes formed by collisionally deactivated association reactions. The weaker peaks are attributed to clusters of the type $\text{VO}_x^+ \cdot (\text{Ar})_l (\text{H}_2)_m (\text{He})_n$ formed by association involving gas impurities (H_2, Ar) present inside the ion trap. Note, only complexes with three or less ligands ($l+m+n=3$), are observed. The absence of larger complexes signals a drop in the sequential binding energy upon addition of a fourth ligand. The interaction between the ion and the rare gas atom is short range in nature and thus steric reasons probably keep the fourth ligand too far away from the positive charge, which is predominantly localized on the vanadium atom.

The VO_3^+ spectrum (spectrum c in Fig. 1) differs from the other two mass spectra. The relative intensities of the He-complexes are considerably larger and only a maximum of two ligands is observed. This indicates that the first two He atoms are bound stronger in VO_3^+ compared to the

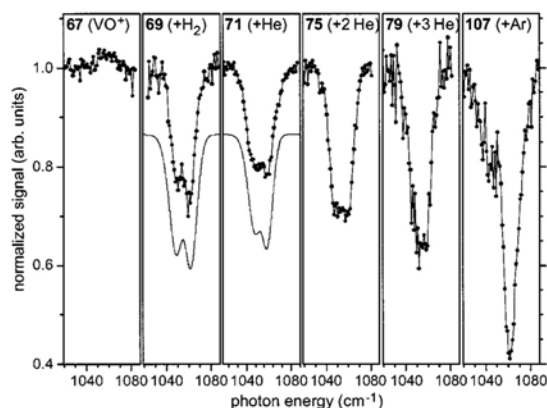


FIG. 2. IR-PD spectra (solid dots) measured by monitoring the yield of VO^+ (67 amu) and $\text{VO}^+\cdot X$ ($X=\text{H}_2$, He, He_2 , He_3 , and Ar) in the region of the fundamental of the $^3\Sigma^-$ ground state of VO^+ . Lines are shown to aid the eye. Simulated spectra (solid lines) are also shown, vertically displaced, for $\text{H}_2\text{-VO}^+$ and He-VO^+ . The double minimum feature can be attributed to rotational resolved structure.

smaller cluster; probably a result of a stronger charge localization on the vanadium atom. Interestingly, the He $n=2$ peak is larger than the $n=1$ peak, which we attribute to the kinetics of the formation process. Note that peaks, albeit very weak, are also observed at lower masses than the parent ion mass. The peak at $\Delta m = -32$ amu is assigned to collision induced loss of O_2 (or $2\cdot\text{O}$). It indicates a lower threshold towards collision induced dissociation for VO_3^+ compared to VO_2^+ and VO^+ . This is in agreement with calculated bond dissociation energies for VO^+ , VO_2^+ and VO_3^+ of 125.9, 85.3 and 29.3 kcal/mol, respectively.¹⁶ A more detailed characterization of the cluster formation energetics and dynamics, in particular a determination of the ion-He atom binding energy from temperature dependent measurements, is currently in progress and will be presented elsewhere. Here we focus on the feasibility of measuring IR-PD spectra by monitoring the cluster ion complex depletion upon irradiation with FELIX.

IR photodissociation spectra of trapped VO^+ ions measured by monitoring the yield of bare VO^+ and various $\text{VO}^+\cdot X$ ($X=\text{He}_n, \text{H}_2, \text{Ar}$) complexes (formed in the ion trap) are shown in Fig. 2. Resonant absorption of IR photons manifests itself as a dip in the signal (photodepletion) of the complex and a signal increase (photoformation) of the bare parent ion. The photoformation signal of VO^+ formed from dissociating complexes is small, roughly $\sim 3\%$, compared to the total VO^+ signal, because the majority of the trapped ions remain uncomplexed under the present conditions. Photoabsorption can be better detected in the depletion spectra and therefore these were measured with a larger number of scans. Depletion of the complex ions varies from 20% in $\text{VO}^+\cdot\text{He}$ to $\sim 60\%$ in $\text{VO}^+\cdot\text{Ar}$. Varying photodepletion yields are a result of different complex reformation rates, which depend on, e.g., neutral atom/molecule concentration and complex binding energy, and indicate that complex reformation proceeds on a similar time scale compared to the time between FELIX firing and ion extraction from the ion

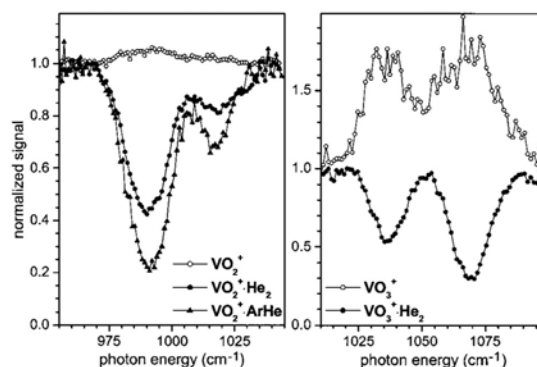


FIG. 3. IR-PD spectra for VO_2^+ parent ions (left) measured in the region from 955 to 1045 cm^{-1} by monitoring bare VO_2^+ (open circles), $\text{VO}_2^+\cdot\text{He}_2$ (solid circles) and $\text{VO}_2^+\cdot\text{ArHe}$ (solid triangles). IR-PD spectra for VO_3^+ parent ions (right) measured in the region from 1010 to 1099 cm^{-1} by monitoring bare VO_3^+ (open circles) and $\text{VO}_3^+\cdot\text{He}_2$ (solid circles).

trap (ms time scale). The band of the He containing messenger complexes are centered around 1053 ± 5 cm^{-1} , in excellent agreement with the only previous experimental value (1060 ± 40 cm^{-1}) and recent high-level *ab initio* calculations of Pykavy and van Wüllen (1058 cm^{-1}) for bare VO^+ .¹⁷ For the $\text{VO}^+\cdot\text{He}_n$ and $\text{VO}^+\cdot\text{H}_2$ clusters the relative shifts of the band centers for different ligands are small (± 1 cm^{-1}), indicating a negligible influence of the lighter ligands (H_2, He) on the vibrational frequency of VO^+ . Interpretation of the peak shift of $+10$ cm^{-1} (relative to the $\text{VO}^+\cdot\text{He}$ spectrum) and the additional structure observed at lower energies in the $\text{VO}^+\cdot\text{Ar}$ spectrum requires further investigation.

The FWHM widths of the depletion features range up to 27 cm^{-1} in $\text{VO}^+\cdot\text{He}$ and are considerably larger than the laser bandwidth of ~ 9 cm^{-1} . This may arise from sequence bands, as well as rotational excitation. Resolved rotational structure in form of a double minimum is observed in the spectra of $\text{VO}^+\cdot\text{He}$ and $\text{VO}^+\cdot\text{H}_2$. Simple spectral simulations (solid lines in Fig. 2) reproduce this structure. The best agreement is obtained for a mean rotational temperature of 70 K, indicating an ion rotational temperature that is higher than the ion trap temperature (~ 20 K). This may be due to several reasons. First, ions entering the ion trap just before FELIX fires will not have undergone sufficient collisions to completely thermalize. Second, the ions can be “reheated” by the trapping RF fields.

IR-PD spectra of trapped VO_2^+ parent ions are shown in Fig. 3 (left). Resonant absorption of IR photons is best observed in the photodepletion spectra of the He_2 complex rather than in the spectra of the He complex or the bare parent ion. Assuming a sequential formation mechanism, this can be attributed to a faster reformation of the $n=1$ complex, compared to the $n=2$ complex, from bare VO_2^+ after photodissociation. The spectrum of $\text{VO}_2^+\cdot\text{He}_2$ reveals two bands at 990 and 1017 cm^{-1} with an intensity ratio of 3:1. The bands appear at similar energies in the $\text{VO}_2^+\cdot\text{ArHe}$ spectrum. Comparison to density functional calculations^{16,18} (DFT) can aid in the assignment of the VO_2^+ spectrum. Taking into account that the DFT harmonic frequencies are sys-

tematically calculated too high¹⁹ a satisfactory agreement is found for the predicted 1A_1 (VO_2^+) electronic ground state, while an assignment to the lowest triplet state ($^3A''$) can be ruled out. VO_2^+ thus has a bent geometry with two equivalent V–O bonds. The two bands are assigned to the antisymmetric (990 cm^{-1}) and symmetric stretch mode (1017 cm^{-1}).

IR-PD spectra for VO_3^+ are shown on the right of Fig. 3. Two bands at slightly higher wave numbers than for VO_2^+ are observed in the spectrum of $VO_3^+ \cdot He_2$ (solid dots in Fig. 3). The band maxima are found at 1037 and 1069 cm^{-1} with an intensity ratio of 1:1.6. The bands appear somewhat broader, when monitoring the parent ion yield (open circles in Fig. 3). The dissociation of all observed ion complexes contribute to the (bare) parent ion signal, and in particular the heavier, spectrally-shifted complexes may lead to the relative broadening of these features. Based on the comparison between experimental and calculated vibrational frequencies best agreement is found for the $^3A''$ state with an oxovanadium(V) peroxide structure.¹⁶ Both, the assignment to the corresponding singlet state ($^1A'$), which has been suggested to be the ground state of VO_3^+ ,¹⁸ and the assignment to the energetically low-lying $^3A''$ state with a trioxide structure, can be ruled out.

Summarizing, the present study yields the first experimental values for the vibrational frequencies of VO_2^+ and VO_3^+ and a considerable more accurate value for the fundamental of VO^+ compared to the previous experiment.¹³ In combination with electronic structure calculations the structure (and electronic state) can be unambiguously identified. The method presented here can be easily extended to larger vanadium oxide cluster ions. The dynamics of complex formation play a central role in this regard. They can be “tuned” by changing the He buffer gas temperature and pressure and have to be chosen such that the rate for complex formation is fast enough to yield a sufficient amount of complexed ions (in order to measure depletion spectra) and at the same time complex reformation after photodissociation is not too fast, such that a large fraction of the photodissociation products can be detected.

This work is supported by the Collaborative Research Center 546 of the Deutsche Forschungsgemeinschaft. The authors thank L. Wöste for his continuous support, J. Sauer, M. Duncan and G. Meijer for valuable discussions, G. Berden for help with simulating the rotational spectra and grate-

fully acknowledge the support of the Stichting voor Fundamenteel Onderzoek der Materie (FOM) in providing the required beam time on FELIX and highly appreciate the skillful assistance of the FELIX staff, in particular Dr. A. F. G. van der Meer.

- ¹K. Müller-Dethlefs, M. Sander, and E. W. Schlag, *Z. Naturforsch. A* **39**, 1089 (1984).
- ²L. Zhu and P. Johnson, *J. Chem. Phys.* **94**, 5769 (1991).
- ³E. J. Bieske and J. P. Maier, *Chem. Rev.* **93**, 2603 (1993); J. M. Lisy, *Int. Rev. Phys. Chem.* **16**, 267 (1997); T. Ebata, A. Fujii, and N. Mikami, *Int. Rev. Phys. Chem.* **17**, 331 (1998); M. A. Duncan, *Int. J. Mass. Spectrom.* **200**, 545 (2000); E. J. Bieske and O. Dopfer, *Chem. Rev.* **100**, 3963 (2000).
- ⁴H. Piest, G. von Helden, and G. Meijer, *J. Chem. Phys.* **110**, 2010 (1999).
- ⁵S. Mukamel and J. Jortner, *J. Chem. Phys.* **65**, 5204 (1976); A. S. Sudbo, P. A. Schulz, E. R. Grant, Y. R. Shen, and Y. T. Lee, *J. Chem. Phys.* **70**, 912 (1979); J. Oomens, G. Meijer, and G. von Helden, *J. Phys. Chem. A* **105**, 8302 (2001).
- ⁶M. Okumura, L. I. Yeh, and Y. T. Lee, *J. Chem. Phys.* **83**, 3705 (1985).
- ⁷N. Kobayashi, T. Kojima, and Y. Kaneko, *J. Phys. Soc. Jpn.* **57**, 1528 (1988); H. Tanuma, J. Sanderson, and N. Kobayashi, *J. Phys. Soc. Jpn.* **68**, 2570 (1999).
- ⁸C. N. R. Rao and B. Raven, *Transition Metal Oxides* (VCH, New York, 1995); D. Yin, N. Xu, J. Zhang, and X. Zheng, *J. Phys. D* **29**, 1051 (1996); B. Grzybowska-Swierkosz, *Appl. Catal., A* **157**, 263 (1997).
- ⁹D. R. Justes, R. Mitrić, N. A. Moore, V. Bonacić-Koutecký, and A. W. Castleman, Jr., *J. Am. Chem. Soc.* **125**, 6289 (2003).
- ¹⁰H. Wu and L.-S. Wang, *J. Chem. Phys.* **108**, 5310 (1998); H. J. Zhai and L.-S. Wang, *J. Chem. Phys.* **117**, 7882 (2002); A. Pramann, K. Koyasu, A. Nakajima, and K. Kaya, *J. Chem. Phys.* **116**, 6521 (2002).
- ¹¹L. B. Knight, Jr., R. Babb, M. Ray, T. J. Banisaukas III, L. Russon, R. S. Dailey, and E. R. Davidson, *J. Chem. Phys.* **105**, 10237 (1996); G. V. Chertihin, W. D. Bare, and L. Andrews, *J. Phys. Chem. A* **101**, 5090 (1997); S. E. Kooi and A. W. Castleman, Jr., *J. Phys. Chem. A* **103**, 5671 (1999); J. Harrington and J. C. Weisshaar, *J. Phys. Chem.* **97**, 2809 (1992); A. Fielicke, R. Mitrić, G. Meijer, V. Bonacić-Koutecký, and G. von Helden, *J. Am. Chem. Soc.* (to be published).
- ¹²K. R. Asmis, M. Brümmer, C. Kaposta, G. Santambrogio, G. von Helden, G. Meijer, K. Rademann, and L. Wöste, *Phys. Chem. Chem. Phys.* **4**, 1101 (2002).
- ¹³J. M. Dyke, B. W. J. Gravenor, M. P. Hastings, and A. Morris, *J. Phys. Chem.* **89**, 4613 (1985).
- ¹⁴G. G. Dolnikowski, M. J. Kristo, C. G. Enke, and J. T. Watson, *Int. J. Mass. Spectrom.* **82**, 1 (1988).
- ¹⁵D. Oepts, A. F. G. van der Meer, and P. W. van Amersfoort, *Infrared Phys. Technol.* **36**, 297 (1995).
- ¹⁶G. K. Koyanagi, D. K. Bohme, I. Kretzschmar, D. Schröder, and H. Schwarz, *J. Phys. Chem. A* **105**, 4259 (2001).
- ¹⁷M. Pykavy and C. van Wüllen, *J. Phys. Chem. A* **107**, 5566 (2003).
- ¹⁸M. Calatayud, B. Silvi, J. Andrés, and A. Beltrán, *Chem. Phys. Lett.* **333**, 493 (2001).
- ¹⁹A. P. Scott and L. Radom, *J. Phys. Chem.* **100**, 16502 (1996).

Gas Phase Infrared Spectroscopy of Mono- and Divanadium Oxide Cluster Cations

Knut R. Asmis and Gerard Meijer

Fritz-Haber-Institut der Max-Planck-Gesellschaft, Faradayweg 4-6, D 14195 Berlin, Germany.

Mathias Brümmer, Cristina Kaposta, Gabriele Santambrogio, and Ludger Wöste

Institut für Experimentalphysik, Freie Universität Berlin, Arnimallee 14, D 14195 Berlin, Germany.

Joachim Sauer

Institut für Chemie, Humboldt-Universität Berlin, Unter den Linden 6, D-10099 Berlin, Germany

Full article in *Journal of Chemical Physics* **120**(14) 6461-70 (2005).

Gas phase infrared spectroscopy of mono- and divanadium oxide cluster cations

Knut R. Asmis^{a)} and Gerard Meijer

Fritz-Haber-Institut der Max-Planck-Gesellschaft, Faradayweg 4-6, D-14195 Berlin, Germany

Mathias Brümmer, Cristina Kaposta, Gabriele Santambrogio, and Ludger Wöste

Institut für Experimentalphysik, Freie Universität Berlin, Arnimallee 14, D-14195 Berlin, Germany

Joachim Sauer^{b)}

Institut für Chemie, Humboldt-Universität Berlin, Unter den Linden 6, D-10099 Berlin, Germany

(Received 3 December 2003; accepted 6 January 2004)

The vibrational spectroscopy of the mono- and divanadium oxide cluster cations VO_{1-3}^+ and $\text{V}_2\text{O}_{2-6}^+$ is studied in the region from 600 to 1600 wave numbers by infrared photodissociation of the corresponding cluster cation-helium atom complexes. The comparison of the experimental depletion spectra with the results of density functional calculations on bare vanadium oxide cluster cations allows for an unambiguous identification of the cluster geometry in most cases and, for VO_{1-3}^+ and $\text{V}_2\text{O}_{5,6}^+$, also of the electronic ground state. A common structural motif of all the studied divanadium cluster cations is a four-membered V–O–V–O ring, with three characteristic absorption bands in the 550–900 wave number region. For the V–O–V and V=O stretch modes the relationship between vibrational frequencies and V–O bond distances follows the Badger rule.

© 2004 American Institute of Physics. [DOI: 10.1063/1.1650833]

INTRODUCTION

Vanadium oxides are important in many technological applications,¹ e.g., in heterogeneous catalysis, semiconductors, optical devices, and coatings. The rational design of supported vanadium oxide catalysts remains difficult,² because of the lack of a consistent model that quantitatively explains the structure/reactivity relationship at a molecular scale. Progress is being made by applying spectroscopic methods *in situ*³ during catalytic operation, but the identification and characterization of the active sites with currently available surface science techniques remains challenging. As many active catalysts contain vanadium oxide highly dispersed on different oxide supports, important contributions can come from gas phase cluster studies.

The formation of isolated vanadium oxide cluster cations and anions as well as their reactivity with various reactants has been studied under well-controlled conditions as a function of their size.^{4–8} While mass spectrometry has become a standard technique to identify charged reactants and products and to provide information about their composition, the determination of their geometric structures remains an experimental challenge. The lack of structural knowledge together with the lack of thermochemical data so far has limited the understanding of the cluster reactivity. Attempts to predict structures from observed reactivity patterns,⁶ for example, are in conflict with later predictions from reliable quantum chemical calculations. Anion photoelectron spectroscopy has proven very useful in characterizing the structure of small,

neutral vanadium oxide clusters;⁵ the spectra of the larger clusters⁹ are too congested to resolve any vibrational structure. The first IR spectra of individual vanadium oxide cluster cations were recently obtained from IR photodissociation studies using a tunable free electron laser.^{10–12}

Quantum mechanical methods, in particular methods based on density functional theory (DFT), have proven very useful in identifying the molecular structure of metal oxide clusters in the gas phase based on a comparison of calculated and measured vibrational frequencies.¹³ The electronic structure of transition metal oxides and other transition metal compounds is more difficult to calculate than main group compounds because partially filled *d* shells and the weak coupling of *d* electrons on different transition metal atoms lead to many nearly degenerate electronic states. Tests have shown^{14,15} that structures of the same quality as for main group compounds can be obtained for transition metal compounds if the B3LYP hybrid density functional¹⁶ is used. DFT predictions for structures of vanadium oxide clusters of increasing size have first been made for neutral clusters and cluster anions.^{17,18} Shortly after this, predictions have also been made for the corresponding cations.^{19–22} Later, the methodology first used for cluster anions¹⁷ has been applied to cationic clusters and their reaction products with ethylene.^{7,11} Reliable structure prediction is also complicated by the large number of low energy isomers in combination with many low lying electronic states. Several previous computational studies on small vanadium oxide cluster cations, for example, do not agree on the lowest electronic state and the global minimum structure, even though they apply very similar computational techniques.^{7,19–21}

We recently reported a novel method¹² of measuring IR spectra of cluster ions by photodissociation of cluster ion–

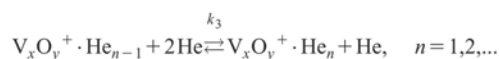
^{a)} Author to whom correspondence should be addressed; electronic mail: asmis@fhi-berlin.mpg.de

^{b)} Author to whom correspondence should be addressed; electronic mail: sek.qc@chemie.hu-berlin.de

rare gas complexes formed in a cold ion trap. In contrast to photodissociation of the bare cluster ion predissociation of the “messenger atom” complex bears several important advantages. For example, the number of adsorbed photons needed to fragment the complex is considerably smaller (and often equal to one) and, more importantly, independent of the dissociation energy of the bare cluster ion. This ensures that structural isomers can be detected with the same efficiency. The present study combines this technique with a systematic DFT study in order to determine the structure of mono- and divanadium oxide cluster cations. The IR depletion spectra are compared to the DFT predictions for different low lying isomers and/or electronic states, leading to an identification of the ground state even if a global optimization method is not used.

EXPERIMENT

The present experiments were carried out on a previously described tandem mass spectrometer-ion trap system.¹⁰ Briefly, vanadium oxide clusters are prepared by a pulsed laser vaporization source. The output of a Nd:YAG laser (Quantel Brilliant Ultra), operated at 20 Hz, is focused on a rotating 6-mm-diam vanadium rod (Alfa Aesar, 99.5% purity). The vanadium atom containing plasma is entrained in a pulse of 0.5% O₂ seeded in He carrier gas, expanded through a clustering channel and passed through a skimmer. The beam of positive ions is collimated in a radio frequency (rf) decapole ion guide and then guided into the first rf quadrupole mass filter, which is typically operated at unit resolution. Mass-selected cluster ions are guided into a cooled, He-filled (~0.02 mbar) rf hexadecapole ion trap, where they are accumulated and thermalized to the ambient temperature (~20 K) through collisions with the He buffer gas (Linde, He 6.0). Under these conditions the formation of cluster ion–rare gas atom complexes by three-body association is observed.



as was previously reported¹² for the monovanadium oxide cluster cations. The ion concentrations are determined by the rates of the forward and the backward reaction, which depend on temperature and pressure of the He buffer gas.

IR photodissociation spectra are obtained by photoexcitation of the trapped ions with pulsed radiation from the “free electron laser for infrared eXperiments” (FELIX),²³ which is operated at 5 Hz. A measurement cycle is initiated by the trigger signal of the previous FELIX pulse and the ion trap is allowed to fill with mass-selected ions for a fixed time t_{fill} . Next, the ions are allowed to thermalize, which is assumed to proceed on a time scale of up to a few milliseconds. Then, the accumulated, cooled ions are irradiated inside the ion trap. Directly after FELIX fires, all ions are extracted and the mass-selected ion yield is monitored. This cycle is repeated multiple times (3–10 times for the present experiments) and then FELIX is set to the next wavelength. Resonant absorption of IR radiation by the ion complexes leads to vibrational predissociation of the complexes. Consequently, the ion concentration of the (absorbing) complex

decreases and that of the bare ion increases temporarily, until the system is able to dissipate all the absorbed energy and return to equilibrium. Thus, if the rate of reformation is slow enough, the infrared spectroscopy of the parent ions $V_xO_y^+$ can be studied by mass-selectively monitoring changes in the $V_xO_y^+ \cdot He_n$ ion yield as a function of photon wavelength directly after irradiation with a tunable IR source.¹² The dependence of the dissociation rate on the initially excited vibrational mode is assumed to be negligible, because, under the present experimental conditions, there is sufficient time (microseconds or more) for the efficient redistribution of the excitation energy. Ideally, with t_{fill} less than 200 ms, the experiment can make use of the FELIX repetition rate of 5 Hz. In practice, longer filling times proved to yield superior signal statistics. An acquisition time $t_{\text{fill}} = 600$ ms was used throughout the experiments described here.

In the present study overview spectra are measured in the region from 6 to 16 μm with a step size of 0.1 μm . Spectra with smaller step sizes and longer accumulation times are then measured in those spectral regions, where signal was observed. The output of FELIX is introduced into the ion trap region through a ZnSe window, a 50 cm focal length KBr lens, and a 5-mm-thick KBr window. Focusing of the FELIX beam is required to avoid light scattering off the ion trap exit and entrance lenses. The transmission of the KBr optics is nearly wavelength independent in the region studied. The transmission of the ZnSe window decreases considerably at longer wavelengths. The accuracy of the determined vibrational frequencies is generally within 1% of the central wavelength. The accuracy of the relative depletion intensities is less well defined, mainly due to the non-monotonic variation of the FELIX beam intensity, bandwidth, and waist size with wavelength. We did not correct for any of these effects and estimate that our relative intensities vary within 10% between 1200 and 700 cm^{-1} and to a larger extent in the region below 700 cm^{-1} .

COMPUTATIONAL METHODS

All calculations are carried out using the TURBOMOLE suite of programs.²⁴ The B3LYP hybrid functional¹⁶ employed combines Becke’s 1988 nonlocal exchange²⁵ with Hartree–Fock exchange along with the Lee–Yang–Parr²⁶ correlation functional. Note that other implementations²⁷ of the B3LYP functional use a slightly different formulation of the Vosko–Wilk–Nusair (VWN) local correlation functional.²⁸ The TZVP basis sets applied are the triple-zeta valence basis sets developed by Ahlrichs and co-workers²⁹ augmented by polarization functions, a *d* set for oxygen and a *p* set for vanadium.³⁰ Harmonic vibrational frequencies are obtained from second analytic derivatives.³¹ Structure optimizations use tight convergence criteria. Structures are optimized until Cartesian gradients are smaller than 1×10^{-4} Hartree/Bohr and the energy change smaller than 1×10^{-6} Hartree. The self-consistent field convergence criterion is 1×10^{-7} Hartree for the energy and 1×10^{-7} a.u. for the root-mean square of the density.

It is known that B3LYP vibrational frequencies are systematically too large (see, e.g., Refs. 32 and 33) and, therefore, agreement with observed frequencies can be improved

TABLE I. Frequency scaling factors for fundamental vibrations and root-mean-square deviation (rms) derived from a least squares fit of frequencies.

	No. of data	Scale factor	rms (cm ⁻¹)
(1a) Vanadyl modes only ^a	10	0.9167	13
(1b) V–O–V modes only ^a	14	0.9832	26
(2) All modes ^a	24	0.9429	35
Ref. 32	1066	0.9614	34
Ref. 33	900	0.9726	42

^aPresent study.

by scaling. Scaling accounts for both anharmonicities (calculated harmonic wave numbers are compared to observed fundamentals including anharmonicities) and systematic errors of the calculated harmonic force constants. For the systems studied anharmonicity effects are expected to be small. We use 24 experimental vibrational frequencies of VO⁺(1), VO₂⁺(2), V₂O₂⁺(2), V₂O₃⁺(4), V₂O₄⁺(5), V₂O₅⁺(5), and V₂O₆⁺(5). The two unassigned modes in VO₃⁺ and the superoxo mode in V₂O₆⁺ are not used. Following the procedure described by Scott and Radom,³² two different types of scaling are done: (1) Individual scaling for two groups of frequencies, (a) vanadyl stretch vibrations (10 values) and (b) V–O–V stretch and all other vibrations below 900 cm⁻¹ (14 values). (2) Global scaling using all 24 frequencies. Table I shows the results. The scale factors obtained and the root-mean-square deviations of the scaled frequencies fall into the known ranges.^{32,33}

RESULTS

Optimized B3LYP/TZVP geometries of selected mono- and divanadium oxide cluster cations are shown in Fig. 1 and their vibrational frequencies are listed in Table II. Infrared photodissociation spectra of the vanadium oxide cluster cations VO₁₋₃⁺ and V₂O₂₋₆⁺, measured by monitoring the depletion of the respective cluster ion–He_n complex ($n=1, 2, \text{ or } 3$), are shown in Figs. 2–4. Experimental vibrational frequencies (band centers) are listed in Table II. He _{$n>1$} complexes were monitored, whenever the depletion signal of the He₁ complex was weak or completely masked either due to partial dissociation of He _{$n>1$} complexes or rapid reformation dynamics. In all cases the influence of the He atoms on the vibrational frequency is assumed to be small, i.e., on the order of a few wave numbers or less. Rotationally resolved vibrational predissociation experiments on proton-bound He complexes revealed redshifts up to 15 cm⁻¹ for hydrogen stretching motions, corresponding to less than 0.5% of the fundamental frequency.³⁴ Due to the considerably higher reduced mass and lower vibrational frequency of the modes considered here, the frequency shift should be comparably smaller. For V₂O₂⁺ the signal level was very low and the spectra of two different complexes ($n=2$ and $n=3$) were summed. The simulated spectra are based on globally scaled harmonic frequencies and relative intensities determined by B3LYP/TZVP calculations, and were convoluted with a Gaussian line shape function, with a width that increases linearly with increasing frequency, in order to correct for the wavelength dependent bandwidth of FELIX. The experimen-

tal data are plotted against a logarithmic scale to aid in the comparison to the simulated absorption spectra. According to Lambert–Beer’s law, the logarithm of the relative depletion (I/I_0) is proportional to the absorption coefficient. Furthermore, it is assumed that if a photon is absorbed, it always leads to dissociation with probability that is independent of wavelength. Binding energies of He atoms to ionic complexes³⁵ are on the order of a few hundred wave numbers or less and thus a single IR photon should be sufficient to dissociate the ion–He atom complexes studied here.

VO⁺

The IR depletion spectrum of VO⁺·He (Fig. 2, left) reveals a single band at 1053 cm⁻¹. Upon closer inspection the band shows additional structure, a double minimum feature, which is attributed to the influence of molecular rotations discussed elsewhere in more detail.¹² The center of the band remains nearly unchanged in the spectra of the VO⁺·He₂ (1053 cm⁻¹) and VO⁺·He₃ (1054 cm⁻¹) complexes (not shown), confirming that the He atoms have a negligible influence on the V–O stretching frequencies. The position of the band center is in good agreement with, but significantly more accurate than, the value obtained for the ³Σ⁻ ground state of bare VO⁺ using photoelectron spectroscopy (1060 ± 40 cm⁻¹).³⁶ The recent high-level *ab initio* calculations (multi-reference average coupled pair functional, MR-ACPF, with basis set extrapolation) of Pykavy and van Wüllen³⁷ for bare VO⁺ yield 1058 cm⁻¹. Our B3LYP/TZVP frequency ($\nu_{\text{scaled}}=1032$ cm⁻¹) is in reasonable agreement with these results, as is the calculated bond length ($r_e=1.55$ Å), which was determined experimentally ($r_0=1.56$ Å) from rotationally resolved pulsed field ionization spectra.³⁸

VO₂⁺

Two bands are observed in the depletion spectrum of VO₂⁺·He₂ (Fig. 2, right) at 1017 and 990 cm⁻¹ with relative intensities of 1–3. Both, the intensity ratio and the splitting of the two bands, are reproduced well by the B3LYP/TZVP calculations, confirming the bent ¹A₁ ground state for VO₂⁺, originally proposed by Harvey *et al.*⁸ The two bands are assigned to the symmetric ($\nu_{\text{scaled}}=1038$ cm⁻¹) and antisymmetric ($\nu_{\text{scaled}}=1011$ cm⁻¹) stretch mode, respectively. The energy of the bending mode, predicted at $\nu_{\text{scaled}}=445$ cm⁻¹ with a relative intensity of 3%, is too small to be observed in the present spectra. The spectrum²⁰ of the lowest triplet state, an ³A^{''} state 156 kJ/mol above the ¹A₁ ground state, with vibrational frequencies of 1171 and 690 cm⁻¹, clearly does not match the experimental spectrum.

VO₃⁺

The depletion spectrum of VO₃⁺·He₂ (Fig. 3, left) shows two bands. The most intense feature is found at 1069 cm⁻¹. The second peak lies 32 cm⁻¹ lower in energy and is roughly half as intense. Overview scans down to 625 cm⁻¹ (not shown) revealed no additional signal at lower photon energies. The lowest electronic state predicted by our B3LYP calculations is the open-shell ³A^{''} state with an oxovanadium(V)-η²-superoxide structure, also found in the

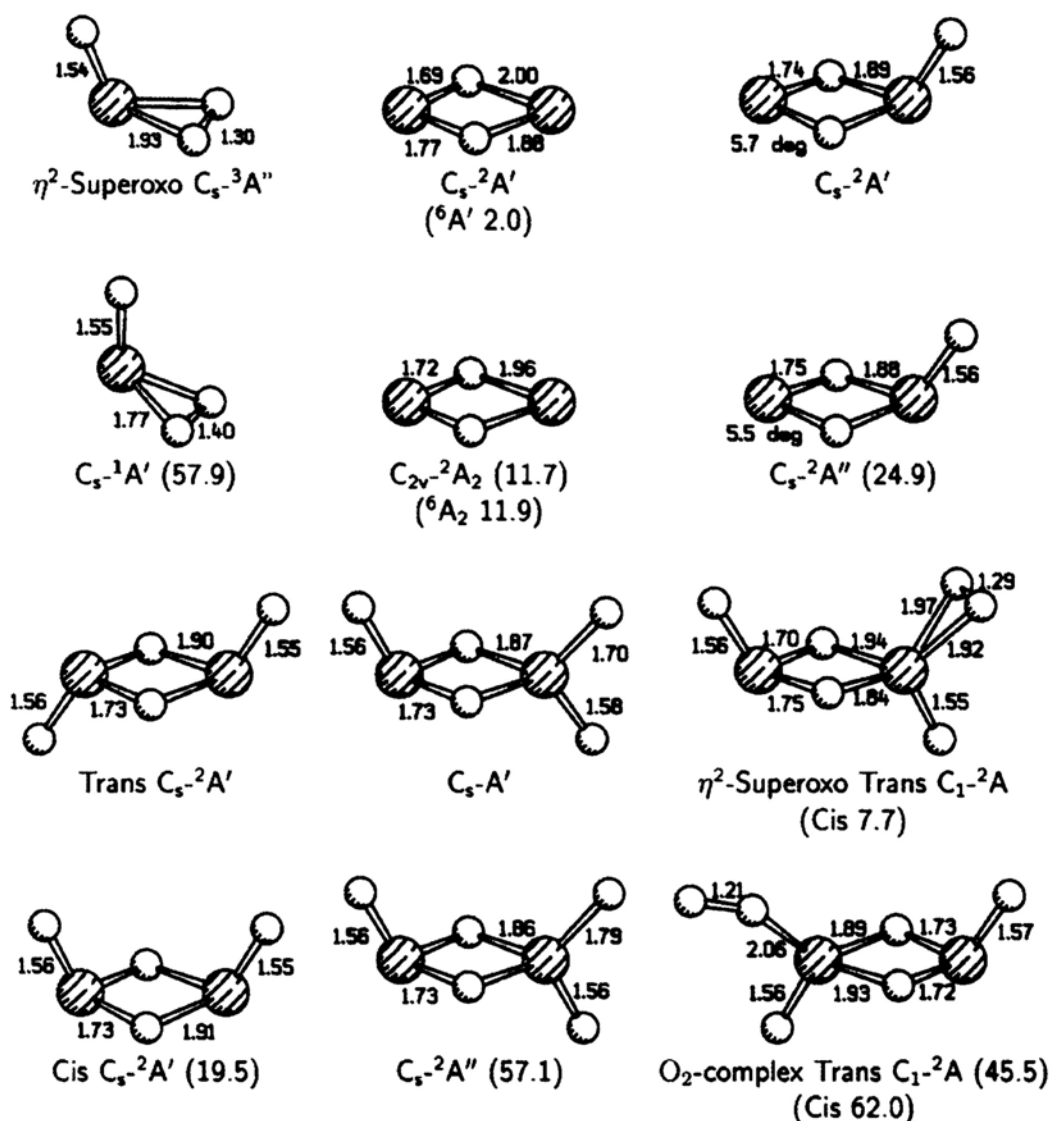


FIG. 1. B3LYP/TZVP optimized structures of selected mono- and divanadium oxide cluster cations. Two structures are shown for each cluster, one of the electronic ground state (top) and the other of an energetically low-lying isomer (bottom). Bond lengths are in Å, bond angles in degrees, and relative energies (in parentheses) with respect to the ground state are in kJ/mol. The structures of VO^+ and VO_2^+ are shown in Fig. 2.

previous calculations by Koyanagi *et al.*¹⁹ Another study²⁰ proposed an $^1A'$ ground state, but did not consider the $^3A''$ state of the η^2 -superoxo structure. We find this $^1A'$ state 57.9 kJ/mol above the $^3A''$ ground state. Both states have similar geometries (see Fig. 1), but characteristically different IR spectra (see Fig. 3). The dioxo group in the $^1A'$ state has larger O–O and smaller OV–O₂ bond lengths, but a stronger redshift of the O–O stretch, 1051 cm^{-1} compared to 1126 cm^{-1} in the $^3A''$ state. Moreover, the spectrum of the $^1A'$ state shows several peaks at low photon energies. Summarizing, we find significantly better agreement between the experimental and calculated spectra of the ground electronic

state ($^3A''$) than for the lowest singlet state ($^1A'$). The assignment of the individual bands, one to the vanadyl- and the other to the oxo-mode, is left open, because the predicted intensity ordering does not match the experimental spectrum.

V_2O_2^+

In contrast to the spectra of the monovanadium oxide cluster cations discussed above, the depletion spectra of $\text{V}_2\text{O}_2^+ \cdot \text{He}_{2,3}$ (Fig. 3, center) do not show any features above 900 cm^{-1} , but rather two bands of similar intensity are found at lower photon energies, namely at 833 and 724 cm^{-1} .

TABLE II. Experimental (ν_{expt}), calculated (ν_{B3LYP}), and scaled (ν_{scaled}) vibrational frequencies, relative intensities (in parentheses), and frequency difference $\Delta\nu = \nu_{\text{scaled}} - \nu_{\text{expt}}$ for mono- and divanadium oxide cluster cations. All frequencies are in wave numbers. Experimental frequencies are based on the IR depletion spectra of the corresponding $\text{V}_x\text{O}_y^+ \cdot \text{He}_n$ cluster ions. Theoretical values are determined by B3LYP/TZVP calculations. Scaled frequencies are calculated using the individual scaling factors (1a,b in Table I).

Experiment		B3LYP calculations					
System	ν_{expt}	State	ν_{B3LYP}	Sym.	Type	ν_{scaled}	$\Delta\nu$
$\text{VO}^+ \cdot \text{He}$	1053	$^3\Sigma^-$	1125 (1.00)	a_1	Vanadyl	1032	-21
$\text{VO}_2^+ \cdot \text{He}_2$	1017	1A_1	1133 (0.13)	a_1	Vanadyl	1038	+21
	990		1103 (1.00)	b_1	Vanadyl	1011	+21
$\text{VO}_3^+ \cdot \text{He}_2$	1069 ^a	$^3A''$	1228 (0.52)	a'	Oxo	1126 ^b	
	1037 ^a		1161 (1.00)	a'	Vanadyl	1064	
$\text{V}_2\text{O}_2^+ \cdot \text{He}_{2,3}$	833	$^2A'$	849 (1.00)	a'	Ring	835	+2
	724		712 (0.98)	a'	Ring	700	-24
			575 (1.32)	a'	Ring	565	
$\text{V}_2\text{O}_3^+ \cdot \text{He}_3$	1044	$^2A'$	1127 (0.63)	a'	Vanadyl	1033	-11
	803		823 (0.46)	a'	Ring	809	+6
	765		718 (0.62)	a''	Ring	706	-59
	666		638 (1.00)	a'	Ring	627	-39
$\text{V}_2\text{O}_4^+ \cdot \text{He}_3$	1049	$^2A'$	1135 (0.19)	a'	Vanadyl	1041	-8
	1029		1116 (1.00)	a'	Vanadyl	1023	-6
	794		844 (0.43)	a'	Ring	830	+36
	776		774 (0.47)	a''	Ring	761	-15
	594		637 (0.75)	a'	Ring	627	+33
$\text{V}_2\text{O}_5^+ \cdot \text{He}$	1034	$^2A'$	1130 (0.52)	a'	Vanadyl	1036	+2
	911		1005 (0.54)	a'	Vanadyl	921	+10
	815		850 (0.66)	a'	Ring	835	20
	738		749 (0.46)	a''	Ring	736	-2
	657		679 (1.00)	a'	Ring	668	11
			597 (0.00)	a'	V-O	587	
$\text{V}_2\text{O}_6^+ \cdot \text{He}$	1160	$^2A'$	1246 (0.31)	a	Oxo	1142 ^b	-18
	1060		1149 (0.34)	a	Vanadyl	1054	-6
	1028		1121 (0.80)	a	Vanadyl	1028	0
	836		873 (0.66)	a	Ring	859	23
	751		765 (0.37)	a	Ring	752	+1
	673		677 (1.00)	a	Ring	665	-8

^aNot assigned.

^bScaled with vanadyl scaling factor.

Therefore the presence of vanadyl (or oxo) groups, which would be expected in the region above 900 cm^{-1} , can be excluded. The width of the observed bands is somewhat larger than for the other systems studied. This is a result of the low parent ion signal level, which we compensated by increasing the FELIX power and thus also its bandwidth. Satisfactory agreement is found with the simulated IR spectra of the lowest energy isomer, an $^2A'$ state with a planar, four-membered V-O-V-O ring. Of the six vibrational modes, the three highest in energy ($\nu_{\text{scaled}} = 835, 700,$ and 565 cm^{-1}) are predicted to be the most intense and therefore they comprise the spectroscopic "fingerprint" of the ring structure. All three of these modes are in-plane deformation modes. The two higher modes match well with the experimental spectrum, while the lowest one lies too low in energy to be observed in our spectra. Note, for the larger cluster ions, starting with V_2O_3^+ , this third band is blueshifted and consequently all three modes comprising the fingerprint are observed in the spectra of the larger species.

A cyclic $^2A'$ ground state agrees with the previous study of Calatayud *et al.*²⁰ However, the next electronic state is not 4B_2 but $^6A'$. Due to the weak coupling of d electrons on the two vanadium sites the $^6A'$ high-spin analogue of $^2A'$ is

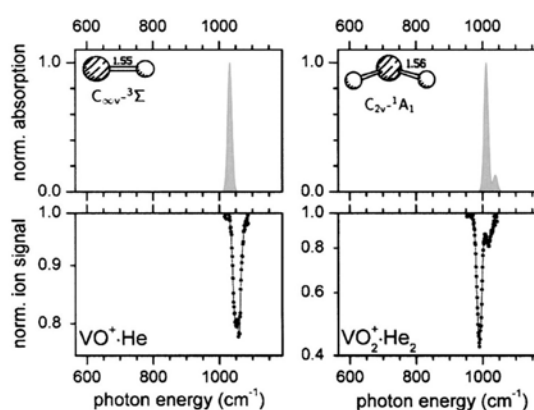


FIG. 2. Simulated IR absorption spectrum (gray line and gray shaded area), based on scaled B3LYP/TZVP frequencies and relative intensities of the ground state (top row) of VO^+ (left) and VO_2^+ (right) in the region from 565 to 1190 cm^{-1} . Higher resolution, experimental IR photodepletion spectrum (solid black dots connected by black lines) of $\text{VO}^+ \cdot \text{He}$ (left) and $\text{VO}_2^+ \cdot \text{He}_2$ (right) in this energy region are shown in the bottom row. Note the logarithmic scale for the ion signal.

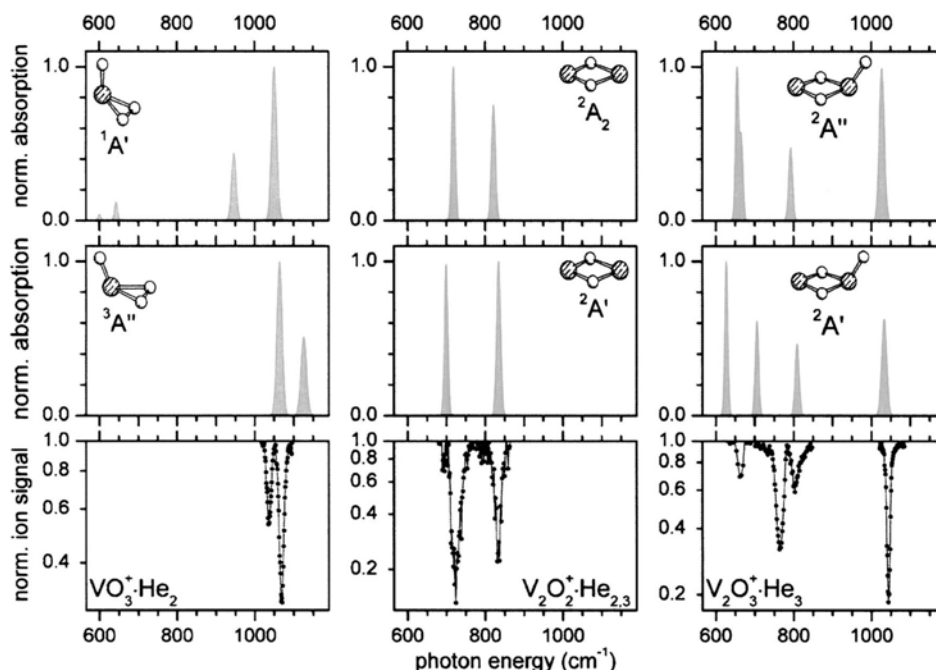


FIG. 3. Simulated IR absorption spectra (gray line and gray shaded area), based on scaled B3LYP/TZVP frequencies and relative intensities of the ground state (middle row) and lowest, electronically excited state (top row), of VO_3^+ (left), V_2O_2^+ (middle), and V_2O_3^+ (right) in the region from 565 to 1190 cm^{-1} . Higher resolution, experimental IR photodepletion spectrum (solid black dots connected by black lines) of $\text{VO}_3^+\cdot\text{He}_2$ (left), $\text{V}_2\text{O}_2^+\cdot\text{He}_{2,3}$ (center), and $\text{V}_2\text{O}_3^+\cdot\text{He}_3$ (right) in this energy region are shown in the bottom row. Note the logarithmic scale for the ion signal.

only two kJ/mol higher in energy and has a virtually identical IR spectrum. A 2A_2 state (C_{2v} symmetry), with a very similar IR spectrum (see Fig. 3) and slightly better agreement with the experimental spectrum, is found only 10 kJ/mol above the ${}^2A'$ state. Its high-spin analog, an 6A_2 state, is only 0.2 kJ/mol above the 2A_2 state. Therefore an unambiguous assignment of the electronic ground state of V_2O_2^+ requires higher level calculations.

V_2O_3^+

The depletion spectrum of $\text{V}_2\text{O}_3^+\cdot\text{He}_3$ is shown on the right of Fig. 3. A single, intense band (1044 cm^{-1}) lies in the vanadyl-stretch region. Three additional bands are observed below 810 cm^{-1} , in the V–O–V–O ring fingerprint region. Consequently, the spectrum supports a ring structure with a single, exocyclic vanadyl group, in contrast to, for example, a linear chain structure, which would reveal two characteristic vanadyl bands.²⁰ The experimental spectrum is in reasonable agreement with the IR spectrum of the lowest electronic state (${}^2A'$) found in our and previous²⁰ calculations. In particular, the number and position of the IR active bands are reproduced satisfactorily. The largest discrepancy is observed for the relative intensity of the 666 cm^{-1} band. The lowest excited state is an ${}^2A''$ state, which lies 24.9 kJ/mol above the ${}^2A'$ state. Its absorption spectrum reveals only three bands plus a shoulder and agrees less well with the observed one.

V_2O_4^+

The IR photodissociation spectrum of $\text{V}_2\text{O}_4\cdot\text{He}_3$ shows four bands at 1049, 1029, 776, and 594 cm^{-1} and a pronounced shoulder at 794 cm^{-1} (see Fig. 4, left). In line with the arguments given above and our calculations for V_2O_4^+ , the three features below 800 cm^{-1} , of which the higher two partially overlap, are attributed to the characteristic modes of the V–O–V–O ring subunit and the two peaks above 1000 cm^{-1} are assigned to the symmetric (1049 cm^{-1}) and the antisymmetric (1029 cm^{-1}) combination of the two exocyclic vanadyl groups, with the antisymmetric stretch being the more intense of the two bands. The two vanadyl groups may either occupy cis or trans positions with respect to the ring plane. Note, that a comparison of the relative intensities of all bands would favor an assignment to the cis isomer. However, our B3LYP/TZVP calculations place the cis isomer 19.5 kJ/mol higher in energy than the trans isomer. This gap is reduced to 8.4 kJ/mol, when high-level *ab initio* calculations (MR-ACPF with basis set extrapolation at the B3LYP geometry) are performed.¹⁵ Since in V_2O_4^+ the unpaired *d* electron localizes at one of the V sites, the V–O–V–O ring has two long and two short V–O bonds. Isomerization into the equivalent structure with the *d* electron at the other V site is possible for both the trans and cis structure via a symmetric transition structure (C_{2h} and C_{2v} symmetry, respectively) with four identical V–O bonds in the ring.¹⁵ The energy barriers are 19.4 and 21.2 kJ/mol, respectively.¹⁵ At suffi-

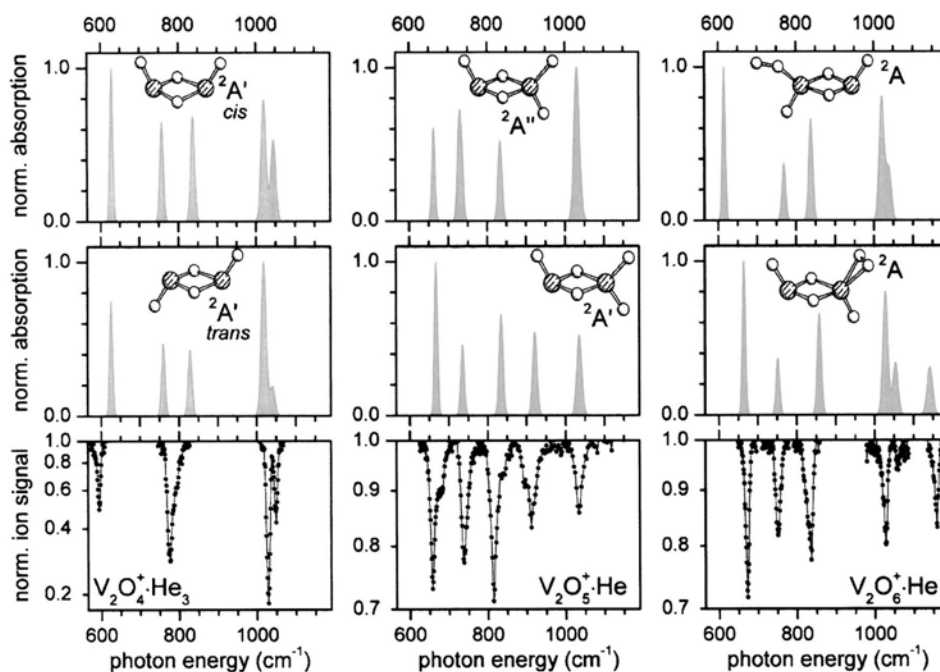


FIG. 4. Simulated IR absorption spectra (gray line and gray shaded area), based on scaled B3LYP/TZVP frequencies and relative intensities of the ground state (middle row) and an energetically low-lying isomer (top row), of $V_2O_4^+$ (left), $V_2O_5^+$ (middle), and $V_2O_6^+$ (right) in the region from 565 to 1190 cm^{-1} . Higher resolution, experimental IR photodepletion spectrum (solid black dots connected by black lines) of $V_2O_4^+ \cdot He_3$ (left), $V_2O_5^+ \cdot He$ (center), and $V_2O_6^+ \cdot He$ (right) in this energy region are shown in the bottom row. Note the logarithmic scale for the ion signal.

ciently high temperatures large amplitude motions along this isomerization coordinate may affect the predictions for the highest (830 cm^{-1}) and lowest (627 cm^{-1}) of the three characteristic V–O–V–O ring modes which are due to stretches of the V–O bonds in the ring (see Fig. 5).

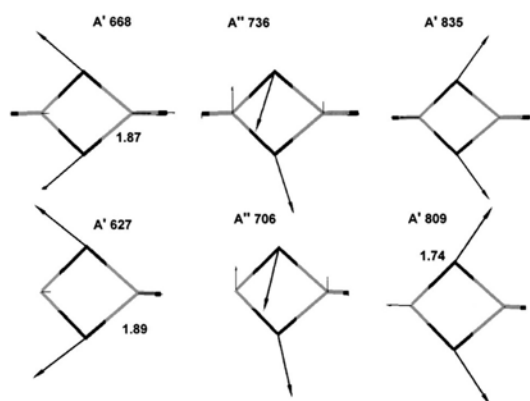


FIG. 5. The three characteristic “in-plane” normal modes of the central V–O–V–O ring in divanadium oxide cluster cations. The relative motion of the atoms, which is predominantly limited to motion in the plane of the ring, is indicated by the arrows. The scaled B3LYP/TZVP vibrational frequencies are (from left to right) 668, 736, and 835 cm^{-1} for $V_2O_5^+$ (top row) and 627, 706, and 809 cm^{-1} for $V_2O_3^+$ (bottom row).

$V_2O_5^+$

The IR photodissociation spectrum of $V_2O_5^+ \cdot He$ (Fig. 4, bottom row, center) shows five bands, two bands in the vanadyl region at 1034 and 911 cm^{-1} and three, roughly twice as intense bands, below 900 cm^{-1} at 815, 738, and 657 cm^{-1} . In addition, shoulders are observed at 896, 839, and 679 cm^{-1} . The position, as well as the intensity pattern of the five main peaks, is in excellent agreement with the simulated IR spectrum of the $^2A'$ state (see Fig. 4), the lowest electronic state we find in our B3LYP/TZVP calculations. Based on these calculations, the 1034 cm^{-1} band, calculated at $\nu_{scaled} = 1036$ cm^{-1} , is assigned to the stretch mode of the isolated vanadyl bond (see Fig. 1). The two geminal V–O bonds form a symmetric and an antisymmetric combination delocalized over both bonds, with scaled frequencies of 922 and 587 cm^{-1} , respectively. The antisymmetric combination is assigned to the 911 cm^{-1} feature in the experimental spectrum, while the 587 cm^{-1} band has virtually no intensity (although IR allowed) and is not observed. Similar to the assignments for $V_2O_{2-4}^+$, the remaining three intense bands below 900 cm^{-1} are attributed to the three characteristic modes of the central V–O–V–O ring.

The next highest electronic state, calculated 57.1 kJ/mol above the ground state, has $^2A''$ symmetry and geometrical parameters which are similar to those of the $^2A'$ ground state. The main difference between the two structures is in the length of the longer of the two geminal V–O bonds (cis

position to the isolated V–O bond). In the ${}^2A'$ state the bond distances for the geminal V–O bonds are 170 and 158 pm, while in the ${}^2A''$ state they are 179 and 156 pm. The effect on the IR spectrum is substantial. In contrast to the ${}^2A'$ state, the two geminal V–O bond stretches do not mix, but remain predominantly localized on the longer and shorter V–O bond, and both have appreciable intensity. The scaled frequency of the mode involving the shorter bond is 1030 cm^{-1} , minimally lower than the frequency of the mode involving the isolated vanadyl bond (1038 cm^{-1}). Consequently, the two modes lead to overlapping bands and form a single, intense feature in the simulated spectrum. The scaled frequency of the mode involving the longer V–O bond is 728 cm^{-1} and overlaps with one of the three ring breathing modes (834, 736, and 663 cm^{-1}), effectively increasing the relative intensity of the central feature of this group of three bands. The predicted spectrum of the ${}^2A''$ state cannot explain the band observed at 911 cm^{-1} and we conclude that the calculated B3LYP/TZVP energies and the comparison of the IR spectra provide convincing evidence for an ${}^2A'$ and against an ${}^2A''$ ground state of V_2O_5^+ . The origin of the observed shoulders is not clear and they are left unassigned. Note, the position of the shoulders does not match the absorption spectrum of the ${}^2A''$ excited state discussed above.

V_2O_6^+

The IR photodissociation spectrum of $\text{V}_2\text{O}_6^+\cdot\text{He}$ is shown on the right of Fig. 4. Six bands are observed. The band at 1160 cm^{-1} is too high in energy for a regular vanadyl group and thus is assigned to a superoxo group. The two bands at 1060 and 1028 cm^{-1} lie in the typical spectral region for vanadyl stretches. Similar to the other spectra of divanadium oxide cluster cations, the three bands at 836, 751, and 673 cm^{-1} are attributed to the three characteristic modes of a four-membered V–O–V–O ring. The experimental spectrum matches exceptionally well with the spectrum calculated for the 2A ground state of V_2O_6^+ , and clearly disagrees with the spectrum of the “O₂-complex” isomer (2A), found 45.5 kJ/mol above the ground state. In the ground state of V_2O_6^+ the two vanadyl groups occupy the trans position and the η^2 -superoxo unit forms a three-membered ring with one of the two vanadium atoms (see Fig. 1). The cis isomer is calculated 7.7 kJ/mol higher in energy. Its IR spectrum is virtually identical with that of the trans isomer and not shown.

DISCUSSION

Comparison of the present results with previous multiphoton IR photodissociation studies on metal oxide cations in the region below 2000 cm^{-1} highlights several important features of the current experimental scheme. (1) In most previous studies on cluster ions and using free electron laser (FEL) radiation the initial ion beam was not mass selected (see, for example, Ref. 39 and references therein) and consequently a mass distribution of cluster ions is irradiated. A mass filter is then used to mass select the “product” ions. Although this method has the multiplex advantage, this procedure does not uniquely identify the signal carrier, because

product ions of identical mass can be formed from different parent ions. Unless one has a detailed understanding of the dissociation pathways, mass selection of the ions *prior* to irradiation is required in order to unambiguously identify the signal carrier. (2) IR photodissociation experiments on bare metal oxide clusters generally require the absorption of multiple IR photons. When multiple isomers are present in the ion beam, the isomer with the lowest dissociation energy, which does not necessarily have to be the thermodynamically most stable one, generally dissociates at the lowest laser fluence and thus is most facile to detect. IR multiphoton dissociation studies on $\text{V}_4\text{O}_{10}^+$, for example, showed that a $\text{V}_4\text{O}_8^+\cdot\text{O}_2$ isomer could be detected, but not the theoretically predicted most stable cage-like isomer of $\text{V}_4\text{O}_{10}^+$, because the dissociation energy is more than 3 eV higher for the cage structure.¹⁰ He tagging reduces the number of photons required in the photodissociation process dramatically, generally down to a single photon, avoiding the complications described above. (3) He tagging also results in a considerable increase of the spectral resolution, because the absorbing species are necessarily the colder subset of the species present in the ion trap, and generally much colder compared to those produced directly by laser vaporization.

The improved experimental scheme combined with the reliable prediction of ground state geometries and frequencies allows for a detailed insight into the structure of metal oxide cluster ions in general and of vanadium oxide cluster cations in this particular study. The central building block of the divanadium oxide cations is a four-membered V_2O_2 ring, in which each vanadium atom is adjacent to two oxygen atoms. For one vanadium atom the two V–O bonds are significantly shorter than for the other. Experimental evidence for four-membered rings as a structural motif in metal oxide clusters was originally found by von Helden *et al.*¹³ in their pioneering study on the infrared spectroscopy of neutral zirconium oxide clusters. They observed two very broad absorption bands centered at 620 and 680 cm^{-1} , respectively, and assigned them to vibrational modes of the Zr–O–Zr–O ring, predicted in the $600\text{--}800\text{ cm}^{-1}$ range. The spectral signature of the V–O–V–O four-membered ring is three absorption bands of comparable intensity in the region from 550 to 900 cm^{-1} . Both the observed and predicted (in parenthesis) wave numbers fall into narrow ranges of 833–794 (859–809), 776–724 (761–700), 673–594 (668–565) cm^{-1} . As the oxygen content increases from V_2O_2^+ to V_2O_6^+ , the number of unpaired *d* electrons on vanadium sites decreases from 3/2 in V_2O_2^+ to 1/0 in V_2O_6^+ and the number of terminal VO groups increases from none to 3. V_2O_6^+ includes an additional η^2 -superoxo ligand. Neither of these changes affects the characteristic V_2O_2 ring modes significantly. Figure 5 sketches the three modes. The highest and the lowest energy modes are couplings of the stretches of the two shorter and longer VO bonds, respectively, with the deformation of the opposite V–O–V angle. Their splitting is indicative of the asymmetry of the VO bond distances in the ring. The third mode is a O–V–O twist.

The present data can be used to deduce information about V–O bond distances of vanadium oxide species, for which the IR spectra (or Raman spectra) are known, but the

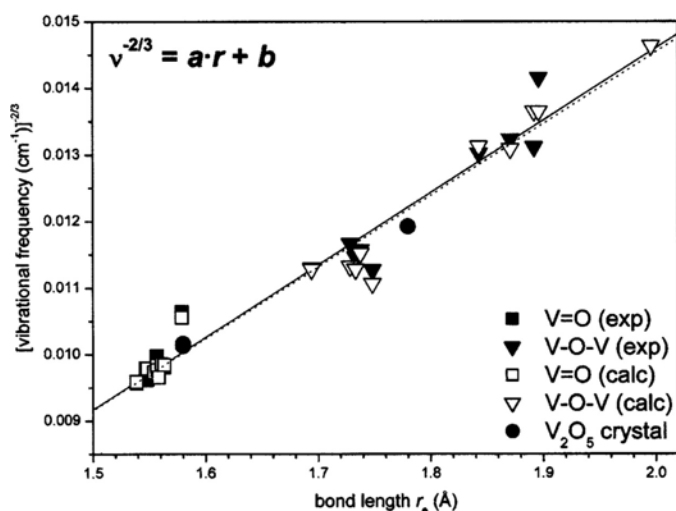


FIG. 6. Badger's rule plot of $\nu^{-2/3}$ against the r_e , where ν is the vanadium–oxygen stretching frequency and r_e the vanadium–oxygen bond length. Scaled harmonic (open symbols) and experimental (solid symbols) vibrational frequencies are shown. Squares and triangles refer to gas phase values from the present study and the solid circles are based on previous results on crystalline V_2O_5 . For the gas phase, data squares indicate frequencies for terminal V=O bonds, while triangles represent V–O–V bonds including divalent oxygen atoms. Solid and dotted lines represent the linear, least squares fit to the experimental (gas phase only) and calculated frequencies, respectively.

structure is not. This is relevant for supported vanadium oxide catalysts, and attempts have been made to predict vanadium oxide bond distances for solid materials of unknown structure involving vanadium oxides.⁴⁰ Figure 6 shows that the frequencies of the vanadium–oxygen stretch modes are indeed a monotonic function of the bond distance. Based on the Badger rule, which assumes that for a given bond type the harmonic force constant k is inversely proportional to the cube of the bond distance r_e , $k = C/(r_e - d)^3$, $\nu^{-2/3}$ is plotted against the equilibrium bond distance r_e . Both scaled harmonic (open symbols) and experimental (solid symbols) vibrational frequencies are shown. Squares indicate terminal V=O bonds, while triangles represent V–O–V bonds including divalent oxygen atoms. Solid and dotted lines represent the linear, least squares fit to the experimental and theoretical frequencies, respectively. The linear fit yields similar values for the experimental ($a = 0.01086 \text{ cm}^{2/3}/\text{\AA}$, $b = 0.00713 \text{ cm}^{2/3}$) and the theoretical frequencies ($a = 0.01076 \text{ cm}^{2/3}/\text{\AA}$, $b = 0.00698 \text{ cm}^{2/3}$). Included in the figure are also observed data for V=O and V–O(–V) bonds of crystalline V_2O_5 (solid circles). The observed IR frequencies (981/976 and 768 cm^{-1} , respectively)⁴¹ and bond distances (1.58 and 1.78 Å, respectively) derived from the x-ray structure⁴² fall on the same line. Hence, use may be made of the present data to derive structure information from IR or Raman spectra of vanadium oxide species supported, for example, on aluminum oxide and silicon dioxide.

Previous theoretical studies had predicted the correct connectivity for most of the clusters, however conflicting assignments for the electronic ground states of VO_3^+ , $V_2O_2^+$, $V_2O_4^+$, $V_2O_5^+$, and $V_2O_6^+$ were made. The assumption of a ${}^2A''$ ground state in $V_2O_5^+$ in Ref. 7 is of particular significance, as many of the reaction energies and also the energy profile shown in Fig. 4 of Ref. 7 will change if the ${}^2A'$ ground state found in the present and a previous study^{21,43} is considered. Our calculation of the reaction energies in Table I of Ref. 7 shows that all four reaction energies for $V_2O_5^+ + C_2H_4$ and two of the reaction energies for

$V_2O_6^+ + C_2H_4$ change by about 0.6 eV. Since the changes for $V_2O_5^+$ and $V_2O_6^+$ are in opposite direction, the predicted reactivity differences between the two oxide species become significantly smaller and additional effort is needed to fully understand the observed reaction patterns.

ACKNOWLEDGMENTS

We thank P. Degelmann (Universität Karlsruhe) for a pre-release version of the aoforce modul which permits unrestricted open shell DFT calculations. This work is supported by the Collaborative Research Center 546 of the Deutsche Forschungsgemeinschaft. The authors thank G. von Helden and A. Fielicke for helpful discussions and gratefully acknowledge the support of the Stichting voor Fundamenteel Onderzoek der Materie (FOM) in providing the required beam time on FELIX and highly appreciate the skillful assistance of the FELIX staff, in particular Dr. A. F. G. van der Meer.

¹C. N. R. Rao and B. Raven, *Transition Metal Oxides* (VCH, New York, 1995).

²B. M. Weckhuysen and D. E. Keller, *Catal. Today* **78**, 25 (2003).

³G. G. Cortez and M. A. Banares, *J. Catal.* **209**, 197 (2002).

⁴D. Schröder, J. Loos, M. Engeser, H. Schwarz, H.-C. Jankowiak, R. Berger, R. Thissen, O. Dutuit, J. Döbler, and J. Sauer, *Inorg. Chem.* (in press); E. B. Rudnyi, E. A. Kaibicheva, and L. N. Sidorov, *J. Chem. Thermodyn.* **25**, 929 (1993); R. C. Bell, K. A. Zemski, and A. W. Castleman, Jr., *J. Phys. Chem. A* **102**, 8293 (1998); R. C. Bell, K. A. Zemski, and A. W. Castleman, Jr., *ibid.* **103**, 1585 (1999); R. C. Bell, K. A. Zemski, D. R. Justes, and A. W. Castleman, Jr., *J. Chem. Phys.* **114**, 798 (2001); K. A. Zemski, D. R. Justes, and A. W. Castleman, Jr., *J. Phys. Chem. A* **105**, 10237 (2001); A. Dinca, T. P. Davis, K. J. Fisher, D. R. Smith, and G. D. Willett, *Int. J. Mass. Spectrom.* **182/183**, 73 (1999); A. Fielicke and K. Rademann, *Phys. Chem. Chem. Phys.* **4**, 2621 (2002).

⁵H. Wu and L.-S. Wang, *J. Chem. Phys.* **108**, 5310 (1998); H. J. Zhai and L.-S. Wang, *ibid.* **117**, 7882 (2002).

⁶R. C. Bell, K. A. Zemski, K. P. Kerns, H. T. Deng, and A. W. Castleman, Jr., *J. Phys. Chem. A* **102**, 1733 (1998).

⁷D. R. Justes, R. Mitric, N. A. Moore, V. Bonacic-Koutecký, and A. W. Castleman, Jr., *J. Am. Chem. Soc.* **125**, 6289 (2003).

⁸J. N. Harvey, M. Diefenbach, D. Schröder, and H. Schwarz, *Int. J. Mass. Spectrom.* **182/183**, 85 (1999).

- ⁹A. Pramann, K. Koyasu, A. Nakajima, and K. Kaya, *J. Chem. Phys.* **116**, 6521 (2002).
- ¹⁰K. R. Asmis, M. Brümmer, C. Kaposta, G. Santambrogio, G. von Helden, G. Meijer, K. Rademann, and L. Wöste, *Phys. Chem. Chem. Phys.* **4**, 1101 (2002).
- ¹¹A. Fielicke, R. Mitric, G. Meijer, V. Bonacic-Koutecky, and G. von Helden, *J. Am. Chem. Soc.* **125**, 15716 (2003).
- ¹²M. Brümmer, C. Kaposta, G. Santambrogio, and K. R. Asmis, *J. Chem. Phys.* **119**, 12700 (2003).
- ¹³G. von Helden, A. Kirilyuk, D. van Heijnsbergen, B. Sartakov, M. A. Duncan, and G. Meijer, *Chem. Phys.* **262**, 31 (2000).
- ¹⁴O. Hübner and J. Sauer, *Phys. Chem. Chem. Phys.* **4**, 5234 (2002).
- ¹⁵M. Pykavy, C. van Wüllen, and J. Sauer, *J. Chem. Phys.* (to be published).
- ¹⁶A. D. Becke, *J. Chem. Phys.* **98**, 5648 (1993).
- ¹⁷S. F. Vyboishchikov and J. Sauer, *J. Phys. Chem. A* **104**, 10913 (2000).
- ¹⁸S. F. Vyboishchikov and J. Sauer, *J. Phys. Chem. A* **105**, 8588 (2001).
- ¹⁹G. K. Koyanagi, D. K. Bohme, I. Kretschmar, D. Schröder, and H. Schwarz, *J. Phys. Chem. A* **105**, 4259 (2001).
- ²⁰M. Calatayud, B. Silvi, J. Andrés, and A. Beltrán, *Chem. Phys. Lett.* **333**, 493 (2001).
- ²¹M. Calatayud, J. Andrés, and A. Beltrán, *J. Phys. Chem. A* **105**, 9760 (2001).
- ²²J. Sauer and S. F. Vyboishchikov, poster presented at the Berichtskolloquium Sfb 546, Humboldt-Universität zu Berlin, February, 2002 (unpublished).
- ²³D. Oepts, A. F. G. van der Meer, and P. W. van Amersfoort, *Infrared Phys. Technol.* **36**, 297 (1995).
- ²⁴R. Ahlrichs, M. Bär, M. Häser, H. Horn, and C. Kölmel, *Chem. Phys. Lett.* **162**, 165 (1989); O. Treutler and R. Ahlrichs, *J. Chem. Phys.* **102**, 346 (1995); K. Eichkorn, O. Treutler, H. Ohm, M. Häser, and R. Ahlrichs, *Chem. Phys. Lett.* **242**, 652 (1995).
- ²⁵A. D. Becke, *Phys. Rev. A* **38**, 3098 (1988).
- ²⁶C. Lee, W. Yang, and R. G. Parr, *Phys. Rev. B* **37**, 785 (1988).
- ²⁷P. J. Stephens, F. J. Devlin, C. F. Chabalowski, and M. J. Frisch, *J. Phys. Chem.* **98**, 11623 (1994).
- ²⁸R. H. Hertwig and W. Koch, *Chem. Phys. Lett.* **268**, 345 (1997).
- ²⁹A. Schäfer, C. Huber, and R. Ahlrichs, *J. Chem. Phys.* **100**, 5829 (1994).
- ³⁰A. J. Wachtters, *J. Chem. Phys.* **52**, 1033 (1970).
- ³¹P. Deglmann, F. Furche, and R. Ahlrichs, *Chem. Phys. Lett.* **362**, 511 (2002).
- ³²A. P. Scott and L. Radom, *J. Phys. Chem.* **100**, 16502 (1996).
- ³³M. D. Halls, J. Velkovski, and H. B. Schlegel, *Theor. Chem. Acc.* **105**, 413 (2001).
- ³⁴S. A. Nizkorodov, J. P. Maier, and E. J. Bieske, *J. Chem. Phys.* **103**, 1297 (1995); D. Roth, O. Dopfer, and J. P. Maier, *Phys. Chem. Chem. Phys.* **3**, 2400 (2001).
- ³⁵E. J. Bieske and O. Dopfer, *Chem. Rev. (Washington, D.C.)* **100**, 3963 (2000).
- ³⁶J. M. Dyke, B. W. J. Gravenor, M. P. Hastings, and A. Morris, *J. Phys. Chem.* **89**, 4613 (1985).
- ³⁷M. Pykavy and C. van Wüllen, *J. Phys. Chem. A* **107**, 5566 (2003).
- ³⁸J. Harrington and J. C. Weisshaar, *J. Phys. Chem.* **97**, 2809 (1992).
- ³⁹A. Fielicke, G. Meijer, and G. von Helden, *J. Am. Chem. Soc.* **125**, 3659 (2003).
- ⁴⁰F. D. Hardcastle and I. E. Wachs, *J. Phys. Chem.* **95**, 5031 (1991).
- ⁴¹P. Clauws and J. Vennik, *Phys. Status Solidi B* **76**, 707 (1976).
- ⁴²R. Enjalbert and J. Galy, *Acta Crystallogr., Sect. C: Cryst. Struct. Commun.* **42**, 1467 (1986).
- ⁴³Calatayud, Andrés, and Beltrán (Ref. 21) incorrectly label the ground state of $V_2O_5^+ {}^2A'$. However, from the agreement of the bond distances and vibrational frequencies reported in Ref. 21 with our ${}^2A'$ results we gather that the state calculated was in fact the correct ${}^2A'$ ground state.

Polyhedral Vanadium Oxide Cages: Infrared Spectra of Cluster Anions and Size-Induced d Electron Localization

Knut R. Asmis

Fritz-Haber-Institut der Max-Planck-Gesellschaft, Faradayweg 4-6, D 14195 Berlin, Germany.

Mathias Brümmer and Gabriele Santambrogio

Institut für Experimentalphysik, Freie Universität Berlin, Arnimallee 14, D 14195 Berlin, Germany.

Joachim Sauer

Institut für Chemie, Humboldt-Universität Berlin, Unter den Linden 6, D-10099 Berlin, Germany

Communication in *Angewandte Chemie - International Edition* **44**(22) 3122-5 (2005).

Communications

Cluster Compounds

Polyhedral Vanadium Oxide Cages: Infrared Spectra of Cluster Anions and Size-Induced d Electron Localization**

Knut R. Asmis,* Gabriele Santambrogio,
Mathias Brümmer, and Joachim Sauer*

The size-dependent properties of transition metal oxide clusters have been intensely studied not only because of interest in this peculiar state of matter, but also because of their relevance as building blocks for nanostructured materials. Vanadium oxides, in particular, are important in supported catalysts,^[1] as cathode materials in lithium batteries,^[2] in bolometric detectors,^[3] and as ferromagnetic nanotubes.^[4] While the structural characterization of vanadium oxide clusters deposited on surfaces^[5] has reached atomic resolution, it remains a major experimental challenge in the gas

[*] Dr. K. R. Asmis
Fritz-Haber-Institut der Max-Planck-Gesellschaft
Faradayweg 4–6, 14195 Berlin (Germany)
Fax: (+49) 308-413-5603
E-mail: asmis@fhi-berlin.mpg.de
Prof. Dr. J. Sauer
Institut für Chemie, Humboldt-Universität Berlin
Unter den Linden 6, 10099 Berlin (Germany)
Fax: (+49) 302-093-7136
E-mail: js@chemie.hu-berlin.de
Dipl.-Phys. G. Santambrogio, Dipl.-Ing. M. Brümmer
Institut für Experimentalphysik, Freie Universität Berlin
Arnimallee 14, 14195 Berlin (Germany)

[**] This work was supported by the German Research Foundation (DFG) as part of the Collaborative Research Center 546. We gratefully acknowledge the support of the “Stichting voor Fundamenteel Onderzoek der Materie (FOM)” in providing the required beam time on FELIX and highly appreciate the skilful assistance of the FELIX staff. We thank L. Wöste and G. Meijer for their continuous support and A. Fielicke for helpful discussions.

Supporting information for this article is available on the WWW under <http://www.angewandte.org> or from the author.

phase.^[6] Infrared photodissociation^[7] paired with quantum chemistry is currently the most generally applicable approach for cluster ions even though it requires intense and tunable infrared radiation sources. Below 2000 cm⁻¹, in the fingerprint region of metal oxide clusters, only free-electron lasers meet these demands.^[8]

Herein we report the first experimental infrared spectra of transition metal oxide cluster anions in the gas phase. We combine infrared multiple photon dissociation (IRMPD) spectroscopy with density functional theory (DFT) to characterize the geometric and electronic structures of a representative series of vanadium oxide cluster anions, (V₂O₅)_n⁻ (*n* = 2, 3, or 4).^[9] Compelling evidence is produced that these anions have the polyhedral cage structures that have been predicted before, but have eluded spectroscopic detection until now.^[10,11] Evidence is also found for a size-induced localization of the extra electron in this series of anions.

The IRMPD spectra of mass-selected V₄O₁₀⁻, V₆O₁₅⁻, and V₈O₂₀⁻ are shown on the left in Figure 1. They were measured by irradiating vibrationally cold, mass-selected parent ions with intense, tunable IR radiation from the free-electron laser FELIX^[12] and monitoring the mass-selected fragment ion yield as a function of laser wavelength. Only when the radiation is resonant with a fundamental vibrational transition can the cluster ions absorb photons, thereby initiating a sequential multiphoton absorption process^[13] which leads to heating of the cluster ion and eventually to photodissociation. The simplicity of the V₄O₁₀⁻ spectrum is striking and immediately suggests a structure of higher symmetry with degenerate transitions. The dominant feature is a single, rather narrow intense band at 990 cm⁻¹. Based on our previous measurements on vanadium oxide cluster cations it is assigned to a vanadyl stretching mode.^[14] The weaker signal below 750 cm⁻¹ is attributed to a V–O–V stretch. The IRMPD spectrum of V₈O₂₀⁻ is markedly different. While the vanadyl band stays nearly unchanged, a new band, much broader and roughly four times stronger than the vanadyl band, is observed centered at 870 cm⁻¹. The appearance of the V₆O₁₅⁻ spectrum is intermediate between the spectra described above. An intense vanadyl band, somewhat broader and red-shifted, is followed by a four times less intense band at 830 cm⁻¹. No signal is observed below 700 cm⁻¹ for the two larger clusters.

To understand these vibrational spectra we performed DFT calculations (B3LYP functional^[15,16]) of cluster geometries and vibrational spectra (see Figure 1). All three anions are open-shell systems with a single unpaired electron. For V₄O₁₀⁻ we find a tetragonal *D*_{2d} structure (**1**) which is minimally Jahn–Teller distorted from the *T*_d structure. Each vanadium atom is fourfold coordinated, forming one short V=O bond (159 pm) and three V–O bonds (181 pm). The four symmetry-equivalent vanadyl bond stretches combine to give three IR-active *b*₂ and *e* modes, which are quasi-degenerate and explain the single intense vanadyl band in the IRMPD spectrum. The six symmetric V–O–V bond stretches also give rise to three IR-active *e* and *b*₂ modes (629 and 609 cm⁻¹, respectively), and they have a cumulative oscillator strength that is about 1/3 that of the vanadyl bands, in good agreement with experiment. The modes resulting from the six antisym-

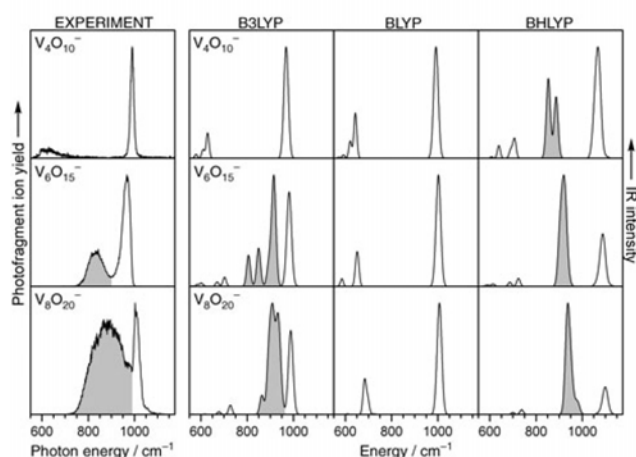
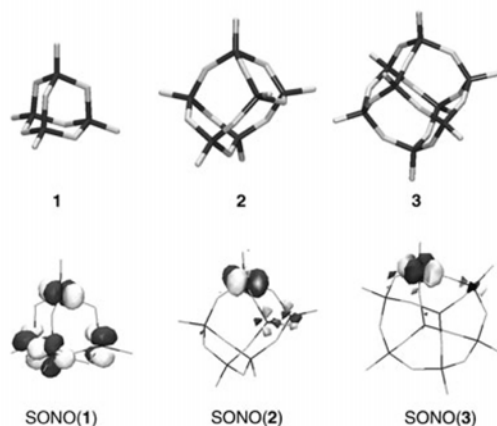


Figure 1. Experimental and simulated vibrational spectra of vanadium oxide cluster anions in the region of the V–O and V=O bond stretch modes. IRMPD spectra (left) of $V_4O_{10}^-$, $V_6O_{15}^-$, and $V_8O_{20}^-$ were measured from 550 to 1175 cm^{-1} by monitoring the dominant fragmentation channel, which leads to the formation of $V_3O_8^-$, $V_4O_{10}^-$, and $V_6O_{10}^-$, respectively. Simulated spectra (right) were obtained from scaled harmonic frequencies and oscillator strengths employing the B3LYP, BLYP, and BHLYP functionals. The calculated stick spectra were convoluted for better comparison with the experiment. Gray shaded peaks indicate localization of the unpaired d electron (see text).

metric V–O–V bond stretches are below 600 cm^{-1} and have vanishingly low intensities.



In $V_4O_{10}^-$ the unpaired electron is completely delocalized over d-states of all four vanadium sites, as illustrated by its singly-occupied natural orbital SONO(1). In contrast, in the larger anions the unpaired electron is localized at a single vanadium site, which lowers the symmetry of their structures to C_s . For $V_6O_{15}^-$ and $V_8O_{20}^-$ we find the distorted trigonal prism and cube structures **2** and **3**. Their singly occupied natural orbitals, SONO(2) and SONO(3), reflect the localization of the unpaired electron. Compared to $V_4O_{10}^-$, the

average V–O(–V) bond distances in $V_8O_{20}^-$ are longer at the electron localization site (189 pm), but shorter at the other sites (177–178 pm), while the V=O bond distances are similar and not affected by the localization. Unlike the closed-shell neutral parent compounds, the D_{3h} structure (trigonal prism) of $V_6O_{15}^-$ and the D_{2d} structure (cube) of $V_8O_{20}^-$ are higher-order saddle points that are 45 and 21 $kJ\,mol^{-1}$, respectively, above the ground state. For both $V_6O_{15}^-$ and $V_8O_{20}^-$ first-order saddle points with C_{2v} symmetry are found 9.8 and 8.7 $kJ\,mol^{-1}$, respectively, above the ground state. They represent transition structures for the interconversion of two equivalent C_s -minimum structures and have the additional electron delocalized over two sites.

The effects of symmetry breaking are directly observed in the vibrational spectra of these species (indicated by the gray-shaded area in Figure 1). Upon localization of the unpaired electron intense V–O–V stretch transitions appear at around 100–200 cm^{-1} below the strong vanadyl band, which replace the weak V–O–V feature more than 350 cm^{-1} below the vanadyl band in the spectrum of the delocalized case ($V_4O_{10}^-$). The calculated ratio of the cumulative oscillator strengths of the V–O–V modes and the V=O modes is 3.3 for $V_8O_{20}^-$ and 0.3 for $V_4O_{10}^-$; these values compare well to the experimental values of 4.4 and 0.4 respectively. The vanadyl modes are not affected by the electron localization and therefore their position and width remain nearly unchanged. Comparison with the experimental infrared spectra confirms the general predictions of the B3LYP model, in particular the pronounced, qualitative changes upon electron localization when the size of the cluster is increased.^[17]

Figure 1 shows not only the B3LYP results discussed so far, but also the results of DFT calculations with the BLYP^[16,18] and BHLYP^[16,19] functionals. The increasing admixture of Fock exchange (0, 20, and 50% in BLYP, B3LYP, and BHLYP, respectively) leads to an increasing tendency for symmetry breaking.^[20–22] BHLYP (right column in Figure 1) yields localization of the unpaired electron for all three cage-type anions, and also for $V_4O_{10}^-$. Consequently, the calculated BHLYP spectrum of $V_4O_{10}^-$ shows additional bands between 800 and 900 cm^{-1} that are absent from the experimental spectrum. In contrast, BLYP predicts delocalization of the unpaired electron for all three cage-type anions studied and C_{2v} and D_{2d} structures become the ground states of $V_6O_{15}^-$ and $V_8O_{20}^-$, respectively. All three BLYP spectra show no bands between 750 and 950 cm^{-1} , which is in clear contrast with the experimental spectra of $V_6O_{15}^-$ and $V_8O_{20}^-$. In summary, Figure 1 shows that only B3LYP reproduces correctly the transition from symmetric (delocalized) to broken-symmetry (localized) structures when passing from $V_4O_{10}^-$ to $V_6O_{15}^-$ in this series of $(V_2O_5)_n^-$ cluster anions.

Figure 2 compares the gas-phase IRMPD spectrum of $V_8O_{20}^-$ with the electron energy loss spectrum of a V_2O_5

Communications

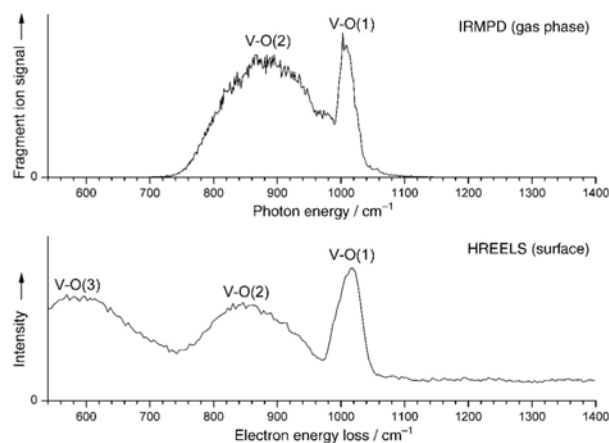


Figure 2. Vibrational spectra of different forms of vanadium oxide: The IRMPD spectrum of the gas-phase cluster anion $V_8O_{20}^-$ (top) and the spectrum of a freshly cleaved 001 surface of V_2O_5 (bottom), measured by high resolution electron energy loss spectroscopy (see text).

surface,^[23] which also probes vibrational states. The spectra are surprisingly similar in the region above 740 cm^{-1} , with both displaying two bands of similar width and relative intensity. Their assignment is identical, that is, to vibrational modes of singly and doubly coordinated oxygen atoms. The third broad band of the surface spectrum is not observed in the gas phase. This can easily be rationalized because this band is assigned^[11,24] to triply coordinated oxygen sites, which do not exist in the $V_8O_{20}^-$ cluster anion. Hence, the vibrational spectra reflect clearly the common (V=O and V–O–V bonds) and the discriminating (triply coordinated O) structural features of gas-phase clusters and solid surfaces.^[25,26]

In this communication the polyhedral cage structures of $(V_2O_5)_n^-$ clusters ($n=2, 3, 4$) have been identified spectroscopically for the first time by IRMPD spectroscopy. We have also found evidence for size-dependent charge localization in these clusters. Symmetry-breaking localization is observed in many other chemical systems for the reverse process—creation of an electron hole.^[21] For example, the electron hole created in quartz when doped with Al is not delocalized over all four oxygen sites of the AlO_4 defect site, but localized at one oxygen only.^[22] The proper description of electron (hole) localization phenomena by DFT depends on the functional used. In the present case we use the measured IRMPD spectra as the criteria for selecting the proper functional and find that only B3LYP has the right admixture of Fock exchange to reproduce the size-dependent change from delocalized to localized d electron states in vanadium oxide cages correctly. Even though the largest cluster anion studied here, $V_8O_{20}^-$, is still rather small, it reveals some striking similarities with the properties of a vanadium oxide single-crystal surface, making it an interesting gas-phase model for surface adsorption and reactivity studies.

Experimental Section

The present experiments were carried out on a previously described tandem mass spectrometer–ion trap system.^[27] Vanadium oxide clusters were prepared by pulsed laser vaporization of a vanadium rod in the presence of O_2 seeded in He. The beam of negative ions was collimated and mass-selected by a quadrupole mass filter. Mass-selected cluster ions were accumulated and cooled to 15 K in a linear radio-frequency ion trap. IR photodissociation spectra were obtained by photoexcitation of the trapped cold ions with pulsed radiation from the FELIX,^[12] and subsequent monitoring of the mass-selective ion yield. A FELIX bandwidth (RMS) of less than 0.3% of the central wavelength and pulse energies up to 60 mJ per macropulse were used.

Unrestricted Kohn–Sham calculations were performed with TURBOMOLE.^[28] Triple-zeta valence plus polarization basis sets (TZVP) were applied.^[29] Harmonic vibrational frequencies were obtained from second analytic derivatives^[30] and were scaled using standard procedures (see Supporting Information).

Received: December 10, 2004

Published online: April 13, 2005

Keywords: cluster compounds · density functional calculations · electronic structure · IR spectroscopy · vanadium

- [1] B. M. Weckhuysen, D. E. Keller, *Catal. Today* **2003**, *78*, 25–46.
- [2] M. S. Whittingham, *Chem. Rev.* **2004**, *104*, 4271–4301.
- [3] L. A. L. de Almeida, G. S. Deep, A. M. N. Lima, I. A. Khrebtov, V. G. Malyarov, H. Neff, *Appl. Phys. Lett.* **2004**, *85*, 3605–3607.
- [4] L. Krusin-Elbaum, D. M. News, H. Zeng, V. Derycke, J. Z. Sun, R. Sandstrom, *Nature* **2004**, *431*, 672–676.
- [5] a) J. Schoiswohl, G. Kresse, S. Surnev, M. Sock, M. G. Ramsey, F. P. Netzer, *Phys. Rev. Lett.* **2004**, *92*, 206103; b) N. Magg, B. Immaraporn, J. B. Giorgi, T. Schroeder, M. Bäumer, J. Döbler, Z. L. Wu, E. Kondratenko, M. Cherian, M. Baerns, P. C. Stair, J. Sauer, H.-J. Freund, *J. Catal.* **2004**, *126*, 88–100.
- [6] a) A. Dinca, T. P. Davis, K. J. Fisher, D. R. Smith, G. D. Willett, *Int. J. Mass Spectrom.* **1999**, *182/183*, 73–84; b) R. C. Bell, K. A. Zemski, D. R. Justes, A. W. Castleman, Jr., *J. Chem. Phys.* **2001**, *114*, 798–811; c) H. J. Zhai, L.-S. Wang, *J. Chem. Phys.* **2002**, *117*, 7882–7888; d) A. Pramann, K. Koyasu, A. Nakajima, K. Kaya, *J. Chem. Phys.* **2002**, *116*, 6521–6528.
- [7] M. A. Duncan, *Int. J. Mass Spectrom.* **2000**, *200*, 545–569.
- [8] G. von Helden, D. van Heijnsbergen, G. Meijer, *J. Phys. Chem. A* **2003**, *107*, 1671–1688.
- [9] A systematic study of vanadium oxide cluster anions containing two to eight vanadium atoms will be reported shortly.
- [10] S. F. Vyboishchikov, J. Sauer, *J. Phys. Chem. A* **2000**, *104*, 10913–10922.
- [11] S. F. Vyboishchikov, J. Sauer, *J. Phys. Chem. A* **2001**, *105*, 8588–8598.
- [12] D. Oepts, A. F. G. van der Meer, P. W. van Amersfoort, *Infrared Phys. Technol.* **1995**, *36*, 297–308.
- [13] J. Oomens, G. Meijer, G. von Helden, *J. Phys. Chem. A* **2001**, *105*, 8302–8309.
- [14] K. R. Asmis, G. Meijer, M. Brümmer, C. Kaposta, G. Santambrogio, L. Wöste, J. Sauer, *J. Chem. Phys.* **2004**, *120*, 6461–6470.
- [15] A. D. Becke, *J. Chem. Phys.* **1993**, *98*, 5648–5652.
- [16] C. Lee, W. Yang, R. G. Parr, *Phys. Rev. B* **1988**, *37*, 785–789.
- [17] Some discrepancies between experimental and simulated spectra remain and are attributed to the approximate nature of the calculations, which neglect the multiphotonic nature of the absorption process and assume that the potentials are single-well and harmonic.

- [18] A. D. Becke, *Phys. Rev. A* **1988**, *38*, 3098–3100.
- [19] A. D. Becke, *J. Chem. Phys.* **1993**, *98*, 1372–1377.
- [20] C. D. Sherrill, M. S. Lee, M. Head-Gordon, *Chem. Phys. Lett.* **1999**, *302*, 425–430.
- [21] M. Sodupe, J. Bertran, L. Rodriguez-Santiago, E. J. Baerends, *J. Phys. Chem. A* **1999**, *103*, 166–170.
- [22] G. Pacchioni, F. Frigoli, D. Ricci, J. A. Weil, *Phys. Rev. B* **2001**, *63*, 054102; X. Solans-Monfort, V. Branchadell, M. Sodupe, M. Sierka, J. Sauer, *J. Chem. Phys.* **2004**, *121*, 6034–6041.
- [23] B. Tepper, B. Richter, A. C. Dupuis, H. Kuhlenbeck, C. Hucho, P. Schilbe, M. A. bin Yarmo, H.-J. Freund, *Surf. Sci.* **2002**, *496*, 64–72.
- [24] V. Brázdová, M. V. Ganduglia-Pirovano, J. Sauer, *Phys. Rev. B* **2004**, *69*, 165420.
- [25] In solid compounds, mixed-valence polyvanadate species, such as $V_{15}O_{36}^{5-}$, are found which also have a cage structure with terminal V=O groups, but contain triply coordinated O in addition to V–O–V bonds. See ref. [26].
- [26] A. Müller, E. Krickemeyer, M. Penk, H.-J. Walberg, H. Bögge, *Angew. Chem.* **1987**, *99*, 1060–1061; *Angew. Chem. Int. Ed. Engl.* **1987**, *26*, 1045–1046.
- [27] K. R. Asmis, M. Brümmer, C. Kaposta, G. Santambrogio, G. von Helden, G. Meijer, K. Rademann, L. Wöste, *Phys. Chem. Chem. Phys.* **2002**, *4*, 1101–1104.
- [28] a) R. Ahlrichs, M. Bär, M. Häser, H. Horn, C. Kölmel, *Chem. Phys. Lett.* **1989**, *162*, 165–169; b) O. Treutler, R. Ahlrichs, *J. Chem. Phys.* **1995**, *102*, 346–354; c) K. Eichkorn, O. Treutler, H. Öhm, M. Häser, R. Ahlrichs, *Chem. Phys. Lett.* **1995**, *242*, 652–660.
- [29] A. Schäfer, C. Huber, R. Ahlrichs, *J. Chem. Phys.* **1994**, *100*, 5829–5835.
- [30] P. Deglmann, F. Furche, R. Ahlrichs, *Chem. Phys. Lett.* **2002**, *362*, 511–518.

D.2 Vibrational Spectroscopy of Strong Hydrogen Bonds

Gas Phase Infrared Spectroscopy of Cluster Anions as a Function of Size: The Effect of Solvation on Hydrogen-Bonding in $\text{Br}^- \cdot (\text{HBr})_{1,2,3}$ Clusters

Nicholas L. Pivonka and Daniel M. Neumark

Department of Chemistry, University of California, Berkeley, California and Chemical Sciences Division, Lawrence Berkeley National Laboratory, Berkeley, California 94720, U.S.A.

Gert von Helden and Gerard Meijer

FOM Institute for Plasmaphysics Rijnhuizen, Edisonbaan 14, NL-3439 MN, Nieuwegein, The Netherlands and Department of Molecular and Laser Physics, University of Nijmegen, Toernooiveld, NL-6525 ED, Nijmegen, The Netherlands

Cristina Kaposta, Ludger Wöste, and Knut R. Asmis

Institut für Experimentalphysik, Freie Universität Berlin, Arnimallee 14, D-14195 Berlin, Germany

Full article in the *Journal of Chemical Physics* **117(14)** 6493-9 (2002).

Gas phase infrared spectroscopy of cluster anions as a function of size: The effect of solvation on hydrogen-bonding in $\text{Br}^{\cdot}(\text{HBr})_{1,2,3}$ clusters

Nicholas L. Pivonka

Department of Chemistry, University of California, Berkeley, California
and Chemical Sciences Division, Lawrence Berkeley National Laboratory, Berkeley, California 94720

Cristina Kaposta

Institut für Experimentalphysik, Freie Universität Berlin, Arnimallee 14, D 14195 Berlin, Germany

Gert von Helden

FOM Institute for Plasmaphysics Rijnhuizen, Edisonbaan 14, NL-3439 MN, Nieuwegein, The Netherlands

Gerard Meijer

FOM Institute for Plasmaphysics Rijnhuizen, Edisonbaan 14, NL-3439 MN, Nieuwegein,
The Netherlands and Department of Molecular and Laser Physics, University of Nijmegen, Toernooiveld,
NL-6525 ED, Nijmegen, The Netherlands

Ludger Wöste

Institut für Experimentalphysik, Freie Universität Berlin, Arnimallee 14, D 14195 Berlin, Germany

Daniel M. Neumark^{a)}

Department of Chemistry, University of California, Berkeley, California
and Chemical Sciences Division, Lawrence Berkeley National Laboratory, Berkeley, California 94720

Knut R. Asmis^{b)}

Institut für Experimentalphysik, Freie Universität Berlin, Arnimallee 14, D 14195 Berlin, Germany

(Received 24 May 2002; accepted 22 July 2002)

The gas phase vibrational spectroscopy of $\text{Br}^{\cdot}(\text{HBr})_{1,2,3}$ clusters has been studied between 6 and 16 μm (625 and 1700 cm^{-1}) by multiphoton infrared photodissociation spectroscopy using the output of the free electron laser for infrared experiments. Infrared (IR) spectra were recorded by monitoring the mass-selected ion yield. In all three systems neutral HBr loss is found to be the dominant photofragmentation channel. BrHBr^{\cdot} exhibits a weak absorption band at 1558 cm^{-1} which is assigned to the overtone of the antisymmetric stretching mode ν_3 . A series of strong absorption bands was observed for $\text{Br}^{\cdot}(\text{HBr})_2$ at energies in the 950–1450 cm^{-1} range. The $\text{Br}^{\cdot}(\text{HBr})_3$ spectra reveal two absorption bands at 884 and 979 cm^{-1} , which are assigned to two H-atom stretching modes. Evidence for the localization of the H atom and destruction of the symmetric BrHBr^{\cdot} hydrogen bond in the larger clusters is presented. Standard electronic structure calculations fail to reproduce the experimental IR spectra, indicating a breakdown of the harmonic approximation. © 2002 American Institute of Physics. [DOI: 10.1063/1.1506308]

I. INTRODUCTION

The hydrogen bond is one of the most important interactions in chemistry, governing diverse phenomena from the properties of liquids to the structure of proteins and DNA.¹ Hydrogen bonds are particularly appealing from the perspective of cluster spectroscopy, which can probe how the properties of a collection of molecules held together by hydrogen bonds evolve with size.² Such studies have shown, for example, how many of the properties of liquid water can be understood in terms of fundamental interactions between water molecules.³

Some of the strongest known hydrogen bonds are the symmetric bihalide anions XHX^{\cdot} (X=F, Cl, Br, I), with dis-

sociation energies ranging from 1.93 eV for FHF^{\cdot} to 0.73 eV for IHI^{\cdot} .⁴ Experiments and calculations indicate these anions to be symmetric, $D_{\infty h}$ species with two equal H–X bond lengths.^{5–16} These anions and their asymmetric counterparts, such as BrHI^{\cdot} , are also of interest as transition state precursors in negative ion photoelectron spectroscopy experiments.^{17,18} However, the very factor that causes these hydrogen bonds to be so strong, namely the extensive sharing of the H-atom between two halogen atoms, also makes these bonds highly susceptible to solvent perturbation that can, for example, destroy the symmetry of the bonds in symmetric XHX^{\cdot} anions. In this paper, we use the tunable infrared (IR) radiation from a free electron laser to obtain the first gas phase spectrum of BrHBr^{\cdot} and probe the effect of solvation on the hydrogen-bonding in this anion via IR spectroscopy of size-selected $\text{Br}^{\cdot}(\text{HBr})_n$ clusters.

Considerable recent progress has been made in the IR spectroscopy of hydrogen-bonded anion clusters, primarily

^{a)} Author to whom correspondence should be addressed. Electronic mail: dan@radon.cchem.berkeley.edu

^{b)} Author to whom correspondence should be addressed. Electronic mail: asmis@physik.fu-berlin.de

TABLE I. Experimental infrared band positions and intensities.

Parent ion	Fragment ion	Position (cm ⁻¹) and normalized intensity
BrHBr ⁻	Br ⁻	1558
Br ⁻ ·(HBr) ₂	BrHBr ⁻	~875 (0.05), ~940 (0.06), 992 (1.00), 1012 (0.74), 1048 (0.73), 1104 (0.75), 1147 (0.56), 1205 (0.16), 1222 (0.10), 1269 (0.10), 1289 (0.10), 1359 (0.66), 1420 (0.27)
Br ⁻ ·(HBr) ₃	Br ⁻ ·(HBr) ₂ BrHBr ⁻	888 (1.00), 979 (0.16) 884 (0.07), 934 (0.08), 984 (1.00), 1052 (0.11), 1098 (0.08), 1142 (0.06), 1203 (0.03), 1225 (0.01), 1264 (0.01), 1289 (0.01), 1359 (0.06), 1416 (0.04)

through IR predissociation experiments in which size-selected clusters are vibrationally excited with one or more IR photons, and then predissociate to daughter ions that can be detected with near-unit efficiency.^{19–23} This type of IR action spectroscopy is extremely sensitive and can be applied to mass-selected ion beams where number densities are as low as 10³–10⁴/cm³. These experiments require intense, tunable laser sources, and have thus been largely restricted to vibrational frequencies above 2350 cm⁻¹. However, for strongly hydrogen-bonded anions such as symmetric bihalides, the antisymmetric stretch (ν_3) fundamental is considerably lower than this; gas phase IR spectroscopy of FHF⁻ and ClHCl⁻ yields ν_3 frequencies of 1331 and 723 cm⁻¹, respectively,^{10,11} while matrix isolation spectroscopy of BrHBr⁻ yields ν_3 frequencies ranging from 728 to 753 cm⁻¹.^{8,12} Hence, the systematic study of the IR spectroscopy of bare and clustered bihalides requires a very different type of light source.

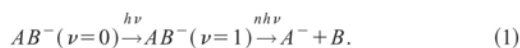
A novel approach to study the vibrational spectroscopy of cations in the spectral region below 2000 cm⁻¹ using infrared photodissociation (IRPD) spectroscopy has recently been demonstrated by Meijer and co-workers using the free electron laser for infrared experiments (FELIX) at the FOM-Institute Rijnhuizen.^{24–27} Multiphoton excitation IRPD spectra of selected polycyclic aromatic hydrocarbons were measured using excimer laser ionization followed with multiphoton excitation with a pulsed free electron laser (FEL) in the 400–1700 cm⁻¹ region. Asmis *et al.*²⁸ extended the technique to study mass-selected parent ions by coupling a tandem-mass spectrometer to the FEL source. In the present study, we apply this technique for the first time to investigate the vibrational spectroscopy of gas phase cluster anions. Our results indicate that the addition of one or more HBr solvent molecules to the BrHBr⁻ cluster destroys the symmetry of the BrHBr⁻ bond, with the resulting system resembling two or three HBr ligands bound to a Br⁻ core.

II. EXPERIMENT

Br⁻·(HBr)_{*n*} clusters are produced at the intersection of a pulsed supersonic molecular beam and a 1 keV, 300 μ A electron beam using an arrangement similar to that used in previous photoelectron spectroscopy studies of BrHBr⁻.¹⁸ The molecular beam is formed from a gas mixture of 4% HBr in Ar, which is expanded through a pulsed valve (General Valve) with a 780 μ m diameter orifice. The pulsed valve is

operated at 20 Hz with a stagnation pressure of 2–5 bar. Br⁻ ions are formed through dissociative electron attachment to HBr and are clustered and internally cooled as the supersonic expansion progresses. Anion clusters generated in the supersonic expansion pass a 2 mm skimmer into a previously described guided ion beam tandem mass spectrometer,²⁸ where they are mass-selected and subsequently trapped in a temperature-adjustable, helium filled radio frequency (RF) hexadecapole ion trap. The ion trap is kept at a constant temperature of ~50 K and He buffer gas pressure of ~80 μ bar.

Infrared excitation is performed with the output of FELIX.²⁹ The FELIX output is composed of 5 μ s long macropulses at 5 Hz, with each macropulse containing a series of ~1 ps micropulses separated by a nanosecond. The FELIX bandwidth is transform limited to ~0.8% of the central frequency and pulse energies of 50 and 25 mJ per macropulse (measured before the ZnSe optics) were employed in these experiments. The FELIX beam is directed through two ZnSe windows and focused within the ion trap by a 600 mm focal length ZnSe lens. The scan range for these experiments was limited by the IR transmission function of the ZnSe windows and lenses which was >85% between 8 and 14 μ m and dropped to <10% below 6 μ m and above 17 μ m. When FELIX is in resonance with an infrared transition of the trapped anion, multiple photon absorption and dissociation can occur, leading to production of ionic photofragments, as follows:



During a measurement cycle, the ion trap is allowed to fill for a period of 290 ms and the ions are then stored until a trigger signal from the FEL is received. During this time either two or three FELIX macropulses interact with the trapped ions, producing photofragment ions if multiphoton dissociation occurs. The trap is partially emptied over a period of 100 ms and the mass-selected ion yield is recorded as a function of the FEL wavelength. Depending on the signal intensity, this process is repeated over 5–20 fill/extraction cycles and for each fragment ion monitored. The stability of the parent ion production is checked by measuring the parent ion yield once at the beginning and once at the end of each wavelength step. The ion trap is completely emptied after

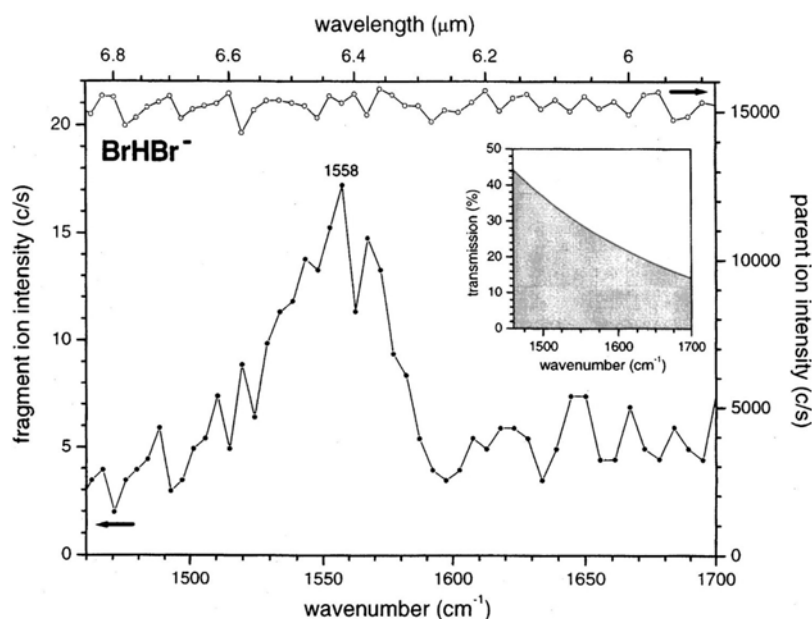


FIG. 1. Parent ion (open dots) and Br^- fragment ion (solid dots) IRPD spectrum of BrHBr^- . Inset shows transmission efficiency of ZnSe optics.

each wavelength step. A typical spectrum is measured in steps of 20–100 nm and takes roughly 30–60 min to record. Peak positions are summarized in Table I.

III. RESULTS

A. BrHBr^-

The IRPD spectrum of BrHBr^- in the range from 1460 to 1700 cm^{-1} is shown in Fig. 1. Both parent ion (open dots) and Br^- fragment ion (solid dots) intensities are plotted. The parent ion signal, which was measured with less signal averaging than the fragment ion signal, varies by $<10\%$ over the acquisition time. A single broad, weak absorption band is observed in the Br^- fragment ion yield (HBr loss channel) at 1558 cm^{-1} with a full width at half maximum of 60 cm^{-1} . Depletion of the parent ion signal is not resolved, because it is three orders of magnitude smaller than the parent ion signal itself. Coarser scans extending from 625 to 1700 cm^{-1} showed no additional features, nor did finer scans from 700– 800 cm^{-1} , where the ν_3 antisymmetric stretch fundamental is expected.^{7,8,12,15,16,30} A constant Br^- background signal resulting from collision induced dissociation of the BrHBr^- parent ions is observed. The Br^- background is on the order of 0.03% of the parent ion signal, and photofragmentation at 1558 cm^{-1} yields approximately three times the background signal. The transmission of the ZnSe optics (inset of Fig. 1) strongly decreases below $8\text{ }\mu\text{m}$ and varies by a factor of ~ 3 in the shown spectral region. As a result of this the band shape may be distorted due to the decreasing pulse energy at the interaction region.

B. $\text{Br}^-(\text{HBr})_2$

Figure 2 shows IRPD spectra of $\text{Br}^-(\text{HBr})_2$. The dominant photofragment channel is production of $\text{HBr} + \text{BrHBr}^-$

(solid dots). The parent ion depletion spectrum is also shown (top right corner). In contrast to BrHBr^- , the parent depletion is quite pronounced. At 992 cm^{-1} , the largest absorption band, roughly 85% of the parent ions are depleted, indicating that photofragmentation does not exclusively occur at the focus of IR beam, but extends over the complete irradiated region of the 23 cm long ion trap. Collisional fragmentation of $\text{Br}^-(\text{HBr})_2$ within the ion trap gave a small baseline BrHBr^- signal of $\sim 70\text{ c/s}$ over the entire scan range. The depletion and fragment ion spectra exhibit a strong correlation, with six distinct, strong absorption peaks appearing at 992, 1048, 1104, 1147, 1359, and 1420 cm^{-1} . The 992 cm^{-1} feature exhibits a shoulder at 1012 cm^{-1} , hinting at an addi-

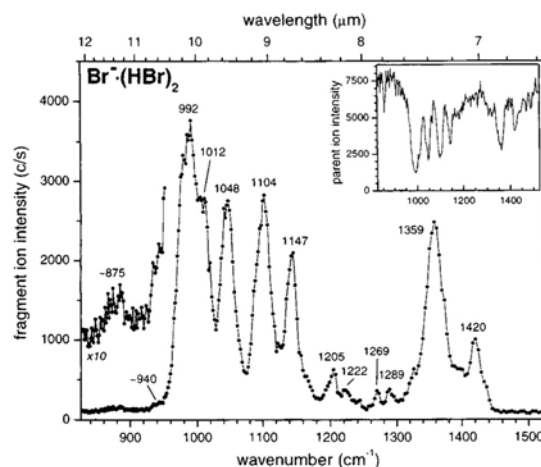


FIG. 2. BrHBr^- fragment ion IRPD spectrum of $\text{Br}^-(\text{HBr})_2$ (solid dots). Inset shows the corresponding $\text{Br}^-(\text{HBr})_2$ parent depletion spectrum.

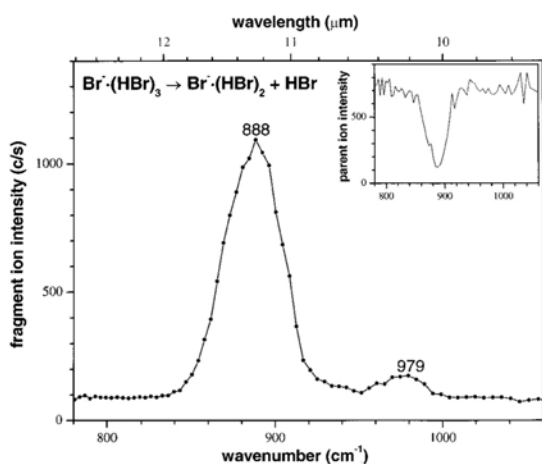


FIG. 3. $\text{Br}^-\cdot(\text{HBr})_2$ fragment ion IRPD spectrum of $\text{Br}^-\cdot(\text{HBr})_3$ (solid dots). Inset shows the corresponding $\text{Br}^-\cdot(\text{HBr})_3$ parent depletion spectrum.

tional, overlapping absorption band. Lorentzian fits of these peaks yield widths (FWHM) of 15–21 cm^{-1} , save the peak at 992 cm^{-1} , which is 40 cm^{-1} wide. Lower intensity absorption bands appear in the BrHBr^- fragment ion spectrum at 875, 940, 1205, 1222, 1269, and 1289 cm^{-1} . The fragment ion yield is not equivalent to the depletion signal, mainly due to the optimization of the mass spectrometer for parent ion detection. All observed peak widths are well in excess of the 8–11 cm^{-1} FELIX bandwidth. A background free Br^- fragment ion spectrum (not shown) was also acquired over the same wavelength range, but <0.2% of the total photoproducts appear as Br^- and no distinct features were observed.

C. $\text{Br}^-\cdot(\text{HBr})_3$

The IRPD spectroscopy of $\text{Br}^-\cdot(\text{HBr})_3$ was studied in the spectral range from 6 to 16 μm with macropulse energies of 50 mJ and 25 mJ (50% attenuation). At the lower laser power (Fig. 3) the dominant fragmentation products are $\text{Br}^-\cdot(\text{HBr})_2 + \text{HBr}$. Loss of two HBr units leading to the formation of BrHBr^- is also observed, but with considerably less efficiency (<1% at 888 cm^{-1}). The photofragment yield spectrum for $\text{Br}^-\cdot(\text{HBr})_2$ production (solid dots) shows two absorption bands at 888 and 979 cm^{-1} . At 888 cm^{-1} more than 80% of the parent ion signal is depleted (inset of Fig. 3). The width of the intense absorption band is >30 cm^{-1} and may be broadened in part from saturation effects. A constant background of $\text{Br}^-\cdot(\text{HBr})_2$ formed by He atom collision induced dissociation in the ion trap is also observed and amounts to <10% of the fragment ion intensity at the maximum of the main absorption band.

IRPD spectra of $\text{Br}^-\cdot(\text{HBr})_3$ taken at a FELIX power of 50 mJ/macropulse are shown in Fig. 4. The parent depletion spectrum differs considerably from the spectrum measured at lower laser power, exhibiting an additional, pronounced minimum at 979 cm^{-1} . Complete saturation of the 884 cm^{-1} transition is effected, with no residual parent ions observed. The single HBr loss spectrum (not shown) looks similar to

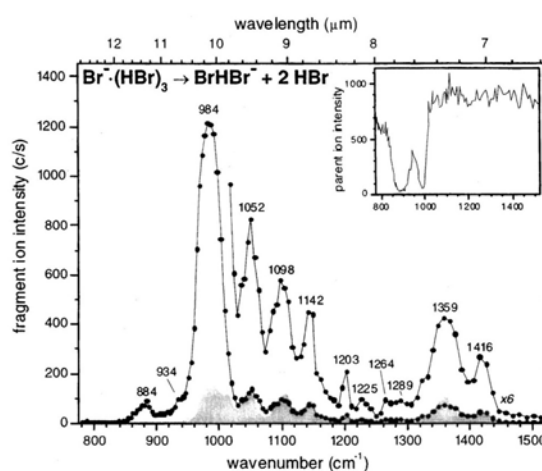
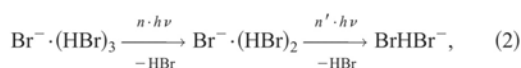


FIG. 4. BrHBr^- fragment ion IRPD spectrum of $\text{Br}^-\cdot(\text{HBr})_3$ (solid dots). Gray shaded area shows the $\text{Br}^-\cdot(\text{HBr})_2$ IRPD spectrum. Inset shows the corresponding $\text{Br}^-\cdot(\text{HBr})_3$ parent depletion spectrum.

the one measured at lower laser power (see Fig. 3), but saturation effects significantly broaden the absorption peaks. However, the intensity of the $\text{BrHBr}^- + 2\text{HBr}$ channel (solid dots, Fig. 4) increases significantly at higher power and looks quite different from the single HBr loss channel in Fig. 3. In particular, the BrHBr^- channel is much more intense at 984 cm^{-1} than at 884 cm^{-1} , totally opposite to the intensity distribution in Fig. 3. In addition, a series of much smaller peaks at higher frequency are observed that do not appear in Fig. 3 nor in the parent depletion spectrum in Fig. 4.

The differences between Figs. 3 and 4 arise from two effects. The peak at 984 cm^{-1} nearly coincides with the peak at 992 cm^{-1} in the IRPD spectrum of $\text{Br}^-\cdot(\text{HBr})_2$ in Fig. 2. We therefore attribute the 984 cm^{-1} peak in Fig. 4 to a sequential process producing BrHBr^- ,



where $h\nu$ is resonant with a vibrational fundamental in both the $n=2$ and $n=3$ clusters. The small peaks seen in the 1000–1500 cm^{-1} region of the spectrum in Fig. 4 appear at the same locations as peaks in the $\text{Br}^-\cdot(\text{HBr})_2$ IRPD spectrum (Fig. 2 and also shown in the gray shaded area of Fig. 4) discussed in the previous section, and these are attributed exclusively to the IRPD of $\text{Br}^-\cdot(\text{HBr})_2$ produced by collisional fragmentation of $\text{Br}^-\cdot(\text{HBr})_3$ in the ion trap. The intensity of the gray shaded peaks is consistent with the magnitude of $\text{Br}^-\cdot(\text{HBr})_2$ fragments observed in the trap in the absence of FELIX excitation, and the absorption cross section of $\text{Br}^-\cdot(\text{HBr})_2$.

D. Electronic structure calculations

A sophisticated theoretical treatment of BrHBr^- has been reported recently, in which vibrational energy levels on a multidimensional potential energy surface were

TABLE II. Normal modes, harmonic vibrational frequencies, and oscillator strengths for the C_{2v} ground state of $\text{Br}^{\cdot-}(\text{HBr})_2$ calculated at the B3LYP/aug-cc-pVTZ level of theory.

Symmetry	Frequency (cm ⁻¹)	Intensity (km/mol)	Description
a_1	1662	1776	symmetric H-atom stretch
b_2	1453	7285	antisymmetric H-atom stretch
a_1	632	<1	in-plane synchronous H-atom wag
a_2	585	0	out-of-plane asynchronous H-atom wag
b_2	568	33	in-plane asynchronous H-atom wag
b_1	567	2	out-of-plane synchronous H-atom wag
a_1	106	13	symmetric Br-Br stretch
b_2	98	123	antisymmetric Br-Br stretch
a_1	11	≪1	Br-Br bend

determined.¹⁶ However, no calculations of any sort have been done for the larger clusters. Therefore, optimized geometries and vibrational frequencies were calculated for the $\text{Br}^{\cdot-}(\text{HBr})_{2,3}$ clusters at the B3LYP (Ref. 31) level of theory, employing the Dunning correlation consistent split valence triple zeta basis set with diffuse functions (aug-cc-pVTZ) (Refs. 32–34) as packaged in GAUSSIAN 98.³⁵ Calculated harmonic vibrational frequencies, IR intensities, and approximate mode descriptions for both clusters are listed in Tables II and III. The minimum energy structures found are shown in Fig. 5. $\text{Br}^{\cdot-}(\text{HBr})_2$ exhibits a C_{2v} minimum energy structure with two HBr ligands complexed to a central $\text{Br}^{\cdot-}$. Addition of a third HBr ligand yields a C_{3v} minimum energy structure for $\text{Br}^{\cdot-}(\text{HBr})_3$.

The inner HBr bond lengths for the $n=2$ and 3 clusters were found to be 2.03 and 2.16 Å and the terminal HBr bond lengths were calculated to be 1.53 and 1.49 Å. The terminal HBr bond lengths in the $n=2$ and 3 clusters are nearer the unperturbed HBr bond length of 1.4144 Å (Ref. 36) than the previously calculated¹⁶ HBr bond lengths of 1.73 Å in $\text{BrHBr}^{\cdot-}$. The Br-Br distances increase by ~0.1 Å per additional HBr ligand. The calculations predict that the addition of even a single HBr to $\text{BrHBr}^{\cdot-}$ destroys the symmetrical hydrogen bond in the bihalide; the two larger cluster ions are

TABLE III. Normal modes, harmonic vibrational frequencies, and oscillator strengths for the C_{3v} ground state of $\text{Br}^{\cdot-}(\text{HBr})_3$ calculated at the B3LYP/aug-cc-pVTZ level of theory.

Symmetry	Frequency (cm ⁻¹)	Intensity (km/mol)	Description
a_1	1981	480	symmetric H atom stretch
e	1807	4669	antisymmetric H atom stretch
e	559	≪1	H atom wag
a_1	527	2	H atom wag
a_2	514	0	H atom wag
e	512	1	H atom wag
e	101	46	antisymmetric HBr stretch
a_1	90	2	symmetric HBr stretch
e	12	≪1	HBr wag
a_1	11	≪1	intramolecular umbrella

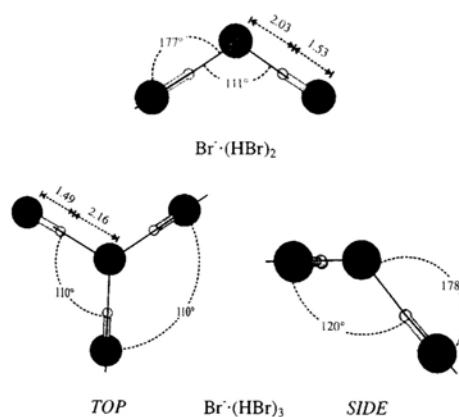


FIG. 5. Structures of $\text{Br}^{\cdot-}(\text{HBr})_2$ (above) and $\text{Br}^{\cdot-}(\text{HBr})_3$ (below) calculated at the B3LYP/aug-cc-pVTZ level of theory. Upper panel shows bond lengths and angles for the C_{2v} $\text{Br}^{\cdot-}(\text{HBr})_2$ complex. Lower panel shows top and side views of the C_{3v} $\text{Br}^{\cdot-}(\text{HBr})_3$ complex ion. H-Br-H and Br-Br-Br bond angles are indicated in the top view, along with inner and outer H-Br bond lengths (Å). Side view shows slight deviation from linearity in the Br-H-Br bond, and also illustrates the 120° dihedral of the third HBr ligand.

better represented as HBr ligands complexed to a central bromide ion. The effect of solvation on binary hydrogen bonds in negatively charged species was recently probed by Robertson *et al.* in an IR study of $\text{Cl}^{\cdot-}(\text{H}_2\text{O})(\text{CCl}_4)_n$ clusters, where addition of a single CCl_4 molecule was shown to perturb the Cl-H-O bond length.³⁷

These trends are reflected in the calculated frequencies and intensities in Tables II and III, according to which the IR spectroscopy of the $n=2$ and $n=3$ clusters should be dominated by two modes representing symmetric and antisymmetric linear combinations of HBr stretches. The calculated frequencies for these modes lie between the $\text{BrHBr}^{\cdot-}$ antisymmetric stretch, 753 cm⁻¹, and the HBr fundamental at 2559 cm⁻¹, indicating significant and increasing perturbation of the hydrogen bond in $\text{BrHBr}^{\cdot-}$ by the additional HBr molecules.

The zero point corrected binding energies of a single HBr ligand to $\text{Br}^{\cdot-}(\text{HBr})_2$ and $\text{Br}^{\cdot-}(\text{HBr})_3$ were calculated to be 2963 and 3918 cm⁻¹. The HBr binding energy of $\text{BrHBr}^{\cdot-}$ calculated by the same method was 7582 cm⁻¹, which agrees reasonably well with the experimental binding energy of 7480 cm⁻¹ reported by Caldwell *et al.*⁴

The C_{2v} structure calculated for $\text{Br}^{\cdot-}(\text{HBr})_2$ is consistent with past experimental and theoretical work on $\text{Cl}^{\cdot-}(\text{HCl})_2$ and $\text{F}^{\cdot-}(\text{HF})_2$ which showed similar structures for these clusters.^{38–44} Likewise, the C_{3v} structure calculated for $\text{Br}^{\cdot-}(\text{HBr})_3$ confirms the trend observed in previously calculated structures for $\text{F}^{\cdot-}(\text{HF})_3$ and $\text{Cl}^{\cdot-}(\text{HCl})_3$ which predicted a geometry change from D_{3h} to C_{3v} in the transition from fluorine to chlorine.^{38,39,42}

IV. DISCUSSION

The observed absorption band of $\text{BrHBr}^{\cdot-}$ at 1558 cm⁻¹ is assigned to the overtone of the ν_3 absorption band previ-

ously observed at 728 and 753 cm^{-1} in matrix IR studies.^{8,12} The high negative anharmonicity implied by this assignment is consistent with the calculations by Del Bene and Jordan,¹⁶ who find a substantial negative anharmonicity for the ν_3 mode in FHF^- , ClHCl^- , and BrHBr^- .

For $\text{Br}^-(\text{HBr})_2$, using the calculated results in Table II as a guide, the experimental peaks at 1359 and 1420 cm^{-1} are closest in frequency to the calculated harmonic frequencies of 1453 and 1662 cm^{-1} for the b_2 and a_1 antisymmetric and symmetric HBr stretches, and the experimental and calculated relative intensities of the two peaks agree reasonably well. The calculated frequencies for the corresponding modes in $\text{Br}^-(\text{HBr})_3$ are higher and would be out of range of the instrument due to the ZnSe windows. One would then assign the peaks around 1000 cm^{-1} for the two clusters to combination bands of the various bending modes for which the calculated fundamentals lie between 500–600 cm^{-1} . However, this assignment is problematic because the calculated IR intensities for the bend fundamentals are several orders of magnitude lower than for the HBr stretches, whereas in the experimental spectrum for $\text{Br}^-(\text{HBr})_2$, the peaks around 1000 cm^{-1} are more intense than the 1359/1416 cm^{-1} doublet.

These considerations lead one to question the reliability of the calculated harmonic frequencies for the asymmetric hydrogen bonds in these clusters. Indeed, in a theoretical study BrHI^- , a prototypical asymmetric bihalide, by Morokuma and co-workers,⁴⁵ the harmonic frequency of the ν_3 mode obtained was found to be 1779 cm^{-1} , substantially higher than the 1267 cm^{-1} frequency obtained by constructing a full three-dimensional surface for BrHI^- and calculating the eigenvalues, and higher still than either of the two reported matrix IR spectroscopy values, 666 and 920 cm^{-1} .⁶ Additionally, the harmonic antisymmetric H-atom stretch of the asymmetric $\text{F}^-(\text{HF})_2$ complex was calculated at 2364 cm^{-1} ,⁴⁰ while experimental work placed the frequency at 1815 cm^{-1} .⁴⁴ As an alternate assignment, the bands at 992 and 1048 cm^{-1} for $\text{Br}^-(\text{HBr})_2$ and 888 and 979 cm^{-1} for $\text{Br}^-(\text{HBr})_3$ could be the fundamentals of the two H-atom stretch vibrations. The higher frequency peaks in the $\text{Br}^-(\text{HBr})_2$ spectrum then result from combination bands; comparison with Table II suggests the likeliest candidates are the b_2 H-atom wag and antisymmetric Br–Br stretch modes, with calculated frequencies of 568 and 98 cm^{-1} , respectively, and small but nonzero IR intensities. While neither set of assignments is wholly satisfactory, both place the antisymmetric HBr stretch at a considerably higher frequency than the ν_3 fundamental in BrHBr^- , providing experimental evidence for destruction of the symmetric hydrogen bond and localization of the H atom in the larger clusters.

Comparison of the three ions studied here suggests that BrHBr^- lies in a different regime with respect to multiphoton absorption and dissociation than the two larger clusters. In the generally accepted picture of multiphoton absorption and dissociation within the low field approximation (the maximum photon flux at the interaction region is on the order of 10^{11} W/cm^2),^{46,47} absorption of the first few photons occurs within the “discrete” regime, in which the photons resonantly excite a particular vibrational mode of a molecule.

Higher excitation accesses the “quasicontinuum” regime in which the density of states is so high that the vibrational energy is rapidly randomized among all vibrational modes of the molecule; the transition between the two regimes depends on the vibrational density of states and the strengths of the interactions between vibrational modes. The molecule continues to absorb photons until the dissociation rate exceeds the up-pumping rate.

In BrHBr^- , the ν_3 mode exhibits significant negative anharmonicity; the fundamental frequency is 730–750 cm^{-1} , but the first overtone is centered at 1558 cm^{-1} . Hence, the absence of the fundamental and low dissociation yield for BrHBr^- for the overtone indicates that the discrete regime acts as an anharmonic bottleneck, with one-color excitation unable to resonantly excite both the 1–0 and 2–1 transitions. On the other hand, observation of the overtone transition suggests the density of states near 3000 cm^{-1} is sufficiently high for absorption of the second (and subsequent) photon to occur under the conditions of our experiment. In addition, ~ 10 collisions with the He buffer gas occur during the 5 μs duration of each macropulse, resulting in additional state mixing that can facilitate multiphoton absorption.

In the $\text{Br}^-(\text{HBr})_{2,3}$ clusters, the additional HBr ligands raises the vibrational density of states relative to BrHBr^- , and based on the calculations in Sec. III, the dissociation energies are lower. The breakdown of the harmonic approximation for the description of the H-atom stretch modes also hints at a considerable coupling of the vibrational modes. All three effects favor multiphoton absorption and dissociation, consistent with the much higher signals seen for the two larger clusters. Hence, these clusters behave more like the cation clusters previously studied with FELIX.^{28,48}

The results presented here show that IRPD studies with FELIX can access the vibrational spectroscopy of anions spanning a wide size range, and in particular can be applied to anions with as few as three atoms. It is therefore an ideal method for observing the size-dependence of the vibrational spectroscopy of anion clusters over an extended frequency range that has previously been inaccessible. In the case of the hydrogen bonded clusters studied here, the inclusion of anharmonic effects is a prerequisite for an adequate theoretical description of the IR spectra of these species.

ACKNOWLEDGMENTS

This work is funded by the Sonderforschungsbereich 546 and the Ph.D. Graduate Study Program 788 of the Deutsche Forschungsgemeinschaft. United States Air Force Office of Scientific Research Grant No. F49620-00-1-0018 provided support for N.L.P. The authors gratefully acknowledge the support of the *Stichting voor Fundamenteel Onderzoek der Materie* (FOM) in providing the required beam time on FELIX and highly appreciate the skillful assistance of the FELIX staff, in particular Dr. A. F. G. van der Meer. This work was supported in part under the “Access to research infrastructure action of the Improving Human Potential Program” of the European Community. The authors would like to thank Professor Dr. W. J. Buma of the University of Amsterdam for the loan of HBr gas.

- ¹G. C. Pimentel and A. L. McClellan, *The Hydrogen Bond* (Freeman, San Francisco, 1960).
- ²U. Buck and F. Huisken, *Chem. Rev.* **100**, 3863 (2000).
- ³F. N. Keutsch and R. J. Saykally, *PNAS* **98**, 10533 (2001).
- ⁴G. Caldwell and P. Kebarle, *Can. J. Chem.* **63**, 1399 (1985).
- ⁵J. Emsley, *Chem. Soc. Rev.* **9**, 91 (1980).
- ⁶B. S. Ault, *Acc. Chem. Res.* **15**, 103 (1982).
- ⁷V. Bondybey, G. C. Pimentel, and P. N. Noble, *J. Chem. Phys.* **55**, 540 (1971).
- ⁸D. E. Milligan and M. E. Jacox, *J. Chem. Phys.* **55**, 2550 (1971).
- ⁹K. Kawaguchi and E. Hirota, *J. Chem. Phys.* **84**, 2953 (1986).
- ¹⁰K. Kawaguchi and E. Hirota, *J. Chem. Phys.* **87**, 6838 (1987).
- ¹¹K. Kawaguchi, *J. Chem. Phys.* **88**, 4186 (1988).
- ¹²C. L. Lugez, M. E. Jacox, and W. E. Thompson, *J. Chem. Phys.* **105**, 3901 (1996).
- ¹³C. L. Janssen, W. D. Allen, H. F. Schaefer, and J. M. Bowman, *Chem. Phys. Lett.* **131**, 352 (1986).
- ¹⁴A. B. Sannigrahi and S. D. Peyerimhoff, *Chem. Phys. Lett.* **148**, 197 (1988).
- ¹⁵S. Ikuta, T. Saitoh, and O. Nomura, *J. Chem. Phys.* **93**, 2530 (1990).
- ¹⁶J. E. Del Bene and M. J. T. Jordan, *Spectrochim. Acta, Part A* **55**, 719 (1999).
- ¹⁷S. E. Bradforth, A. Weaver, D. W. Arnold, R. B. Metz, and D. M. Neumark, *J. Chem. Phys.* **92**, 7205 (1990).
- ¹⁸R. B. Metz, A. Weaver, S. E. Bradforth, T. N. Kitsopoulos, and D. M. Neumark, *J. Phys. Chem.* **94**, 1377 (1990).
- ¹⁹M. S. Johnson, K. T. Kuwata, C. K. Wong, and M. Okumura, *Chem. Phys. Lett.* **260**, 551 (1996).
- ²⁰C. G. Bailey, J. Kim, C. E. H. Dessent, and M. A. Johnson, *Chem. Phys. Lett.* **269**, 122 (1997).
- ²¹P. Ayotte, G. H. Weddle, J. Kim, and M. A. Johnson, *Chem. Phys.* **239**, 485 (1998).
- ²²O. M. Cabarcos, C. J. Weinheimer, J. M. Lisy, and S. S. Xantheas, *J. Chem. Phys.* **110**, 5 (1999).
- ²³P. S. Weiser, D. A. Wild, and E. J. Bieske, *J. Chem. Phys.* **110**, 9443 (1999).
- ²⁴H. Piest, G. von Helden, and G. Meijer, *J. Chem. Phys.* **110**, 2010 (1999).
- ²⁵J. Oomens, A. J. A. van Roij, G. Meijer, and G. von Helden, *Astrophys. J.* **542**, 404 (2000).
- ²⁶J. Oomens, B. G. Sartakov, A. G. G. M. Tielens, G. Meijer, and G. von Helden, *Astrophys. J. Lett.* **560**, L99 (2001).
- ²⁷J. Oomens, G. Meijer, and G. von Helden, *J. Phys. Chem. A* **105**, 8302 (2001).
- ²⁸K. R. Asmis, M. Brummer, C. Kaposta, G. Santambrogio, G. von Helden, G. Meijer, K. Rademann, and L. Woste, *Phys. Chem. Chem. Phys.* **4**, 1101 (2002).
- ²⁹D. Oepts, A. F. G. Vandermeer, and P. W. Vanamersfoort, *Infrared Phys. Technol.* **36**, 297 (1995).
- ³⁰M. Rasanen, J. Seetula, and H. Kunttu, *J. Chem. Phys.* **98**, 3914 (1993).
- ³¹A. D. Becke, *J. Chem. Phys.* **98**, 5648 (1993).
- ³²T. H. Dunning, *J. Chem. Phys.* **90**, 1007 (1989).
- ³³R. A. Kendall, T. H. Dunning, and R. J. Harrison, *J. Chem. Phys.* **96**, 6796 (1992).
- ³⁴A. K. Wilson, D. E. Woon, K. A. Peterson, and T. H. Dunning, *J. Chem. Phys.* **110**, 7667 (1999).
- ³⁵M. J. Frisch, G. W. Trucks, H. B. Schlegel *et al.*, GAUSSIAN 98, Gaussian, Inc., Pittsburgh, PA, 1998.
- ³⁶D. H. Rank, U. Fink, and T. A. Wiggins, *J. Mol. Spectrosc.* **18**, 170 (1965).
- ³⁷W. H. Robertson, G. H. Weddle, J. A. Kelley, and M. A. Johnson, *J. Phys. Chem. A* **106**, 1205 (2002).
- ³⁸W. D. Chandler, K. E. Johnson, and J. L. E. Campbell, *Inorg. Chem.* **34**, 4943 (1995).
- ³⁹W. D. Chandler, K. E. Johnson, B. D. Fahlman, and J. L. E. Campbell, *Inorg. Chem.* **36**, 776 (1997).
- ⁴⁰V. P. Bulychev, G. S. Denisov, H. H. Limbach, and R. M. Shukailov, *Opt. Spectrosc.* **90**, 356 (2001).
- ⁴¹J. E. Del Bene, M. J. T. Jordan, S. A. Perera, and R. J. Bartlett, *J. Phys. Chem. A* **105**, 8399 (2001).
- ⁴²K. N. Rankin, W. D. Chandler, and K. E. Johnson, *Can. J. Chem.* **77**, 1599 (1999).
- ⁴³T. von Rosenvinge, M. Parrinello, and M. L. Klein, *J. Chem. Phys.* **107**, 8012 (1997).
- ⁴⁴R. D. Hunt and L. Andrews, *J. Chem. Phys.* **87**, 6819 (1987).
- ⁴⁵A. Kaledin, S. Skokov, J. M. Bowman, and K. Morokuma, *J. Chem. Phys.* **113**, 9479 (2000).
- ⁴⁶A. S. Sudbo, P. A. Schulz, E. R. Grant, Y. R. Shen, and Y. T. Lee, *J. Chem. Phys.* **70**, 912 (1979).
- ⁴⁷M. Quack, *Ber. Bunsenges. Phys. Chem.* **83**, 757 (1979).
- ⁴⁸D. Heijnsbergen, M. A. Duncan, G. Meijer, and G. von Helden, *Chem. Phys. Lett.* **349**, 220 (2001).

**Probing a Strong Hydrogen Bond with Infrared Spectroscopy:
Vibrational Predissociation of $\text{BrHBr}^- \cdot \text{Ar}$**

Nicholas L. Pivonka and Daniel M. Neumark

*Department of Chemistry, University of California, Berkeley, California and Chemical Sciences Division,
Lawrence Berkeley National Laboratory, Berkeley, California 94720, U.S.A.*

Gert von Helden and Gerard Meijer

*FOM Institute for Plasmaphysics Rijnhuizen, Edisonbaan 14, NL-3439 MN, Nieuwegein, The
Netherlands and Department of Molecular and Laser Physics, University of Nijmegen, Toernooiveld, NL-
6525 ED, Nijmegen, The Netherlands*

Cristina Kaposta, Mathias Brümmer, Ludger Wöste, and Knut R. Asmis

Institut für Experimentalphysik, Freie Universität Berlin, Arnimallee 14, D 14195 Berlin, Germany

Communication in *Journal of Chemical Physics* **118** 5275-8 (2003).

COMMUNICATIONS

**Probing a strong hydrogen bond with infrared spectroscopy:
Vibrational predissociation of $\text{BrHBr}^- \cdot \text{Ar}$**

Nicholas L. Pivonka

Department of Chemistry, University of California, Berkeley, California 94720 and Chemical Sciences Division, Lawrence Berkeley National Laboratory, Berkeley, California 94720

Cristina Kaposta and Mathias Brümmer

Institut für Experimentalphysik, Freie Universität Berlin, Arnimallee 14, D 14195 Berlin, Germany

Gert von Helden

FOM Institute for Plasmaphysics Rijnhuizen, Edisonbaan 14, NL-3439 MN, Nieuwegein, The Netherlands

Gerard Meijer

FOM Institute for Plasmaphysics Rijnhuizen, Edisonbaan 14, NL-3439 MN, Nieuwegein, The Netherlands; Department of Molecular and Laser Physics, University of Nijmegen, Toernooiveld, NL-6525 ED, Nijmegen, The Netherlands; and Department of Molecular Physics, Fritz Haber Institute of the Max Planck Society, Faradayweg 4-6, Berlin, Germany

Ludger Wöste

*Institut für Experimentalphysik, Freie Universität Berlin, Arnimallee 14, D 14195 Berlin, Germany*Daniel M. Neumark^{a)}*Department of Chemistry, University of California, Berkeley, California 94720 and Chemical Sciences Division, Lawrence Berkeley National Laboratory, Berkeley, California 94720*Knut R. Asmis^{a)}*Institut für Experimentalphysik, Freie Universität Berlin, Arnimallee 14, D 14195 Berlin, Germany*

(Received 4 November 2002; accepted 21 January 2003)

The gas phase vibrational spectroscopy of BrHBr^- , a prototypical strongly hydrogen-bonded species, has been studied between 6 and 17 μm (590 and 1670 cm^{-1}) by infrared vibrational predissociation of the $\text{BrHBr}^- \cdot \text{Ar}$ ion. Infrared excitation was accomplished using the output of the free electron laser for infrared experiments (FELIX). Predissociation spectra were recorded by monitoring depletion of mass-selected $\text{BrHBr}^- \cdot \text{Ar}$ ions as a function of excitation wavelength. Four prominent absorption bands are observed at 733, 890, 1048, and 1201 cm^{-1} . They are assigned to the fundamental of the hydrogenic stretching mode ν_3 and a sequence of $\nu_3 + n\nu_1$ combinations ($n = 1-3$). Additional features to the blue of these bands spaced by $\sim 21 \text{ cm}^{-1}$ are attributed to combination bands involving motion of the Ar messenger atom. Differences in the relative intensities of the $\nu_3 + n\nu_1$ combinations bands in comparison to previous matrix experiments are rationalized on the basis of the underlying dissociation dynamics. © 2003 American Institute of Physics. [DOI: 10.1063/1.1559478]

Hydrogen bonding governs a number of diverse and important chemical interactions, ranging from the solvent properties of water and other liquids to the structure of proteins and nucleic acids.¹ An important classification used in this context is based on the strength of the hydrogen bond, which is reflected in the distance between the heteroatoms sharing the hydrogen atom. As the bond strength increases, the distance between the heteroatoms as well as the hydrogen exchange barrier decreases. In the limit of strong or low-barrier hydrogen bonds, the barrier to hydrogen exchange has dropped below the zero point vibration, and the hydrogen assumes a symmetric position between the heteroatoms. These types of hydrogen bonds play an important role in both enzyme catalysis^{2,3} and proton exchange phenomena in acidic and basic aqueous solutions (e.g., H_3O_2^- and H_5O_2^+).^{4,5}

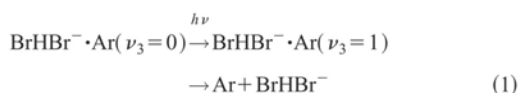
The simplest strongly hydrogen-bonded species are the triatomic bihalide anions XHX^- and XHY^- . The vibrational spectroscopy of these anions has been studied extensively in cryogenic matrices.⁶ This work showed that the hydrogenic stretching frequencies were extremely low, ranging from 1330 cm^{-1} in FHF^- to 645 cm^{-1} in IHI^- , in contrast to the uncomplexed HX frequencies of 4138 cm^{-1} in HF and 2309 cm^{-1} in HI.^{7,8} This frequency shift is a direct consequence of extensive sharing of the central hydrogen between the two halogen atoms. However, these studies indicated that the effects of the matrix on the vibrational frequencies could be significant, providing strong motivation to measure the unperturbed gas phase infrared (IR) spectra of these bihalide anions. High resolution gas phase IR spectra over narrow frequency ranges have been measured for FHF^- and ClHCl^- using diode laser absorption.⁹⁻¹² In this paper, we report a

different and more general approach to gas phase ion vibrational spectroscopy, combining excitation by means of a tunable infrared free electron laser [free electron laser for infrared experiments (FELIX)] with vibrational predissociation spectroscopy.^{13–15} The result is the first broadband infrared spectrum (from 590–1670 cm^{-1}) of a gas phase bihalide anion, BrHBr^- , measured by vibrational predissociation of $\text{BrHBr}^- \cdot \text{Ar}$.

The bihalide anion BrHBr^- is believed to be symmetric ($D_{\infty h}$),⁶ and its high dissociation energy of 0.93 eV makes it a model strong hydrogen bonding system.¹⁶ Inorganic salt and solution phase experiments yielded the first IR absorptions attributed to the BrHBr^- complex in the region between 500 and 1300 cm^{-1} .¹⁷ Further IR absorption experiments performed by several groups in rare gas matrices assigned asymmetric stretch absorptions between 646 and 753 cm^{-1} .^{18–21} These experiments also yielded $\nu_3 + n\nu_1$ combination bands, with $(\nu_3 + \nu_1) - \nu_3$ values near 160 cm^{-1} .

Evaluation of the BrHBr^- infrared spectrum through electronic structure calculations is complicated by the strong coupling between the vibrational modes. Del Bene and Jordan²² have shown that vibrational frequencies determined by one-dimensional harmonic analysis are inadequate, regardless of the level of theory used in the calculation, and that it is instead necessary to construct a two-dimensional potential energy surface upon which energy levels involving symmetric and asymmetric stretch excitation can be computed accurately. Their calculated frequencies agree well with the earliest sets of Ar matrix results.^{18–20}

For many years, the photoelectron spectrum of BrHBr^- has represented the only gas phase data on this anion.^{23,24} However, as part of a recent study of larger clusters, we performed tunable infrared multiphoton dissociation (IRMPD) experiments on BrHBr^- using a free electron laser and observed a single broad peak near 1550 cm^{-1} ; this feature was tentatively assigned to the overtone of the ν_3 vibrational mode.²⁵ The IRMPD approach, which relies on a high density of states to overcome the anharmonic bottleneck in the multiphoton dissociation process, was less than ideal for bare BrHBr^- with its relatively high HBr binding energy (7480 cm^{-1}) and low number of vibrational degrees of freedom.¹⁶ Drawing on previous cation and anion spectroscopy experiments by Lee¹³ and Johnson,^{14,15} we present results here on the vibrational predissociation of $\text{BrHBr}^- \cdot \text{Ar}$. The Ar atom acts as a “messenger” or “spy” atom, and its expected low binding energy allows detection of the absorption of a *single* IR photon via vibrational predissociation:



By monitoring depletion of the $\text{BrHBr}^- \cdot \text{Ar}$ complex or production of BrHBr^- as a function of excitation energy, the vibrational spectrum of BrHBr^- can be obtained.

The present experiments were carried out on a previously described tandem mass spectrometer ion trap system.²⁶ Briefly, $\text{BrHBr}^- \cdot \text{Ar}$ cluster anions are created by crossing a

pulsed supersonic expansion of $\sim 0.1\%$ HBr in Ar with a 300 μA , 1 keV electron beam. The supersonic expansion is generated by a pulsed valve operating at 100 Hz with a backing pressure of 5 bar. The anions pass through a 2 mm skimmer, are collimated by a linear radio frequency (RF) ion guide, then mass-selected by a quadrupole mass spectrometer. Subsequently the mass-selected ions are collected in a He filled linear RF hexadecapole ion trap which is connected to a helium cryostat and kept at a temperature of < 70 K. Collisions with the He buffer gas (~ 0.03 mbar) slow the ions and cool them to the ambient temperature. Roughly 80% of the (“fast”) $\text{BrHBr}^- \cdot \text{Ar}$ ions entering the ion trap fragment through collisions with the He atoms, forming BrHBr^- . Because of this wavelength independent BrHBr^- background signal, a better signal-to-noise ratio is achieved by monitoring $\text{BrHBr}^- \cdot \text{Ar}$ depletion rather than the BrHBr^- formation.

The ion trap is continuously filled for 160 ms. Trapped ions interact with a single macropulse of the 5 Hz output of FELIX, composed of 5 μs long macropulses, with each macropulse comprising a series of ~ 1 ps micropulses separated by a nanosecond.²⁷ Pulse energies used in these experiments were on the order of 15 mJ/macropulse, with a Gaussian bandwidth of $\sim 0.8\%$ of the central energy (FWHM). The output of FELIX was introduced into the ion trap region through a KBr lens (focal length 478 mm) and a 5 mm thick KBr window. Focusing of the FELIX beam is required to avoid light scattering off the ion trap exit and entrance lenses. One millisecond after irradiation, the ion trap is emptied, and the $\text{BrHBr}^- \cdot \text{Ar}$ signal is mass-selectively monitored using a (second) quadrupole mass spectrometer. The ion trap is then refilled again and the cycle repeated multiple times at each wavelength step in order to assure sufficient signal averaging.

Infrared predissociation spectra of $^{81}\text{Br}^{81}\text{Br}^- \cdot \text{Ar}$ are shown in Fig. 1. Observed peak positions and assignments are listed in Table 1. Overview scans (main spectrum) were measured from 6 to 17 μm with a step size of 0.1 μm . Higher resolution spectra (step size: 0.01–0.02 μm) were measured with an increased number of shots per data point in selected regions and are shown in the inset. Four prominent depletion features are readily identifiable at 733, 890, 1048 and 1201 cm^{-1} . Gaussian peak widths (FWHM) were found to be 15, 13, 11, and 10 cm^{-1} and are chiefly limited by the bandwidth of FELIX. An assignment of these features based on the previous matrix experiments is straightforward (see Tables 1 and 2). The peak at 733 cm^{-1} is assigned to the fundamental of the $\text{BrHBr}^- \nu_3$ mode and the sequence observed at shorter wavelengths to $\nu_3 + n\nu_1$ ($n = 1–3$) combinations bands involving the symmetric stretch vibration. Weaker features are observed in the (smoothed) higher resolution spectra at 754, 775, 911, 929 and 1070 cm^{-1} , which we attribute to combination bands involving excitation of the Ar motion with a characteristic fundamental frequency of 21 cm^{-1} . There is also suggestion of a weak depletion feature near 650 cm^{-1} , in the anticipated region of the ν_2 fundamental, but further study will be necessary to confirm this observation.

In the overview spectra, depletion of the parent ion signal is as high as $\sim 75\%$, with baseline fluctuations on the

TABLE I. Observed depletion features, bandwidths and assignments.

Frequency (cm ⁻¹)	Width (cm ⁻¹)	Assignment
733	15	1 ν_3
754		1 $\nu_3 + 1 \nu_{Ar}$
775		1 $\nu_3 + 2 \nu_{Ar}$
890	13	1 $\nu_3 + 1 \nu_1$
911		1 $\nu_3 + 1 \nu_1 + 1 \nu_{Ar}$
929		1 $\nu_3 + 1 \nu_1 + 2 \nu_{Ar}$
1048	11	1 $\nu_3 + 2 \nu_1$
1070		1 $\nu_3 + 2 \nu_1 + 1 \nu_{Ar}$
1202	10	1 $\nu_3 + 3 \nu_1$

order of 5%–10%. The fluctuations are mainly a result of variations in source conditions. No Br⁻ ions were observed over the entire scan region, indicating (a) no collisionally induced rupture of the hydrogen bond and (b) no IRMPD processes resulting in BrHBr⁻ breakdown. No features are found at the location of the previously assigned overtone near 1550 cm⁻¹, calling that assignment into question.²⁵

A comparison of the experimental peak energies and those calculated by Del Bene and Jordan²² for the $\nu_3 + n\nu_1$ series ($n=0-3$) is shown in Table 2. The calculated and experimental ν_3 fundamentals (731 and 733 cm⁻¹) are in excellent agreement. The absolute deviations across the series are small (≤ 10 cm⁻¹), so the assignment of the experimental peaks to this series is straightforward. The experimental peak spacings between adjacent peaks are 157, 158 and 154 cm⁻¹ for $n=0-1$, 1-2, and 2-3, i.e., decreasing slightly with increasing n . These spacings are 4–6 cm⁻¹ less than the corresponding spacings between the calculated peak positions in Table 2. One of the more striking features of the calculation by Del Bene and Jordan was that the spacing between the peaks of the $\nu_3 + n\nu_1$ series was 20–30 cm⁻¹ less than the calculated energy of the ν_1 fundamental, 189 cm⁻¹, indicating that antisymmetric stretch excitation reduces the symmetric stretch frequency, and the overall agreement between experiment and theory in Table 2 supports this conclusion. The very presence of the $\nu_3 + n\nu_1$ sequence further demonstrates the breakdown of the harmonic approximation in the presence of a strong hydrogen bond such as this one, and emphasizes the need for explicit consideration of intermode coupling when calculating the properties of strongly hydrogen bonded systems.^{28,29}

TABLE II. Comparison of experimental and calculated vibrational frequencies for the BrHBr-complex ion.

Assignment	Gas phase	Matrix				Calculated ^d
		Ne ^a	Ar ^b	Kr ^c	Xe ^c	
ν_3	733	741	728	687	646	731
$(\nu_3 + 1\nu_1) - \nu_3$	+157	+163	+164	+158	+152	+162
$(\nu_3 + 2\nu_1) - \nu_3$	+315		+325	+313	+300	+323
$(\nu_3 + 3\nu_1) - \nu_3$	+469			+466	+446	+481

^aReference 16.

^bReference 17.

^cReference 18.

^dReference 19.

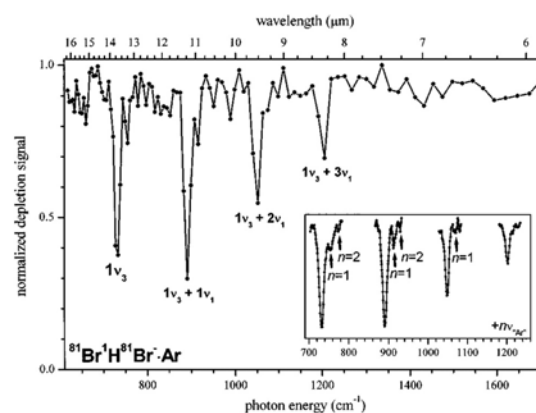


FIG. 1. Infrared predissociation overview spectrum of ⁸¹BrH⁸¹Br⁻·Ar measured by monitoring the depletion of the parent ion. Inset shows smoothed (3-point average) spectra measured with smaller step size (see text).

The depletion peak intensities in Fig. 1 differ significantly from the intensities previously observed in matrix IR absorption experiments, in which the absorption decreased by a factor of two from ν_3 to $\nu_3 + \nu_1$ and a factor of ten from ν_3 to $\nu_3 + 2\nu_1$.¹⁸⁻²¹ The depletion intensities observed in the present experiment cannot be directly compared to the absorption intensities reported in the previous matrix studies, since the depletion signal reflects not only the oscillator strengths of the IR transitions, but also (a) the variation in FELIX power and bandwidth over the scan range and (b) the cluster predissociation rate. FELIX characteristics were optimized such that power and bandwidth change as little as possible in the energy range of interest. It is more likely that the dissociation rate of the vibrationally excited clusters influences the intensity distribution, with a lower dissociation rate for less vibrationally excited anions resulting in a smaller than expected relative depletion signal.

In order for the dissociation rate to effect peak intensities, the dissociation lifetime must be at least a few microseconds, since this is the time scale for collisions between the trapped ions and the He buffer gas inside the trap. The ions are extracted 1 ms after the irradiation pulse, so it can be assumed that all photoexcited ions have either dissociated or been collisionally quenched before the extraction pulse is applied to the ion trap exit lens. It thus appears that the cluster predissociation rate increases with excitation of the symmetric stretch of the BrHBr⁻ chromophore. This could be a “total energy” effect, in which the total excess energy above the dissociation threshold (estimated³⁰⁻³² to be 300–400 cm⁻¹) determines the dissociation rate. Alternatively, the predissociation rate may be mode-specific, with ν_1 excitation promoting dissociation more efficiently than ν_3 excitation.

The combination of vibrational predissociation spectroscopy with FELIX excitation opens up a new frontier in the study of hydrogen bonded ions. The effect of solvation upon the hydrogen bond is of particular interest. Simulations based on pairwise sums of empirical potentials carried out by McCoy and co-workers predict a ν_3 shift of only -1 cm⁻¹ upon addition of an Ar atom to ClHCl⁻.³³ Vibrational predissocia-

tion experiments by Kelley *et al.*³⁴ on $\text{Cl}^- \cdot \text{H}_2\text{O} \cdot \text{Ar}_n$ found a sequential shift in the hydrogen bonded OH stretch of less than 3 cm^{-1} upon addition of 1–5 Ar atoms. Hence, the addition of a single Ar atom is expected to result in a negligible shift of the BrHBr^- frequency from its gas phase value. On the other hand, vibrational²⁵ and photoelectron³⁵ spectroscopy have shown that the addition of a single HBr to BrHBr^- profoundly alters the anionic hydrogen bond, resulting in a structure more akin to $\text{Br}^-(\text{HBr})_2$. The photoelectron spectrum of $\text{BrHBr}^-(\text{H}_2\text{O})$ suggests an intermediate degree of hydrogen bond perturbation by the water molecule.³⁵ This inference can be tested more directly through measurement of the IR spectrum of this species, an experiment planned for the very near future. The determination of vibrational frequencies in bihalide anions can also be exploited in transition state spectroscopy experiments in which the photoelectron spectrum of a vibrationally excited state is measured, because photodetachment of vibrationally excited anions will allow for Franck–Condon overlap with a larger region of the neutral $\text{X}+\text{HY}$ hydrogen exchange transition state region than can be accessed by photodetachment of ground state anions.^{36,37}

This work is supported by the Sonderforschungsbereich 546 and the Ph.D. Graduate Study Program 788 of the DFG. United States AFOSR Grant No. F49620-00-1-0018 provided support for N.L.P and D.M.N. We gratefully acknowledge the support of the *Stichting voor Fundamenteel Onderzoek der Materie* (FOM) in providing the required beam time on FELIX and highly appreciate the skillful assistance of the FELIX staff, in particular Dr. A. F. G. van der Meer.

³¹Authors to whom correspondence should be addressed. Electronic mail: dan@radon.cchem.berkeley.edu and asmis@physik.fu-berlin.de

¹G. C. Pimentel and A. L. McClellan, *The Hydrogen Bond* (W. H. Freeman, San Francisco, 1960).

²P. A. Frey, S. A. Whitt, and J. B. Tobin, *Science* **264**, 1927 (1994).

³W. W. Cleland and M. M. Kreevoy, *Science* **264**, 1887 (1994).

⁴M. E. Tuckerman, D. Marx, M. L. Klein, and M. Parrinello, *Science* **275**, 817 (1997).

⁵C. C. M. Samson and W. Klopper, *J. Mol. Struct.: THEOCHEM* **586**, 201 (2002).

⁶B. S. Ault, *Acc. Chem. Res.* **15**, 103 (1982).

⁷D. U. Webb and K. N. Rao, *J. Mol. Spectrosc.* **28**, 121 (1968).

⁸D. R. J. Boyd and H. W. Thompson, *Spectrochim. Acta* **5**, 308 (1952).

⁹K. Kawaguchi and E. Hirota, *J. Chem. Phys.* **84**, 2953 (1986).

¹⁰K. Kawaguchi and E. Hirota, *J. Chem. Phys.* **87**, 6838 (1987).

¹¹K. Kawaguchi, *J. Chem. Phys.* **88**, 4186 (1988).

¹²K. Kawaguchi and E. Hirota, *J. Mol. Struct.* **352**, 389 (1995).

¹³M. Okumura, L. I. Yeh, and Y. T. Lee, *J. Chem. Phys.* **83**, 3705 (1985).

¹⁴C. G. Bailey, J. Kim, C. E. H. Dessent, and M. A. Johnson, *Chem. Phys. Lett.* **269**, 122 (1997).

¹⁵P. Ayotte, C. G. Bailey, G. H. Weddle, and M. A. Johnson, *J. Phys. Chem. A* **102**, 3067 (1998).

¹⁶G. Caldwell and P. Kebarle, *Can. J. Chem.* **63**, 1399 (1985).

¹⁷J. C. Evans and G. Y. S. Lo, *J. Phys. Chem.* **71**, 3942 (1967).

¹⁸V. Bondybey, G. C. Pimentel, and P. N. Noble, *J. Chem. Phys.* **55**, 540 (1971).

¹⁹C. L. Lugez, M. E. Jacox, and W. E. Thompson, *J. Chem. Phys.* **105**, 3901 (1996).

²⁰D. E. Milligan and M. E. Jacox, *J. Chem. Phys.* **55**, 2550 (1971).

²¹M. Rasanen, J. Seetula, and H. Kunttu, *J. Chem. Phys.* **98**, 3914 (1993).

²²J. E. Del Bene and M. J. T. Jordan, *Spectrochim. Acta, Part A* **55**, 719 (1999).

²³R. B. Metz, A. Weaver, S. E. Bradforth, T. N. Kitsopoulos, and D. M. Neumark, *J. Phys. Chem.* **94**, 1377 (1990).

²⁴R. B. Metz and D. M. Neumark, *J. Chem. Phys.* **97**, 962 (1992).

²⁵N. L. Pivonka, C. Kaposta, G. von Helden, G. Meijer, L. Woste, D. M. Neumark, and K. R. Asmis, *J. Chem. Phys.* **117**, 6493 (2002).

²⁶K. R. Asmis, M. Brümmer, C. Kaposta, G. Santambrogio, G. von Helden, G. Meijer, K. Rademann, and L. Wöste, *Phys. Chem. Chem. Phys.* **4**, 1101 (2002).

²⁷D. Oepts, A. F. G. Vandermeer, and P. W. Vanamersfoort, *Infrared Phys. Technol.* **36**, 297 (1995).

²⁸M. V. Vener, O. Kuhn, and J. Sauer, *J. Chem. Phys.* **114**, 240 (2001).

²⁹J. E. Del Bene and M. J. T. Jordan, *J. Mol. Struct.: THEOCHEM* **573**, 11 (2001).

³⁰Y. X. Zhao, I. Yourshaw, G. Reiser, C. C. Arnold, and D. M. Neumark, *J. Chem. Phys.* **101**, 6538 (1994).

³¹K. R. Asmis, T. R. Taylor, C. S. Xu, and D. M. Neumark, *J. Chem. Phys.* **109**, 4389 (1998).

³²Z. Liu, H. Gomez, and D. M. Neumark, *Chem. Phys. Lett.* **332**, 65 (2000).

³³H. B. Lavender and A. B. McCoy, *J. Phys. Chem. A* **104**, 644 (2000).

³⁴J. A. Kelley, J. M. Weber, K. M. Lisle, W. H. Robertson, P. Ayotte, and M. A. Johnson, *Chem. Phys. Lett.* **327**, 1 (2000).

³⁵H. Gomez, A. Meloni, J. Madrid, and D. M. Neumark, *J. Chem. Phys.* (to be published).

³⁶S. E. Bradforth, A. Weaver, D. W. Arnold, R. B. Metz, and D. M. Neumark, *J. Chem. Phys.* **92**, 7205 (1990).

³⁷D. M. Neumark, *PhysChemComm* **5**, 76 (2002).

The Gasphase Infrared Spectrum of the Protonated Water Dimer

Knut R. Asmis, Gabriele Santambrogio, Mathias Brümmer, Cristina Kaposta, and
Ludger Wöste

Institut für Experimentalphysik, Freie Universität Berlin, Arnimallee 14, D 14195 Berlin, Germany

Nicholas L. Pivonka and Daniel M. Neumark

*Department of Chemistry, University of California, Berkeley, California and Chemical Sciences Division,
Lawrence Berkeley National Laboratory, Berkeley, California 94720, U.S.A.*

Report in *Science* **299** 1375-7 (2003).

Gas-Phase Infrared Spectrum of the Protonated Water Dimer

Knut R. Asmis,^{1*} Nicholas L. Pivonka,^{2,3} Gabriele Santambrogio,¹
Mathias Brümmer,¹ Cristina Kaposta,¹ Daniel M. Neumark,^{2,3*}
Ludger Wöste¹

The protonated water dimer is a prototypical system for the study of proton transfer in aqueous solution. We report infrared photodissociation spectra of cooled $\text{H}^+(\text{H}_2\text{O})_2$ [and $\text{D}^+(\text{D}_2\text{O}_2)$] ions, measured between 620 and 1900 wave numbers (cm^{-1}). The experiment directly probes the shared proton region of the potential energy surface and reveals three strong bands below 1600 cm^{-1} and one at 1740 cm^{-1} (for H_5O_2^+). From a comparison to multidimensional quantum calculations, the three lower energy bands were assigned to stretching and bending fundamentals involving the $\text{O}\cdots\text{H}^+\cdots\text{O}$ moiety, and the highest energy band was assigned to a terminal water bend. These results highlight the importance of intermode coupling in shared proton systems.

Proton transfer through hydrogen bonds plays an essential role in many chemical and biological processes. The dynamics of proton transfer across biomembranes, for example, governs the bioenergetic functions of protein assemblies like the adenosine triphosphate synthetase complex (1) and bacteriorhodopsin (2). The detailed molecular mechanisms of these “proton pumps” remain elusive (3, 4). The anomalously high proton mobility of liquid water (5) indicates that, unlike other ions, the transport of protons in aqueous solutions does not require the net diffusion of atomic (or molecular) species but instead involves chemical exchange of hydrogen nuclei along charge-conducting “water wires” in which the hydrated proton forms a fluxional defect in the hydrogen-bonded network (6–8). Important limiting structures in these networks are the hydrated hydronium and hydrated proton complexes $\text{H}_3\text{O}^+(\text{H}_2\text{O})_3$ and $\text{H}^+(\text{H}_2\text{O})_2$ (9).

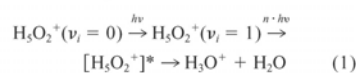
The interpretation of the spectroscopic signature of hydrated protons in liquid water, characterized by a quasi-continuous absorption observed in the infrared (IR), has been a long-running controversy (10), in particular the attribution of specific bands to the hydrated proton structures H_5O_2^+ and H_9O_4^+ (11, 12). Spectroscopic information on the corresponding isolated gas-phase cluster ions, which could aid in the assignment, remains scarce. The vibrational spectroscopy of H_5O_2^+ has been studied in the region of the free O–H stretch modes ($>3500 \text{ cm}^{-1}$) with the use of infrared multiphoton photodissociation (IRMPD) spectroscopy (13, 14). The

experiments support a “solution-like” $\text{H}_2\text{O}\cdots\text{H}^+\cdots\text{OH}_2$ structure, in which the proton is located symmetrically between the two water ligands; electronic structure calculations (15, 16) confirm that this species has a minimum energy structure with C_2 symmetry as shown in the inset of Fig. 1. However, the vibrational modes involving the central proton, which are key to the understanding of proton transfer on the H_5O_2^+ potential energy surface, have remained experimentally unexplored.

Here, we describe an experimental study of the gas-phase vibrational spectroscopy of H_5O_2^+ and its deuterated analog, D_5O_2^+ , between 620 and 1900 cm^{-1} , the region of the $\text{O}\cdots\text{H}^+\cdots\text{O}$ fundamentals. The experiments were performed with a novel tandem mass spectrometer–ion trap setup (17) in combination with radiation from the free electron laser for infrared experiments (FELIX) (18). These experiments draw on the pioneering work of Meijer and co-workers (19), who showed that FEL radiation is well suited to study the gas-phase vibrational spectroscopy of atomic and molecular clusters and cluster ions in the region below 2000 cm^{-1} . In particular, one can perform vibrational “action” spectroscopy of positive and negative ions in this frequency range (17, 20), in which absorption of IR light by mass-selected ions yields charged fragments that can be detected with nearly unit efficiency. Continuously tunable tabletop lasers do not have sufficient intensity below 2000 cm^{-1} for this type of experiment.

For the measurement of the IRMPD spectra, we formed a continuous beam of water-cluster cations in a Perkin Elmer SCIEX atmospheric ion spray source and transferred it through a $60\text{-}\mu\text{m}$ orifice into a high vacuum chamber. H_5O_2^+ cations were mass-selected and accumulated in a linear radio-frequency hexadecapole ion trap kept at a temperature

of $\sim 100 \text{ K}$. The ion trap was filled with helium buffer gas, which collisionally cooled the trapped cluster ions down to the ambient temperature within several microseconds. Cooling of the floppy H_5O_2^+ ions before irradiation minimized the contribution of vibrational hot bands and energetically low-lying isomers to the spectra. The trapped ions were irradiated by a single FEL macropulse, for which the overall pulse energy and duration were 20 to 40 mJ and $5 \mu\text{s}$, respectively. The full width at half maximum bandwidth was $\sim 0.5\%$ of the central frequency. The IR beam was focused through a 5-mm KBr window into the center of the ion trap with a 48-cm focal length KBr lens. The IRMPD spectrum was measured by mass-selectively monitoring the formation of H_3O^+ as a function of FELIX wavelength. H_3O^+ ions were formed by dissociation of H_5O_2^+ subsequent to the absorption of multiple IR photons, as is shown in Eq. 1:



Here, h is Planck’s constant, v_i is the vibrational quantum number of the i th vibrational mode and n is the total number of absorbed photons. Although Eq. 1 is a multiphoton process, no production of H_3O^+ occurs unless the first photon is resonant with a vibrational transition of the cold parent ion. In more detail (21–24), absorption of the first few photons occurs within the “discrete” regime, in which a particular vibrational mode of a molecule is excited resonantly. Higher excitation accesses the “quasi-continuum” regime in which the density of states is so high that the vibrational energy is rapidly randomized among all vibrational modes of the molecule. The transition between the two regimes depends on the vibrational density of states and the strengths of the interactions between vibrational modes. The cluster continues to absorb photons until it has enough energy to dissociate. The dissociation energy of H_5O_2^+ is 31.6 kcal/mol (25), so 6 to 18 photons are needed for dissociation in the frequency range studied here.

The IRMPD spectrum of H_5O_2^+ (Fig. 1A) comprises four bands of higher intensity (b to e) at 921, 1043, 1317, and 1741 cm^{-1} and an additional weaker feature at 788 cm^{-1} (a). The bands are more than 20 times wider ($>100 \text{ cm}^{-1}$) than the laser bandwidth ($\sim 5 \text{ cm}^{-1}$ at $10 \mu\text{m}$). Additional fine structure is observed for bands b to e, with a spacing on the order of 30 (b and c) and $\sim 70 \text{ cm}^{-1}$ (d), respectively (Table 1). In order to aid in the assignment of the bands, we recorded IRMPD spectra of D_5O_2^+ (Fig. 1B). Four bands (b’ to e’), somewhat narrower, with less pronounced fine structure and with different relative intensities than in the H_5O_2^+

¹Institut für Experimentalphysik, Freie Universität Berlin, Arnimallee 14, D 14195 Berlin, Germany. ²Department of Chemistry, University of California, ³Chemical Sciences Division, Lawrence Berkeley National Laboratory, Berkeley, CA 94720, USA.

*To whom correspondence should be addressed. E-mail: asmis@physik.fu-berlin.de (K.R.A.); dan@radon.chem.berkeley.edu (D.M.N.)

REPORTS

spectra, are observed. All four band maxima are red-shifted upon H-D substitution, with isotope shifts of 1.32 (b-b'), 1.31 (c-c'), 1.37 (d-d'), and 1.34 (e-e').

Previous theoretical studies have indicated that the IR spectrum of $\text{H}_2\text{O}\cdots\text{H}^+\cdots\text{OH}_2$ is adequately described within the harmonic approximation only for those vibrational modes that predominantly involve the terminal water molecules (26, 27). These modes include the H-O-H rock, wag, and twist below 600 cm^{-1} ; the H-O-H bend around 1750 cm^{-1} ; and the O-H stretch above 3600 cm^{-1} . Thus, we assigned band e at 1741 cm^{-1} to the asymmetric bending motion of the water molecules in H_5O_2^+ , calculated at 1787 cm^{-1} at the B-CCD(T)/TZ2P (28) level of theory (16). We attribute the remaining bands (a to d) to modes involving the central $\text{O}\cdots\text{H}^+\cdots\text{O}$ moiety, which include the symmetric and asymmetric stretch as well as two bending modes. The B-CCD(T)/TZ2P harmonic frequencies of these modes are 650, 794, 1505, and 1596 cm^{-1} (16). Only the latter three transitions are dipole-allowed, and the asymmetric stretch (794 cm^{-1}) has the largest calculated oscillator strength. The experimental spectrum reveals no

substantial signal in the region between 1500 to 1650 cm^{-1} and only a weak band below 850 cm^{-1} . Thus, we find no satisfactory agreement between the experimental spectrum and the calculated harmonic frequencies in the region between 600 and 1600 cm^{-1} .

The failure of the harmonic picture for H_5O_2^+ is not surprising, because the shared proton vibrates in a rather flat potential and will undergo large amplitude motion, similar to the bialkali anions such as BrHBr^- that have been studied by a similar technique (20). Several calculations have been undertaken to correct for anharmonic effects in the IR spectrum of H_5O_2^+ (26, 27, 29). Compared to the harmonic frequencies, these models (Table 2) predict that the asymmetric stretch is blue-shifted above 1000 cm^{-1} and that the bend modes are red-shifted below 1500 cm^{-1} , thus improving the overlap with the experimental spectrum. However, the various calculations disagree on the ordering and the relative intensities of the transitions. The most extensive calculations to date are the four-dimensional (4D) simulations of Sauer and co-workers (27), which account for coupling between all four modes involving the shared proton. At this level of theory, the asymmetric stretch is calculated at 1158 cm^{-1} . The two bend fundamentals are red-shifted by roughly 500 cm^{-1} , to 968 and 1026 cm^{-1} , so that they lie below the asymmetric stretch. These three values compare rather favorably with the three experimental values of 921 (b), 1043 (c), and 1317 cm^{-1} (d), in particular when the origin (1252 cm^{-1}) and not the maximum of band d is considered.

The assignment suggested by this comparison is supported by the isotope shifts in the D_5O_2^+ spectrum. The 4D simulations predict a 5% larger isotope shift for the

asymmetric stretch (H-D shift of 1.49) than for the bends (1.42 and 1.43). Experimentally (Table 1), we find a 4% larger shift between peaks d and d' than that for the other two sets of peaks, although our absolute values are somewhat smaller. Changes in the relative band intensities upon deuteration, in particular those of band e', can be attributed to the influence of combination bands involving the $\text{O}\cdots\text{H}^+\cdots\text{O}$ modes. The 4D simulations predict strong combination bands in the 1300 to 1450 cm^{-1} region of the D_5O_2^+ spectrum. These could account for the strong increase of the relative intensity of band e' in the D_5O_2^+ spectrum, nominally the terminal D_2O bend, as compared to that of band e in the H_5O_2^+ spectrum. In H_5O_2^+ , most of these combination bands are predicted above 1950 cm^{-1} , i.e., outside our measurement window.

The origin of the finer structure in the H_5O_2^+ spectrum is less clear. This species is a nearly prolate top with rotational constant $A_e = 5.8\text{ cm}^{-1}$ (30). The 30-cm^{-1} spacing in bands b and c is much larger than $2A_e$ and thus cannot be from $\Delta K = \pm 1$ rotational transitions associated with excitation of the bend vibrations. However, this spacing and the larger spacing in band d is probably too small to originate from combination bands involving the low-frequency torsional and/or wagging modes of the terminal water molecules; calculated (harmonic) values for the lowest frequency modes of this type range from 120 to 240 cm^{-1} (15, 16, 29). A third possibility is that this structure originates from $\Delta v = 0$ sequence bands involving at least one of these low-frequency modes. For this to be the case, there must be a substantial population of one to two excited levels of the mode in question,

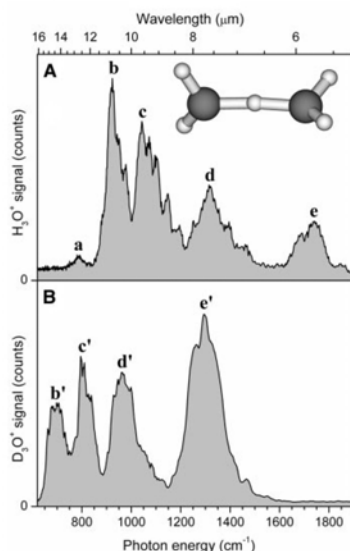


Fig. 1. IRMPD spectra of (A) H_5O_2^+ and (B) D_5O_2^+ in the spectral range from 620 to 1900 cm^{-1} . Bands are labeled with lowercase letters. The shown traces are composite spectra, and the data was smoothed. The spectra were measured by monitoring the formation of H_3O^+ (D_3O^+) as a function of FELIX wavelength. The H_3O^+ signal is superimposed over a small and wavelength-independent background resulting from collision-induced dissociation of the mass-selected H_5O_2^+ ions with the He buffer gas atoms within the ion trap.

Table 1. Experimental vibrational frequencies [in wave numbers (cm^{-1})] for H_5O_2^+ and D_5O_2^+ and isotope effects determined from IRMPD spectra. The position of each band maximum is underlined.

H_5O_2^+ band	Frequency	D_5O_2^+ band	Frequency	H-D shift
a	788			
b	888, <u>921</u> , 947, 975	b'	<u>697</u>	1.32
c	<u>1043</u> , 1071, 1100, 1145, 1195	c'	<u>795</u>	1.31
d	1252, <u>1317</u> , 1390, ~1460	d'	<u>960</u>	1.37
e	1687, <u>1741</u> , ~1850	e'	<u>1296</u>	1.34

Table 2. Comparison of experimental and calculated vibrational frequencies (in wave numbers) of the $\text{O}\cdots\text{H}^+\cdots\text{O}$ moiety in H_5O_2^+ (sym., symmetric; asym., asymmetric; x, out of plane; y, in plane). Tentative assignments based on the present study, frequencies from 4D simulation of Vener *et al.* (27), correlation-corrected vibrational self-consistent field frequencies (29), and harmonic frequencies at the B-CCD(T) level of theory (16) are listed.

Vibrational mode	Experiment	4D	CC-VSCF	Harmonic
$(\text{O}\cdots\text{H}\cdots\text{O})$ sym. stretch		587	599	650
$(\text{O}\cdots\text{H}\cdots\text{O})_x$ bend	921	968	1442	1505
$(\text{O}\cdots\text{H}\cdots\text{O})_y$ bend	1043	1026	1494	1596
$(\text{O}\cdots\text{H}\cdots\text{O})$ asym. stretch	1317	1158	1209	794

and its frequency must be 30 cm^{-1} higher in the $\nu = 1$ bend levels than in their ground states. A frequency shift of this type would be another example of the breakdown of the harmonic picture in H_5O_2^+ .

In the 4D vibrational calculations, the asymmetric stretch was predicted to be more than three times more intense than the two bending bands in H_5O_2^+ , which does not agree well with the experimental spectrum. This discrepancy can arise from at least two factors: (i) The calculations refer to the linear absorption spectrum, whereas the photoinduced vibrational predissociation mechanism (Eq. 1) governing our IRMPD experiments requires the absorption of multiple photons (6 to 18 photons in the frequency range studied). The absorption of the first few photons within the discrete (in contrast to quasi-continuum) regime (21, 22) generally governs the relative intensities observed in the IRMPD spectrum. Meijer and co-workers have found satisfactory agreement between the IRMPD and linear absorption spectrum for bi- and tricyclic hydrocarbon cations even though as many as 100 photons are required for dissociation (23, 24). However, these ions are larger than the protonated water dimer, and there may be more deviation from the linear absorption intensities over the spectral range probed by our experiment if more photons are needed to reach the quasi-continuum, a particular concern at the lowest frequencies in Fig. 1. (ii) Anharmonic coupling to vibrational modes other than the four $\text{O}\cdots\text{H}^+\cdots\text{O}$ vibrations was not included in these calculations. The multiconfigurational self-consistent field calculations of Muguet (15) indicate that coupling to the water wags and bends is important. The fine structure in the experimental spectrum shows evidence for this type of coupling, which is likely to alter the overall intensity pattern.

The present results provide previously unstudied insight regarding the assignment of the liquid-phase spectra (12, 31). Hydrated protons in aqueous solution are characterized by four broad absorption bands at 1200, 1760, 2900, and 3350 cm^{-1} and a continuous absorption over the 1000 to 3400 cm^{-1} range. In heavy water, the spectral features are red-shifted to 920, 1420, 2130, and 2480 cm^{-1} . On the basis of a comparison with the gas-phase spectra, the absorption of the hydrated proton (deuteron) in the 1200 and 1760 cm^{-1} (920 and 1420 cm^{-1}) region can be attributed to the presence of H_5O_2^+ -type structures in the aqueous solution. The bulk 1760 cm^{-1} absorption is attributed to the blue-shifted bend vibration of the terminal water, which is found at 1741 cm^{-1} in the present gas-phase spectrum. This result confirms the original assignment of Librovich *et al.* (11)

and recent multistate empirical valence-bond simulations by Kim *et al.* (12). The broad 1200 cm^{-1} absorption is attributed to three modes, namely the asymmetric stretch and the two bend modes of the $\text{O}\cdots\text{H}^+\cdots\text{O}$ moiety, that we find in the 920 to 1320 cm^{-1} region. We note that the liquid-phase difference spectra also show a very weak absorption at around 750 cm^{-1} and that a similar absorption is observed in our spectra at 788 cm^{-1} (band a).

References and Notes

1. M. Saraste, *Science* **283**, 1488 (1999).
2. J. K. Lanyi, *J. Phys. Chem. B* **104**, 11441 (2000).
3. R. Pomès, B. Roux, *Biophys. J.* **82**, 2304 (2002).
4. A. M. Smondyrev, G. A. Voth, *Biophys. J.* **82**, 1460 (2002).
5. M. Eigen, L. D. Maeyer, *Proc. R. Soc. London* **247**, 505 (1958).
6. C. J. T. d. Grothuss, *Ann. Chim. (Paris)* **58**, 54 (1806).
7. J. D. Lear, Z. R. Wasserman, W. F. DeGrado, *Science* **240**, 1177 (1988).
8. N. Agmon, *Chem. Phys. Lett.* **244**, 456 (1995).
9. D. Marx, M. E. Tuckerman, J. Hutter, M. Parrinello, *Nature* **397**, 601 (1999).
10. G. Zundel, *Adv. Chem. Phys.* **111**, 1 (2000).
11. N. B. Librovich, V. P. Sakun, N. D. Sokolov, *Chem. Phys.* **39**, 351 (1979).
12. J. Kim, U. W. Schmitt, J. A. Gruetzmacher, G. A. Voth, N. E. Scherer, *J. Chem. Phys.* **116**, 737 (2002).
13. L. I. Yeh, J. D. Myers, J. M. Price, Y. T. Lee, *J. Chem. Phys.* **91**, 7319 (1989).
14. L. I. Yeh, Y. T. Lee, J. T. Hougen, *J. Mol. Spectrosc.* **164**, 473 (1994).
15. F. F. Muguet, *J. Mol. Struct.* **368**, 173 (1996).
16. E. D. Valeev, H. F. Schaefer III, *J. Chem. Phys.* **108**, 7197 (1998).
17. K. R. Asmis *et al.*, *Phys. Chem. Chem. Phys.* **4**, 1101 (2002).
18. G. M. H. Knippels, R. F. X. A. M. Mols, A. F. G. van der Meer, D. Oepts, P. W. van Amersfoort, *Phys. Rev. Lett.* **75**, 1755 (1995).
19. M. Putter, G. von Helden, G. Meijer, *Chem. Phys. Lett.* **258**, 118 (1996).
20. N. L. Pivonka *et al.*, *J. Chem. Phys.* **117**, 6493 (2002).
21. S. Mukamel, J. Jortner, *J. Chem. Phys.* **65**, 5204 (1976).
22. A. S. Sudbo, P. A. Schulz, E. R. Grant, Y. R. Shen, Y. T. Lee, *J. Chem. Phys.* **70**, 912 (1979).
23. J. Oomens, A. J. A. van Rooij, G. Meijer, G. von Helden, *Astrophys. J.* **542**, 404 (2000).
24. J. Oomens, G. Meijer, G. von Helden, *J. Phys. Chem. A* **105**, 8302 (2001).
25. Y. K. Lau, S. Ikuta, P. Kebarle, *J. Am. Chem. Soc.* **104**, 1462 (1982).
26. L. Ojamäe, I. Shavitt, S. J. Singer, *Int. J. Quantum Chem. Symp.* **29**, 657 (1995).
27. M. V. Vener, O. Kühn, J. Sauer, *J. Chem. Phys.* **114**, 240 (2001).
28. B-CCD(T) is the Brueckner coupled cluster doubles method with a perturbational triple-excitation correction. TZZP is the triple- ζ plus double polarization basis set.
29. G. M. Chaban, J. O. Jung, R. B. Gerber, *J. Phys. Chem. A* **104**, 2772 (2000).
30. D. J. Wales, *J. Chem. Phys.* **110**, 10403 (1999).
31. R. Vuilleumier, D. Borgis, *J. Chem. Phys.* **111**, 4251 (1999).
32. Supported by the Collaborative Research Center 546 and the Ph.D. Graduate Study Program 788 of the Deutsche Forschungsgemeinschaft. U.S. Air Force Office of Scientific Research grant F49620-00-1-0018 provided support for N.L.P. and D.M.N. We thank M. V. Vener and J. Sauer for helpful discussions, the Stichting voor Fundamenteel Onderzoek der Materie for providing the required beam time on FELIX, and the FELIX staff, in particular A. F. G. van der Meer, for skillful assistance.

18 December 2002; accepted 29 January 2003
Published online 4 January 2003;
10.1126/science.1081634

Include this information when citing this paper.

Experimental and Theoretical Study of the Infrared Spectra of BrHI⁻ and BrDI⁻

M. J. Nee, A. Osterwalder, and D. M. Neumark

Department of Chemistry, University of California, Berkeley, California 94720 and Chemical Sciences Division, Lawrence Berkeley Laboratory, Berkeley, California 94720

C. Kaposta and C. Cibrián Uhalte

Institut für Experimentalphysik, Freie Universität Berlin, Arnimallee 14, 14195 Berlin, Germany

T. Xie, A. Kaledin, and J. M. Bowman

Department of Chemistry and Cherry L. Emerson Center for Scientific Computation, Emory University, Atlanta, Georgia 30322

S. Carter

Department of Chemistry, University of Reading, Reading, United Kingdom

K. R. Asmis

Fritz-Haber-Institut der Max-Planck-Gesellschaft, Faradayweg 4-6, 14195 Berlin, Germany

Full article in the *Journal of Chemical Physics* **121(15)** 7259-68 (2004).

Experimental and theoretical study of the infrared spectra of BrHI^- and BrDI^-

M. J. Nee, A. Osterwalder, and D. M. Neumark^{a)}

Department of Chemistry, University of California, Berkeley, California 94720 and Chemical Sciences Division, Lawrence Berkeley Laboratory, Berkeley, California 94720

C. Kaposta and C. Cibrián Uhalte

Institut für Experimentalphysik, Freie Universität Berlin, Arnimallee 14, 14195 Berlin, Germany

T. Xie, A. Kaledin, and J. M. Bowman^{b)}

Department of Chemistry and Cherry L. Emerson Center for Scientific Computation, Emory University, Atlanta, Georgia 30322

S. Carter

Department of Chemistry, University of Reading, Reading, United Kingdom

K. R. Asmis^{c)}

Fritz-Haber-Institut der Max-Planck-Gesellschaft, Faradayweg 4-6, 14195 Berlin, Germany

(Received 19 July 2004; accepted 27 July 2004)

Gas phase vibrational spectra of BrHI^- and BrDI^- have been measured from 6 to 17 μm (590–1666 cm^{-1}) using tunable infrared radiation from the free electron laser for infrared experiments in order to characterize the strong hydrogen bond in these species. $\text{BrHI}^- \cdot \text{Ar}$ and $\text{BrDI}^- \cdot \text{Ar}$ complexes were produced and mass selected, and the depletion of their signal due to vibrational predissociation was monitored as a function of photon energy. Additionally, BrHI^- and BrDI^- were dissociated into HBr (DBr) and I^- via resonant infrared multiphoton dissociation. The spectra show numerous transitions, which had not been observed by previous matrix studies. New *ab initio* calculations of the potential-energy surface and the dipole moment are presented and are used in variational ro-vibrational calculations to assign the spectral features. These calculations highlight the importance of basis set in the simulation of heavy atoms such as iodine. Further, they demonstrate extensive mode mixing between the bend and the H-atom stretch modes in BrHI^- and BrDI^- due to Fermi resonances. These interactions result in major deviations from simple harmonic estimates of the vibrational energies. As a result of this new analysis, previous matrix-isolation spectra assignments are reevaluated. © 2004 American Institute of Physics.

[DOI: 10.1063/1.1794671]

I. INTRODUCTION

The triatomic hydrogen bihalide anions, XHY^- , where X and Y are halogen atoms, are of fundamental chemical interest. From the perspective of electronic structure, these anions are an important model system for understanding three-center bonding.^{1,2} They have some of the strongest hydrogen bonds known, as evidenced by their high dissociation energies relative to $\text{X}^- + \text{HY}$ (1.7 eV for FHF^-)³ and low-frequency hydrogen stretch vibrations (723 cm^{-1} for BrHBr^-).⁴ Bihalide anions also serve as transition state precursors in negative ion photoelectron (PE) spectroscopy experiments, in which it has been shown that photodetachment of the anion can access the transition state region of the $\text{X} + \text{HY}$ reaction.^{5,6} Interpretation of these experiments is strongly dependent on the quality of the spectroscopic and structural data available for the anion. Infrared (IR) spectra of several symmetric XHX^- anions have been measured via

matrix-isolation spectroscopy⁷ and in the gas phase,^{4,8,9} and are reasonably well understood. The matrix IR spectra of the asymmetric ($\text{X} \neq \text{Y}$) bihalides¹⁰ are more complex, however, and have so far only been interpreted by assuming the simultaneous presence of two structural forms of the anions. Clearly, gas phase IR spectra are desirable to gain an improved understanding of these species. Here, we report the first such spectrum of an asymmetric bihalide, BrHI^- , using a tunable infrared free electron laser (FEL) to perform vibrational predissociation spectroscopy on $\text{BrHI}^- \cdot \text{Ar}$ and resonant infrared multiphoton dissociation (IRMPD) experiments on bare BrHI^- . Identical experiments are described for the deuterated analogs.

The BrHI^- anion was first observed by Ellison and Ault¹⁰ using IR matrix-isolation spectroscopy. They observed four bands at 666, 799, 920, and 1171 cm^{-1} for BrHI^- and three bands at 470, 728, and 862 cm^{-1} for BrDI^- . Previous work on symmetric bihalides¹¹ in matrices showed that, depending on conditions, one could generate symmetric (type II) and asymmetric (type I) forms of the anion, with type II anions exhibiting considerably lower H-atom stretch (ν_3) frequencies owing to a greater delocalization of the hydro-

^{a)}Electronic mail: dan@radon.cchem.berkeley.edu

^{b)}Electronic mail: bowman@euch4e.chem.emory.edu

^{c)}Electronic mail: asmis@physik.fu-berlin.de

gen. Ellison and Ault¹⁰ assigned the BrHI⁻ spectrum assuming that this ion also existed in two forms, both with asymmetric hydrogen bonds, but with a more localized and asymmetric hydrogen bond in the type I structure than the type II structure. The BrHI⁻ peaks at 920 and 1171 cm⁻¹ were assigned to the type I ion; the peak at 920 cm⁻¹ was assigned to the ν_3 fundamental and that at 1171 cm⁻¹ to either the fundamental or overtone of the ν_2 bending mode. The other two peaks at 666 and 799 cm⁻¹ were assigned to the type II structure, in which the hydrogen is shared more equally between the bromine and iodine. Unlike their symmetric counterparts, all of the BrHI⁻ matrix peaks were seen regardless of the preparation conditions. For the XHX⁻ anions, the type I structures were attributed to strong perturbation by the matrix, implying that the gas phase geometry would be closer to the type II structure. This expectation has been borne out in the gas phase IR spectra of FHF⁻, ClHCl⁻, and BrHBr⁻,^{4,8,9} in which the ν_3 antisymmetric stretch frequencies seen are very close to the type II matrix values. However, the question of which structure, if either, exists in the gas phase has remained open for the asymmetric bihalides.

In the gas phase, Caldwell and Kebablar³ measured the dissociation energy of BrHI⁻ relative to the I⁻ + HBr limit at 0.70 eV. The gas phase PE spectra of BrHI⁻ and BrHI⁻·Ar have been reported and analyzed in a series of papers by Neumark and co-workers.¹²⁻¹⁴ These spectra showed resolved vibrational structure that was close to but noticeably lower in frequency than the diatomic HBr vibrational frequency, indicating that photodetachment of the anion accessed the I+HBr product valley of the neutral Br+HI potential energy surface (PES) rather than the [BrHI][‡] transition state. This interpretation is consistent with the expected asymmetric I⁻···HBr structure of the anion, reflecting the higher proton affinity of Br⁻ relative to I⁻ (by 0.40 eV).¹⁵ Wave packet simulations by Bradforth *et al.*,¹² using a highly simplified potential function for the anion and a model potential energy surface¹⁶ for the Br+HI reaction, produced reasonable agreement with the experimental spectra. In these simulations, the anion ν_3 frequency was assumed to be 920 cm⁻¹ based on the type I value from the matrix studies; a satisfactory simulation of the PE spectra could not be obtained using the type II value (666 cm⁻¹). However, given the approximations made by Bradforth *et al.*, this result alone does not constitute definitive support for the type I anion in the gas phase.

In order to gain a more complete understanding of the photoelectron spectrum of BrHI⁻, Kaledin *et al.*¹⁷ constructed an *ab initio* potential energy surface for the anion and performed variational ro-vibrational calculations to determine the energy eigenvalues. These calculations recovered the experimental dissociation energy of the complex and confirmed the linear, asymmetric geometry. The calculations found the H–Br equilibrium bond distance, r_{HBr} , to be substantially shorter than the H–I distance, r_{HI} (1.50 versus 2.31 Å) and only slightly longer than the equilibrium bond length in diatomic H–Br (1.414 Å).¹⁸ The full-dimensionality calculation of the vibrational energy levels yielded 1266.7 cm⁻¹ for the ν_3 fundamental, considerably lower than the *ab initio*

harmonic value, 1779 cm⁻¹, but more than 300 cm⁻¹ above the type I matrix value, 920 cm⁻¹ (and even further above the type II value). If these calculations are correct, they indicate that either the matrix experiment was misassigned or that the matrix shift was abnormally large.

Measurement of the gas phase infrared spectra of these ions should resolve the discrepancies between the matrix spectra and the calculations. However, the frequency range of interest is too low for the tunable IR lasers typically used in the vibrational spectroscopy of ions. Meijer and co-workers¹⁹⁻²¹ have measured low-frequency vibrations in clusters and other species with vibrational action spectroscopy using a tunable infrared free-electron laser. Asmis and co-workers^{8,22,23} used this light source to obtain vibrational spectra of strongly hydrogen-bonded cationic and anionic complexes from 600 to 1500 cm⁻¹, where vibrational frequencies associated with the shared hydrogen are expected. As in the experiments by Okumura *et al.*,²⁴ Bieske *et al.*,²⁵ and Ayotte *et al.*,²⁶ a weakly bound “messenger” atom may be added to the species being investigated, which leaves the vibrationally excited ion via vibrational predissociation (VPD). Alternatively, resonant IRMPD may be used to dissociate the unclustered chromophore. In either case, detection is accomplished by monitoring parent ion depletion or fragment ion formation as a function of photon energy. In this work, we obtain gas phase vibrational spectra of BrHI⁻ and BrDI⁻ using VPD on BrHI⁻·Ar and BrDI⁻·Ar and IRMPD on the bare anions in order to gain further insight into hydrogen bonding in the asymmetric hydrogen bihalides and to aid in the construction of an improved anion potential energy surface.

The spectra presented here are then compared with the new calculations on BrHI⁻ and BrDI⁻. These calculations are similar to those presented previously by Kaledin *et al.*¹⁷ but use a better method and a larger electronic basis to calculate the anion potential energy surface; a calculation of the dipole moment surface is also done for the first time. The new potential energy and dipole surfaces are used to simulate ro-vibrational energies and transition intensities. The new calculations reproduce the experimental transition energies and intensities and are in significantly better agreement with the experiment than the earlier calculations of Kaledin *et al.*¹⁷ They show considerable mode mixing between the H-atom stretch and bending modes, thus explaining the complexity of the new infrared spectra. The spectra and calculations provide the most complete picture currently available for an asymmetric bihalide anion.

II. EXPERIMENT

All experiments were performed on a tandem mass spectrometer ion trap system at the free electron laser for infrared experiments (FELIX) facility [Stichting voor Fundamenteel Onderzoek der Materie (FOM)-Institute for Plasma Physics “Rijnhuizen,” Nieuwegein, The Netherlands]. The apparatus, including its use in conjunction with the FELIX, has been discussed previously²⁷ and is described only briefly here. All ions are generated by crossing a pulsed (100 Hz) supersonic expansion of the appropriate gas mix with a beam of electrons from a 300- μA , 1-keV electron gun. The gas

TABLE I. Comparison of the optimized geometries (angstroms or deg) and normal-mode frequencies (cm⁻¹) with different basis sets. All calculations were done by the coupled cluster method [CCSD(T)] if not specified otherwise. For the vibrational frequencies, ω_1 , ω_2 , and ω_3 correspond to the halogen stretch, bend, and H-atom stretch modes, respectively.

Basis sets	r_{HBr}	r_{HI}	θ_{BrHI}	ω_1	ω_2	ω_3
Previous study ^a	1.499	2.318	180	85	550	1726
AVTZ	1.530	2.186	180	110	600	1481
AVTZ (cpp) ^b	1.527	2.171	180	112	604	1476
AVQZ ^c	1.524	2.196	180	105	587	1500
AVQZ ^c (cpp)	1.521	2.180	180	107	592	1487
AVQZ	1.525	2.203	180	106	574	1513
AVQZ (cpp)	1.523	2.185	180	108	581	1500
AVQZ ^c (cpp)/MRCI	1.512	2.206	180	108	591	1570
Fitted surface by MRCI	1.512	2.207	180	100	613	1543

^aFrom Ref. 17: Stuttgart quasirelativistic ECP with valence $3s3p1d$ contraction with a diffuse s augmentation for the halogens and $6-311G(p)$ for the hydrogen.

^bCore polarization potential.

^cNo g functions included in the basis set.

mix used was between 0.05% and 0.5% HBr (or DBr) in argon (higher HBr concentrations for bare BrHI⁻ clusters, lower for BrHI⁻·Ar), passed over a small quantity of methyl iodide, then expanded into the vacuum via a pulsed molecular beam valve (General Valve). The ions produced from the expansion pass through a 2-mm-diameter skimmer. The negative ion beam is collimated by a gas-filled radio frequency (rf) decapole ion guide and then directed into a quadrupole mass filter. The mass-selected anions are collected in a linear rf hexadecapole ion trap, which is filled with a background pressure of approximately 0.015 mbar of helium and connected to the head of a close-to helium cryostat held at 16 K. For typical IRMPD experiments, the trap is filled for 150 ms (500 ms for the VPD experiments), corresponding to approximately 15 gas pulses being stored before interacting with the field. Because FELIX runs at 5 Hz, it is preferable to store for less than 200 ms to take full advantage of each FELIX pulse. However, for the BrHI⁻·Ar and BrDI⁻·Ar experiments, longer storage times were needed to compensate for the lower numbers produced and for the loss in the trap.

The FELIX radiation used for these experiments ranges from 6 to 17 μm (1666–590 cm⁻¹) with a bandwidth on the order of 0.4% of the central energy (full width at half maximum); it enters the trap collinearly with the ions. Typical powers are the order of 300 mW at the center of the range but decrease significantly at the lower wavelengths in the range used (less than 7 μm) to about 100 mW. Additionally, each 5- μs macropulse contains a series of several thousand micropulses, each approximately 1 ps in duration, with about 1 ns between micropulses. To increase the photon density in the trap, the beam is focused at the center of the interaction region using a 50-cm focal length KBr lens. The calibration of FELIX is achieved by an external spectral analyzer.

Approximately 1 ms after their interaction with the radiation field, the ions are emptied from the trap and directed into a second quadrupole mass filter, which separates the fragment ions from their undissociated parent ions for detection. For the weakly bound BrHI⁻·Ar and BrDI⁻·Ar complexes, collisional cooling with the helium in the ion trap

causes significant dissociation. Approximately 80% of the complexes dissociate due to collisions in this case, but because this number is constant over the course of a stably running experiment, the parent complex depletion is monitored to produce a predissociation spectrum. In the BrHI⁻ and BrDI⁻ multiphoton experiments, monitoring the I⁻ daughter fragment produces more satisfactory results because of a near-zero background. Although parent ion depletion was sometimes visible, it was generally much smaller than in the VPD experiments and was difficult to detect on such a large background. Br⁻ appearance could also sometimes be observed but yielded no additional peaks.

III. THEORETICAL METHODS

A. Potential-energy surface and dipole moment

The electronic energy calculations and fitting are similar to the procedures used previously by Kaledin *et al.*¹⁷ In those calculations of the anion surface, the coupled cluster method was used and several high-energy configurations posed convergence problems. Moreover, bond breaking and the breakup limit, i.e., I⁻···H···Br, cannot be properly described with a single reference method. In this work, we use the more versatile multireference configuration interaction (MRCI) approach to map the surface with a future aim of investigating excited electronic states and spin-orbit coupling. We correct for non-size extensivity of MRCI by including Davidson's correction. Also, several basis sets, larger than those used previously, were investigated. For the effective core potential (ECP) for Br and I, the Stuttgart ECP set, which includes both f [for (AVTZ) basis] and g [for (AVQZ) basis] functions for Br and I, was used.²⁸ In our MRCI calculations, we use 31 reference configurations out of full valence complete active space with 16 electrons distributed in nine molecular orbitals. The final contracted configuration interaction contains around half a million configurations for the AVQZ basis without g functions. These calculations were performed with the MOLPRO quantum chemistry package.²⁹

In Table I, we compare the geometries and harmonic frequencies calculated with different basis sets. In order to

make a comparison with our previous work,¹⁷ we have used the coupled cluster singles and doubles with perturbative triples [CCSD(T)] method (which was used previously) in these calculations. We also include the results from the present MRCI calculations using the basis that was used to obtain the potential surface and the results from the potential surface. Comparison of the optimized geometries from the old and new basis sets shows that the biggest difference lies in r_{HI} , which is compressed by 0.13 Å using the new basis. In contrast, r_{HBr} increases by only about 0.02 Å. The harmonic frequencies at the equilibrium structure are also shifted significantly. The halogen stretch is blueshifted by about 20 cm^{-1} , a relative change of 23%; the H-atom stretch is redshifted by about 220 cm^{-1} , a relative change of 13%. This comparison clearly shows the importance of the f function for the halogen atoms and the necessity of constructing a PES using a large basis set. To determine the optimal basis set for the new PES, the convergence of the properties shown in Table I was monitored. As seen, the inclusion of g functions does not have a significant effect on the optimized geometries or the vibrational frequencies. On the other hand, the core-polarization potential (cpp)³⁰ term seems to give an appreciable correction with very little additional cost. Thus, the AVQZ basis (without g functions) with the Stuttgart ECP, including the core-polarization effect, was used as the basis for the electronic energy and dipole moment calculations. The CCSD(T) and MRCI optimized geometry and harmonic frequencies are in good agreement with each other (for the same basis), as expected. Also, the fitted potential reproduces the *ab initio* MRCI values well.

The IR intensities were calculated using MOLPRO in the standard double-harmonic approximation, yielding 0.00, (0.04 0.04), and 4908 km/mol for the halogen stretch, the (doubly degenerate) bend, and the H-atom stretch, respectively. Thus, these approximate calculations predict virtually no IR intensity for the halogen stretch and bend modes.

For the construction of the PES, 2268 *ab initio* energy points were computed on a regular three-dimensional (3D) grid defined by r_{HBr} [1.0,1.15,1.28,1.38,1.46, r_e = 1.513, 1.57, 1.65, 1.75,2.0,2.4,3.0,4.0,5.0] Å, r_{HI} [1.35,1.62,1.82, 1.94, 2.02,2.09,2.15, r_e = 2.205, 2.25, 2.32, 2.41, 2.53, 2.7,3.0, 3.7,5.0,7.0,9.0] Å, and θ_{BrHI} [180,177,172,165,155,140,120, 100,80] deg. It should be noted that there is another stationary collinear structure of the anion with Br in the middle, which is not covered in this grid. As has been discussed in the previous paper,¹⁷ the energy for this second minimum is too high to contribute to the low-lying vibrational states. The electronic energies and dipole moment were fit by a 3D spline, which was used in the ro-vibrational calculations described next.

B. Ro-vibrational calculations

The ro-vibrational bound-state variational calculations were carried out using two very different codes. One uses a Hamiltonian in Jacobi coordinates and a truncation/recoupling procedure as described in detail previously.¹⁷ The other code, RVIB3,^{31–33} uses a Hamiltonian in terms of two bond lengths, r_{HBr} and r_{HI} , and the bond angle θ_{BrHI} . Infrared transition probabilities were obtained from both codes by

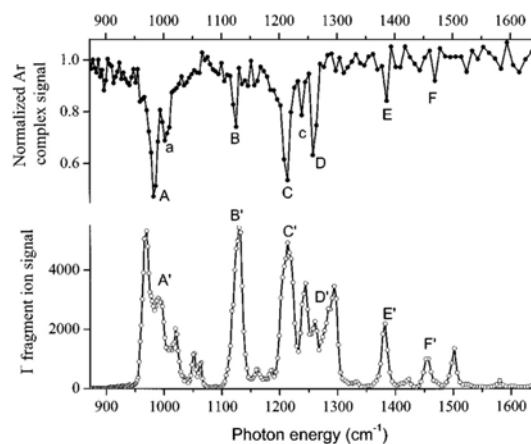


FIG. 1. Infrared dissociation spectra of $\text{BrHI} \cdot \text{Ar}$ (closed circles, upper trace) and BrHI^- (open circles, lower trace). Peaks in the $\text{BrHI} \cdot \text{Ar}$ predissociation spectrum, where the parent ion depletion is monitored, point downward, whereas the multiphoton spectrum of BrHI^- has upward peaks because the I^- fragment ion is monitored.

integrating dipole moment matrix elements over both the vibrational and rotational coordinates (the details of the “exact” calculations done in RVIB3 can be found in Ref. 32). These intensity calculations assumed $J=0$ to be the initial state of the anion and were done for final $J=1$ and $|\Delta K| = 0$ or 1, in accord with standard dipole selection rules. Parallel transitions, i.e., $\Delta K=0$, couple the initial state to excited bending states with an even quanta of bend excitation.

IV. RESULTS

A. Predissociation spectra

Parent ion depletion spectra for $\text{BrHI} \cdot \text{Ar}$ and $\text{BrDI}^- \cdot \text{Ar}$ are shown in the top traces of Figs. 1 and 2, respectively. Both spectra are scaled to the field-free background. The corresponding peak positions are given in Tables II and III.

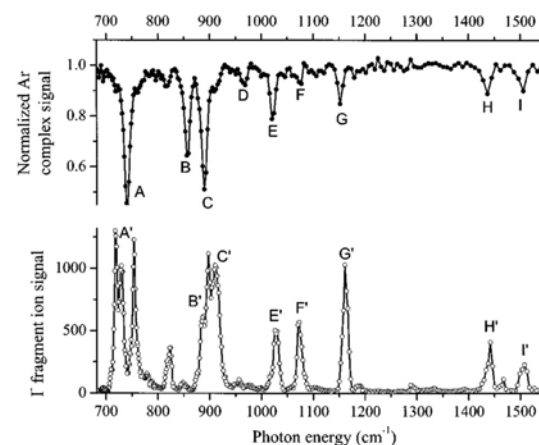


FIG. 2. Infrared dissociation spectra of $\text{BrDI} \cdot \text{Ar}$ (closed circles, upper trace) and BrDI^- (open circles, lower trace).

TABLE II. Peak assignments for predissociation spectra of BrHI⁻·Ar. Experimental intensities in brackets have been corrected and rescaled to the largest value to account for the number of photons.

Peak label	Peak position (cm ⁻¹)		Assignment (n ₁ n ₂ n ₃)	Intensity	
	Experiment	Calculation		Experiment [Corrected]	Calculation
<i>A</i>	984	983.2	0 2 0+0 0 1	1.0	1.0
<i>a</i>	1003	...	(0 2 0+0 0 1)+v _{Ar}	[0.75] 0.58	...
<i>B</i>	1127	1126.9	1 2 0+1 0 1	[0.39] 0.49	0.014
<i>C</i>	1215	1228.0	0 2 0-0 0 1	[0.40] 0.86	0.23
<i>c</i>	1238	...	(0 2 0-0 0 1)+v _{Ar}	[1.00] 0.39	...
<i>D</i>	1259	1268.1	2 2 0+2 0 1	[0.40] 0.70	0.12
<i>E</i>	1380	1390.0	3 2 0+3 0 1	[0.80] 0.30	0.0029
<i>F</i>	1468	1462.4	2 2 0-2 0 1	[0.40] 0.14	0.00050
				[0.25]	

The spectra in each case were taken at steps of 0.01 μm. Peaks *A* and *C* at 984 and 1215 cm⁻¹ for BrHI⁻·Ar and 742 and 890 cm⁻¹ for BrDI⁻·Ar are the most intense features in each spectrum. In each case, they correspond closely to the two higher energy peaks seen in Ellison and Ault's matrix work (920 and 1171 cm⁻¹ in BrHI⁻, 730 and 861 cm⁻¹ for BrDI⁻).¹⁰ All four matrix values are lower than the corresponding gas phase frequencies, with redshifts varying from 12 cm⁻¹ (peak *A*, BrDI⁻) to 64 cm⁻¹ (peak *A*, BrHI⁻). As discussed in Sec. I, the higher-energy matrix peaks were attributed to the more asymmetric type I anion structure. No peaks assigned to the type II structure are observed in the gas phase, although the peaks should be well within the range of the FELIX radiation used, implying that only the type I

structure is observed in the gas phase. However, as will be discussed below, the peaks presented cannot be assigned as simply as was done in the matrix work.

In addition, several peaks that were not seen previously are present in both spectra. Peaks *A*, *B*, and *D* in BrHI⁻·Ar are approximately evenly spaced (143 cm⁻¹ between *A* and *B*, 132 cm⁻¹ between *B* and *D*). In BrDI⁻·Ar, peaks *A*, *B*, *D*, and *F* are spaced by approximately 110 cm⁻¹ and *C*, *E*, and *G* by about 130 cm⁻¹. This pattern suggests combination bands involving the low-frequency *v*₁ stretch, primarily a heavy-atom vibration in these anions. A more definitive assignment emerges from comparison with the simulations in Sec. V. Also present is a small peak (labeled peak *a*) to the blue of peak *A* in BrHI⁻·Ar, which does not appear as

TABLE III. Peak Assignments for predissociation spectra of BrDI⁻·Ar. Experimental intensities in brackets have been corrected and rescaled to the largest value to account for the number of photons.

Peak label	Peak position (cm ⁻¹)		Assignment (n ₁ n ₂ n ₃)	Intensity	
	Experiment	Calculation		Experiment [Corrected]	Calculation
<i>A</i>	742	747.9	020+001	1.0	1.0
<i>B</i>	857	864.2	120+101	[0.95] 0.65	0.15
<i>C</i>	890	910.5	020-001	[0.64] 0.89	0.53
<i>D</i>	970	971.7	220+201	[1.00] 0.15	0.00070
<i>E</i>	1021	1041.9	120-101	[0.14] 0.38	0.025
<i>F</i>	1080	1077.3	320+301	[0.45] 0.13	0.0084
<i>G</i>	1154	1165.4	220-201	[0.17] 0.27	0.0074
<i>H</i>	1433	1448.2	040+002	[0.38] 0.20	0.095
<i>I</i>	1502	1520.9	040-002	[0.57] 0.18	0.026
				[0.66]	

TABLE IV. Peak assignments for multiphoton dissociation of BrHI⁻. Values in brackets are divided by two to show the expected two-photon frequency.

Peak label	Peak position (cm ⁻¹)			Number of photons
	Experiment	Calculation [$\div 2$]	Assignment	
<i>A'</i>	971	1939.3 [969.7]	040+002	2
	988	983.2	020+001	1
	1018	2035.6 [1017.8]	040-002	2
	1051	2107.9 [1054.0]	140+102	2
	1064	2123.4 [1061.7]	140-102	2
<i>B'</i>	1127	1126.9	120+101	1
	1162	2332.2 [1166.1]	240-202	2
	1187	2375.6 [1187.8]	340+302	2
<i>C'</i>	1213	1228.0	020-001	1
	1244	2445.2 [1222.6]	340-302	2
		2457.7 [1228.9]	021	2
<i>D'</i>	1262	1268.1	220+201	1
	1294	2599.6 [1299.8]	121	2
	1333	1339.0	120-101	1
<i>E'</i>	1382	1390.0	320+301	1
	1423	2857 [1428.5]	221	2
<i>F</i>	1455	1462.4	220-201	1
	1498	1498.9	420+401	1
	1580	1587.1	520+501	1

prominently in the BrDI⁻·Ar spectrum. Similarly, a small peak (peak *c*) is seen to the blue of peak *C* in BrHI⁻·Ar. Both of these small peaks are approximately 20 cm⁻¹ separated from the preceding peak.

Finally, Tables II and III present the experimental depletion intensities for comparison with the theoretical transition strengths. The experimental values are actually given by $-\ln(c/c_0)$, where c/c_0 is the depletion signal read from Figs. 1 and 2. Here, we assume that all the complexes vibrationally excited by each micropulse dissociate before the next micropulse 1 ns later, so that there is a steadily decreasing number of ions interacting with the successive micropulses. Under these circumstances, it is $-\ln(c/c_0)$ that is proportional to the transition strength. Additionally, the intensities scaled to the photon flux at each wavelength are listed in square brackets in order to account for the decreased flux at the higher-frequency range of the spectra in Figs. 1 and 2. Both sets of values have been normalized to set the most intense peak to unity.

B. Multiphoton spectra

The dissociation spectra of bare BrHI⁻ and BrDI⁻ obtained by monitoring I⁻ fragment production are shown in the lower traces of Figs. 1 and 2, respectively. Line positions are given in Tables IV and V. There are clear correspondences between the vibrational predissociation and multiphoton spectra, as is emphasized by the labeling scheme (*A* versus *A'*, etc.) used in the two sets of spectra. There are, however, significant differences. There are more peaks in the multiphoton spectra and many of the smaller peaks are more intense than in the VPD spectra. The main peaks (*A* and *C*) in the VPD spectra appear as clusters of closely spaced peaks in the IRMPD spectra. Finally, there is usually a small fre-

TABLE V. Peak assignments for multiphoton dissociation of BrDI⁻. Values in brackets are divided by two to show the expected two-photon frequency.

Peak label	Peak position (cm ⁻¹)			Number of photons
	Experiment	Calculation [$\div 2$]	Assignment	
<i>A'</i>	719	1448.2 [724.1]	040+002	2
	730	747.9	020+001	1
	755	1520.9 [760.5]	040-002	2
	779	1582.9 [791.5]	140+102	2
	827	1645.3 [822.7]	140-102	2
	848	1691.1 [845.6]	240+202	2
<i>B'</i>	886	864.2	120+101	1
	900	1801.1 [900.6]	240-202	2
<i>C'</i>	911	910.5	020-001	1
		1819.9 [910.0]	021	2
	956	1939.4 [969.7]	121	2
		971.7	220+201	1
<i>E'</i>	1029	1041.9	120-101	1
<i>F'</i>	1073	1077.3	320+301	1
<i>G'</i>	1164	1165.4	220-201	1
	1188	1185.7	320-301	1
	1291	1305.5	420+401	1
<i>H'</i>	1442	1448.2	040+002	1
	1466	1429.3	420-401	1
<i>I'</i>	1509	1520.9	040-002	1

quency shift (up to 30 cm⁻¹) between pairs of corresponding peaks in the two sets of spectra.

C. Theoretical results

Selected bound-state energies of BrHI⁻ and BrDI⁻ are given in Tables II and III (for initial $J=0$, obtained with the truncation/recoupling code) along with the corresponding assignments based on inspection of expectation values of the Jacobi coordinates and visual analysis of the wave functions. The RVIB3 code produced nearly identical results. Inspection of these wave functions revealed extensive mode mixing between the bending and the H-atom stretch modes due to Fermi resonance. For example, there is a strong mixing between the $(v_1 v_2 v_3) = (0 0 1)$ and $(0 2 0)$ zero-order states. To demonstrate this, a simple deperturbation procedure was performed, where the sum and difference of these two eigenstates were determined. Contour plots of the resulting wave functions, along with the original eigenstates, are shown in Fig. 3. The two top plots in Fig. 3 show the two-dimensional cuts of the wave functions of the 983 and 1228 cm⁻¹ eigenstates, whereas the two bottom plots present the sum (on the left) and the difference (on the right) of these two wave functions. After the deperturbation process, the two unassignable eigenstates become the $(0 2 0)$ state (for the sum) and the $(0 0 1)$ state (for the difference). The bend overtone (as opposed to the fundamental) is assigned based on the presence of two nodes along the angular coordinate, only half of which is shown in the figure. As a result of these observations, a special assignment representation has been used to indicate the Fermi resonances formed by two pure states.

The transition energies calculated using the Jacobi coordinate truncation/recoupling procedure and infrared intensi-

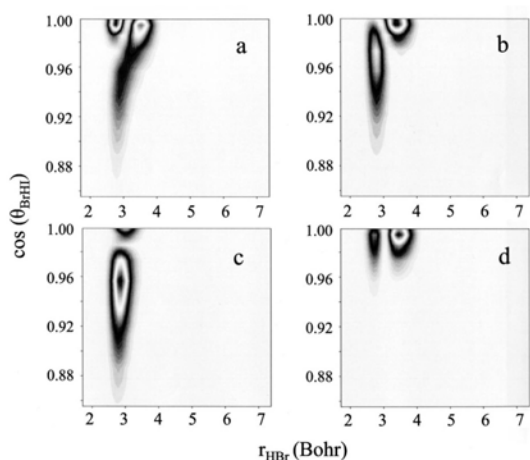


FIG. 3. Contour plots of the eigenfunctions at (a) 983.2 and (b) 1126.9 cm^{-1} , and (c) sum and (d) difference of the two, representing the pure states of the bending overtone and the H-atom stretch modes, respectively. The plots are two-dimensional slices in the plane defined by r_{HBr} and the bond angle θ_{BrHI} .

ties calculated by the RVIB3 code are listed in Tables II and III. These have been scaled relative to the highest intensity, which is assigned to unity. The relative intensities are shown against the predissociation spectra of BrHI^- and BrDI^- in Fig. 4. In this figure, the experimental data are plotted on a logarithmic scale for reasons discussed in Sec. IV A. The correspondence between the calculated and the experimental peak positions is strikingly clear, and the intensities of the strongest peaks are also in good agreement. There is more divergence between the theoretical and experimental intensities for many of the smaller features, with considerably more dynamic range in the calculated values.

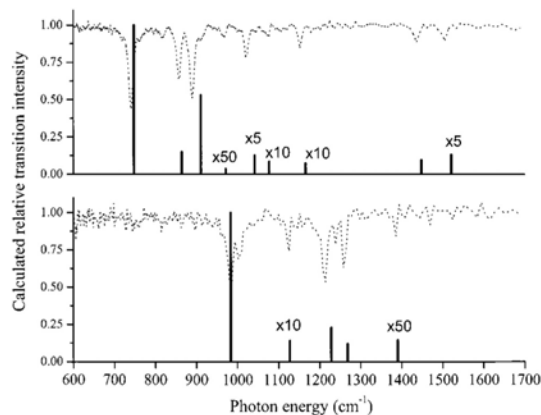


FIG. 4. Comparison of the predissociation spectra (dotted traces) with the calculated frequencies and intensities based on the dipole moment matrix elements. The lower portion shows BrHI^- ; BrDI^- is shown above it. The experimental data are normalized to the background and shown on a logarithmic scale. Calculated intensities are normalized to the largest intensity and plotted on a linear scale for comparison.

To estimate the effect of argon on the vibrations of BrHI^- , we optimized the $\text{BrHI}^- \cdot \text{Ar}$ complex using the CCSD(T) method with the AVTZ basis and ECP for Br, I, and Ar atoms. Three stationary structures were located with binding energy ranging from 275 to 377 cm^{-1} . The lowest energy structure has a T-shaped geometry with the Ar atom closer to I than to the Br atom. A full normal-mode analysis at the three stationary points revealed shifts in the BrHI^- modes of at most 5 and 13 cm^{-1} for the bending and H-atom stretch harmonic frequencies, respectively. Although this is slightly smaller than some of the shifts observed in the experiment, it is clear from the full-dimensional simulations that harmonic frequencies are not sufficient to describe quantitatively the vibrational energies of these anions. Regardless, interpretation of the experimental data must not assume unreasonably large argon shifts.

V. ANALYSIS AND DISCUSSION

A. VPD spectra

The close correspondence between the matrix work of Ellison and Ault¹⁰ and peaks A and C in our VPD spectra would suggest the same assignment for our spectra as were assigned to the matrix, namely, that peaks A and C are the (0 0 1) and (0 n 0) transitions, with $n=1$ or 2. On the other hand, Kaledin *et al.*¹⁷ calculated the (0 0 1) and (0 2 0) transitions in BrHI^- to lie slightly to the blue of the gas phase peaks C and A, respectively, at 1266 and 1026 cm^{-1} . This result suggests that the matrix assignment needs to be reversed. Neither assignment, however, explains why the two transitions are of comparable intensity; as shown earlier, the harmonic calculations predict the (0 0 1) transition to be considerably more intense than the bending fundamental, let alone the overtone. In addition, assigning either peak A or C to the (0 2 0) transition is somewhat awkward, as there is no corresponding (0 1 0) transition at approximately half the frequency in the gas phase infrared spectrum or in the matrix. Assignment of the BrHI^- and BrDI^- VPD spectra is therefore less straightforward than might be expected for a triatomic molecule.

The ambiguity regarding the assignment of the major peaks is removed by the calculations presented here, in which we determine accurate ro-vibrational eigenstates and eigenfunctions on a high-level, three-dimensional potential-energy surface. These new calculations show a significant degree of mode mixing between the bending and the H-atom stretch modes. Consequently, peaks A and C are best described as transitions to (0 2 0 ± 0 0 1) states, both of which have significant zero-order bend and H-atom stretch character. The striking agreement between the experiment and simulated peak positions, as shown in Tables II and III, is compelling evidence for the assignments provided in those tables and an indication that the potential energy surface used here is satisfactory to describe the vibrational modes of the BrHI^- and BrDI^- anions. The strong mode mixing also explains the comparable intensities of peaks A and C because each eigenstate has a significant (0 0 1) admixture.

The calculations support our conjecture in Sec. IV A that peaks B and D in the $\text{BrHI}^- \cdot \text{Ar}$ spectrum and peaks B, D, E,

F, and *G* are combination bands based on peaks *A* and *C* involving the low-frequency ν_1 mode. The calculated frequencies and assignments based on the wave-function analysis are given in Tables II and III. The calculations also suggest assignments for the two highest energy peaks *H* and *I* in the $\text{BrDI}^- \cdot \text{Ar}$ spectrum to the $(0\ 4\ 0 \pm 0\ 0\ 2)$ transitions. The small peaks *a* and *c* in the $\text{BrHI}^- \cdot \text{Ar}$ spectrum are also identified in Table II as the addition of some mode involving the argon atom. The spacings of peaks *a* and *c* from peaks *A* and *C*, respectively, is approximately the same as in $\text{BrHBr}^- \cdot \text{Ar}$,⁸ where similar argon modes were observed.

Overall, the agreement between the experimental and calculated peak positions is excellent, as can be seen in Tables II and III and in Fig. 4. However, the intensities do not agree nearly as well. Many of the smaller peaks are considerably more intense in the experimental VPD spectra than in the calculations, particularly the combination bands involving excitation of the ν_1 mode. This discrepancy may reflect saturation effects in the experiment; the FEL beam does not fully overlap the trapped ions, so even if all the ions in the laser field are excited, one would not observe a 100% depletion. This effect reduces the relative intensity of the strongest transitions in the experiment, making the weaker peaks look more intense than they actually are. It is also possible that anharmonic effects involving the ν_1 mode are underestimated in the calculations. However, the ν_1 combination bands to the blue of peaks *A* and *C* are essentially absent from the matrix absorption spectra, lending support to the intensity discrepancies originating in the VPD spectra rather than in the calculations.

Finally, the full ro-vibrational calculations find the $(0\ 1\ 0)$ transition strength to be comparable to that of the $(0\ 0\ 1)$ transition, in contrast to the harmonic results. It thus appears that the harmonic approximation breaks down badly even in describing the bend fundamental of BrHI^- . The calculated positions for the $(0\ 1\ 0)$ peaks of BrHI^- and BrDI^- are 597.2 and $426.8\ \text{cm}^{-1}$, respectively. This result has interesting implications for the matrix IR spectra because the $666\ \text{cm}^{-1}$ peak for BrHI^- and $470\ \text{cm}^{-1}$ peak for BrDI^- , which were originally assigned to the type II structure, could actually be the $(0\ 1\ 0)$ peaks, both blueshifted by less than $70\ \text{cm}^{-1}$ from the calculated values. This assignment would imply that only one form of the anion exists in the matrix. The observation of $(0\ 1\ 0)$ transitions in the gas phase experiments near the calculated values would confirm this new interpretation. Unfortunately, the calculated $(0\ 1\ 0)$ frequency for BrDI^- is well below the lowest frequency available to the gas phase experiment in its current configuration, $590\ \text{cm}^{-1}$, whereas that for BrHI^- is very close to this lower limit and may also be out of range.

B. Multiphoton spectra

There are clearly more peaks in the multiphoton spectra than in the VPD spectra, and the additional peaks appear to cluster near the frequencies at which peaks *A* and *C* are observed in the VPD spectra. In the frequency range probed by our experiments, four to ten photons are required to reach the dissociation limit of BrHI^- . Moreover, a triatomic anion is less favorable for resonant IRMPD than the larger systems

we have studied with this method^{22,23} owing to the lower density of states at comparable levels of vibrational excitation. Under these circumstances, it is not totally unexpected that the VPD and the IRMPD spectra are not identical, presenting us with the challenge of assigning the extra peaks in the IRMPD spectra.

The additional peaks could be vibrational hot bands, but these should be largely eliminated in the spectra because the ions are cooled by collisions with cold He atoms in the ion trap prior to the interaction with the laser pulse. Alternatively, these bands could result from multiphoton transitions in which two (or more) photons are resonant with a vibrational transition in the anion. The photon energies at which these transitions would be excited will be shifted from the single-photon transitions owing to anharmonicities in the anion. While such transitions would normally be very weak, we point out that the peak intensities of the FEL are quite high ($10\text{--}100\ \text{MW}/\text{cm}^2$). In addition, resonant excitation to a higher-lying vibrational level, i.e., an overtone versus a fundamental, should result in more facile subsequent multiphoton absorption and dissociation.

In order to explore this possibility further, the energies of several vibrational levels of BrHI^- and BrDI^- lying at about twice the frequency of those seen in the VPD spectra were calculated and tabulated in Tables IV and V; assuming that these are accessible by two-photon transitions, the photon energy at which each level would be excited is given in square brackets. The calculated peak positions are listed alongside the experimental peak positions. In doing so, one finds a remarkably good agreement with both the one- and the two-photon transitions. For example, a comparison of the five peaks in the lowest energy cluster for BrHI^- (collectively labeled as *A'* in Table IV) shows that no pair of calculated and experimental frequencies differs by more than $5\ \text{cm}^{-1}$, supporting the proposed assignments. The correspondence between experiment and theory for some of the highest energy transitions is tenuous because the experimental peaks are barely above the noise level.

The assignments given in Tables IV and V have the seemingly undesirable feature that the most intense peak in a particular cluster is often a two-photon rather than a one-photon transition. For example, in BrHI^- , the most intense peak at $971\ \text{cm}^{-1}$ is assigned as the two-photon transition to the $(0\ 4\ 0+0\ 0\ 2)$ level, whereas the less-intense neighboring peak at $988\ \text{cm}^{-1}$ is assigned as the one-photon transition to the $(0\ 2\ 0+0\ 0\ 1)$ level. However, as discussed earlier, the intensities in the multiphoton spectra do not necessarily represent the transition strengths, because subsequent absorption from higher-lying levels is expected to be more facile. Similarly, one might expect that the one-photon transition to the $(0\ 4\ 0+0\ 0\ 2)$ level in BrDI^- (peak *H'* at $1442\ \text{cm}^{-1}$, Fig. 2) would be more intense than the two-photon transition to the same level (peak *A'* at $719\ \text{cm}^{-1}$). Here, however, there is the additional compensating factor that the FEL intensity is about a factor of 3 lower at peak *H'* compared to peak *A'*.

Finally, as can be seen from the tables, the peaks in the VPD and IRMPD spectra assigned to the same transitions

occur at slightly different energies. These shifts are largest at lower photon energies and appear to be more significant for BrDI⁻ than for BrHI⁻, as can be seen by inspection of the two sets of spectra in Figs. 1 and 2. In BrHI⁻, the shifts due to argon are at most 13 cm⁻¹, much smaller than in BrDI⁻, where several shifts larger than 20 cm⁻¹ are present. Some of the larger shifts in BrDI⁻ may reflect ambiguities in the assignment of the IRMPD spectra. For example, the (1 2 0+1 0 1) peak (*B* in the VPD spectrum, *B'* in the IRMPD spectrum), which shows no discernible shift upon addition of the argon atom in BrHI⁻, shows a shift in BrDI⁻ of 29 cm⁻¹ to the red. In the case of the BrDI⁻ multiphoton spectrum, the (1 2 0+1 0 1) transition could also have been assigned to the peak at 848 cm⁻¹, for a shift of only 9 cm⁻¹ (this time to the blue). However, assigning the very weak peak at 848 cm⁻¹ to an allowed one-photon transition seems less desirable than the assignment given in Table V. The question arises as to whether these shifts are from Ar complexation, the multiphoton nature of the IRMPD process, or some combination of the two. In fact, the shifts in the BrHI⁻·Ar VPD spectrum relative to the bare-ion IRMPD spectrum are within the range expected for the Ar complexation, as predicted by the harmonic calculations in Sec. IV C. The origin of the larger shifts in BrDI⁻ are less clear at this time and their interpretation may require a more sophisticated theoretical treatment of the vibrational energy levels in BrHI⁻·Ar.

VI. SUMMARY

The gas phase vibrational predissociation of BrHI⁻·Ar and BrHI⁻·Ar and multiphoton dissociation spectra of BrHI⁻ and BrDI⁻ have been measured using a tunable infrared free-electron laser. In addition, high-level calculations of the anion potential energy surface and the vibrational eigenstates and eigenfunctions supported by this surface have been carried out. Comparison of the experimental and theoretical results leads to a detailed assignment of all the spectral features. Multiphoton dissociation spectra revealed some additional structure assigned to transitions to higher-energy states via two-photon transitions.

The gas phase frequencies observed here are close to those seen in earlier matrix-isolation experiments and attributed to the type I form of the anion. However, our assignment differs from the original assignment of the matrix spectra. In particular, the calculated vibrational energy levels show a remarkable extent of mode mixing between the H-atom stretch and the bend modes, which manifests itself in numerous Fermi resonance states, leading to a more complex spectrum than would be expected otherwise. These mixed states help explain the difficulties in modeling the system under the harmonic approximation, both because of the perturbation of states and because of the extreme mechanical anharmonicity, that allows those perturbations. The work presented here also suggests that the matrix features attributed to the symmetric (type II) anion may arise from the bend fundamental and/or the associated combination band with the heavy atom stretch rather than that from a form of the ion different from that seen in the gas phase.

ACKNOWLEDGMENTS

This work is supported by the Specialized Research Center 546 and the Ph.D. Graduate Study Program 788 of the German Research Foundation DFG. The authors gratefully acknowledge the support of the *Stichting voor Fundamenteel Onderzoek der Materie* (FOM) in providing the required beam time on FELIX and highly appreciate the skillful assistance of the FELIX staff. C.K., C.C.U., and K.R.A. gratefully acknowledge the helpful discussions with and technical expertise from Professor Ludger Wöste, Professor Gerard Meijer, and Dr. Gert von Helden. D.M.N. thanks the Air Force Office of Scientific Research for the support under Grant No. F49620-03-1-0085. A.O. thanks the Swiss National Science Foundation for funding. J.M.B. thanks the National Science Foundation (Grant Nos. CHE-0131482 and ITR CHE-0219331) for funding.

- ¹G. C. Pimentel, *J. Chem. Phys.* **19**, 446 (1951).
- ²G. A. Landrum, N. Goldberg, and R. Hoffman, *J. Chem. Soc. Dalton Trans.* **1997**, 3605.
- ³G. Caldwell and P. Kebarle, *Can. J. Chem.* **63**, 1399 (1985).
- ⁴K. Kawaguchi, *J. Chem. Phys.* **88**, 4186 (1988).
- ⁵D. M. Neumark, *Acc. Chem. Res.* **26**, 33 (1993).
- ⁶D. M. Neumark, *PhysChemComm* **5**, 76 (2002).
- ⁷B. S. Ault, *Acc. Chem. Res.* **15**, 103 (1982).
- ⁸N. L. Pivonka, C. Kaposta, M. Brummer, G. von Helden, G. Meijer, L. Wöste, D. M. Neumark, and K. R. Asmis, *J. Chem. Phys.* **118**, 5275 (2003).
- ⁹K. Kawaguchi and E. Hirota, *J. Chem. Phys.* **87**, 6838 (1987).
- ¹⁰C. M. Ellison and B. S. Ault, *J. Phys. Chem.* **83**, 832 (1979).
- ¹¹B. S. Ault, *J. Phys. Chem.* **83**, 837 (1979).
- ¹²S. E. Bradforth, A. Weaver, D. W. Arnold, R. B. Metz, and D. M. Neumark, *J. Chem. Phys.* **92**, 7205 (1990).
- ¹³Z. Liu, H. Gomez, and D. M. Neumark, *Chem. Phys. Lett.* **332**, 65 (2000).
- ¹⁴R. B. Metz and D. M. Neumark, *J. Chem. Phys.* **97**, 962 (1992).
- ¹⁵S. G. Lias, J. E. Bartmess, J. F. Liebman, J. L. Holmes, R. D. Levin, and W. G. Mallard, *J. Phys. Chem. Ref. Data* **17**, 1 (1988).
- ¹⁶M. Broida and A. Persky, *Chem. Phys.* **133**, 405 (1989).
- ¹⁷A. Kaledin, S. Skokov, J. M. Bowman, and K. Morokuma, *J. Chem. Phys.* **113**, 9479 (2000).
- ¹⁸K. P. Huber and G. Herzberg, *Molecular Spectra and Molecular Structure IV: Constants of Diatomic Molecules* (Van Nostrand-Reinhold, New York, 1977).
- ¹⁹G. von Helden, D. van Heijnsbergen, and G. Meijer, *J. Phys. Chem. A* **107**, 1671 (2003).
- ²⁰G. von Helden, I. Holleman, G. M. H. Knippels, A. F. G. van der Meer, and G. Meijer, *Phys. Rev. Lett.* **79**, 5234 (1997).
- ²¹H. Piest, G. von Helden, and G. Meijer, *J. Chem. Phys.* **110**, 2010 (1999).
- ²²N. L. Pivonka, C. Kaposta, G. von Helden, G. Meijer, L. Wöste, D. M. Neumark, and K. R. Asmis, *J. Chem. Phys.* **117**, 6493 (2002).
- ²³K. R. Asmis, N. L. Pivonka, G. Santambrogio, M. Brummer, C. Kaposta, D. M. Neumark, and L. Wöste, *Science* **299**, 1375 (2003).
- ²⁴M. Okumura, L. I. Yeh, and Y. T. Lee, *J. Chem. Phys.* **83**, 3705 (1985).
- ²⁵E. J. Bieske, S. A. Nizkorodov, O. Dopfer, J. P. Maier, R. J. Strickland, B. J. Cottrell, and B. J. Howard, *Chem. Phys. Lett.* **250**, 266 (1996).
- ²⁶P. Ayotte, C. G. Bailey, G. H. Weddle, and M. A. Johnson, *J. Phys. Chem. A* **102**, 3067 (1998).
- ²⁷K. R. Asmis, M. Brummer, C. Kaposta, G. Santambrogio, G. von Helden, G. Meijer, K. Rademann, and L. Wöste, *Phys. Chem. Chem. Phys.* **4**, 1101 (2002).
- ²⁸M. Dolg, Ph.D. thesis, Universität Stuttgart, 1989.
- ²⁹MOLPRO is a package of ab initio programs written by H.-J. Werner and P. J. Knowles, with contributions from R. D. Amos, A. Berning, D. L. Co-

- per, M. J. O. Deegan, A. J. Dobbyn, F. Eckert, C. Hampel, G. Hetzer, T. Leninger, R. Lindh, A. W. Lloyd, W. Meyer, M. E. Mura, A. Nicklaß, P. Palmieri, K. Peterson, R. Pitzer, P. Pulay, G. Rauhut, M. Schütz, H. Stoll, A. J. Stone, and T. Thorsteinsson.
- ³⁰W. Müller, J. Flesch, and W. Meyer, *J. Chem. Phys.* **80**, 3297 (1984).
- ³¹S. Carter, N. C. Handy, R. Puzzarini, R. Tarroni, and P. Palmieri, *Mol. Phys.* **98**, 1713 (2000).
- ³²S. Carter, N. C. Senekowitsch, N. C. Handy, and P. Rosmus, *Mol. Phys.* **65**, 143 (1988).
- ³³T. Taketsugu, K. Ishii, and S. Carter, *Chem. Phys. Lett.* **380**, 213 (2003).

Gas Phase Vibrational Spectroscopy of Strong Hydrogen Bonds

Knut R. Asmis

Department of Molecular Physics, Fritz-Haber-Institut der Max-Planck-Gesellschaft, Berlin, Germany

Daniel M. Neumark

Department of Chemistry, University of California, Berkeley, CA, USA

Joel M. Bowman

Department of Chemistry and Cherry L. Emerson Center for Scientific Computation, Emory University, Atlanta, USA

Chapter in

Physical and Chemical Aspects of Hydrogen Transfer, edited by J. T. Hynes and H. H. Limbach; Vol. 1 of *Handbook of Hydrogen Transfer*, edited by R. L. Schowen (Wiley-VCH, Weinheim, Germany, 2005).

Gas Phase Vibrational Spectroscopy of Strong Hydrogen Bonds

Knut R. Asmis

*Department of Molecular Physics, Fritz-Haber-Institut der Max-Planck-Gesellschaft, Berlin,
Germany*

Daniel M. Neumark

Department of Chemistry, University of California, Berkeley, CA, USA

and

Joel M. Bowman

*Department of Chemistry and Cherry L. Emerson Center for Scientific Computation,
Emory University, Atlanta, USA*

1	Introduction.....	2
2	Methods.....	3
2.1	Vibrational Spectroscopy of Gas Phase Ions.....	3
2.2	Experimental Setup.....	5
2.3	Potential Energy Surfaces.....	6
2.4	Vibrational Calculations.....	8
3	Selected Systems.....	9
3.1	Bihalide Anions.....	9
3.2	The Protonated Water Dimer ($\text{H}_2\text{O}\cdots\text{H}\cdots\text{OH}_2$) ⁺	14
4	Outlook.....	23

1 Introduction

The hydrogen bond interaction is key to understanding the structure and properties of water, biomolecules, self-assembled nanostructures and molecular crystals. However, much confusion remains about its electronic nature, a combination of van der Waals, electrostatic and covalent contributions, leading to a wide variety of hydrogen bonds with bond strengths ranging from 2 to 40 kcal/mol. In particular, our understanding of strong, low-barrier hydrogen bonds and their central role in enzyme catalysis^[1], biomolecular recognition^[2], proton transfer across biomembranes^[3] and proton transport in aqueous media^[4] remains sketchy. The central aim of this chapter is to outline some recent advances in the research on strongly hydrogen bonded model systems in the gas phase with emphasis on the work from our research groups.

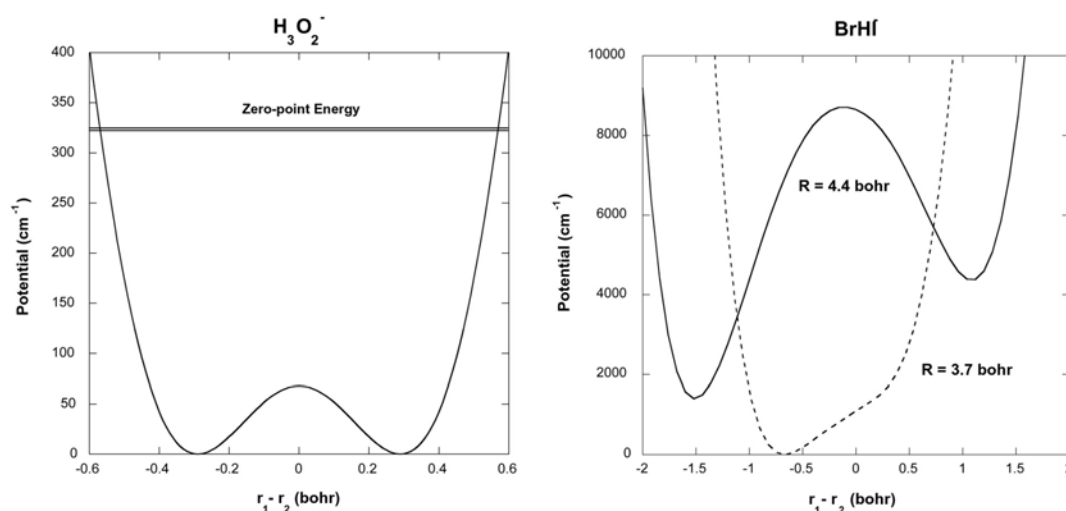


Figure 1: Typical potential energy curves for strong, low-barrier hydrogen bonds. The homoconjugated $H_3O_2^-$ (left) exhibits a (relaxed) symmetric, double-well potential as a function of the difference of the bridging hydrogen distance with the two oxygen atoms. The heteroconjugated $BrHI^-$ (right) is characterized by an asymmetric single-well potential at equilibrium and an asymmetric double well at a larger $Br-I^-$ distance.

Strong hydrogen bonds ($A\cdots H\cdots B$) are often classified based on their hydrogen bond energy; a typically cited lower limit is >15 kcal/mol.^[5] Their most prominent physical properties are large NMR downfield chemical shifts and considerably red-shifted hydrogen stretch frequencies. Moreover, the H-atom transfer barrier, a characteristic feature of weak hydrogen bonds $A-H\cdots B$, is either absent or very small in these systems (at their minimum energy geometry). Consequently, the H-atom in homoconjugated ($A=B$) strong hydrogen bonds is equally shared by the two heavy atoms forming two identical strong hydrogen bonds. This symmetry is lost in heteroconjugated ($A\neq B$) systems, but the H-atom remains in a more centered position, i.e., the distance between the heavy

atoms is smaller than in weaker hydrogen bonded systems. Strong hydrogen bonds can either be low-barrier, as in $(\text{HO}\cdots\text{H}\cdots\text{OH})^-$, or single-well, as in $(\text{Br}\cdots\text{H}\cdots\text{I})^-$, depending on the form of the potential curve along the H-atom exchange coordinate (see Figure 1 and below).

Hydrogen bonds are very sensitive to perturbation, due to an intimate interdependence between heavy atom separation, H-atom exchange barrier and position of the light H-atom leading to unusually high proton polarizabilities. Therefore it can prove advantageous to study strong hydrogen bonds in the gas phase, in the absence of any perturbations from surrounding solvent or host molecules. Standard experimental techniques to study strong hydrogen bonds, including NMR, as well as x-ray and neutron diffraction, are currently limited to condensed phase probes. Gas phase experiments are hindered by low number densities and only vibrational spectroscopy exhibits the required sensitivity and selectivity to perform such studies.

Recently, advances in laser technology as well as in computational approaches have allowed for significant progress in the study of strongly hydrogen bonded model systems. We first describe these improved experimental and theoretical methods and then discuss experiments and calculations on three prototypical systems containing strong hydrogen bonds: BrHBr^- , BrHI^- and H_5O_2^+ . These results demonstrate that the vibrational spectroscopy of triatomic systems involving strong hydrogen bonds has now been successfully solved, even when heavy atoms like iodine are involved. However, the study of slightly larger systems like the protonated water dimer remains challenging.

2 Methods

2.1 Vibrational Spectroscopy of Gas Phase Ions

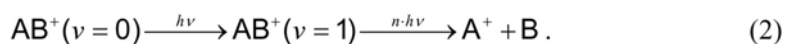
Vibrational spectroscopy paired with quantum chemistry currently offers the most direct and generally applicable experimental approach to structural investigation of neutral and charged cluster in the gas phase.^[6] Direct absorption measurements based ion discharge modulation methods^[7] can yield high resolution spectra of small and light molecular ions. Problems associated with high discharge temperatures can nowadays be overcome by using pulsed-slit supersonic expansions.^[8] However, these types of experiments become increasingly difficult for larger and heavier molecular ions, particularly ion clusters, owing to spectral congestion, lower gas phase number densities and presence of other absorbing species. Therefore alternative techniques have been developed in which the absorption of photons can be measured indirectly, by way of resonance enhanced photodissociation (or action) spectroscopy. Photodissociation techniques have the advantage that fragment ions can be detected background-free and with nearly 100% detection efficiency. A high

selectivity can be achieved through mass selection of parent and fragment ions using appropriate mass filters.

An infrared photodissociation (IR-PD) spectrum is measured by irradiating ions with infrared radiation and monitoring the yield of fragment ions as a function of the irradiation wavelength. In order to induce fragmentation the parent ion AB^+ (the same line of argumentation holds for negative ions) is required to absorb sufficient energy to overcome the (lowest) dissociation threshold. Once a metastable ro-vibronic state is reached, intramolecular energy redistribution will eventually lead to dissociation, producing a charged and a neutral fragment:

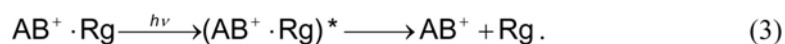


As noted before the dissociation energy of strong hydrogen bonds is roughly 5000 cm^{-1} or higher, while the fundamentals of the shared H-atom modes are found well below this limit. Process (1) therefore requires the absorption of multiple infrared photons. The coherent stepwise multiphoton excitation, where all photons are absorbed in one vibrational ladder, is unfavorable and becomes unrealistic for higher dissociation thresholds, because the laser runs out of resonance, due to the anharmonicity of vibrational potentials. The multiphoton process is better viewed as a sequential absorption of photons enhanced by rapid intramolecular vibrational energy redistribution at higher excitation.^[9] Only the first few photons are absorbed in the “discrete” regime, in which a particular mode is excited resonantly. Higher excitation accesses the “quasi-continuum”, in which the density of states is so high that the vibrational energy is rapidly randomized among all vibrational modes of the molecular ion. The ion continues to absorb photons until it has enough energy to dissociate. The transition between the two regimes depends on the vibrational density of states and the strengths of the interactions between vibrational modes. For larger molecular systems the IR-PD spectrum often resembles the linear absorption spectrum.^[10] For smaller systems with less internal degrees of freedom the relative intensities may be different. However, if the laser fluence is kept at a moderate level, signal is only detected, if the laser wavelength is resonant with a fundamental transition, that is,



At high laser fluence the probability of directly exciting overtones is enhanced, complicating the interpretation of the IR-PD spectrum.^[11]

A useful method to avoid multiphoton excitation and measure IR-PD spectra in the linear regime is the messenger atom technique^[12]:



By forming ion-rare gas atom (Rg) complexes the dissociation threshold of the system is lowered, generally below the photon energy and these predissociation spectra directly reflect the linear absorption spectrum. This technique has also been used to great effect in anion spectroscopy experiments.^[13] The multiphoton dissociation approach remains attractive for systems, in which the perturbation of the messenger atom cannot be neglected or in instruments where rare gas attachment is difficult.

IR-PD experiments generally require intense and tunable radiation sources which for many years were only commercially available in the wavelength region up to ~ 4 microns ($>2500\text{ cm}^{-1}$), that is the region of O-H stretches and overtones. The spectral signature of strong hydrogen bonds, however, is found at longer wavelengths. The application of free electron lasers (FELs) to molecular spectroscopy by Meijer and coworkers has bridged this gap.^[14] More recently, several groups^[15, 16] were able to access the region below 2000 cm^{-1} with higher energy, narrow bandwidth table-top laser systems, which make use of difference frequency mixing in an AgGaSe₂ crystal.^[17] Even though the pulse energy in these table-top systems is roughly three orders of magnitude smaller than from FEL sources and generally not sufficient to perform multiphoton absorption experiments, it is enough to photodissociate messenger atom-ion complexes.^[16]

2.2 Experimental Setup

The experiments described here were performed on a guided ion beam tandem mass spectrometer^[18] that was temporarily installed at the free electron laser facility FELIX (Free Electron Laser for Infrared Experiments, FOM Institute for Plasma Physics, Nieuwegein, The Netherlands).^[19] A schematic of the experimental setup is shown in Figure 2. Ions are generated in the ion source region (not shown) using either a pulsed supersonic jet crossed by a 1 keV electron beam for the bihalide anions or an ion spray source for the protonated water clusters. The ion beam containing a distribution of cluster ions of different size is collimated and compressed in phase space in a gas-filled radio frequency (RF) ion guide and directed into the first quadrupole mass filter. Mass-selected ions are then guided into a temperature-adjustable RF ion trap. The trap consists of a linear RF ion guide and two electrostatic ion lenses contained in a cylindrical housing, which is connected to the cold head of a closed-cycle He cryostat. The cylinder is continuously filled with He (~ 0.2 mbar). The use of a buffer gas has several advantages. (i) The trap can be operated in a continuous ion-fill-mode. (ii) Trapped ions are collisionally cooled to the ambient temperature (approximately within a few milliseconds). Experiments can currently be performed at temperatures between 14 K and 350 K.

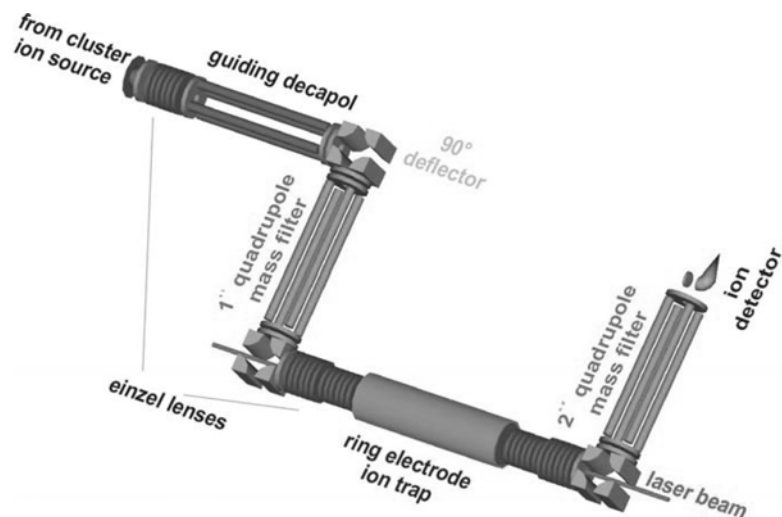


Figure 2: Schematic of the guided-ion-beam-tandem-mass-spectrometer used in the present studies.^[60] The instrument is housed in a 5-stage differentially pumped vacuum chamber. The FEL radiation is applied collinearly to the axis of the ion trap.

IR-PD spectra are obtained by photoexcitation of the trapped ions with the pulsed FEL radiation and subsequent monitoring of the fragment ion signal. The FEL generates 5- μ s macropulses at a repetition rate of 5 Hz. Each macropulse contains a series of several thousand \sim 1-ps micropulses with about 1 ns between micropulses. A new measurement cycle is triggered by the previous FEL macropulse. First, the ion trap is filled with mass-selected ions; typically for 150 ms. The trap is then closed and the ions are allowed to thermalize. Directly after FELIX fires, all ions are extracted and the mass-selected ion yield is monitored. This cycle is repeated multiple times, the signal is summed and then the FEL is set to the next wavelength. Overview spectra are measured first, in the region from 5.5 to 18 μ m with a step size of 0.1 μ m. Spectra with smaller step sizes and longer accumulation times are then measured in those spectral regions, where signal is observed. The accuracy of the determined vibrational frequencies is generally within 1% of the central wavelength. The accuracy of the relative depletion intensities is less well defined, mainly due to the non-monotonic variation of the FELIX beam intensity, bandwidth, and waist size with wavelength. We try to minimize these variations and do not correct for them in our spectra.

2.3 Potential Energy Surfaces

Rigorous theoretical modeling of IR spectra of hydrogen bonded complexes consists of two parts. The first is the calculation of the potential energy surface and the dipole moment. The second is appropriate dynamics calculations using the potential and dipole moment surfaces. For simulations of the IR spectrum quantum, semi-classical or purely classical dynamics calculations

are straightforward to do in principle in the weak-field limit. Practically, quantum dynamics calculations can be quite computationally demanding, depending on the number of degrees of freedom. Both aspects of this theoretical modeling are briefly reviewed next, followed by a review of recent applications to BrHI^- and H_5O_2^+

For triatomic molecules, even with heavy atoms, such as BrHI^- , it is now straightforward to obtain global potential energy surfaces, based on highly accurate *ab initio* calculations. One fairly common approach is to obtain the *ab initio* energies (and dipole moment) on a regular grid of roughly ten points per degree of freedom and to use interpolation, e.g., splines, to obtain the potential between grid points. This approach will be described below for BrHI^- . For larger systems, such as H_5O_2^+ , the proton bound water dimer, and H_3O_2^- , mono-hydrated hydroxyl, the grid approach is impractical. For these systems a "scattered" approach has proved successful. In this approach tens of thousands of *ab initio* calculations are done at configurations of relevance to the dynamics, including stationary points, etc. The *ab initio* data are then fit using standard least-squares procedures with, however, some important new features of the basis functions. In the least-squares approach the data are represented by the compact expression

$$V(x_1, \dots, x_d) = \sum_{n=0} C_n g_n(x_1, \dots, x_d), \quad (4)$$

where x_i are the variables of the fit, g_n are a known set of linearly independent basis functions, and the C_n are coefficients that are determined by the least-squares procedure. The key to a successful fit to the data is the choice of basis functions and the variables of the fit. Somewhat surprisingly, fitting approaches done prior to our work did not explicitly incorporate permutational symmetry of like atoms into the basis functions. This was done recently in applications to CH_5^+ ,^[20] H_3O_2^- ,^[21] and H_5O_2^+ .^[22] The approach is to use all internuclear distances, r_i , as the basic variables and x_i is a suitable function of r_i . These variables form a closed set under permutation of atoms. Then, symbolically, V is given by

$$V(x_1, \dots, x_d) = \sum_{i_1 \dots i_d} C_{i_1 \dots i_d} S\{x_1^{i_1} \dots x_d^{i_d}\}, \quad (5)$$

where the symbol S indicates a symmetrization operator so that the symmetrized monomial $S\{x_1^{i_1} \dots x_d^{i_d}\}$ is invariant with respect to interchange of any two identical nuclei. The approach we actually use is more involved and is described elsewhere.^[22]

With this new approach we have been able to obtain full-dimensional potentials using high quality *ab initio* calculations of electronic energies and dipole moments. Some of these results for H_5O_2^+ will be presented below.

2.4 Vibrational Calculations

As with potential surfaces, exact vibrational calculations for triatomics are essentially a "solved" problem. There are several numerically equivalent exact approaches that are currently in use. These basically differ in the choice of coordinates. Our recent calculations on BrHI^- made use of two such approaches; one used so-called Jacobi coordinates and the other used internal valence coordinates, i.e., the BrH , HI^- bond lengths and the BrHI^- bond angle. The kinetic energy operator in these coordinates is complex and so we refer the reader to the original literature^[23] instead of giving it here. In Jacobi coordinates this operator is much simpler, and the full Hamiltonian for an "ABC" triatomic for a given value of the total nuclear angular momentum J (in a rotating frame) is given by

$$H = T_R + T_r + \frac{(\mathbf{J} - \mathbf{j})^2}{2\mu R^2} + V(R, r, \theta), \quad (6)$$

where R is the distance of one atom, say A , to the center of mass of the diatom, say BC , r is the diatom internuclear distance, θ is angle between the vectors \mathbf{R} and \mathbf{r} , \mathbf{J} is the total nuclear angular momentum operator, \mathbf{j} is the diatom angular momentum operator, and V is the full potential.

For the BrHI^- calculations, reviewed below, codes based on Jacobi coordinates and valence coordinates were used to obtain vibrational energies and wave functions. IR transition intensities were obtained for $J = 0$ to $J' = 1$ transitions using the exact wave functions and the *ab initio* dipole moment.

For larger hydrogen-bonded systems, rigorous calculations are far more difficult to carry out, both from the point of view of obtaining full-dimensional potentials and the subsequent quantum vibrational calculations. Reduced dimensionality approaches are therefore often necessary and several chapters in this volume illustrate this approach. With increasing computational power, coupled with some new approaches, it is possible to treat modest sized H-bonded systems in full dimensionality. We have already briefly reviewed the approach we have developed for potentials; for the vibrations we have primarily used the code Multimode (MM). The methods used in MM have been reviewed recently,^[24 and references therein., 25] and so we only give a very brief overview of the method here.

There are two versions of MM. One, that we refer to as "single-reference" MM is based on the exact Watson Hamiltonian, which is the Hamiltonian in rectilinear mass-weighted normal coordinates. The normal coordinates, as usual, are referenced to a single stationary point, which does not have to be a minimum. For calculations we review below the reference geometry was chosen as a saddle point, not a minimum. The other version of MM, which is much better suited for highly floppy systems, is based on the Reaction Path Hamiltonian.^[25] A key element of both

versions is the n-mode representation of the potential. In the single-reference version of MM, the potential in N normal modes is represented as

$$V(Q_1, \dots, Q_N) = \sum_i V^{(i)}(Q_i) + \sum_{i \neq j} V^{(2)}(Q_i, Q_j) + \sum_{i \neq j \neq k} V^{(3)}(Q_i, Q_j, Q_k) + \sum_{i \neq j \neq k \neq l} V^{(4)}(Q_i, Q_j, Q_k, Q_l) + \dots \quad (7a)$$

For the Reaction-Path version of MM the potential is given by

$$V(\tau, Q_1, Q_2, \dots) = V^{(0)}(\tau) + \sum_i V_i^{(1)}(\tau, Q_i) + \sum_{ij} V_{ij}^{(2)}(\tau, Q_i, Q_j) + \sum_{ijk} V_{ijk}^{(3)}(\tau, Q_i, Q_j, Q_k) + \sum_{ijkl} V_{ijkl}^{(4)}(\tau, Q_i, Q_j, Q_k, Q_l) + \dots \quad (7b)$$

where the Q_i are rectilinear normal modes and τ is the large amplitude coordinate. In these representations n is less than N but the sums run over all sets of normal modes. This representation of the potential makes it feasible to perform the high-dimensional numerical quadratures, etc. needed to set up the Hamiltonian matrix for diagonalization. In recent applications n is typically 4 or 5 in eq. (7a) and 3 or 4 in eq. (7b). The basis used to construct the Hamiltonian matrix is the set of virtual excitations of an exact Vibrational-Self Consistent Field Hamiltonian, typically for the zero-point state. This virtual "CI" approach is denoted "VCI".

Relevant calculations using both versions of MM have been reported for $(\text{OH})\text{H}_2\text{O}$ ^[21, 26] and H_5O_2^+ ^[27, 28] and some very recent results will be presented below. Diffusion Monte Carlo calculations, done by and in collaboration with Anne McCoy have also been done on these systems, however, these are not reviewed in detail here.

3 Selected Systems

3.1 Bihalide Anions

The bihalide anions XHY^- , where X and Y are halogen atoms, are among the simplest systems containing strong hydrogen bonds. In fact, these triatomic systems exhibit some of the strongest hydrogen bonds known, reaching 1.93 eV (44.5 kcal/mol) in FHF^- .^[29] All bihalide anions are linear and have $D_{\infty h}$ (X=Y) or $C_{\infty h}$ (X≠Y) symmetry. As a result of the strong three-center bonding, the interatomic distance between the heavy atoms is small, leading to a pronounced red-shift of the antisymmetric stretch frequency ν_3 compared to the vibrational frequency of the diatomic X-H. Unusually low frequencies of the shared proton modes are a characteristic trademark for strong hydrogen bonds in general. The extensive sharing of the H-atom between the two halogen

atoms makes these bonds highly susceptible to solvent perturbation.^[30] In larger $\text{Br}^{\cdot-}(\text{HBr})_n$ clusters ($n>1$), for example, the additional HBr molecules destroy the symmetry of the H-bonds and the H-atom is localized.^[31] XHY^- anions are also of interest as transition state precursors in negative ion photoelectron spectroscopy experiments^[32] and are isoelectronic with the rare gas compounds RgHRg^+ , which exhibit very similar vibrational spectra.^[33]

The vibrational spectroscopy of bihalide anions has been studied extensively in cryogenic matrices.^[34] This work showed that the hydrogenic stretching frequencies were very low, ranging from 1330 cm^{-1} in FHF^- to 645 cm^{-1} in IHI^- , in contrast to the uncomplexed HX frequencies of 4138 cm^{-1} in HF and 2309 cm^{-1} in HI.^[35] These studies also indicated that the effects of the matrix on the vibrational frequencies could be significant, providing strong motivation to measure the unperturbed gas phase IR spectra of these bihalide anions. High resolution gas phase IR spectra over narrow frequency ranges have been measured for FHF^- and ClHCl^- using diode laser absorption.^[36] We recently applied a different and more general approach to gas phase ion vibrational spectroscopy. The result was the first broadband infrared spectra in the range from 600 to 1675 cm^{-1} of a homoconjugated (BrHBr^-) and a heteroconjugated (BrHI^-) gas phase bihalide anion measured by vibrational predissociation of the corresponding anion-Ar complex.^[11, 37]

The results of the BrHBr^- study^[37], together with recent data on BrDBr^- are shown in Figure 3. The spectra were measured by IR-PD of the anion-Ar complex. The addition of a single Ar atom is expected to result in only minor shift ($<5\text{ cm}^{-1}$) of the ν_3 frequency compared to bare BrHBr^- . The fundamental of the antisymmetric stretch mode ν_3 is observed at 733 cm^{-1} and peaks at higher energies are attributed to $\nu_3+n\nu_1$ combination bands. As expected, the antisymmetric stretch frequency is red-shifted upon deuteration, while the peak spacing, related to the symmetric stretch mode ν_1 , remains nearly unchanged. The ratio of $\nu_3(\text{H})/\nu_3(\text{D})$ is 1.45, slightly larger than the harmonic value of $\sqrt{2}$ and considerably larger than 1.2-1.3, the value usually quoted for strong hydrogen bonds.^[38] The measured peak positions are in excellent agreement with the results from anharmonic calculations of Del Bene and Jordan^[39], indicated by the black bars in Figure 3. They calculated two-dimensional vibrational eigenfunctions and eigenvalues on a high level *ab initio* potential energy surface for a collinear XHX^- system. The relative intensities in our gas phase spectra differ from the previously measured matrix spectra, presumably due to the underlying dissociation dynamics. Nonetheless, the strong relative intensity of the combination bands in both experiments indicate a complete breakdown of the (uncoupled) harmonic oscillator model in these prototypical systems and underline that explicit consideration of intermode coupling is needed when calculating vibrational properties of strongly hydrogen bonded systems.

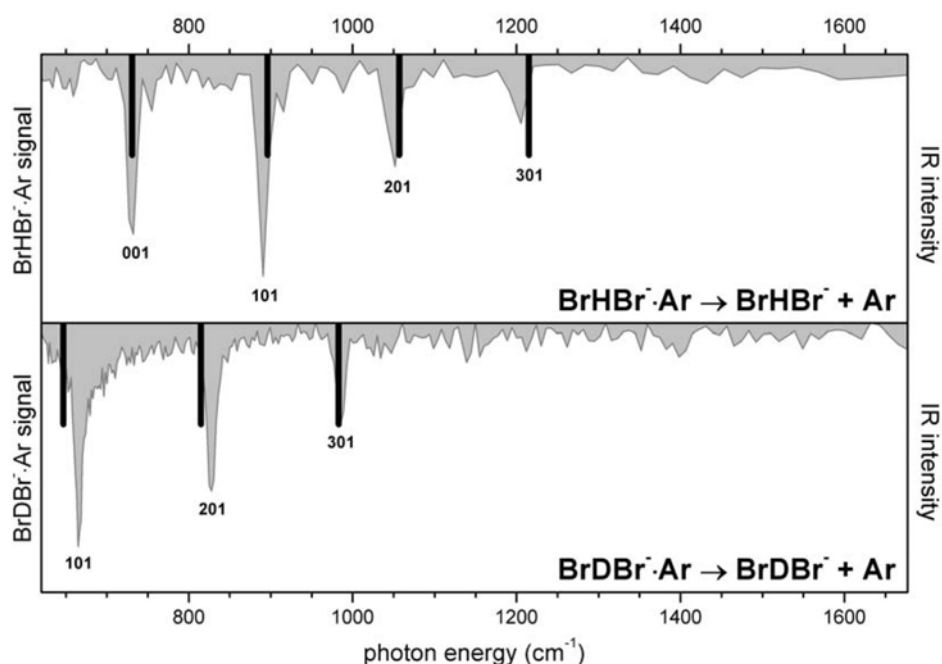


Figure 3: IR-PD spectra of $\text{BrHBr}^- \cdot \text{Ar}$ (top) and $\text{BrDBr}^- \cdot \text{Ar}$ (bottom) from 620 to 1680 cm^{-1} . The depletion of the parent ion signal is shown (gray trace and gray shaded-area) and compared to the eigenvalues (black bars) from a variational calculation on a two dimensional CCSD(T)/aug-cc-pVTZ-based potential energy surface for bare BrHBr^- and BrDBr^- anions, respectively. The peak assignment is indicated by three numbers which give the vibrational quantum number for each mode (symmetric stretch ν_1 , bend ν_2 , antisymmetric stretch ν_3).

The vibrational spectra of the asymmetric bihalides are more complex and their assignment was only recently unraveled satisfactorily.^[11] Earlier matrix IR work^[40] on BrHI^- indicated the presence of two absorbing species, a strongly asymmetric form, referred to as type I, and a more symmetric form (type II), the latter exhibiting a considerably lower H-atom stretch frequency owing to greater delocalization of hydrogen atom, similar to the symmetric bihalides discussed above. To investigate this possible dual structure, spectra of BrHI^- in the gas phase in the region of the bridging hydrogen stretch were recorded.

Parent ion depletion spectra for $\text{BrHI}^- \cdot \text{Ar}$ and $\text{BrDI}^- \cdot \text{Ar}$ are shown Figure 4. Compared to the IR spectra of the symmetric bihalides, these spectra are considerably more complex and their assignment, based on previous calculations^[41], was problematic. The two most intense peaks in both spectra correspond closely to the peaks seen in the previous matrix works. Their frequencies exhibit red-shifts when going from the gas phase to the matrix from 12 to 64 cm^{-1} . All these peaks were assigned to the type I structure in the matrix. No peaks assigned to type II anions are observed in the gas phase, but additional peaks are observed in the gas phase spectra. In order to reach a satisfactory assignment of all the peaks observed in the gas phase spectra new calculations on an improved potential energy surface had to be performed.

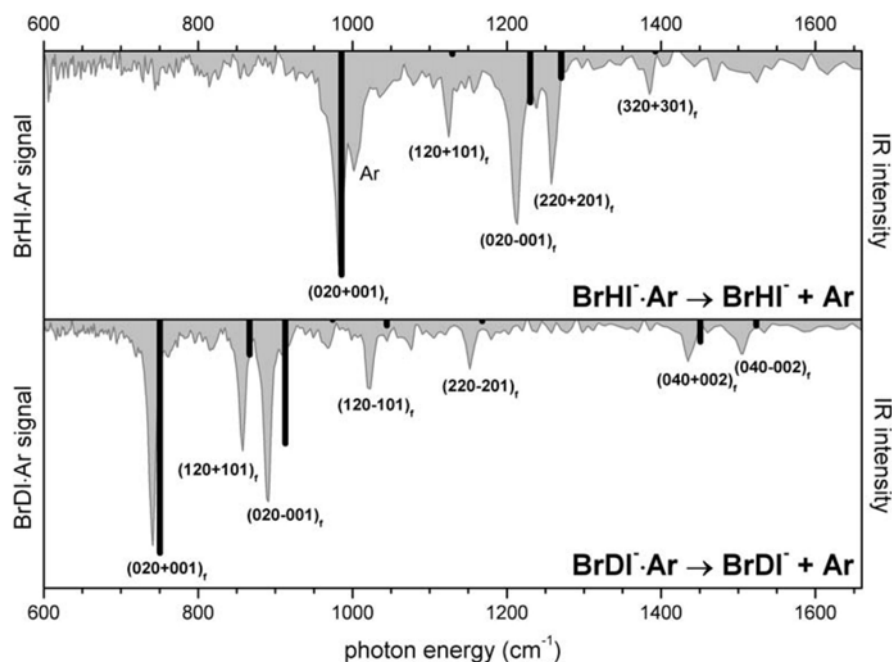


Figure 4: IR-PD spectra of $\text{BrHI}^- \cdot \text{Ar}$ (top) and $\text{BrDI}^- \cdot \text{Ar}$ (bottom). The depletion of the parent ion signal is shown (gray trace and gray shaded-area) and compared to the calculated frequencies and absorption intensities (black bars). Calculations were performed on the bare BrHI^- and BrDI^- anions and involved construction of a three dimensional MRCI/AVQZ(cpp) potential energy surface, followed by ro-vibrational bound-state variational calculations (see text).

Such calculations were recently done. These included a new potential for this anion using multi-reference CI *ab initio* methods with large basis sets; the details are given elsewhere.^[13] *Ab initio* energies and dipole moment values were obtained at roughly 2300 configurations taken from regular grids. Both the energy and dipole moment were subsequently interpolated using 3d splines. The potential along two cuts of this potential for the collinear geometry are shown in Figure 1. In these plots the distance between the Br and I^- , denoted R, is fixed while the potential is plotted as a function of the difference coordinate $r_1 - r_2$ where r_1 and r_2 are the distances between the H atom and Br and I^- , respectively. As seen for large R the potential is a double-minimum, however, near the global minimum, where $R = 3.7$ bohr, the potential is a single minimum. This surface and the corresponding *ab initio* dipole moment were used to calculate the IR spectra of BrHI^- and BrDI^- using two variational codes, one using valence coordinates and one using Jacobi coordinates. The results from the two calculations agree very well, as they should. The comparisons with experiment, given in Figure 4, show very good agreement. This is especially satisfying because there was uncertainty about the assignment of the bands at 920 and 1171 cm^{-1} . The difficulty in making experimental assignments was illuminated and resolved by the calculations, which indicated a strong 2:1 Fermi mixing between the bend and the "antisymmetric-stretch" modes. This mixing is depicted in Figure 5 where plots of the corresponding wave functions are given in the upper two

panels and plots of "deperturbed" wave functions are given in the lower two panels. The plots are in the Jacobi coordinates r and θ described above (and in the figure caption). The energies of these two perturbed states are 983 and 1127 cm^{-1} , in very good agreement with experiment. This analysis presents a satisfactory resolution of the assignment issue for these two lines. (A corresponding and completely analogous situation pertains to BrDI^- for the two lines at 742 and 980 cm^{-1} .) Also, it was shown that these 2:1 resonances pervade the entire spectrum for both BrHI^- and BrDI^- .

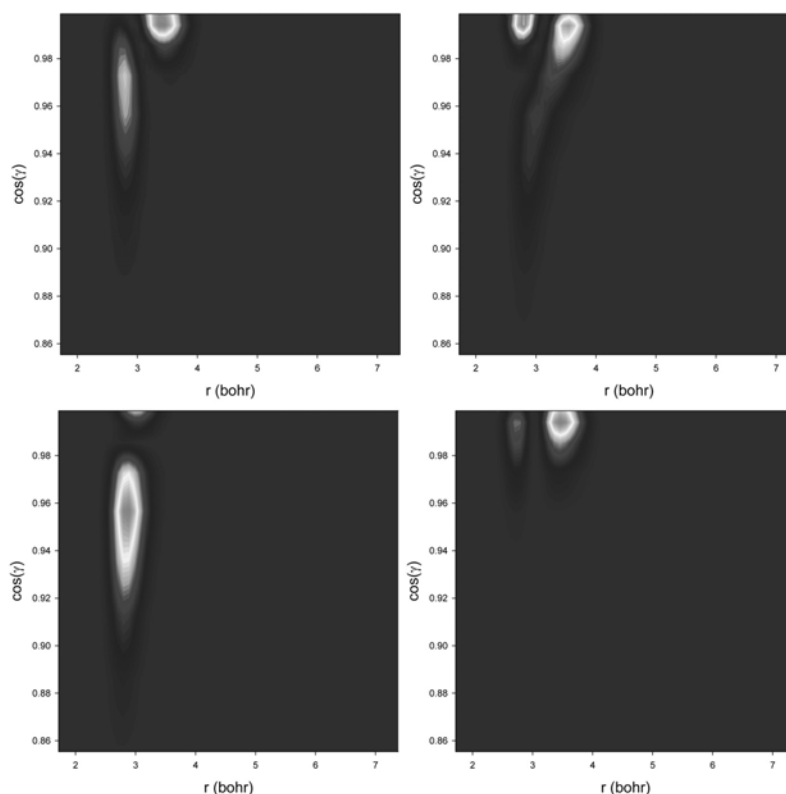


Figure 5: Contour plots of the eigen functions at 983 cm^{-1} (upper left panel) and 1127 cm^{-1} (upper right panel) and sum (lower right panel) and difference of the two (lower left panel), representing the pure states of the bending overtone and the H-atom stretch modes, respectively, in BrHI^- . The plots are two-dimensional slices in the plane defined by r_{HBr} and the bond angle θ_{BrHI^-} .

In summary, the gas phase vibrational frequencies observed for $\text{BrHI}^- \cdot \text{Ar}$ and $\text{BrDI}^- \cdot \text{Ar}$ are close to those seen in earlier matrix-isolation experiments and attributed to the type I form of the anion. The calculated vibrational energy levels show a remarkable extent of mode mixing between the H-atom stretch and bend modes, resulting in numerous Fermi resonance states, and thus more complex spectra than for the symmetric XH(D)X^- bihalide anions. The calculations also suggest a reassignment of the matrix spectra. The matrix features originally attributed to the symmetric type II anion may actually arise from the bend fundamental and/or the associated combination band with

the heavy atom stretch, rather than from a second form of the ion (type II) not observed in the gas phase. These results underline the breakdown of the harmonic approximation; mechanical anharmonicities lead to extended mixing of states, evidenced in the IR spectra by pronounced intensity borrowing effects in the form of Fermi resonances.

3.2 The Protonated Water Dimer ($\text{H}_2\text{O}\cdots\text{H}\cdots\text{OH}_2$)⁺

The protonated water dimer is one of the most prominent ions containing strong hydrogen bonds. It plays a crucial role in the explanation of the unusually high proton mobility in water.^[42] Protonated water clusters and H_5O_2^+ in particular have been suggested as proton release groups in bimolecular proton pumps like bacteriorhodopsin.^[3, 43] The interpretation of the spectroscopic signature of hydrated protons in liquid water, characterized by a quasi-continuous absorption observed in the IR has been a long running controversy^[44], in particular the attribution of specific bands to the hydrated proton structures H_5O_2^+ and H_9O_4^+ .^[45] More recently, *ab initio* molecular dynamics simulations have shown that the hydrated proton actually forms a fluxional defect in the hydrogen-bonded network with both H_5O_2^+ and H_9O_4^+ occurring only in the sense of limiting structures.^[4]

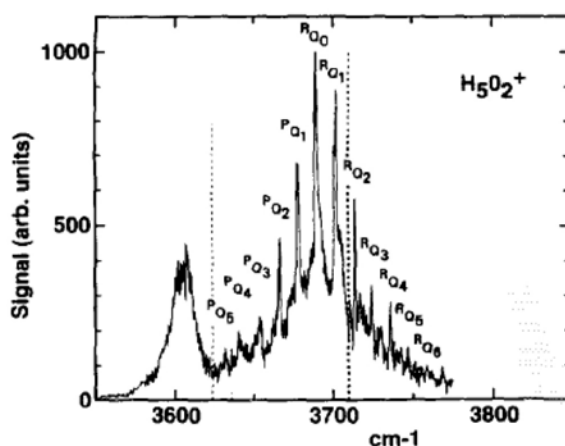


Figure 6: IR-PD spectrum of H_5O_2^+ measured in the region of the monomer O-H stretches. Figure taken from Ref. ^[48].

3.2.1 Experiments

For more than 30 years, starting with X-ray diffraction experiments of hydrated crystals,^[46] H_5O_2^+ has been the subject of extensive theoretical and experimental studies and its spectroscopy remains challenging until today.^[47 and references therein] The vibrational spectroscopy of H_5O_2^+ in the gas phase was first studied in the region above 3500 cm^{-1} , the region of the free O-H stretch modes. The groundbreaking IR-PD experiments of Lee and coworkers^[48] (see Figure 6) in 1989 support a hydrated-crystal-like, C_2 symmetry $\text{H}_2\text{O}\cdots\text{H}^+\cdots\text{OH}_2$ structure, in which the proton is located

symmetrically between the two water ligands. These experiments made use of a two-color excitation scheme; the first, tunable laser was used to probe the linear absorption regime and the second, fixed-frequency laser to overcome the H_5O_2^+ dissociation energy of 31.6 kcal/mol (11055 cm^{-1}) via multiphoton absorption.^[49] The two bands in Figure 6 were assigned to the symmetric and antisymmetric O-H stretches (either in phase or out of phase) of the two H_2O groups. The rotational progression is assigned to a series of Q branches. The observed peak spacing of 11.6 cm^{-1} is in good agreement with the calculated C_2 , near symmetric top structure. In a later study^[50], performed at considerably higher spectral resolution, more evidence for a very floppy molecule was found. The number of observed rovibrational lines was considerably more than one would expect for a rigid molecule and speculatively attributed to tunneling splittings caused by large amplitude motion.^[51]

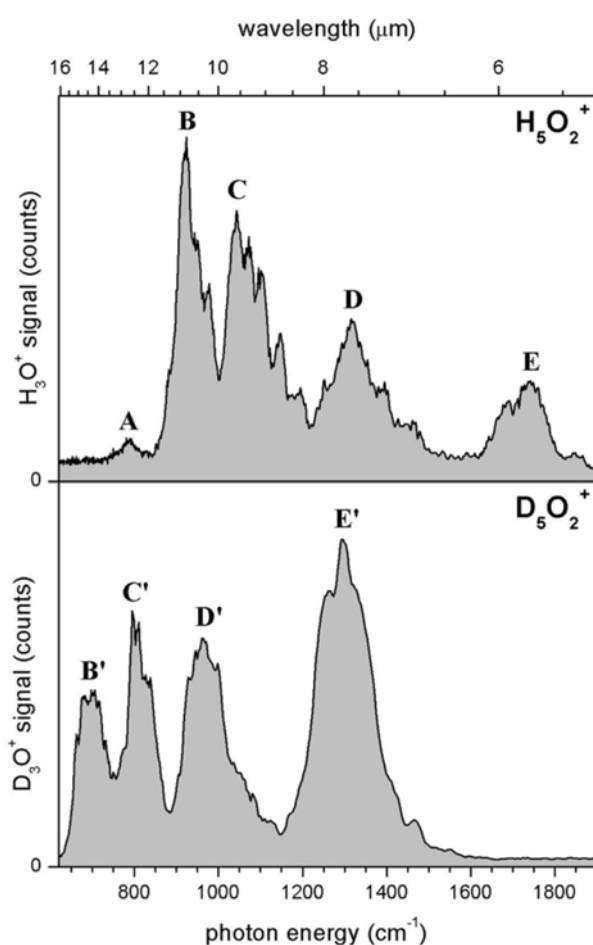


Figure 7: IR-PD spectra of H_5O_2^+ (top) and D_5O_2^+ (bottom). The spectra were measured by monitoring the formation of H_3O^+ and D_3O^+ as a function of FELIX wavelength (top axis). The spectra are plotted linearly against the photon energy (bottom axis). See ref. ^[52] for experimental details.

Interestingly, four (compared to two in Figure 6) O-H stretching bands were observed in the IR-PD spectrum of the $\text{H}_5\text{O}_2^+\cdot\text{H}_2$ complex.^[49] Based on a comparison to computed vibrational frequencies it was concluded that the perturbation exerted by H_2 , which is bound by less than 4 kcal/mol, is already sufficient to break the symmetry and stabilizes an “asymmetric” $\text{H}_2\text{O}\cdots\text{H}_3\text{O}^+$ structure, for which four O-H bands are predicted.

The spectral region containing the shared proton modes, key to characterizing the potential energy surface for proton transfer, lies much lower in energy ($<1600\text{ cm}^{-1}$) and remained experimentally unexplored until 2003. Advances in free electron laser technology can be credited for making the spectral region of strong hydrogen bonds finally accessible to gas phase spectroscopic techniques. These experiments make use of a simpler one-color excitation scheme in contrast to the two-color approach applied in the Lee experiments. The vibrational spectra of H_5O_2^+ and D_5O_2^+ measured in the region from 620 to 1900 cm^{-1} using radiation from the Free Electron Laser for Infrared Experiments FELIX are plotted in Figure 7.^[52] The spectrum of H_5O_2^+ exhibits four main bands, labeled B to E. Upon H-D substitution four bands (B'-E') of similar width but different relative intensities appear red shifted with isotope shifts varying between 1.3-1.4. Based on previous theoretical studies band E was assigned to the bending motion of the terminal water molecules and bands B to D to vibrations predominantly involving the shared proton. The assignment of the shared proton modes to specific vibrational states remains somewhat controversial and will be discussed in more detail together with the most recent calculations below.

The observed bands are more than twenty times broader than the bandwidth of the laser radiation ($\sim 5\text{-}15\text{ cm}^{-1}$). The increased width could be caused by vibrational hot-bands, but these should be largely eliminated in the spectra because the ions are collisionally cooled prior to interaction with the laser pulse. However, the zero-point motion of the central proton on the extremely flat PES likely extends over an unusually large area, leading to the exploration of a much larger part of the configurational space than for a typical rigid molecule, even at 0 K. Additionally, the anharmonicity of the shared proton modes is pronounced, leading to strong anharmonic coupling terms and closely related intensity borrowing effects. The result is an increase in the intensity of bands, which are normally weak or forbidden, like combination bands with low-frequency modes in the present case. Alternatively, multiphoton transitions in which two or more photons are resonant with a vibrational transition may contribute.^[11] These transitions appear at shifted photon energies (compared to the single photon transition) due to the anharmonicity of the vibrational potential. In this way a negative anharmonicity may lead to multiphoton transitions that contribute to the high energy tails of bands B and C. Information on the underlying potential energy

surface may also be hidden in the structure observed for bands B to D, which we can currently not assign; its spacing is too large to be attributed to rotational transitions of a near symmetric top.

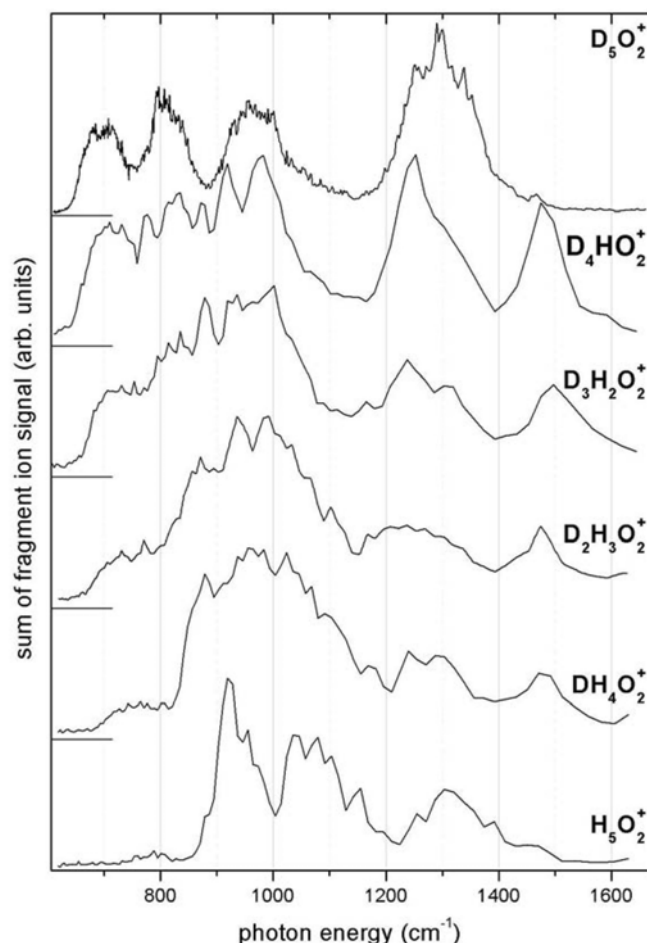


Figure 8: IR-PD spectra of $H_xD_{5-x}O_2^+$ with $x = 0$ to 5 (top to bottom) in the region of the shared proton (deuteron) modes (see text).

Additional information can be gained from the IR-PD spectra of the partially deuterated isomers $D_xH_{5-x}O_2^+$ ($x=0,1,\dots,5$) and these are shown in Figure 8. Fragment ions of different mass are produced upon photodissociation of partially deuterated species and we measured IR-PD spectra for each possible fragment ion mass. We find nearly identical spectra for all fragment ions of a particular parent ion mass, indicating that efficient H/D scrambling occurs, and therefore only representative sum spectra over all fragment ions are shown for each parent ion mass in Figure 8. Efficient intramolecular H/D exchange is made possible by the underlying sequential absorption mechanism in which the cluster ion can absorb photons during the complete duration of a FEL macropulse (~ 5 ms). If the barrier to internal rotation in $D_xH_{5-x}O_2^+$ ions is smaller than the

dissociation limit, efficient intramolecular energy redistribution leads to complete H/D scrambling after sufficient energy is absorbed but before dissociation can occur. The mixed H/D spectra are more congested than the pure spectra, because multiple isomers are present. Nonetheless, some interesting features can be observed. The band at 1500 cm^{-1} , only present in the mixed H/D spectra is assigned to the bending motion of the terminal HDO monomers. The band centered at 770 cm^{-1} in DH_4O_2^+ is attributed to a shared proton mode of the symmetric $\text{H}_2\text{O}\cdots\text{D}^+\cdots\text{OH}_2$ isomer, red-shifted by 118 cm^{-1} compared to band B in Figure 7. This band grows in intensity as the degree of deuteration is increased. Interestingly, it also continues to red-shift, from 770 cm^{-1} in $\text{H}_2\text{O}\cdots\text{D}^+\cdots\text{OH}_2$ to 700 cm^{-1} in $\text{D}_2\text{O}\cdots\text{D}^+\cdots\text{OD}_2$, indicating significant coupling between this shared proton mode and the modes of the terminal monomers. The intermediate region is more complex and its assignment requires a simulation of the vibrational spectra of the partially deuterated species.

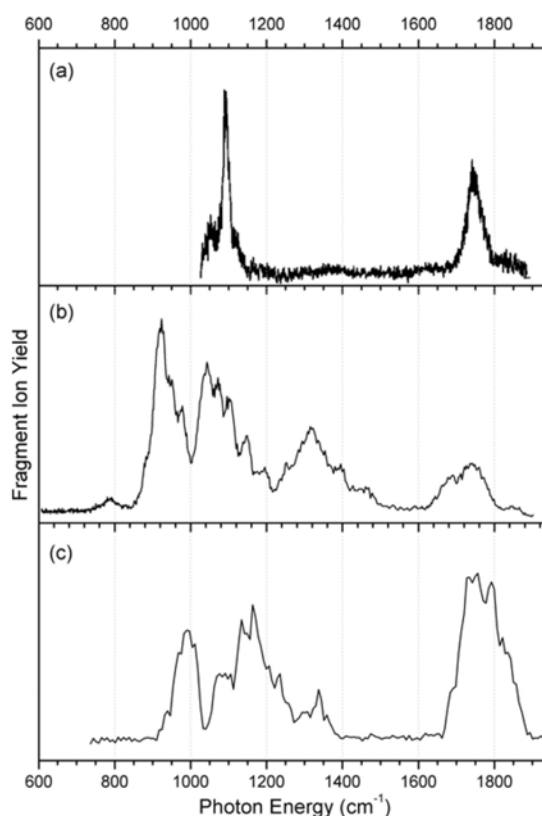


Figure 9: IR-PD spectra of (a) $\text{H}_5\text{O}_2^+\cdot\text{Ar}$,^[16] (b) H_5O_2^+ measured at FELIX,^[52] and (c) H_5O_2^+ measured at CLIO.^[53]

Predissociation spectroscopy of argon-tagged H_5O_2^+ ,^[16] which probes the complex in the linear absorption regime, yields a similar but simpler spectrum compared to the multiphoton dissociation spectrum of bare H_5O_2^+ discussed above (see Figure 9). Headrick *et al.* argue that unlike for H_2 ,^[48] the extent of the Ar perturbation is not sufficient to stabilize the “asymmetric”

$\text{H}_2\text{O}\cdots\text{H}_3\text{O}^+$ complex and change its chemical nature, but only leads to a small shift of the vibrational frequencies. Assuming an additive argon perturbation, they show that the 1080 cm^{-1} band of the $\text{H}_5\text{O}_2^+\cdot\text{Ar}$ complex, found at 1140 cm^{-1} in $\text{H}_5\text{O}_2^+\cdot\text{Ar}_2$, is placed close to the maximum of band C (in the multiphoton spectrum) in the bare ion. No feature corresponding to band D is found in the Headrick *et al.* spectrum. However a peak in this region is found in the recent (multiphoton) IR-PD by Fridgen *et al.*^[53] (see Figure 9) measured at the French free electron laser facility CLIO^[54]. VCI multimode calculations (see Figure 11) also predict transitions with significant intensity in this spectral region. Below 1300 cm^{-1} the spectra measured at FELIX and CLIO do not agree very well; the band maxima at 921 and 1043 cm^{-1} in the FELIX spectrum coincide with regions of low signal in the CLIO spectrum. Such discrepancies are surprising and can only in part be rationalized by different ion internal temperature distributions, $<100\text{ K}$ in the FELIX- vs. room temperature in the CLIO-study. More recent Ar- and Ne-tagged predissociation spectra extending below 1000 cm^{-1} ^[55] are in better agreement overall with the FELIX experiments than with the CLIO experiments.

3.2.2 Calculations

There have been a number of calculations recently on the vibrations of H_5O_2^+ beyond the harmonic approximation. As noted already such calculations are essential due to the highly anharmonic nature of these vibrations. Attempts to go beyond the harmonic approximation have been done in reduced dimensionality^[27, 56] and also with the additional vibrational adiabatic approximation.^[56] These calculations selected the three proton degrees of freedom and the OO-stretch as the reduced dimensionality space. While such approaches are better in some respects than harmonic calculations in full dimensionality, they can miss important coupling with the monomer degrees of freedom. This was demonstrated in comparisons of fully coupled 4d and full dimensionality virtual configuration interaction (VCI) calculations.^[27] The results of the comparison showed that for some states the reduced dimensionality treatment was quite realistic, but not for the proton "anti-symmetric" stretch. For that important mode the 4d estimate for the fundamental is nearly 300 cm^{-1} higher than the full dimensional calculation. The reason for this large difference was traced to the neglect of coupling of that mode to the monomer modes in 4d. This coupling is large and can be understood simply by noting that as the proton moves towards one monomer and away from the other, the closer monomer takes on H_3O^+ character while the other monomer takes on H_2O character and this clearly introduces monomer coupling into the proton anti-symmetric stretch.

The full-dimensional VCI calculations, mentioned above, were done with the single-reference version of Multimode. The calculations used a full-dimensional potential due to Ojamae, Shavitt, and Singer,^[57] version OSS3(p), and considered all four-mode couplings among the 15

normal modes. Until just recently, this was the only full dimensional potential surface for H_5O_2^+ . In many respects the OSS3(p) potential is quite realistic; however, it is not spectroscopically accurate.

Table 1. Selected vibrational energies (cm^{-1}) of H_5O_2^+ calculated by a variety of methods and experiment for the OH-monomer stretches. "2d+2d" are the adiabatic 4d calculations of ref. [56], "4d" are the fully coupled 4d calculations of ref. [27], "CC-VSCF" are the Correlation-Consistent Vibrational Self-Consistent Field calculations of ref. [58] and "VCI" are the virtual configuration interaction calculations of ref. [27]. The potential used in these calculations is indicated after the back-slash

Mode	2d+2d/MP2	4d/OSS3(p)	CC-VSCF/MP2	VCI/OSS3(p)	Exp ^a
OO-stretch	587	571	599	569	
OH ⁺ O-asym st	1158	1185	1209	902	
OH ⁺ O-x bend	968	1328	1442	1354	
OH ⁺ O-y bend	1026	1344	1494	1388	
OH-monomer1	NA	NA	3579	3320	--
OH-monomer2	NA	NA	3577	3420	3609
OH-monomer3	NA	NA	3593	3470	--
OH-monomer4	NA	NA	3518	3470	3684

A summary of these published vibrational energies of H_5O_2^+ is given in Table 1 along with full-dimensionality Correlation-Consistent Vibrational Self-Consistent Field calculations^[58] (CC-VSCF), which were restricted to two-mode coupling. All the calculations find the OO-stretch in the range 569-599 cm^{-1} . However, only the 2d+2d calculations predict the fundamental energy of the OH⁺O-x bend below the asymmetric stretch; they also are alone in predicting the OH⁺O-y bend at around 1000 cm^{-1} . With regard to the highly interesting OH⁺O-anti-symmetric stretch, only the VCI/OSS3(p) calculations predict the fundamental below 1000 cm^{-1} . (Based on this prediction, the intense band labeled "B" in Fig. 7 was re-assigned^[27] as the OH⁺O-anti-symmetric stretch.) However, for the OH-monomer stretches agreement between the VCI/OSS3(p) calculations and experiment is only fair to poor. This appears to be due primarily to a shortcoming of the OSS3(p) potential. The CC-VSCF/MP2 calculations^[58] for these stretches are in somewhat better agreement with experiment; however, not close to "spectroscopic" accuracy.

In reviewing published calculations on H_5O_2^+ it should be noted that Diffusion Monte Carlo (DMC) calculations of the zero-point state using the OSS potential^[47,59] and the more recent *ab initio* potential^[28] (see below) have been reported. These calculations clearly indicate the highly

delocalized nature of the zero-point state. In quite recent work Correlation Function DMC calculations of the IR spectrum were reported using the OSS3(p) potential.^[28] These calculations indicate a quite complex spectrum with much mixing among low-frequency modes. Two states with substantial OH⁺O-anti-symmetric stretch character were identified at 737 and 870 cm⁻¹. The latter number is fairly close to the 902 cm⁻¹ result for this state obtained in VCI calculations on the same potential energy surface (and shown in Table 1).

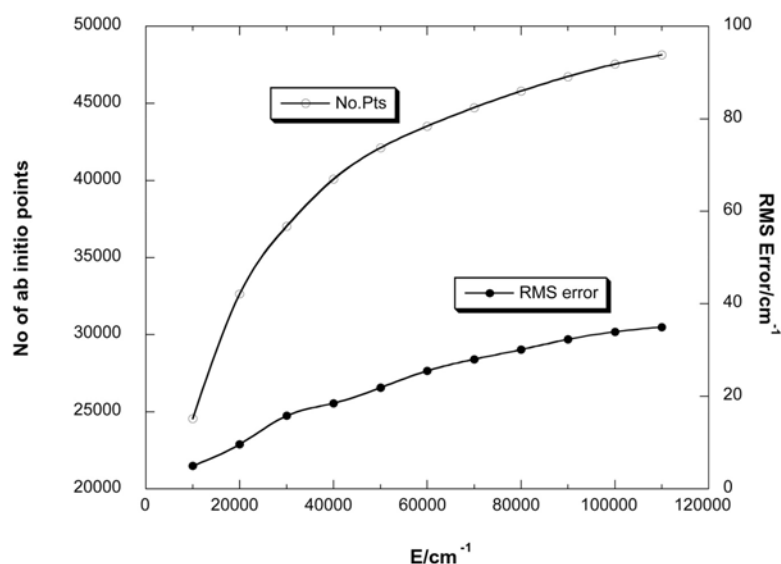


Figure 10: The number of configurations and RMS fitting error as a function of the energy cut-off as explained in the text.

Clearly an accurate simulation of the vibrational energies and IR spectrum of H₅O₂⁺ requires accurate full-dimensional potential energy and dipole moment surfaces and a full-dimensional treatment of the dynamics. Very recently we reported a new *ab initio*, full dimensional potential energy surface and dipole moment for H₅O₂⁺.^[22] The *ab initio* calculations were done at the CCSD(T) level of theory with an aug-cc-pVTZ basis for roughly 50 000 configurations. The potential energy surface is a fit to these energies. It is permutationally invariant with respect to like atoms and dissociates properly to H₂O + H₃O⁺. It was obtained using the methods briefly reviewed in section 2.3. The variables of the fit are given by $x_{i,j} = \exp(-r_{i,j}/a)$ where $r_{i,j}$ are all the internuclear distances and a was fixed at 0.5 bohr⁻¹. The fit is highly precise and RMS fitting error is shown in Figure 10 as a function of the maximum energy of the data set used in determining the error. As seen the RMS error is quite small and is roughly 20 cm⁻¹ for total energies up to 40,000 cm⁻¹ above the global minimum. This value of the RMS is not in the range of "spectroscopic" accuracy, i.e., within 1 cm⁻¹; however, it is close to the expected accuracy of the *ab initio* method used.

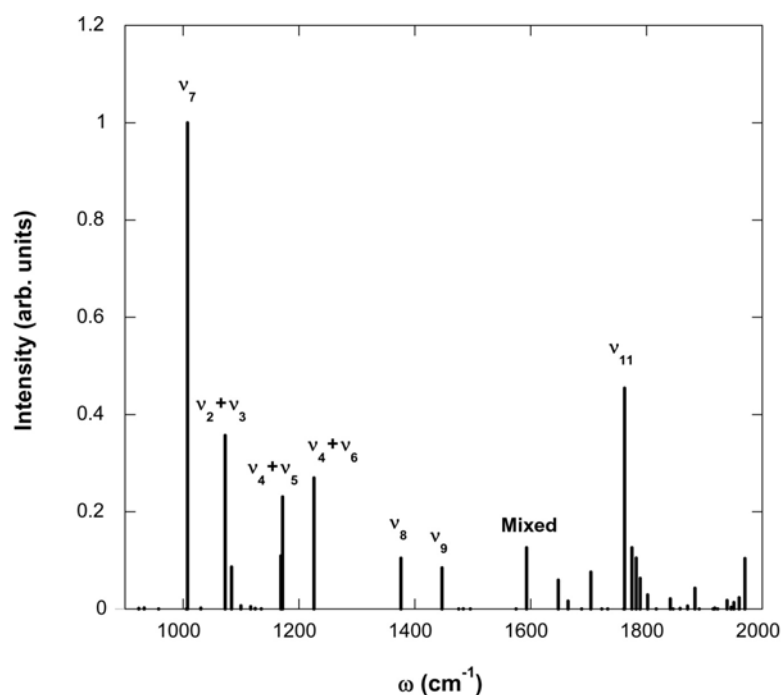


Figure 11: 0 K IR spectrum obtained using "Single-Reference" VCI Multimode calculations using the new potential of reference^[22]. Modes 2 - 5 are various low-frequency rock, wag and torsion modes, mode 6 is the OO-stretch, mode 7 is the OH⁺O-asymmetric stretch, modes 8 and 9 are the OH+O x and y bends, and mode 11 is the asymmetric monomer bends.

This new potential is highly anharmonic and fluxional with numerous low energy saddle points. Together with Anne McCoy, Stuart Carter and Xinchuan Huang, we have begun large-scale vibrational calculations using the new potential and dipole moment surfaces. These calculations are quite demanding and are being done with the single reference and reaction path versions of Multimode briefly described above and also with the DMC method. Some preliminary results have very recently been reported;^[28] however, at present we only have a "rough" IR spectrum based on VCI calculations using the single-reference version of Multimode. This version of the code cannot describe internal torsional motion fully; however it can do crude IR simulations using the exact dipole moment. We present two plots of the calculated 0 K IR spectrum below. The first one, Figure 11, is in the spectral region of the recent IR experiments, shown in Figs 7-9. Based on unpublished comparisons of the VCI energies in this region with excited state DMC ones of McCoy we believe the VCI energies in this region are high by roughly 100 cm⁻¹. Thus, we have shifted this VCI spectrum to the red by 100 cm⁻¹. As seen there are peaks in this calculated spectrum that correspond approximately to the experimental spectra shown in Figs. 7-9. (Note there is only rough agreement among these experimental spectra, as noted already.)

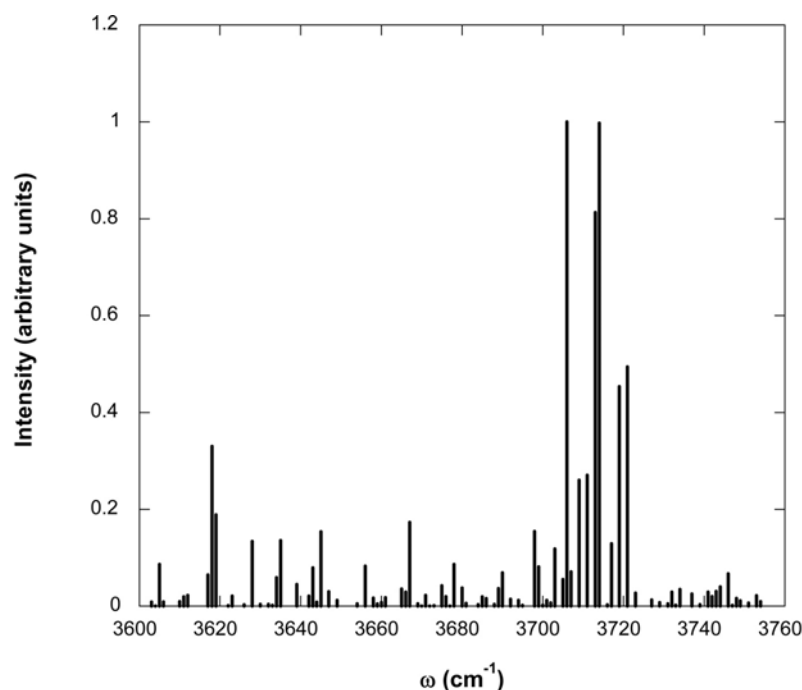


Figure 12: 0 K IR spectrum obtained using "Single-Reference" VCI Multimode calculations using the new potential of reference^[22].

The 0 K IR spectrum in the range 3600-3800 cm^{-1} is shown in Fig. 12 and is presented with no energy shift. As seen the spectrum is fairly complex but does show intensities in qualitative accord with experiment, shown in Fig. 6. Our analysis indicates that the relatively intense lines at 3620 cm^{-1} (the monomer OH-symmetric stretch) and 3710 cm^{-1} (the asymmetric stretch). We stress that these are preliminary results and likely not well converged. More accurate DMC and Multimode-reaction path calculations for the four monomer stretches indicate that the single reference energies are 40 - 100 cm^{-1} high.^[28]

4 Outlook

The vibrational signature of strong hydrogen bonds is found in a spectral region which can be accessed directly with novel radiation sources operating in the mid IR. The photodissociation experiments described above all yield spectra without rotational resolution mainly due to the inherent broad bandwidth of the FELIX radiation. Recent advances in the technology of table top tunable IR lasers are promising and these narrower bandwidth systems have the potential to go beyond this barrier and elucidate the structures of the clusters with considerably more detail based on high resolution spectra. The experiments using FELs should remain interesting, due to the considerably higher pulse energies, different temporal pulse structure and greater tunability

available. Multiphoton absorption photodissociation spectra measured at high pulse energies, above the “quasi-linear” regime, contain additional information on the underlying PES that in principle could be extracted, if theoretical models could directly simulate the more complex multiphoton absorption processes.

The experimental vibrational spectra of strongly hydrogen bonded systems, especially H_5O_2^+ are complex, owing to strong mode-mixing. Their interpretation requires theoretical approaches beyond the harmonic approximation. The calculated spectra for H_5O_2^+ presented here look promising, but more work is needed using better converged calculations and also for non-zero temperature. Calculations for the various isotopomers of H_5O_2^+ are also needed and this will be forthcoming. More challenging will be calculations that directly address the experimental spectra that use either Ar-messenger or multiphoton dissociation techniques.

Acknowledgements

JMB thanks the National Science Foundation and the Office of Naval Research for financial support. He also gratefully acknowledges collaborators Bastiaan Braams, Stuart Carter, Xinchuan Huang and Anne McCoy. KRA and DMN wish to acknowledge contributions from their collaborators Nicholas L. Pivonka, Matthew J. Nee and Andreas Osterwalder at the University of California Berkeley; Ludger Wöste, Cristina Kaposta, Mathias Brümmer, Gabriele Santambrogio and Carlos Cibrián Uhalte at the Freie Universität Berlin and Gerard Meijer and Gert von Helden at the Fritz-Haber-Institut der Max-Planck-Gesellschaft in Berlin. KRA gratefully acknowledges financial support by the German Research Foundation DFG as part of the Collaborative Research Center 546 and the Research Training Group 788, as well as the “Stichting voor Fundamenteel Onderzoek der Materie (FOM)” in providing the required beam time on FELIX and the skillful assistance of the complete FELIX staff. He also thanks Travis Fridgen for supplying a copy of the CLIO spectrum. DMN acknowledges support from the Air Force Office of Scientific Research.

References

- [1] J. Trylska, P. Grochowski, J. A. McCammon, *Protein Sci.* **2004**, *13*, 513-528.
- [2] C. A. Hunter, *Angew. Chem., Int. Ed.* **2004**, *43*, 5310-5324.
- [3] V. Z. Spassov, H. Luecke, K. Gerwert, D. Bashford, *J. Mol. Biol.* **2001**, *312*, 203-219.
- [4] D. Marx, M. E. Tuckerman, J. Hutter, M. Parinello, *Nature* **1999**, *397*, 601.
- [5] T. Steiner, *Angew. Chem., Int. Ed.* **2002**, *41*, 48-76.
- [6] M. A. Duncan, *Int. J. Mass Spectrom.* **2000**, *200*, 545-569; E. J. Bieske, O. Dopfer, *Chem. Rev.* **2000**, *100*, 3963-3998.
- [7] N. H. Rosenbaum, J. C. Owrutsky, L. M. Tack, R. J. Saykally, *J. Chem. Phys.* **1986**, *84*, 5308-5313.
- [8] S. Davis, M. Fárník, D. Uy, D. J. Nesbitt, *Chem. Phys. Lett.* **2001**, *344*, 23-30.
- [9] S. Mukamel, J. Jortner, *J. Chem. Phys.* **1976**, *65*, 5204.
- [10] J. Oomens, G. Meijer, G. von Helden, *J. Phys. Chem. A* **2001**, *105*, 8302-8309.
- [11] M. Nee, C. Kaposta, A. Osterwalder, C. Cibrian Uhalte, T. Xie, A. Kaledin, S. Carter, J. M. Bowman, G. Meijer, D. M. Neumark, K. R. Asmis, *J. Chem. Phys.* **2004**, *121*, 7259.
- [12] M. Okumura, L. I. Yeh, Y. T. Lee, *J. Chem. Phys.* **1985**, *83*, 3705-3706.
- [13] W. H. Robertson, M. A. Johnson, *Annu. Rev. Phys. Chem.* **2003**, *54*, 173-213.
- [14] G. von Helden, I. Holleman, G. M. H. Knippels, A. F. G. van der Meer, G. Meijer, *Phys. Rev. Lett.* **1997**, *79*, 5234-5237.
- [15] M. Gerhards, C. Unterberg, A. Gerlach, *Phys. Chem. Chem. Phys.* **2002**, *4*, 5563-5565; M. Gerhards, *Optics Communications* **2004**, *241*, 493-497; J. A. Stearns, A. Das, T. S. Zwier, *Phys. Chem. Chem. Phys.* **2004**, *6*, 2605-2610.
- [16] J. M. Headrick, J. C. Bopp, M. A. Johnson, *J. Chem. Phys.* **2004**, *121*, 11523-11526.
- [17] W. R. Bosenberg, D. R. Guyer, *Journal Of the Optical Society Of America B-Optical Physics* **1993**, *10*, 1716.
- [18] K. R. Asmis, M. Brümmer, C. Kaposta, G. Santambrogio, G. von Helden, G. Meijer, K. Rademann, L. Wöste, *Phys. Chem. Chem. Phys.* **2002**, *4*, 1101-1104.
- [19] G. M. H. Knippels, G. H. C. Vanwerkhoven, E. H. Haselhoff, B. Faatz, D. Oepts, P. W. Vanamersfoort, *Nucl Instrum Meth A* **1995**, *358*, 308-310; D. Oepts, A. F. G. van der Meer, P. W. van Amersfoort, *Infrared Phys. Technol.* **1995**, *36*, 297-308.
- [20] A. Brown, B. J. Braams, K. Christoffel, Z. Jin, J. M. Bowman, *J. Chem. Phys.* **2003**, *119*, 8790-8793; A. B. McCoy, B. J. Braams, A. Brown, X. C. Huang, Z. Jin, J. M. Bowman, *J. Phys. Chem. A* **2004**, *108*, 4991-4994.
- [21] X. C. Huang, B. J. Braams, S. Carter, J. M. Bowman, *J. Am. Chem. Soc.* **2004**, *126*, 5042-5043.
- [22] X. Huang, B. J. Braams, J. M. Bowman, *Journal of Chemical Physics* **in press**.
- [23] S. Carter, N. C. Handy, C. Puzzarini, R. Tarroni, P. Palmieri, *Mol. Phys.* **2000**, *98*, 1697-1712.
- [24] J. M. Bowman, S. Carter, X. C. Huang, *Int. Rev. Phys. Chem.* **2003**, *22*, 533-549; S. Carter, N. C. Handy, *J. Chem. Phys.* **2000**, *113*, 987-993; J. M. Bowman, S. Carter, N. C. Handy, in *Theory and Applications of Computational Chemistry: The First 40 Years* (Eds.: Clifford Dykstra, Gernot Frenking, Kwang S. Kim, G. E. Scuseria), **to appear in**.
- [25] W. H. Miller, N. C. Handy, J. E. Adams, *J. Chem. Phys.* **1980**, *72*, 99-112; J. T. Hougen, P. R. Bunker, J. W. C. Johns, *J. Mol. Spec.* **1970**, *34*, 136-172.
- [26] E. G. Diken, J. M. Headrick, J. R. Roscioli, J. C. Bopp, M. A. Johnson, A. B. McCoy, X. Huang, S. Carter, J. M. Bowman, *J. Phys. Chem. A* **in press**.
- [27] J. Dai, Z. Bacic, X. Huang, S. Carter, J. M. Bowman, *J. Chem. Phys.* **2003**, *119*, 6571-6580.

- [28] A. B. McCoy, X. Huang, S. Carter, M. Y. Landeweer, J. M. Bowman, *J. Chem. Phys.* **accepted for publication**.
- [29] G. Caldwell, P. Kebarle, *Can J Chem* **1985**, *63*, 1399-1406.
- [30] H. Gomez, G. Meloni, J. Madrid, D. M. Neumark, *J. Chem. Phys.* **2003**, *119*, 872-879.
- [31] N. L. Pivonka, C. Kaposta, G. von Helden, G. Meijer, L. Wöste, D. M. Neumark, K. R. Asmis, *J. Chem. Phys.* **2002**, *117*, 6493-6499.
- [32] D. M. Neumark, *Accts. Chem. Res.* **1993**, *26*, 33-39.
- [33] H. Kunttu, J. Seetula, M. Räsänen, V. A. Apkarian, *J. Chem. Phys.* **1992**, *96*, 5630-5635.
- [34] B. S. Ault, *Accts. Chem. Res.* **1982**, *15*, 103-109.
- [35] D. U. Webb, K. N. Rao, *J. Mol. Spectrosc.* **1968**, *28*, 121; D. R. J. Boyd, H. W. Thompson, *Spectrochim. Acta* **1952**, *5*, 308.
- [36] K. Kawaguchi, *J. Chem. Phys.* **1988**, *88*, 4186-4189; K. Kawaguchi, E. Hirota, *J. Chem. Phys.* **1986**, *84*, 2953-2960; K. Kawaguchi, E. Hirota, *J. Chem. Phys.* **1987**, *87*, 6838-6841; K. Kawaguchi, E. Hirota, *J. Mol. Struct.* **1995**, *352*, 389-394.
- [37] N. L. Pivonka, C. Kaposta, M. Brümmer, G. von Helden, G. Meijer, L. Wöste, D. M. Neumark, K. R. Asmis, *J. Chem. Phys.* **2003**, *118*, 5275-5278.
- [38] P. A. Frey, *Journal of Physical Organic Chemistry* **2004**, *17*, 511-520.
- [39] J. E. Del Bene, M. J. T. Jordan, *Spectrochim Acta A* **1999**, *55*, 719-729.
- [40] C. M. Ellison, B. S. Ault, *J. Phys. Chem.* **1979**, *83*, 832-837.
- [41] A. Kaledin, S. Skokov, J. M. Bowman, K. Morokuma, *J. Chem. Phys.* **2000**, *113*, 9479-9487.
- [42] N. Agmon, *Chem. Phys. Lett.* **1995**, *244*, 456-462.
- [43] R. Rousseau, V. Kleinschmidt, U. W. Schmitt, D. Marx, *Phys. Chem. Chem. Phys.* **2004**, *6*, 1848-1859.
- [44] G. Zundel, *Adv. Chem. Phys.* **2000**, *111*, 1-217.
- [45] N. B. Librovich, V. P. Sakun, N. D. Sokolov, *Chem. Phys.* **1979**, *39*, 351; J. Kim, U. W. Schmitt, J. A. Gruetzmacher, G. A. Voth, N. E. Scherer, *J. Chem. Phys.* **2002**, *116*, 737-746.
- [46] I. Olovsson, *J. Chem. Phys.* **1968**, *49*, 1063-1067.
- [47] X. Huang, H. M. Cho, S. Carter, J. Ojamae, J. M. Bowman, S. J. Singer, *J. Phys. Chem. A* **2003**, *107*, 7142-7151.
- [48] L. I. Yeh, J. D. Myers, J. M. Price, Y. T. Lee, *J. Chem. Phys.* **1989**, *91*, 7319-7330.
- [49] Y. K. Lau, S. Ikuta, P. Kebarle, *J. Am. Chem. Soc.* **1982**, *104*, 1462-1469.
- [50] L. I. Yeh, Y. T. Lee, J. T. Hougen, *J. Mol. Spec.* **1994**, *164*, 473-488.
- [51] D. J. Wales, *J. Chem. Phys.* **1999**, *110*, 10403-10409.
- [52] K. R. Asmis, N. L. Pivonka, G. Santambrogio, M. Brümmer, C. Kaposta, D. M. Neumark, L. Wöste, *Science* **2003**, *299*, 1375.
- [53] T. D. Fridgen, T. B. McMahon, L. MacAleese, J. Lemaire, P. Maitre, *J. Phys. Chem. A* **2004**, *108*, 9008-9010.
- [54] R. Prazeres, F. Glotin, C. Insa, D. A. Jaroszynski, J. M. Ortega, *Eur Phys J D* **1998**, *3*, 87.
- [55] M.A. Johnson, private communication.
- [56] M. V. Vener, O. Kühn, J. Sauer, *J. Chem. Phys.* **2001**, *114*, 240-249.
- [57] L. Ojamäe, I. Shavitt, S. J. Singer, *J. Chem. Phys.* **1998**, *109*, 5547-5564.
- [58] G. M. Chaban, J. O. Jung, R. B. Gerber, *J. Phys. Chem. A* **2000**, *104*, 2772-2779.
- [59] M. Mella, D. C. Clary, *J. Chem. Phys.* **2003**, *119*, 10048-10062.
- [60] K. R. Asmis, M. Brummer, C. Kaposta, G. Santambrogio, G. von Helden, G. Meijer, K. Rademann, L. Wöste, *Phys. Chem. Chem. Phys.* **2002**, *4*, 1101-1104.

E ACKNOWLEDGEMENTS

The present work was realized under the supervision of Prof. Dr. Ludger Wöste, who conceived of and initiated central aspects of this project. In its later stages it was essentially supported by Prof. Dr. Gerard Meijer. I am greatly indebted to both of them for their guidance and for generously sharing their expertise, dedication, and profound knowledge of science with me. I am especially grateful to them for granting me the freedom to pursue my particular scientific goals.

I wish to express sincere gratitude to Cristina Kaposta, Gabriele Santambrogio and Mathias Brümmer for their dedication and friendship without which this project would not have been a success and, more important, would not have been nearly as fun. My special thanks goes to them as well as to Thomas Leisner, Gert von Helden, Albrecht Lindinger, Andre Fielicke, Martin Beyer, Nick Pivonka, Oliver Kühn, Detlef Schröder, Uli Heiz, Marcel Krenz and Henry Hess for the many stimulating scientific and non-scientific exchanges during this time, which all have left memorable impressions.

I thank Michael Kregielski, Detlef Müller and the complete team in the workshop of the Department of Physics at the FUB for their competent contribution to the design and construction of the vacuum chamber and most of the parts that comprise the newly built instrument. I thank the electronics shop team, in particular Herr Marian Luft, for the design and assembly of the electronic components. Thanks to all the helping hands in the administration of the FUB and the FHI, in particular Inge Siegel, Sigrid Apelt, Silvana Pophal, Christa Hermanni, Inga von Dölln and Beatrix Wieczorek for their most competent assistance with respect to all administrative as well as other matters and may they forgive me for asking all those questions.

Special thanks also to all the wonderful people I have met at the FOM Institute Rijnhuizen and that have helped to make this project such a success, in particular, Deniz van Heijnsbergen, Rob Satink, Joost Bakker, Jos Oomens, Giel Berden, Britta Redlich, Lex van der Meer, René van Buren, Wim Mastop, Theo Ram, Peter Delmee, Dave Moore, Boris Sartakov and the charming crew at the front desk and all the people I forgot to mention.

I'm very appreciative of the fruitful collaborations with and significant contributions to this thesis work from the following professors (in alphabetical order) and their groups: Joel Bowman, Michael Duncan, Daniel Neumark, Klaus Rademann, and Joachim Sauer. I'd also like to thank professors Hajo Freund, Mark Johnson, Hans-Heinrich Limbach, Jörn Manz, and Dietmar Stehlik for their support.

I gratefully acknowledge funding from the German Research Foundation DFG, the Max-Planck-Society MPG and the European Union and wish to especially thank the Swiss National Science Foundation for their continuing support throughout my scientific career.

My warmest thanks to my family and my love Cate for their support and encouragement during the last years.

F REFERENCES

- [1] M. S. Whittingham, *Chem. Rev.* **2004**, *104*, 4271-4301.
- [2] L. A. L. de Almeida, G. S. Deep, A. M. N. Lima, I. A. Khrebtov, V. G. Malyarov, H. Neff, *Appl. Phys. Lett.* **2004**, *85*, 3605-3607.
- [3] L. Krusin-Elbaum, D. M. Newns, H. Zeng, V. Derycke, J. Z. Sun, R. Sandstrom, *Nature* **2004**, *431*, 672-676.
- [4] B. M. Weckhuysen, D. E. Keller, *Catal. Today* **2003**, *78*, 25-46.
- [5] J. Trylska, P. Grochowski, J. A. McCammon, *Protein Sci.* **2004**, *13*, 513-528.
- [6] C. A. Hunter, *Angew. Chem., Int. Ed.* **2004**, *43*, 5310-5324.
- [7] V. Z. Spassov, H. Luecke, K. Gerwert, D. Bashford, *J. Mol. Biol.* **2001**, *312*, 203-219.
- [8] D. Marx, M. E. Tuckerman, J. Hutter, M. Parinello, *Nature* **1999**, *397*, 601.
- [9] M. V. Basilevsky, M. V. Vener, *Russ. Chem. Rev.* **2003**, *72*, 1-33.
- [10] T. Steiner, *Angew. Chem., Int. Ed.* **2002**, *41*, 48-76.
- [11] C. J. T. d. Grotthuss, *Ann. Chim.* **1806**, *58*, 54-74; N. Agmon, *Chem. Phys. Lett.* **1995**, *244*, 456-462.
- [12] G. Zundel, in *The Hydrogen Bond - Recent Developments in Theory and Experiments*. (Eds.: P. Schuster, G. Zundel, C. Sandorf), North-Holland, Amsterdam, **1976**, pp. 683-766.
- [13] M. Eigen, *Angew. Chem., Int. Ed. Engl.* **1964**, *3*, 1.
- [14] V. N. Bagratashvili, V. S. Letokhov, A. A. Makarov, E. A. Ryabov, *Multiple Photon Infrared Laser Photophysics and Photochemistry*, Harwood Academic Publishers GmbH, Amsterdam, **1985**; C. D. Cantrell, in *Topics in Current Physics, Vol. 35*, Springer Verlag, Berlin Heidelberg, **1986**.
- [15] M. A. Duncan, *Int. J. Mass Spectrom.* **2000**, *200*, 545-569.
- [16] E. J. Bieske, O. Dopfer, *Chem. Rev.* **2000**, *100*, 3963-3998.
- [17] N. H. Rosenbaum, J. C. Owrutsky, L. M. Tack, R. J. Saykally, *J. Chem. Phys.* **1986**, *84*, 5308-5313.
- [18] S. Davis, M. Fárnik, D. Uy, D. J. Nesbitt, *Chem. Phys. Lett.* **2001**, *344*, 23-30.
- [19] S. Mukamel, J. Jortner, *J. Chem. Phys.* **1976**, *65*, 5204.
- [20] J. Oomens, G. Meijer, G. von Helden, *J. Phys. Chem. A* **2001**, *105*, 8302-8309.
- [21] M. Nee, C. Kaposta, A. Osterwalder, C. Cibrian Uhalte, T. Xie, A. Kaledin, S. Carter, J. M. Bowman, G. Meijer, D. M. Neumark, K. R. Asmis, *J. Chem. Phys.* **2004**, *121*, 7259.
- [22] M. Okumura, L. I. Yeh, Y. T. Lee, *J. Chem. Phys.* **1985**, *83*, 3705-3706.
- [23] W. H. Robertson, M. A. Johnson, *Annu. Rev. Phys. Chem.* **2003**, *54*, 173-213.
- [24] T. H. Maiman, *Nature* **1960**, *187*, 493-494.
- [25] C. Bordé, A. Henry, L. Henry, *Compt. Rend. Acad. Sci.* **1966**, *B262*, 1389.
- [26] N. R. Isenor, M. C. Richardson, *Appl. Phys. Lett.* **1971**, *18*, 224.
- [27] A. J. Beaulieu, *Appl. Phys. Lett.* **1970**, *16*, 504-505.
- [28] R. V. Ambartsumian, V. S. Letokhov, E. A. Ryabov, N. V. Chekalin, *JETP Lett.* **1974**, *20*, 273-274; R. V. Ambartsumian, Y. A. Gorokhov, V. S. Letokhov, G. N. Makarov, *JETP Lett.* **1975**, *21*, 171.
- [29] R. V. Ambartsumian, Y. A. Gorokhov, G. N. Makarov, A. A. Puretzki, N. P. Furzikov, *Chem. Phys. Lett.* **1977**, *45*, 231-234.
- [30] M. J. Coggiola, P. A. Schulz, Y. T. Lee, Y. R. Shen, *Phys. Rev. Lett.* **1977**, *38*, 17-20.
- [31] A. S. Sudbo, P. A. Schulz, Y. R. Shen, Y. T. Lee, in *Multiple-Photon Excitation and Dissociation of Polyatomic Molecules, Vol. 35* (Ed.: C. D. Cantrell), Springer-Verlag, Berlin, **1986**, pp. 95-122.
- [32] W. H. Wing, G. A. Ruff, W. E. Lamb, J. J. Spezeski, *Phys. Rev. Lett.* **1976**, *36*, 1488-1491.
- [33] A. Carrington, D. R. J. Milverton, P. J. Sarre, *Mol. Phys.* **1978**, *35*, 1505-1521.
- [34] R. R. Corderman, W. C. Lineberger, *Annu. Rev. Phys. Chem.* **1979**, *30*, 347-378.
- [35] H. A. Schwarz, *J. Chem. Phys.* **1977**, *67*, 5525-5534; H. A. Schwarz, *J. Chem. Phys.* **1980**, *72*, 284-287.
- [36] T. Oka, *Phys. Rev. Lett.* **1980**, *45*, 531-534.
- [37] F. C. van den Heuvel, A. Dymanus, *Chem. Phys. Lett.* **1982**, *92*, 219.
- [38] R. J. Saykally, K. M. Evenson, *Phys. Rev. Lett.* **1979**, *43*, 515-518.
- [39] L. I. Yeh, J. D. Myers, J. M. Price, Y. T. Lee, *J. Chem. Phys.* **1989**, *91*, 7319-7330.
- [40] M. Okumura, L. I. Yeh, Y. T. Lee, *J. Chem. Phys.* **1988**, *88*, 79-91.

- [41] M. Okumura, L. I. Yeh, J. D. Myers, Y. T. Lee, *J. Chem. Phys.* **1986**, *85*, 2328-2329; M. Okumura, L. I. Yeh, J. D. Myers, Y. T. Lee, *J. Phys. Chem.* **1990**, *94*, 3416-3427.
- [42] J. M. Price, M. W. Crofton, Y. T. Lee, *J. Chem. Phys.* **1989**, *91*, 2749-2751; J. M. Price, M. W. Crofton, Y. T. Lee, *J. Phys. Chem.* **1991**, *95*, 2182-2195.
- [43] L. I. Yeh, Y. T. Lee, *J. Am. Chem. Soc.* **1989**, *111*, 5597-5604.
- [44] W. L. Liu, J. M. Lisy, *J. Chem. Phys.* **1988**, *89*, 605-606; T. J. Selegue, N. Moe, J. A. Draves, J. M. Lisy, *J. Chem. Phys.* **1992**, *96*, 7268-7278; C. J. Weinheimer, J. M. Lisy, *J. Chem. Phys.* **1996**, *105*, 2938-2941; J. M. Lisy, *Int. Rev. Phys. Chem.* **1997**, *16*, 267-289.
- [45] E. J. Bieske, S. A. Nizkorodov, F. R. Bennett, J. P. Maier, *J. Chem. Phys.* **1995**, *102*, 5152-5164.
- [46] Y. B. Cao, J. H. Choi, B. M. Haas, M. S. Johnson, M. Okumura, *J. Phys. Chem.* **1993**, *97*, 5215-5217; M. S. Johnson, K. T. Kuwata, C. K. Wong, M. Okumura, *Chem. Phys. Lett.* **1996**, *260*, 551-557.
- [47] K. Müller-Dethlefs, M. Sander, E. W. Schlag, *Z. Naturforsch. A* **1984**, *39*, 1089; K. Müller-Dethlefs, E. W. Schlag, *Annu. Rev. Phys. Chem.* **1991**, *42*, 109.
- [48] G. K. Jarvis, Y. Song, C. Y. Ng, E. R. Grant, *J. Chem. Phys.* **1999**, *111*, 9568-9573.
- [49] L. Zhu, P. Johnson, *J. Chem. Phys.* **1991**, *94*, 5769-5771.
- [50] M. Putter, G. von Helden, G. Meijer, *Chem. Phys. Lett.* **1996**, *258*, 118-122.
- [51] G. M. H. Knippels, G. H. C. Van Werkhoven, E. H. Haselhoff, B. Faatz, D. Oepts, P. W. Van Amersfoort, *Nucl. Instrum. Meth. A* **1995**, *358*, 308-310; D. Oepts, A. F. G. van der Meer, P. W. van Amersfoort, *Infrared Phys. Technol.* **1995**, *36*, 297-308.
- [52] G. von Helden, I. Holleman, G. M. H. Knippels, A. F. G. van der Meer, G. Meijer, *Phys. Rev. Lett.* **1997**, *79*, 5234-5237; G. von Helden, I. Holleman, A. J. A. van Roij, G. M. H. Knippels, A. F. G. van der Meer, G. Meijer, *Phys. Rev. Lett.* **1998**, *81*, 1825-1828; G. von Helden, I. Holleman, M. Putter, A. J. A. van Roij, G. Meijer, *Chem. Phys. Lett.* **1999**, *299*, 171-176.
- [53] G. von Helden, I. Holleman, G. Meijer, B. Sartakov, *Optics Express* **1999**, *4*, 46-52.
- [54] H. Piest, G. von Helden, G. Meijer, *J. Chem. Phys.* **1999**, *110*, 2010-2015; H. Piest, G. von Helden, G. Meijer, *Astrophys. J.* **1999**, *520*, L75-L78; R. G. Satink, H. Piest, G. von Helden, G. Meijer, *J. Chem. Phys.* **1999**, *111*, 10750-10753; J. Oomens, A. J. A. van Roij, G. Meijer, G. von Helden, *Astrophys. J.* **2000**, *542*, 404.
- [55] D. van Heijnsbergen, G. von Helden, M. A. Duncan, A. J. A. van Roij, G. Meijer, *Phys. Rev. Lett.* **1999**, *83*, 4983-4986; G. von Helden, A. C. G. M. Tielens, D. van Heijnsbergen, M. A. Duncan, S. Hony, L. B. F. M. Waters, G. Meijer, *Science* **2000**, *288*, 313-316; D. van Heijnsbergen, A. Fielicke, G. Meijer, G. von Helden, *Phys. Rev. Lett.* **2002**, *89*, 013401.
- [56] G. von Helden, A. Kirilyuk, D. van Heijnsbergen, B. Sartakov, M. A. Duncan, G. Meijer, *Chem. Phys.* **2000**, *262*, 31-39; D. van Heijnsbergen, G. von Helden, G. Meijer, M. A. Duncan, *J. Chem. Phys.* **2002**, *116*, 2400-2406.
- [57] B. Simard, S. Denomme, D. M. Rayner, D. van Heijnsbergen, G. Meijer, G. von Helden, *Chem. Phys. Lett.* **2002**, *357*, 195-203; A. Fielicke, G. von Helden, G. Meijer, B. Simard, S. Denomme, D. M. Rayner, *J. Am. Chem. Soc.* **2003**, *125*, 11184-11185.
- [58] A. Fielicke, A. Kirilyuk, C. Ratsch, J. Behler, M. Scheffler, G. von Helden, G. Meijer, *Phys. Rev. Lett.* **2004**, *93*, 023401; A. Fielicke, C. Ratsch, G. von Helden, G. Meijer, *J. Chem. Phys.* **2005**, *122*, 091105.
- [59] J. M. Bakker, L. Mac Aleese, G. Meijer, G. von Helden, *Phys. Rev. Lett.* **2003**, *91*, 203003; P. Carcabal, R. T. Kroemer, L. C. Snoek, J. P. Simons, J. M. Bakker, I. Compagnon, G. Meijer, G. von Helden, *Phys. Chem. Chem. Phys.* **2004**, *6*, 4546-4552.
- [60] J. Oomens, N. Polfer, D. T. Moore, L. van der Meer, A. G. Marshall, J. R. Eyler, G. Meijer, G. von Helden, *Phys. Chem. Chem. Phys.* **2005**, *7*, 1345-1348.
- [61] K. R. Asmis, M. Brummer, C. Kaposta, G. Santambrogio, G. von Helden, G. Meijer, K. Rademann, L. Woste, *Phys. Chem. Chem. Phys.* **2002**, *4*, 1101-1104.
- [62] N. L. Pivonka, C. Kaposta, G. von Helden, G. Meijer, L. Wöste, D. M. Neumark, K. R. Asmis, *J. Chem. Phys.* **2002**, *117*, 6493-6499.
- [63] J. Lemaire, P. Boissel, M. Heninger, G. Mauclaire, G. Bellec, H. Mestdag, A. Simon, S. Caer, J. M. Ortega, F. Glotin, P. Maitre, *Phys. Rev. Lett.* **2002**, *89*, 273002.
- [64] J. Banisaukas, J. Szczepanski, J. Eyler, M. Vala, S. Hirata, M. Head-Gordon, J. Oomens, G. Meijer, G. von Helden, *J. Phys. Chem. A* **2003**, *107*, 782-793; J. J. Valle, J. R. Eyler, J. Oomens, D. T. Moore, A. F. G. van der Meer, G. von Helden, G. Meijer, C. L. Hendrickson, A. G. Marshall, G. T. Blakney, *Rev. Sci. Instrum.* **2005**, *76*, 023103.
- [65] J. G. Black, E. Yablonovitch, N. Bloembergen, S. Mukamel, *Phys. Rev. Lett.* **1977**, *38*, 1131-1134.

-
- [66] A. A. Makarov, I. Y. Petrova, E. A. Ryabov, V. S. Letokhov, *J. Phys. Chem. A* **1998**, *102*, 1438-1449.
- [67] J. D. Rynbrandt, B. S. Rabinovitch, *J. Chem. Phys.* **1971**, *54*, 2275-2276.
- [68] E. R. Grant, P. A. Schulz, A. S. Sudbo, Y. R. Shen, Y. T. Lee, *Phys. Rev. Lett.* **1978**, *40*, 115-118.
- [69] T. Beyer, D. F. Swinehart, *Commun Acm* **1973**, *16*, 379-379.
- [70] S. Wolf, Freie Universität Berlin (Berlin), **1997**.
- [71] H. Hess, Diplomarbeit thesis, Freie Universität Berlin (Berlin), **1999**.
- [72] E. Teloy, D. Gerlich, *Chem. Phys.* **1974**, *4*, 417-427; B. Krämer, Diplom thesis, Freie Universität Berlin (Berlin), **1993**.
- [73] T. G. Dietz, M. A. Duncan, D. E. Powers, R. E. Smalley, *J. Chem. Phys.* **1981**, *74*, 6511-6512.
- [74] G. Santambrogio, Università Degli Studi di Milano (Milano), **2001**.
- [75] J. B. Fenn, M. Mann, C. K. Meng, S. F. Wong, C. M. Whitehouse, *Mass Spectrom. Rev.* **1990**, *9*, 37-70.
- [76] C. Kaposta, Ph.D. thesis, Freie Universität Berlin (Berlin), **2005**.
- [77] G. G. Dolnikowski, M. J. Kristo, C. G. Enke, J. T. Watson, *Int. J. Mass Spectrom. Ion. Proc.* **1988**, *82*, 1-15.
- [78] D. Gerlich, *Adv. Chem. Phys.* **1992**, *82*, 1.
- [79] J. Raffy, T. Debuisschert, J. P. Pocholle, M. Papuchon, *Applied Optics* **1994**, *33*, 985-987.
- [80] M. Gerhards, C. Unterberg, A. Gerlach, *Phys. Chem. Chem. Phys.* **2002**, *4*, 5563-5565; M. Gerhards, *Opt. Commun.* **2004**, *241*, 493-497.
- [81] W. R. Bosenberg, D. R. Guyer, *J. Opt. Soc. Am. Soc. B* **1993**, *10*, 1716.
- [82] J. M. Headrick, J. C. Bopp, M. A. Johnson, *J. Chem. Phys.* **2004**, *121*, 11523-11526; E. G. Diken, J. M. Headrick, J. R. Roscioli, J. C. Bopp, M. A. Johnson, A. B. McCoy, *J. Phys. Chem. A* **2005**, *109*, 1487-1490.
- [83] K. E. Kuyanov, T. Momose, A. F. Vilesov, *Applied Optics* **2004**, *43*, 6023-6029.
- [84] J. M. Smith, D. A. Hrovat, W. T. Borden, M. Allan, K. R. Asmis, C. Bulliard, E. Haselbach, U. C. Meier, *J. Am. Chem. Soc.* **1993**, *115*, 3816-3817.

G APPENDIX

G.1 Other Publications

The following two publications are part of my work done at the FUB, but did not fit in the framework of this thesis work. The first, "Bausteine des Wassers unter der Laserlupe", written together with Oliver Kühn from the Department of Chemistry at the FUB, is an article in German and published in the university science magazine *fundiert*. It describes our work on protonated water clusters and is aimed at a general, science-interested audience. The second publication describes femtosecond experiments on silver clusters; work done together with Henry Hess and Thomas Leisner shortly after I came to Berlin in 1999. The paper introduces a new method to study the vibrational spectroscopy of mass-selected *neutral* clusters.

Bausteine des Wassers unter der "Laserlupe"

Knut R. Asmis

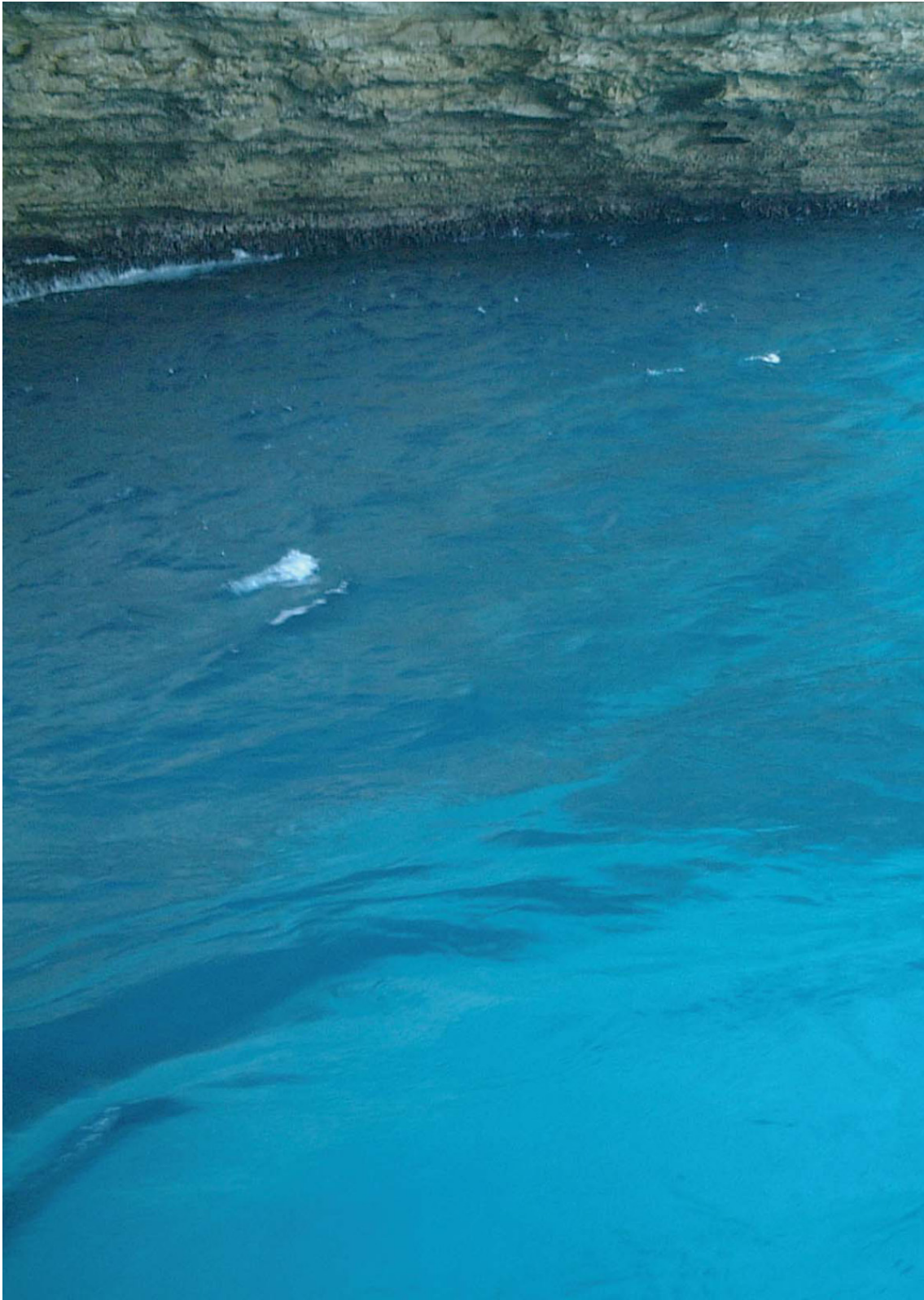
Fritz-Haber-Institut der Max-Planck-Gesellschaft, Faradayweg 4-6, 14195 Berlin, Germany

Oliver Kühn

Institut für Chemie, Freie Universität Berlin, Takustr. 3, 14195 Berlin, Germany

Artikel in

fundiert - Das Wissenschaftsmagazin der Freien Universität Berlin **2** 84-91 (2004).







KNUT ASMIS UND OLIVER KÜHN

Das Vertrautsein, ja die Allgegenwart des Wassers, lässt es unmöglich erscheinen, dass es in Bezug auf das Verständnis der makro- und mikroskopischen Eigenschaften des Wassers irgendwache substantiellen Unklarheiten geben könnte. Und doch, ungeachtet einer langen Geschichte der wissenschaftlichen Erforschung gibt uns das Wasser immer noch Rätsel auf, die erst in der jüngsten Vergangenheit durch den konzentrierten Einsatz moderner experimenteller und theoretischer Methoden allmählich entschlüsselt werden.

Eine Eigenschaft des Wassers, deren Konsequenzen uns geläufig sind, ist seine maximale Dichte bei 4°C. Dies führt zum Beispiel dazu, dass Eis auf flüssigem Wasser schwimmt oder dass im Winter Seen immer erst an der Oberfläche und dann von „oben nach unten“ gefrieren. So bleibt auch bei Temperaturen unter dem Gefrierpunkt das Wasser am Grund eines Sees oft flüssig.

Dieses Verhalten ist uns unter dem Begriff der Anomalie des Wassers bekannt. Es handelt sich dabei um eine makroskopische Eigenschaft, die sich auf atomarer Ebene aus dessen netzwerkartigem Aufbau aus Wassermolekülen ableiten lässt. Neben dieser Unregelmäßigkeit in der Temperaturabhängigkeit der Wasserdichte gibt es eine Vielzahl anderer physikochemischer Eigenschaften des Wassers, welche auf diesen molekularen Verbund von Wassermolekülen zurückzuführen sind. Von diesen wollen wir eine ganz besondere, nämlich die erhöh-

te Mobilität von protonierten Wassermolekülen, hier näher unter die Lupe nehmen.

Die Vernetzung einzelner Wassermoleküle ist auf die Ausbildung von Wasserstoffbrückenbindungen (O-H...O), oder kurz Wasserstoffbrücken, zurückzuführen. Sie spannen einerseits Tetraeder auf, in deren Zentren sich jeweils ein Sauerstoffatom befindet. Andererseits ist die chemische Bindungsenergie einer Wasserstoffbrücke nicht sehr viel größer als die thermische Energie der atomaren Bewegungen bei Raumtemperatur. Dies hat zur Folge, dass die thermische Bewegung allein schon dazu führt, dass Wasserstoffbrücken ständig aufgebrochen und neu gebildet werden. Mit abnehmender Temperatur friert dieses Netzwerk aus und man hat es mit Eis in seiner Vielfalt an Formen zu tun. Grosse Aufmerksamkeit ist der Diffusion von Ionen in wässriger Lösung gewidmet worden. Hierbei fällt insbesondere [Der Grotthuss Mechanismus](#)

auf, dass protonierte Wassermoleküle im Vergleich zu anderen Ionen (zum Beispiel Natriumionen) substantiell „beweglicher“ sind. Dies ist deswegen so bemerkenswert, da ein protoniertes Wassermolekül, das Oxonium-Ion H_3O^+ , hinsichtlich seiner Größe vergleichbar mit einem Na^+ Ion ist, aber seine Mobilität in Experimenten als fünfmal höher nachgewiesen wurde. Der zugrunde liegende Mechanismus wurde bereits vor ca. 200 Jahren durch Theodor von Grotthuss – einem nonkonformen Gelehrten aus baltischem Adelsgeschlecht – postuliert. Jedoch erst nach der Einführung des Konzepts der Wasserstoffbrückenbindung durch M.L. Huggins, W.M. Latimer und W.H. Rodebush von der Universität Berkeley um 1920 konnte der Mechanismus der

Wasser gefriert, wie hier an der Ostsee, immer von oben nach unten – bekannt als Anomalie des Wassers



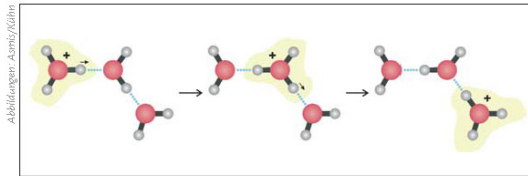


Abbildung 1: Vereinfachte Darstellung des Grotthuss Mechanismus, der die erhöhte Mobilität von protonierten Wassermolekülen erklärt. Ausgangspunkt ist ein Oxonium-Ion H_3O^+ (gelber Bereich). Durch Umlagerung der Bindungselektronen kann die positive Ladung über größere Distanzen durch ein Netzwerk von Wasserstoffbrücken (blau) befördert werden, ohne dass die Protonen (grau) sich dabei substantiell bewegen. Eine geringfügige Verschiebung, angedeutet durch die kleinen Pfeile, reicht aus, damit ein Proton seinen Platz von einem Sauerstoffatom (rot) zum benachbarten wechselt.

Dr. Knut R. Asmis



Geboren am 25. Juni 1968 in Berlin. Studium der Chemie zuerst in an der Freien Universität Berlin dann an der Universität Freiburg i. Ü. (Schweiz) von 1988 bis 1991. Die Promotion zum Dr. rer. nat. erfolgte 1996 zum Thema „Electron-Molecule Collision: A Novel Instrument for Measuring Inelastic Differential Cross Sections at 180° Angle and Applications“. Von 1996 bis 1999 Postdoctoral Fellow des Schweizer

Nationalfonds am Department of Chemistry, University of California, Berkeley, USA (Professor Daniel M. Neumark). 1999 bis 2003 wissenschaftlicher Mitarbeiter und Gruppenleiter am Institut für Experimentalphysik der Freien Universität Berlin (Professor Ludger Wöste). Seit 2003 in der Abteilung Molekülphysik am Fritz-Haber-Institut (Professor Gerard Meijer) tätig.

Kontakt

Freie Universität Berlin | Institut für Experimentalphysik
 Arnimallee 14 | 14195 Berlin
 Tel.: 030-838-56120
 E-Mail: asmis@physik.fu-berlin.de
 www: <http://www.physik.fu-berlin.de/~asmis>

und

Fritz-Haber-Institut der Max-Planck-Gesellschaft
 Faradayweg 4-6 | 14195 Berlin
 Tel.: 030-8413-5735
 E-Mail: asmis@fhi-berlin.mpg.de

Diffusion zumindest qualitativ auf mikroskopischer Ebene erklärt werden (siehe Abb. 1). Ausgangspunkt ist ein Oxonium-Ion, welches über eine Wasserstoffbrücke mit einem benachbarten Wassermolekül verbunden ist. Die thermische Bewegung der Sauerstoffatome kann nun zu einer Verkürzung der Wasserstoffbrücke führen, wodurch es dem Proton ermöglicht wird, seinen Platz von einem Sauerstoffatom zum nächsten zu wechseln. In diesem Sinne kann sich die positive Ladung schließlich durch das Wassernetzwerk bewegen, ohne dass sich die daran beteiligten Atome selbst substantiell von ihren Positionen entfernen müssen. Anhand dieses Mechanismus ist auch klar, wieso die Protonenmobilität im Eis nicht verschwindend klein wird, sondern noch etwa halb so groß wie in flüssigem Wasser bei Raumtemperatur ist. Denn auch im Eis sind zwar die Atomkerne in ihrer Beweglichkeit eingeschränkt, jedoch die viel leichteren Elektronen nicht. Dieser Mechanismus funktioniert natürlich nur, da Protonen selber Bestandteile von Wassermolekülen sind und sich problemlos in bestehende Wasserstoffbrückennetzwerke integrieren lassen. Für andere Ionen ist dies nicht der Fall, so dass deren Mobilität deutlich geringer ist.

Um dieses Verhalten auch quantitativ beschreiben zu können, muss man auch die benachbarten Wassermoleküle in Betracht ziehen, welche sich in Hüllen um das geladene Oxonium-Ion anlagern. Dabei spielen zwei wichtige Strukturen, das Eigen-Kation und das Zundel-Kation, zentrale Rollen (siehe Abb. 2). Bei längeren O-O Abständen bildet sich bevorzugt das Eigen-Kation, ein Oxonium-Ion mit drei Wassermolekülen in seiner nächsten Umgebung, während bei kürzeren O-O Abständen das Zundel-Kation, ein symmetrischer $\text{H}_2\text{O} \cdots \text{H}^+ \cdots \text{OH}_2$ Komplex, in dem sich zwei Wassermoleküle das zentrale Proton gleichermaßen teilen, stabiler ist. Man beachte, dass es sich hierbei um idealisierte Strukturen handelt; die thermische Bewegung sorgt dafür, dass das System ständig zwischen diesen Grenzstrukturen fluktuiert. Auf die Bedeutung des $\text{H}_2\text{O} \cdots \text{H}^+ \cdots \text{OH}_2$ Komplexes für die Protonenmobilität, wurde bereits in den 1930er Jahren durch M.L. Huggins aufmerksam gemacht. Eine detaillierte Entschlüsselung des Grotthuss Mechanismus auf atomarer Ebene wurde jedoch erst Mitte der Neunziger Jahre durch die rasante Entwicklung leistungstarker Rechner und den dazugehörigen Modellierungsprogrammen ermöglicht, mit denen man erstmals ganze Wassernetzwerke im Rahmen der Quantenmechanik simulieren konnte.

Das Zundel-Kation taucht als wichtiges Motiv erneut auf, wenn man von den ausgedehnten Wasserstoffbrü-

Das Zundel-Kation

ckennetzwerken des Wassers zu kleinen Wasserclustern oder Wasserdrähten übergeht, wie sie in biologischen Systemen im Zusammenhang mit Protonenpumpen vorkommen können. Solche Protonenpumpen spielen z.B. bei Redoxreaktionen in Zellmembranen eine Rolle. Protonen „wandern“ hier entlang von Kanälen, die durch Ketten von Wassermolekülen und Proteinseitenketten gebildet werden. Ein intensiv studiertes Beispiel ist das Bacteriorhodopsin, in welchem der Protonentransport durch Absorption von Licht getrieben wird (siehe Abb. 3).

Für die Identifikation und Charakterisierung solcher Protonentransferketten ist offensichtlich ein detailliertes Verständnis der Eigenschaften protonierter Wassercluster erforderlich, wobei das protonierte Wasserdimer (Zundel-Kation) den einfachsten Grenzfall darstellt. Diesem Forschungsfeld haben sich seit kurzem die Arbeitsgruppen von Oliver Kühn, Knut Asmis und Ludger Wöste vom Institut für Chemie bzw. Experimentalphysik im Rahmen eines von der Deutschen Forschungsgemeinschaft geförderten Graduiertenkollegs „Wasserstoffbrücken und Wasserstofftransfer“ gewidmet.

Eine bewährte Methode zur Untersuchung der Eigenschaften von Wasserstoffbrücken ist die Infrarotschwingungsspektroskopie. Hierbei wird durch Absorption elektromagnetischer Strahlung einer bestimmten Frequenz eine Schwingung des Moleküls angeregt (siehe

Gekoppelte Schwingungen von Wasserstoffbrücken

Abb. 4). Quantenmechanisch können nur Lichtquanten absorbiert werden, deren Energie $h\nu$ der Energie eines Schwingungsüberganges $h\nu_{\text{vib}}$ entspricht. Dies kann man mit Hilfe eines Potentialenergiendiagramms, wie es im rechten Teil der Abb. 4 gezeigt ist, veranschaulichen. In der Abbildung haben wir den möglichen Übergang entsprechend der O-H Schwingungsfrequenz eingezeichnet.

Das Bild harmonischer Schwingungen kann erfolgreich auf eine große Anzahl von Molekülen angewandt werden und man ist mit Hilfe von quantenchemischen Berechnungen oftmals in der Lage, Infrarotspektren quantitativ zu erklären. Die Situation für geladene Wassercluster, wie das protonierte Wasserdimer, ist allerdings komplizierter, da die Bewegung der Wasserstoffbrücke gekoppelt ist, und das anschauliche Bild der harmonischen Schwingung (Abb. 4) hier seine Gültigkeit verliert. Einen Hinweis darauf findet man bereits in einer Arbeit von M. L. Huggins aus dem Jahre 1936, aber erst die Methodenentwicklung in der Quantenchemie gepaart mit der Verfügbarkeit leistungsfähiger Computer erlauben eine quantitative Analyse derartiger Systeme. Die Eigenschaften des Potentials für die Bewe-

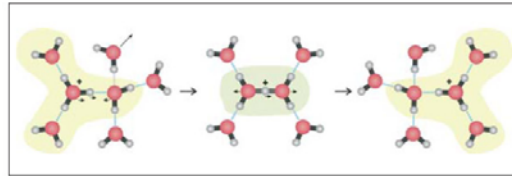


Abbildung 2: Detaillierte Darstellung des Protonentransports in Wasser. Ausgangs- und Endpunkt ist das sogenannte Eigen-Kation $\text{H}_3\text{O}^+(\text{H}_2\text{O})_3$ (links und rechts, gelber Bereich), welches unwesentlich stabiler ist, als das Zundel-Kation $\text{H}^+(\text{H}_2\text{O})_2$ (Mitte, grüner Bereich). Ausgelöst wird der Protonentransport (von links nach rechts) durch den Bruch einer Wasserstoffbrückenbindung (grün) in der näheren Umgebung eines Eigen-Kations und Reorientierung der benachbarten Wassermoleküle

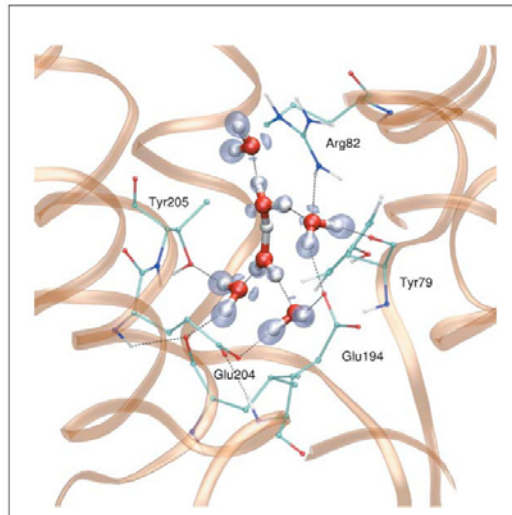


Abbildung 3: Das Zundel-Kation $\text{H}_2\text{O}\cdots\text{H}^+\cdots\text{OH}_2$ (im Zentrum der Abb. - O: rot, H: grau) taucht als strukturelles Motiv zum Beispiel in der Protonentransferkette des Bacteriorhodopsins auf

gung des Protons in der Wasserstoffbrücke, $\text{O}\cdots\text{H}^+\cdots\text{O}$, hängen stark vom Abstand der Sauerstoffatome ab (siehe Abb. 5). Links ist der Fall eines kleinen Sauerstoffabstands, wie im Zundel-Kation (siehe Abb. 2) gezeigt. Hier „sieht“ das Proton im wesentlichen ein Potential, in dem die quantenmechanische Aufenthaltswahrscheinlichkeit im Zentrum der Wasserstoffbrücke maximal ist. Vergrößert sich der Abstand zwischen den Sauerstoffatomen, wie im Eigen-Kation (siehe Abb. 2), wird ein Potential mit zwei Minima realisiert (rechts) und das Proton kann sich entweder in der Nähe des einen oder des anderen Sauerstoffatoms aufhalten. Diese Flexibilität des Potentials und insbesondere seine

Beeinflussung durch die Variation des Abstands der Sauerstoffatome ist letztendlich für den o.g. Grothuss Mechanismus des Protonentransfers verantwortlich. Für das Infrarotspektrum des Zundel-Kations gibt sich aus diesem Bild, dass eine Schwingungsanregung des O-O Abstands notwendig zu einer periodischen Modulation des Potentials für die Protonenbewegung führt

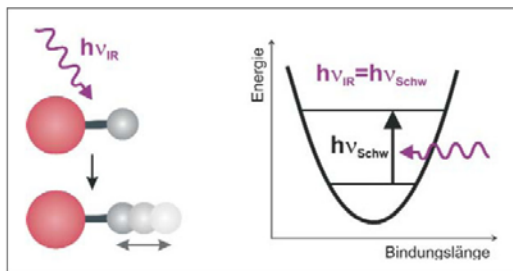


Abbildung 4: Schematische Darstellung einer Infrarotlaseranregung einer O(rot)-H(grau) Stretschwingung (links). Im rechten Bild ist das harmonische Potential für die Schwingungsbewegung dargestellt, wobei man sich die Situation so vorstellen kann, dass zwei Kugeln stark unterschiedlicher Masse über eine Feder verbunden sind. Die Energie der möglichen Schwingungsübergänge $h\nu_{Schw}$ hängt unmittelbar mit der Federkonstanten zusammen

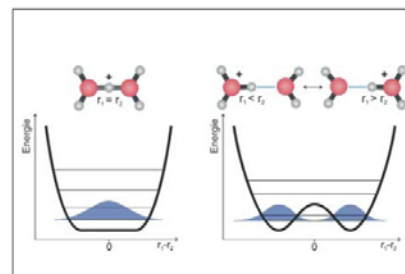
und sich somit, wie in Abb. 5 angedeutet, die möglichen Übergangsenergien zeitlich verändern. Man spricht davon, dass die O-O Schwingung und die Schwingungsbewegung des Protons gekoppelt sind. Der daraus resultierende Effekt auf das Infrarotspektrum wird schon seit den 1930er Jahren als allgemeine charakteristische Eigenschaft von Wasserstoffbrücken diskutiert, entzog sich aber bis vor kurzem dem direkten, experimentellen Nachweis.

Die Messung des Infrarotschwingungsspektrums von in Wasser gelösten Protonen ist experimentell leicht zugänglich. Die Aussagekraft dieses Spektrums wird jedoch durch die, schon oben erwähnten, dynamischen Eigenschaften des Wassernetzwerkes stark beeinträchtigt, da die Überlagerung der sich ständig ineinander umwandelnden Strukturen zu einem weitgehend unstrukturierten Infrarotspektrum im Bereich der starken Wasserstoffbrückenbindungen führt. Im Gegensatz dazu, bietet die Spektroskopie an molekularen Systemen unter isolierten Bedingungen in der Gasphase den entscheidenden Vorteil, dass maßgeschneiderte Struktureinheiten synthetisiert, nach Ihrer Größe bzw. Masse selektiert und dann unter genau definierten Bedingungen untersucht werden können (siehe Abb. 6). Die niedrigen Teilchen-

FELIX – die „Laserlupe“

dichten bei diesen Experimenten bedingen den Einsatz intensiver Lichtquellen. Laser, die entsprechende Strahlungsintensitäten erzeugen können, sind jedoch in der Regel nur in beschränkten Frequenzbereichen einsetzbar, so dass bis vor kurzem keine geeigneten, in der Frequenz durchstimmbaren, Infrarotlichtquellen zur direkten Charakterisierung von starken Wasserstoffbrücken

Abbildung 5: Potentialenergiekurven für die Bewegung des Protons (grau) zwischen den Sauerstoffatomen (rot) im Fall kleiner (links) und grosser (rechts) fixierter O-O Abstände. Thermische Fluktuationen des O-O Abstands können eine Bewegung des Protons entlang der Wasserstoffbrücke ermöglichen und somit zur Mobilität der Protonen im Wassernetzwerk beitragen. Im isolierten Zundel-Kation ist die Situation des linken Bildes vorherrschend, man spricht von einer starken Wasserstoffbrücke



PD Dr. Oliver Kühn



Geboren 1964 in Berlin. Physikstudium an der Humboldt Universität Berlin, Abschluss als Diplom-Physiker 1990, 1995 Promotion an der HU Berlin zum Dr. rer.nat. Von 1995 bis 97 Postdoctoral Fellow an der University of Rochester (USA) und an der Universität Lund (Schweden) als Stipendiat des DAAD, 2000 Habilitation in Theoretischer Chemie an der FU Berlin, seit 2004 Oberassistent an der FU

Berlin. Von 2002 bis 2003 Gastprofessor am Institute for Molecular Science in Okazaki, Japan. Forschungsschwerpunkte: Femtosekundenchemie und -biologie, Quantendynamik und Spektroskopie in Gas- und kondensierter Phase, Wasserstoffbrücken, matrixisierte Moleküle, Primärprozesse der Photosynthese.

Kontakt

Freie Universität Berlin
 Institut für Chemie, Physikalische und Theoretische Chemie
 Takustr. 3 | 14195 Berlin
 Tel.: 030 – 838 55342
 E-Mail: ok@chemie.fu-berlin.de

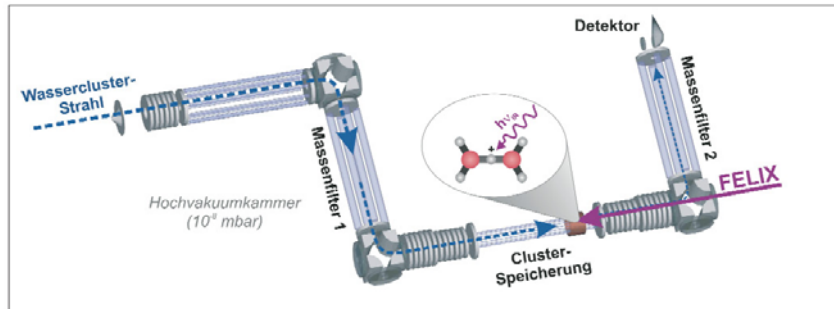


Abbildung 6: Schematische Darstellung des Spektrometers mit dem die Messungen an den Wasserclustern durchgeführt wurden. Auf Grund der extrem niedrigen Teilchendichten kann die Absorption der Infrarotstrahlung durch die Wassercluster nicht direkt (durch Messung der Abschwächung der Intensität des Laserstrahls) gemessen werden, sondern muss indirekt mittels der so genannten Photodissoziationspektroskopie nachgewiesen werden. Wassercluster einer bestimmten Größe und Masse (in diesem Fall $\text{H}_2\text{O}\cdots\text{H}^+\cdots\text{OH}_2$) werden dazu in einer Ionenfalle eingefangen, auf -250°C abgekühlt und mit intensiver Laserstrahlung beschossen. Nur bei den für ein Teilchen ganz charakteristischen Frequenzen $h\nu_{\text{Schw}}$ (siehe auch Abb. 4) kommt es zur Absorption von Photonen, die schlussendlich zur Fragmentation des Wasserclusters führt. Das Infrarotspektrum wird dann durch Messung der Anzahl der erzeugten Fragmente als Funktion der eingestrahlenen Frequenz des Laserlichtes gemessen. Details zum Experiment können unter <http://www.physik.fu-berlin.de/~asmis> nachgelesen werden

ckenbindungen zur Verfügung standen. Erst die Entwicklung Freier-Elektronen-Laser im Infrarotbereich und insbesondere deren Anwendung auf das Gebiet der Molekülphysik durch die Arbeitsgruppe um Gerard Meijer und Gert von Helden (Fritz-Haber-Institut der Max-Planck Gesellschaft, Berlin), ermöglichten der Arbeitsgruppe um Knut Asmis und Ludger Wöste im Rahmen einer internationalen Kooperation mit den Arbeitsgruppe von Daniel Neumark (University of California, Berkeley, USA), erstmalig ein Gasphasen-Infrarotspektrum des Zundel-Kations im Bereich der starken Wasserstoffbrücken zu messen. Dazu wurde das an der Freien Universität Berlin in zweijähriger Arbeit aufgebaute Vakuumspektrometer (Abb. 6) zeitweise in die Niederlande an das FOM Institut für Plasmaphysik Rijnhuizen transportiert, um dort am Freien-Elektronen-Laser-für-Infrarot-Experimente FELIX (Abb. 7) die angestrebten Messungen durchzuführen.

Das gemessene Infrarotschwingungsspektrum des Zundelkations ist in Abb. 8 dargestellt. Seine Interpretation ist bis heute nur teilweise aufgeklärt, da insbesondere die theoretische Modellierung weit komplexer ist als ursprünglich erwartet. Die bis vor kurzem hochwertigsten quantenmechanischen Berechnungen, von Oliver Kühn in Zusammenarbeit mit Mikhail Vener (Karpov Institut Moskau) und Joachim Sauer (Humboldt Universität Berlin) durchgeführt, zeigten eindeutig, dass drei der vier beobachteten Banden den Schwingungen der $\text{O}\cdots\text{H}^+\cdots\text{O}$ Einheit, also der gekoppelten Bewegung

des zentralen Protons zuzuordnen sind. Die endgültige Zuordnung bleibt jedoch bis heute offen, da die theoretische Modellierung nur unter starken Näherungen durchgeführt werden kann. Im Prinzip müssten alle fünfzehn Schwingungsfreiheitsgrade des $\text{H}_2\text{O}\cdots\text{H}^+\cdots\text{OH}_2$ explizit berücksichtigt werden. Dies wäre völlig unproblematisch, wenn die Bewegung der beteiligten Atome nicht den Gesetzen der Quantenmechanik unterliegen würde. Letzteres hat zur Folge, dass der numerische Aufwand einer hochgenauen Simulation der Infrarotspektren extreme Anforderungen an die verfügbare Hard- und Software stellt. Die vollständige Interpretation des Schwingungsspektrums lässt somit noch auf sich warten, scheint mittlerweile aber nur eine Frage der Zeit zu sein. Gelänge dies, würde man anhand der theoretischen Daten eine äußerst genaue topographische Landkarte, im Fachjargon Potentialenergiehyperfläche genannt (vergleiche Abb. 5), erhalten. Damit hätte man den Schlüssel zur Beschreibung der dynamischen Prozesse nicht nur im Zundelkation, sondern auch einen wichtigen Meilenstein auf dem Weg zum besseren Verständnis vieler Eigenschaften, die sowohl auf lokalisierte wie auch ausgedehnte Wassermolekülnetzwerke zurückzuführen sind.

Die Arbeitsgruppen von Oliver Kühn und Knut Asmis haben sich mittlerweile einem neuen, aber direkt verwandten Problem zugewandt und wollen nun *Ausblick* die Schwingungsspektroskopie der analogen, negativ geladenen Verbindung, dem deprotonierten Wasserdimer $\text{OH}^-\cdots\text{H}_2\text{O}$, aufklären. Die Bedeutung die-

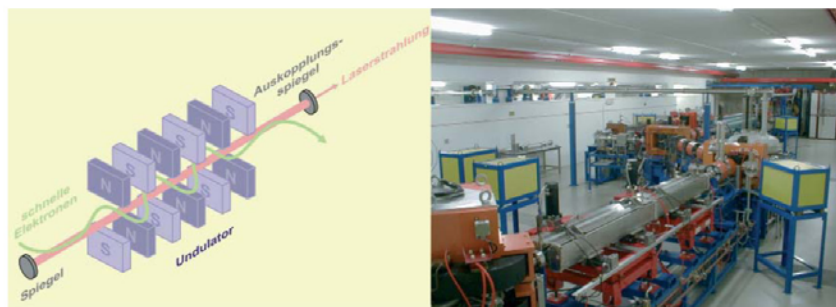


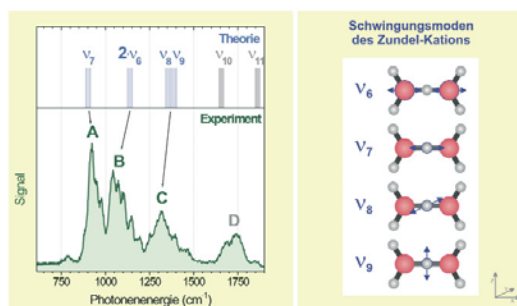
Abbildung 7: Funktionsweise des Freien Elektronenlasers FELIX. Auf relativistische Energien beschleunigte Elektronen (grüner Pfeil) werden in einem alternierenden Magnetfeld (Undulator) auf Grund der Lorentzkraft zu Oszillationen gezwungen, die der Ursprung der erzeugten Strahlung sind. Die Verstärkung wird durch zwei hochreflektierende Spiegel erreicht, welche den Großteil der Strahlung (roter Pfeil) im Bereich des Undulators halten. Die folgenden Elektronen wechselwirken sowohl mit dem Magnetfeld, als auch mit dem Strahlungsfeld, was schlussendlich zur Erzeugung hoch kohärenter Strahlung führt. Ein geringer Teil der Laserstrahlung wird durch ein kleines Loch im zweiten Spiegel ausgekoppelt (roter Pfeil) und zum Experiment geführt. Die mittlere Frequenz der Strahlung wird beim FELIX (rechts) mechanisch durch Veränderung der Magnetfeldstärke (Abstand der Magnete) eingestellt. Die Länge des gesamten Lasersystems beträgt ca. 22 Meter

ses Komplexes hängt wiederum eng mit der Mobilität von Hydroxyl-Ionen (OH^-) in Wassernetzwerken zusammen. Auch hier ist die Voraussetzung ähnlich: Sowohl experimentell wie auch theoretisch sind die Aufgaben äußerst anspruchsvoll und gehen an die Grenze des derzeit Möglichen. Trotzdem erhoffen sich die Forscher durch das enge Zusammenspiel von Theorie und Experiment eine detaillierte Charakterisierung der Potentialenergiehyperflächen und der darauf stattfinden

den molekularen Quantendynamik in diesem Modellsystem. Auf lange Sicht gilt es, die für diese prototypischen Systeme gewonnenen Erkenntnisse zum Beispiel auf komplexe biologische Systeme (siehe Abb. 3) anzuwenden und damit zum Verständnis des Zusammenspiels von strukturellen und funktionellen Aspekten beizutragen.

Die Autoren bedanken sich bei der Deutschen Forschungsgemeinschaft, sowie beim Fonds der Chemischen Industrie für die finanzielle Unterstützung ihrer Forschung.

Abbildung 8: Infrarotspektren des Zundel-Kations (links). Das experimentelle Spektrum ist im unteren Teil aufgetragen. Der Vergleich mit den aktuellsten Rechnungen von Dal et al. (oben dargestellt) legt nahe, dass die Banden A, B und C den Schwingungen, die hauptsächlich der gekoppelten Bewegung des zentralen Protons (siehe rechts) entsprechen, zuzuordnen sind. Die Bande D rührt dagegen von den Biegeschwingungen der endständigen Wassermoleküle her. Aber auch diese neuesten Rechnungen liefern nur Aufschluss über die energetische Position der Schwingungsübergänge. Intensität und Bandenprofil können auf diesem theoretischen Niveau derzeit noch nicht befriedigend vorausgesagt werden



Literaturhinweise

- N. Agmon:** „The Grotthuss Mechanism“ *Chemical Physics Letters* 244 456 (1995).
- K.R. Asmis, N.L. Pivonka, G. Santambrogio, M. Brämmer, C. Kaposta, D.M. Neumark and L. Wöste:** „The Gasphase Infrared Spectrum of the Protonated Water Dimer“ *Science* 299 1375 (2003).
- M. Eigen:** „Proton Transfer, Acid-Base Catalysis and Enzymatic Hydrolysis“ *Angewandte Chemie International Edition in English* 3 1 (1964).
- M. L. Huggins:** „Hydrogen Bridges in Ice and Liquid Water“ *Journal of Physical Chemistry* 40 723 (1936).
- R. Rousseau, V. Kleinschmidt, U. W. Schmitt, D. Marx:** „Modeling protonated water networks in bacteriorhodopsin“ *Physical Chemistry Chemical Physics* 6 1848 (2004).
- V.Z. Spassov, H. Luecke, D. Bashford, K. Genert:** „pK(a) Calculations Suggest Storage of an Excess Proton in a Hydrogen-Bonded Water Network in Bacteriorhodopsin“ *Journal of Molecular Biology* 312 203 (2001).
- M.E. Tuckerman, K. Laasonen, M. Sprik, and M. Parrinello:** „Ab Initio Molecular Dynamics Simulation of the Solvation and Transport of Hydronium and Hydroxyl Ions in Water“ *Journal of Chemical Physics* 103 150 (1995).
- M. V. Vener, O. Kühn, J. Sauer:** „The Infrared Spectrum of the O-H-O Fragment of H_3O_2^+ “ *Journal of Chemical Physics* 114 240 (2001).

**Vibrational Wave Packet Dynamics in the Silver Tetramer Probed by
NeNePo Femtosecond Pump-probe Spectroscopy**

Henry Hess, Knut R. Asmis, Thomas Leisner and Ludger Wöste

Institut für Experimentalphysik, Freie Universität Berlin, Arnimallee 14, D 14195 Berlin, Germany.

Article in *European Physical Journal D* **16**(1-3) 145-9 (2001).

Vibrational wave packet dynamics in the silver tetramer probed by NeNePo femtosecond pump-probe spectroscopy

H. Hess^a, K.R. Asmis^b, T. Leisner^c, and L. Wöste

Institut für Experimentalphysik, Freie Universität Berlin, D-14195 Berlin, Germany

Received 30 November 2000

Abstract. We present results on the ultrafast dynamics of mass-selected neutral Ag_4 clusters using NeNePo (negative ion - neutral - positive ion) femtosecond pump-probe spectroscopy. One-color pump-probe spectra of the $\text{Ag}_4^-/\text{Ag}_4/\text{Ag}_4^+$ system measured at 385 nm and an internal cluster temperature of 20 K display a complex beat structure over more than 60 ps. The oscillatory structure is attributed to vibrational wave packet dynamics in an excited “dark” state of neutral Ag_4 . A dominant 740 fs wave packet period as well as wave packet dephasing and rephasing are observed in the spectra. Fourier analysis of the spectra yields a group of frequencies centered around 45 cm^{-1} and an anharmonicity $|2\nu_0\chi_e|$ of 2.65 cm^{-1} for the active vibrational mode.

PACS. 36.40.-c Atomic and molecular clusters – 33.15.Mt Rotation, vibration, and vibration-rotation constants – 33.80.Eh Autoionization, photoionization, and photodetachment

1 Introduction

The development of ultrafast spectroscopic techniques has enabled scientists to probe dynamical processes in matter with unprecedented temporal resolution [1–3]. NeNePo (negative ion - neutral - positive ion) femtosecond pump-probe spectroscopy is a versatile tool to study nuclear dynamics on the potential energy surface (PES) of mass-selected, isolated neutral clusters and molecules in real time [4,5]. In comparison to femtosecond pump-probe experiments on (neutral) molecular beams three main advantages may be pointed out. (1) Mass selection prior to interaction with the laser field uniquely identifies the signal carrier even when highly fragmentative systems are investigated. (2) Photodetachment of the anion often allows to populate regions of the neutral PES by vertical transitions, which are not accessible by photoabsorption of the neutral species. (3) Due to the different selection rules for photodetachment of the anion compared to photoabsorption of the neutral species so-called “dark” states can be accessed.

NeNePo femtosecond pump-probe spectroscopy was pioneered by Wöste and coworkers, who studied the isomerization reaction from linear to cyclic Ag_3 in real time [4]. This experiment stimulated further experimen-

tal [5–8] and theoretical efforts [9–12], which allowed for a detailed description of the rearrangement process on the ground state PES of the silver trimer. Experimental and theoretical efforts were then extended to larger silver clusters [13–15]. Yannouleas and Landman predicted that the NeNePo scheme should be useful to characterize low frequency vibrations in Ag_{14} , manifested by coherent revivals in the Ag_{14}^+ signal [15]. However, no recurrences were observed in the experiments on Ag_3 and larger uneven numbered silver clusters. In Ag_3 this was attributed to resonant intramolecular vibrational energy distribution (IVR) taking place on a time scale of a few ps, *i.e.*, on a similar time scale as the turnaround time of the vibrational wave packet [12]. For larger metal clusters IVR is expected to be even faster, due to the increase of the degrees of freedom with cluster size. The question thus arises, if NeNePo femtosecond pump-probe spectroscopy can be used to monitor nuclear dynamics in larger metal clusters or if energy dissipative effects result in a too rapid dephasing of the wave packet motion and thus mask its spectral signature?

In the present study we present the NeNePo spectra of the $\text{Ag}_4^-/\text{Ag}_4/\text{Ag}_4^+$ system. The energetics of this system have been studied in some detail both experimentally and theoretically. The 351 nm anion photoelectron spectrum of Ag_4^- reveals three peaks at binding energies of 1.65 eV, 2.39 eV, and 2.76 eV assigned to the 1A_g ground state and $^3B_{1g}$ and $^1B_{1g}$ excited states of neutral Ag_4 with rhombic geometry (D_{2h}) [16–20]. Fluorescence and excitation spectra of Ag_4 deposited in an argon matrix as well as anion photoelectron spectra recorded at higher photon energies reveal additional excited states of Ag_4 at

^a Present address: Department of Bioengineering, University of Washington, Seattle WA 98195, USA.

^b e-mail: asmis@physik.fu-berlin.de

^c Present address: Institut für Experimentalphysik II / Umweltphysik, Technische Universität Illmenau, D-98684 Illmenau, Germany.

higher energies [21,22]. An ionization energy of 6.65 eV for Ag_4 has been deduced from electron impact ionization measurements [23]. Theoretical calculations predict rhombic D_{2h} ground state geometries for all investigated three charge states [24–28].

The present study is a continuation of our efforts on studying the dynamics and reactivity of noble metal clusters, which have received considerable attention, *e.g.*, due to the important role these clusters play in catalytic and photographic processes [29,30]. The paper is structured as follows. After a brief description of the experimental apparatus, we present the results of real time measurements of the $\text{Ag}_4^-/\text{Ag}_4/\text{Ag}_4^+$ system combined with an interpretation and discussion of the data. We conclude with an outlook on future experiments.

2 Experimental methods

The pump-probe experiments were performed in a modified guided ion beam apparatus using ultra-short laser pulses from a regeneratively amplified femtosecond laser system. Both have been described previously, and only the salient features will be summarized [7, 8].

The ultrashort laser pulses are generated by a Nd:YLF laser-pumped regenerative amplifier (Quantronix 4800), seeded by a titanium-sapphire oscillator (Spectra Physics Tsunami) which is pumped by a Nd:YAG laser (Spectra Physics Millennia V). After an additional multi-pass amplifier tunable pulses in the wavelength range from 765 nm to 845 nm with energies of up to 1.6 mJ at a repetition rate of 1 kHz are generated. The light is frequency doubled in a 0.5 mm thick BBO crystal, resulting in bandwidth limited pulses with a duration of 130 fs. The laser beam is then divided by a beam splitter. One beam passes through a computer-controlled delay stage and is recombined with the other beam. Before being introduced collinearly with the quadrupole arrangement through the detector flange of the quadrupole system both beams are focused with a 100 cm lens into the center of the ion trap.

Silver clusters are generated in a modified cold reflex discharge ion source (CORDIS). Negatively charged clusters are guided into a He-filled quadrupole ion guide, which collimates the ion beam and cools the initially hot ions to room temperature. Subsequently, the cluster ions of interest are mass-selected by a quadrupole mass filter. Mass-selected ions are guided via a second quadrupole ion guide into a temperature-controlled, He-filled octopole ion trap. The He pressure inside the trap is 0.1 mbar, which assures a sufficient amount of collisions ($\sim 5 \times 10^6 \text{ s}^{-1}$) to thermalize the injected cluster anions to the ambient temperature. The trapped anions interact with the laser light. Light absorption can lead to photodetachment followed by photoionisation of the mass selected clusters. Positively charged ions are no longer confined along the axis of the octopole and are extracted from the trap. Clusters leaving the trap *via* the exit lens enter a second mass selecting quadrupole. The yield of mass-selected cations is measured by a subsequent off-axis conversion dynode detector.

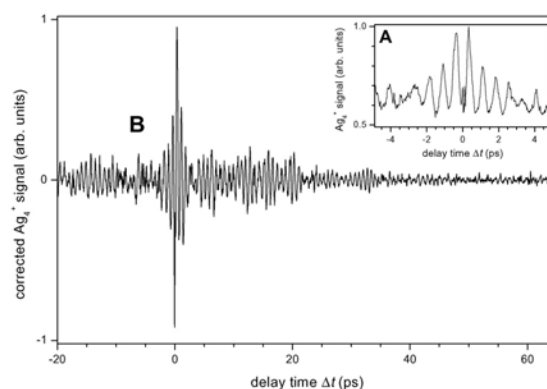


Fig. 1. One-color NeNePo spectra of Ag_4^- recorded at $\lambda_{max} = 385 \text{ nm}$ and a mean anion temperature of 20 K. Trace A (top right) shows the uncorrected, mass selected Ag_4^- yield. Trace B (center) is a composite of two measurements and the signal has been corrected for the following FFT analysis (see text).

3 Results

One-color ($h\nu_{pump} = h\nu_{probe}$) NeNePo spectra of Ag_4^- (432 amu) measured at $\lambda_{max} = 385 \text{ nm}$ and a mean anion temperature of 20 K are shown in Figure 1. Trace A (top right) shows the (uncorrected) mass selected Ag_4^- yield as function of the delay time Δt between the pump and probe pulses from -4.9 ps to $+4.9 \text{ ps}$ in steps of 20 fs. The spectrum was normalized to the highest peak in the spectrum. $\Delta t = 0 \text{ fs}$ was calibrated using the well known NeNePo spectra of Ag_3^- . It can also be identified by the sharp interference pattern due to the temporal and spatial overlap of the two pulses. The pulse energy for both pulses was $7 \mu\text{J}$.

Trace B is a composite of two measurements covering delay times from -20 ps to $+20 \text{ ps}$ and $+20 \text{ ps}$ to $+65 \text{ ps}$. These spectra were measured with pulse energies of $7 \mu\text{J}$ for the pump pulse and $23 \mu\text{J}$ for the probe pulse (at positive delay times). The spectra have been baseline corrected and transformed for the following fast Fourier transformation (FFT). This procedure has been described in detail elsewhere [31]. The raw spectra were normalized in such a way that the observed beat structure oscillates around zero. To this end a mean ion intensity averaged over 4 ps is determined and subtracted from the data set.

Trace A in Figure 1 shows a pronounced oscillatory structure, characterized by a period of $\sim 740 \text{ fs}$. The widths of the peaks are $\sim 290 \text{ fs}$. The intensity of the maxima decrease for larger values of $|\Delta t|$. Additional, weaker structures are observed at delay times $> 2.8 \text{ ps}$ overlapping the 740 fs beat structure. Note, that the oscillation in the signal intensity, which comprises up to 45 percent of the total signal, is superimposed on a constant signal background. The signal background stems from Ag_4^+ production by a single laser pulse. Because we focus the laser

beams into the center of the ion trap, the cross section for photodetachment followed by photoionization of the Ag_4 clusters is not negligible.

Trace B in Figure 1 shows oscillations in the corrected Ag_4^+ signal up to 60 ps, with decreasing intensity. Pronounced partial recurrences are observed at irregular intervals centered at 6, 12, 16, 20, 27 and 33 ps. At longer delay times oscillatory structure is still observed, but the decreasing signal-to-noise ratio makes a more detailed characterization of the structure increasingly difficult. Comparison of the data at positive delay times with the data at negative delay times shows a weak dependence on laser power. Positive delay times correspond to $E(h\nu_{\text{pump}}) = 7 \mu\text{J}$ and $E(h\nu_{\text{probe}}) = 23 \mu\text{J}$ and a roughly two times larger oscillatory signal is observed than for the reversed pulse sequence at negative time delays. More signal at positive delay times therefore indicates that an additional photon is required in the photoionization step compared to the photodetachment step.

The spectra in Figure 1 strongly resemble the pump-probe spectra of the related neutral alkali metal dimers and trimers measured in a molecular beam [31–33]. In these experiments pronounced oscillations in the ionization yield were interpreted in terms of vibrational wave packet dynamics. An ultrashort pump pulse generated a localized wave packet on an excited potential energy surface of the neutral. The wave packet motion was then probed by a second ultrafast pulse. The “location” of the wave packet could be characterized, due to a strong dependence of the ionization cross section on the normal coordinate of the involved vibrational mode(s), *i.e.*, on the relative position of the nuclei. Based on similar arguments we identify the main features in Figure 1 to result from vibrational wave packet dynamics on a potential energy surface of neutral Ag_4 . A more detailed assignment will be discussed later. Assuming a single vibrational mode the roundtrip time of the wave packet is 740 ± 50 fs, yielding a mean vibrational frequency of $45 \pm 4 \text{ cm}^{-1}$. We attribute the recurrences to effects of the anharmonicity of the potential, on which the wave packet propagates, resulting in dephasing and rephasing of the wave packet with time [34]. Complete recurrences are not observed. This is attributed to energy dissipative effects, mainly, IVR.

In order to characterize the main frequency components responsible for the oscillatory structure observed, the time domain spectrum was converted into the frequency domain using a standard fast Fourier transformation algorithm. In Figure 2 the FFT amplitude of trace B shown in Figure 1 is displayed as a function of energy. The dominant feature consists of several peaks centered around 45 cm^{-1} . At least eight peaks can be identified in the region from 32 to 60 cm^{-1} . Additional features are observed at 29 cm^{-1} (peak B) and at higher energies up to 100 cm^{-1} , in particular at 96 cm^{-1} (peak C).

Peaks A_1 to A_8 in Figure 2 are assigned to the difference in energy between adjacent vibrational levels of a single vibrational mode. If we denote the vibrational quantum number with v then this corresponds to the energy difference between levels with $\Delta v = \pm 1$. Assuming

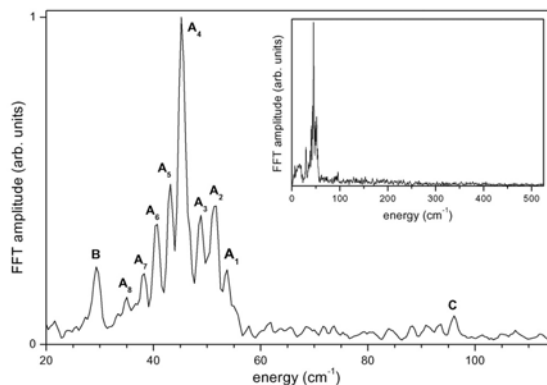


Fig. 2. Fast Fourier transform of trace B shown in Figure 1 for a spectral range from 20 cm^{-1} to 115 cm^{-1} , whereas the insert shows the same sequence in a range from 0 cm^{-1} to 520 cm^{-1} . The Fourier amplitude is plotted as a function of energy. See text for description of peak labels.

a Morse potential, for which the vibrational energy level spacings $\Delta G(v)$ are defined as

$$\Delta G(v) = \nu_0 [1 - 2\chi_e(v + 1)],$$

a linear least square fit yields an anharmonicity (slope) of $|2\nu_0\chi_e| = 2.65 \pm 0.05 \text{ cm}^{-1}$. Determination of the anharmonicity constant is not straight forward, as no experimental evidence for the $v = 0$ level of this mode is available. The weak features observed in the region between 75 cm^{-1} to 100 cm^{-1} , *i.e.*, at roughly twice the mean frequency of 45 cm^{-1} , may then be assigned to vibrational energy level spacings with $\Delta G(v) = \pm 2$. The feature at 29 cm^{-1} (peak B) cannot be assigned.

4 Discussion

We now discuss the underlying energetics involved in the observed wave packet dynamics in neutral Ag_4 . The anion photoelectron spectra of Ag_4^- show that three states of neutral Ag_4 are populated by a one photon process using 385 nm (3.22 eV) photons. These are the 1A_g ground state and the $^3B_{1g}$ and $^1B_{1g}$ excited states of rhombic Ag_4 with vertical detachment energies of 1.65 eV , 2.39 eV , and 2.76 eV , respectively [17]. We thus narrow our following discussion to only involve these three states of neutral Ag_4 . Multiphotonic photodetachment processes are in principle possible, but neglected in the following discussion due to their considerably smaller cross section compared to one-photon processes.

From each of the three mentioned states of neutral Ag_4 ionization into the rhombic $^2B_{3u}$ ground state of Ag_4^+ is allowed by a one-electron process [17]. The experimentally determined ionization energy of Ag_4 is 6.65 eV . Therefore

only the two excited states ${}^3B_{1g}$ and ${}^1B_{1g}$ may be ionized by a two photon process using 385 nm photons, while three 385 nm photons are required for ionization of the neutral ground state. Furthermore, the observation of oscillations in the NeNePo spectra require a dependence of the ionization cross section on the position of the nuclei, such that the ionization probability for one arrangement of the nuclei is considerably different from the ionization probability of another arrangement. In terms of wave packet dynamics these nuclear arrangements may be visualized as a wave packet, which is predominantly localized at either the inner or outer turning point of the PES it is propagating on. Thus the photoionization energy should be in the vicinity of the vertical ionization potential. This holds for ${}^3B_{1g}$ and ${}^1B_{1g}$ states but not the 1A_g ground state.

Ab initio calculations on the harmonic frequencies of the low-lying electronic states of rhombic Ag_4 clearly favor the excited states ${}^3B_{1g}$ and ${}^1B_{1g}$ over the 1A_g state to be involved in the observed wave packet dynamics [35]. In general, only totally symmetric modes of the neutral cluster may be directly excited upon photodetachment. Among the six normal modes of rhombic Ag_4 , only two of them, both in-plane ring-breathing modes, have a_g symmetry. The calculated frequencies for the $1a_g$ mode are 196 cm^{-1} (1A_g), 144 cm^{-1} (${}^3B_{1g}$) and 142 cm^{-1} (${}^1B_{1g}$). The calculated frequencies for the $2a_g$ mode are 114 cm^{-1} (1A_g), 53 cm^{-1} (${}^3B_{1g}$) and 50 cm^{-1} (${}^1B_{1g}$). Reasonable agreement with the present experiment (45 cm^{-1}) is only found for the $2a_g$ mode of either the ${}^3B_{1g}$ or ${}^1B_{1g}$ electronically excited state of Ag_4 . These calculations also confirm the pronounced anharmonicity of this vibrational mode.

We conclude that the oscillations observed in the NeNePo spectra of Ag_4 are due to vibrational wave packet dynamics in the $2a_g$ mode of either the ${}^3B_{1g}$ or ${}^1B_{1g}$ ‘dark’ electronically excited state of rhombic Ag_4 . A localized wave packet is created on the electronically excited PES of neutral Ag_4 by one-photon detachment of Ag_4^- in its electronic ground state. The wave packet motion is then probed by a two-photon photoionization step to the ground state of Ag_4^+ . The $2a_g$ mode was not resolved in the previous anion photoelectron spectroscopy studies, due to its low frequency of 45 cm^{-1} , which lies below the energy resolution ($\geq 80\text{ cm}^{-1}$) of conventional anion photoelectron spectrometers.

The present results demonstrate the first successful application of femtosecond NeNePo spectroscopy to study the wave packet dynamics, manifested by a beat structure in the cation yield, in real time in a ‘purely’ bound potential, in contrast to the previous transition-state experiments on the silver trimer which connected linear with triangular structures. The spectra enable us to precisely characterize a selected vibrational mode with a resolution, which is superior to that of conventional frequency domain techniques that have been applied to the study of the silver tetramer. We are planning to extend these studies and access the vibrational wave packet dynamics in the ground state of Ag_4 . Experimental modifications necessary for this experiment are currently in progress in our laboratory and when finished they will enable us to

use shorter pulses (40 fs) and continuously tune the pulse wave length in the region from 250 nm to 2600 nm.

The authors wish to express their thanks to V. Bonačić-Koutecký, M. Hartmann, and R. Mitrić for providing us with their results prior to publication and for helpful discussions. K.R.A. gratefully acknowledges a stipend from the Swiss National Science Foundation. The research was supported by the Deutsche Forschungsgesellschaft as part of the SFB 450 and SFB 546.

References

1. *Ultrafast Phenomena XII*, edited by T. Elsaesser, S. Mukamel, M. Murnane, N.F. Scherer (Springer, Berlin, 2000), Vol. 66.
2. A. Zewail, *J. Phys. Chem. A* **104**, 5660 (2000).
3. *Femtosecond Chemistry*, edited by J. Manz, L. Wöste (VCH, Weinheim, 1995).
4. S. Wolf, G. Sommerer, S. Rutz, E. Schreiber, T. Leisner, L. Wöste, *Phys. Rev Lett.* **74**, 4177 (1995).
5. D.W. Boo, Y. Ozaki, L.H. Anderson, W.C. Lineberger, *J. Phys. Chem. A* **101**, 6688 (1997).
6. S. Wolf, Ph.D. thesis, Freie Universität Berlin, Berlin, 1997.
7. T. Leisner, S. Vajda, S. Wolf, L. Wöste, R.S. Berry, *J. Chem. Phys.* **111**, 1017 (1999).
8. H. Hess, S. Kwiet, L. Socaciu, S. Wolf, T. Leisner, L. Wöste, *Appl. Phys. B* **71**, 337 (2000).
9. H.O. Jeschke, M.E. Garcia, K.H. Bennemann, *Phys. Rev. A* **54**, R4601 (1996).
10. M. Hartmann, J. Pittner, V. Bonačić-Koutecký, A. Heidenreich, J. Jortner, *J. Chem. Phys.* **108**, 3096 (1998).
11. M. Hartmann, A. Heidenreich, J. Pittner, V. Bonačić-Koutecký, J. Jortner, *J. Phys. Chem. A* **102**, 4069 (1998).
12. I. Andrianov, V. Bonačić-Koutecký, M. Hartmann, J. Manz, J. Pittner, K. Sundermann, *Chem. Phys. Lett.* **318**, 256 (2000).
13. T. Leisner, S. Rutz, G. Sommerer, S. Vajda, S. Wolf, E. Schreiber, L. Wöste, in *Fast Elementary Processes in Chemical and Biological Systems*, edited by A. Tramer (AIP Press, Woodbury, New York, 1996), pp. 603-609.
14. M. Warken, V. Bonačić-Koutecký, *Chem. Phys. Lett.* **272**, 284 (1997).
15. C. Yannouleas, U. Landman, *J. Phys. Chem. A* **102**, 2505 (1998).
16. G. Ganteför, M. Gausa, K.-H. Meiwes-Broer, H.O. Lutz, *J. Chem. Soc. Faraday Trans.* **86**, 2483 (1990).
17. J. Ho, K.M. Ervin, W.C. Lineberger, *J. Chem. Phys.* **93**, 6987 (1990).
18. H. Handschuh, C.-Y. Cha, H. Möller, P.S. Bechthold, G. Ganteför, W. Eberhardt, *Chem. Phys. Lett.* **227**, 496 (1994).
19. H. Handschuh, C.-Y. Cha, P.S. Bechthold, G. Ganteför, W. Eberhardt, *J. Chem. Phys.* **102**, 6406 (1995).
20. K.J. Taylor, C.L. Pettiette-Hall, O. Cheshnovsky, R.E. Smalley, *J. Chem. Phys.* **96**, 3319 (1992).
21. C. Félix, C. Sieber, W. Harbich, J. Buttet, I. Rabin, W. Schulze, G. Ertl, *Chem. Phys. Lett.* **313**, 105 (1999).
22. P.R. Taylor, J.M.L. Martin, J.P. Francois, R. Gijbels, *J. Phys. Chem.* **95**, 6530 (1991).

23. C. Jackschath, I. Rabin, W. Schulze, *Z. Phys. D* **22**, 517 (1992).
24. V. Bonačić-Koutecký, L. Češpiva, P. Fantucci, J. Pittner, J. Koutecký, *J. Chem. Phys.* **98**, 7981 (1993).
25. V. Bonačić-Koutecký, L. Češpiva, P. Fantucci, J. Pittner, J. Koutecký, *J. Chem. Phys.* **100**, 490 (1994).
26. R. Santamaria, I.G. Kaplan, O. Novaro, *Chem. Phys. Lett.* **218**, 395 (1994).
27. V. Bonačić-Koutecký, J. Pittner, M. Boiron, P. Fantucci, *J. Chem. Phys.* **110**, 3876 (1999).
28. Z.F. Liu, W.L. Yim, J.S. Tse, J. Hafner, *Eur. Phys. J. D* **10**, 105 (2000).
29. U. Heiz, W.-D. Schneider, *J. Phys. D* **33**, R85 (2000).
30. P. Fayet, F. Granzer, G. Hegenbart, E. Moisar, B. Pishel, L. Wöste, *Phys. Rev. Lett.* **55**, 3002 (1985).
31. S. Rutz, Ph.D. thesis, Freie Universität Berlin, Berlin, 1996.
32. T. Baumert, M. Grosser, R. Thalweiser, G. Gerber, *Phys. Rev. Lett.* **67**, 3753 (1991).
33. S. Rutz, K. Kobe, H. Kuhling, E. Schreiber, L. Wöste, *Z. Phys. D* **26**, 276 (1993).
34. M. Gruebele, A.H. Zewail, *J. Chem. Phys.* **98**, 883 (1993).
35. M. Hartmann, V. Bonačić-Koutecký, private communication (2000).

G.2 List of Publications

Academic Publications

1. "Infrared Photodissociation Spectroscopy of Mass-Selected Cluster Ions in the Gas Phase", Habilitation thesis (submitted), Institut für Experimentalphysik, Freie Universität Berlin (2005).
2. "Electron-Molecule Collisions: A Novel Instrument for Measuring Inelastic Differential Cross Sections at 180° Angle and Applications", Ph.D. thesis, Nr. 1142, Université de Fribourg (1996).
3. "Characterization of Complex Formation in the Gas Phase Using Fourier-Transform-IR-Spectroscopy", Diploma thesis, Institut für Anorganische Chemie, Université de Fribourg (1992).
4. "Characterization of Excited States of Neutral Molecules and Their Negatively and Positively Charged Ions Using UV-Photoelectron and Electron-Impact Spectroscopy", Diploma thesis, Institut für Physikalische Chemie, Université de Fribourg (1992).

Peer Reviewed Publications

1. G. Santambrogio, M. Brümmer, L. Wöste, J. Sauer, G. Meijer, K.R. Asmis, "Gas Phase Infrared Spectroscopy of Vanadium Oxide Cluster Anions", in preparation.
2. K.R. Asmis, G. Santambrogio, M. Brümmer, J. Sauer, "Polyhedral Vanadium Oxide Cages: Infrared Spectra of Cluster Anions and Size-Induced d-Electron Localization", Communication in *Angew. Chem. Int. Ed.* **44** 3122-5 (2005).
3. M.J. Nee, C. Kaposta, A. Osterwalder, C. Cibrián Uhalte, T. Xie, A. Kaledin, S. Carter, J.M. Bowman, D.M. Neumark, K.R. Asmis, "Experimental and theoretical study of the infrared spectra of BrHI^- and BrDI^- ", Article in *J. Chem. Phys.* **121** 7259 (2004).
4. K.R. Asmis, M. Brümmer, C. Kaposta, G. Santambrogio, J. Sauer, G. Meijer, and L. Wöste, "Infrared Vibrational Predissociation Spectroscopy of Mono- and Divanadium Oxide Cluster Cations: A Combined Experimental and Ab Initio Study", Article in *J. Chem. Phys.* **120** 6461 (2004).
5. M. Brümmer, C. Kaposta, G. Santambrogio, K.R. Asmis, "Formation and Photodepletion of Cluster Ion–Messenger Atom Complexes in a Cold Ion Trap: Infrared Spectroscopy of VO^+ , VO_2^+ and VO_3^+ ", Communication in *J. Chem. Phys.* **119** 12700 (2003).
6. H. Haberkern, K.R. Asmis, M. Allan, P. Swiderek, "Triplet states in Oligomeric Materials: Electron Energy Loss Spectroscopy of Thiophene and Bithiophene and Extrapolation to the Polymer", Article in *Phys. Chem. Chem. Phys.* **5** 827 (2003).
7. K.R. Asmis, N.L. Pivonka, G. Santambrogio, M. Brümmer, C. Kaposta, D.M. Neumark, L. Wöste, "The Gasphase Infrared Spectrum of the Protonated Water Dimer", Report in *Science* **299** 1375 (2003).
8. N.L. Pivonka, C. Kaposta, M. Brümmer, G. von Helden, G. Meijer, L. Wöste, D.M. Neumark, K.R. Asmis, "Probing a Strong Hydrogen Bond with Infrared Spectroscopy: Vibrational Predissociation of $\text{BrHBr}^- \cdot \text{Ar}$ ", Communication in *J. Chem. Phys.* **118** 5275 (2003).

9. N.L. Pivonka, C. Kaposta, G. von Helden, G. Meijer, L. Wöste, D.M. Neumark, K.R. Asmis, "Gas Phase Infrared Spectroscopy of Cluster Anions as a Function of Size: The Effect of Solvation on Hydrogen-Bonding in $\text{Br}^-(\text{HBr})_{1,2,3}$ Clusters", Full article in *J. Chem. Phys.* **117** 6493 (2002).
10. K.R. Asmis, M. Brümmer, C. Kaposta, G. Santambrogio, G. von Helden, G. Meijer, K. Rademann, L. Wöste, "Mass-selected Infrared Photodissociation Spectroscopy of $\text{V}_4\text{O}_{10}^+$ ", Communication in *Phys. Chem. Chem. Phys.* **4** 1101 (2002).
11. H. Hess, K.R. Asmis, T. Leisner, L. Wöste, "Vibrational Wave Packet Dynamics in the Silver Tetramer Probed by NeNePo Femtosecond Pump-Probe Spectroscopy", Article in *Eur. Phys. J. D* **16** 145 (2001).
12. T.R. Taylor, H. Gomez, K.R. Asmis, D.M. Neumark, "Photoelectron Spectroscopy of GaX_2^- , Ga_2X^- , Ga_2X_2^- , and Ga_2X_3^- ($X = \text{P}, \text{As}$)", Article in *J. Chem. Phys.* **115** 4620-31 (2001).
13. K.R. Asmis, T.R. Taylor, D.M. Neumark, "Anion Photoelectron Spectroscopy of Small Boron Nitride Clusters: Adiabatic Detachment Energies and Vibrational Frequencies of B_2N and B_3N ", Article in *Eur. Phys. J. D* **9** 257-61 (1999).
14. T.R. Taylor, K.R. Asmis, H. Gomez, D.M. Neumark, "Vibrationally Resolved Anion Photoelectron Spectra of the Low Lying Electronic States of GaP_2^- , Ga_2P^- and Ga_2P_3^- ", Article in *Eur. Phys. J. D* **9** 317-21 (1999).
15. K.R. Asmis, T.R. Taylor, D.M. Neumark, "Anion Photoelectron Spectroscopy of B_3N^- ", *J. Chem. Phys.* **111** 10491 (1999).
16. K.R. Asmis, T.R. Taylor, D.M. Neumark, "Anion Photoelectron Spectroscopy of B_2N^- ", Article in *J. Chem. Phys.* **111** 8838-51 (1999).
17. K.R. Asmis, T.R. Taylor, D.M. Neumark, "Electronic Structure of Indium Phosphide Clusters: Anion Photoelectron Spectroscopy of In_xP_x^- and $\text{In}_{x+1}\text{P}_x^-$ ($x = 1-13$) Clusters", Article in *Chem. Phys. Lett.* **308** 347-54 (1999).
18. T.R. Taylor, K.R. Asmis, M.T. Zanni, D.M. Neumark, "Characterization of the I3 Radical by Anion Photoelectron Spectroscopy", Communication in *J. Chem. Phys.* **110** 7607-9 (1999).
19. T.R. Taylor, R.T. Bise, K.R. Asmis, D.M. Neumark, "The Singlet-Triplet Splittings of NCN^- ", Article in *Chem. Phys. Lett.* **301** 413-6 (1999).
20. T.R. Taylor, K.R. Asmis, C. Xu, D.M. Neumark, "Evolution of Electronic Structure as a Function of Size in Gallium Phosphide Semiconductor Clusters", Article in *Chem. Phys. Lett.* **297** 133-40 (1998).
21. T. Lenzer, M.R. Furlanetto, K.R. Asmis, D.M. Neumark, "Zero Electron Kinetic Energy and Photoelectron Spectroscopy of the XeI^- Anion", Article in *J. Chem. Phys.* **109** 10754-66 (1998).
22. K.R. Asmis, T.R. Taylor, D.M. Neumark, "Anion Photoelectron Spectroscopy of BN^- ", Article in *Chem. Phys. Lett.* **295** 75-81 (1998).
23. K.R. Asmis, T.R. Taylor, C. Xu, D.M. Neumark, "Anion Photoelectron Spectroscopy of $\text{I}_2^- \cdot \text{Ar}_n$ ($n = 0 - 14, 16, 20$) Clusters", Article in *J. Chem. Phys.* **109** 4389-95 (1998).
24. V. Huber, K.R. Asmis, A.-C. Sergenton, M. Allan, S. Grimme, "Electron-Energy-Loss and DFT/SCI Study of the Singlet and Triplet Excited States and Electron Attachment Energies of Tetramethylsilane, Hexamethyldisilane, Tris-(trimethylsilyl)-Silane, and Tetra-Methoxysilane", Article in *J. Chem. Phys. A* **102** 3524 (1998).

25. K.R. Asmis, M. Allan, "Measurement of Absolute Differential Cross Sections for the Excitation of the p,p^* Triplet State of Ethene by Electron Impact at 0 and 180 Degrees", Article in *J. Chem. Phys.* **106** 7044 (1997).
26. K.R. Asmis, M. Allan, "Measurement of Absolute Differential Cross Sections for the Excitation of the $n = 2$ States of Helium at 0 and 180 Degrees", Article in *J. Phys. B* **30** 1961 (1997).
27. K.R. Asmis, M. Allan, "Excess Energy Partition Between Electrons Departing at 0 and 180 Degrees in the Ionization of Helium Near Threshold", Letter in *J. Phys. B* **30** L167 (1997).
28. K.R. Asmis, M. Allan, M. Fülcher, "Electron Energy-Loss Spectroscopy and Theoretical Study of Triplet and Singlet Excited States of Fulvene", Article in *J. Phys. Chem. A* **101** 2089 (1997).
29. M. Allan, K.R. Asmis, D.B. Popovic, M. Stepanovic, N.J. Mason, J.A. Davies, "Resonances in Collisions of Low-Energy Electrons with Ozone: Experimental Elastic and Vibrationally Inelastic Differential Cross Sections and Dissociative Attachment Spectra", Article in *J. Phys. B* **29** 4727 (1996).
30. M. Allan, K.R. Asmis, D.B. Popovic, M. Stepanovic, N.J. Mason, J.A. Davies, "Production of Vibrationally Autodetaching O_2^- Produced in Low-Energy Electron Impact on Ozone", Article in *J. Phys. B* **29** 3487 (1996).
31. L. Truttmann, K.R. Asmis, T. Bally, "Electronic and Vibrational Structure and Scaled Density Functional Force Field of Cyclopentadiene and Its Radical Cation", Article in *J. Phys. Chem.* **99** 17844 (1995).
32. M. Allan, K.R. Asmis, S. El houar, E. Haselbach, M. Capponi, B. Urwyler, J. Wirz, "Triplet Energy of 2,2-Dimethylisoindene from Electron Energy-Loss Spectroscopy and Photoinduced Triplet Energy Transfer", Article in *Helv. Chim. Acta* **77** 1541 (1994).
33. J.M. Smith, D.A. Hrovat, W.T. Borden, M. Allan, K.R. Asmis, C. Bulliard, E. Haselbach, U.C. Meier, "Synthesis and Spectroscopy of Tricyclo^[84]undec-3(7)-ene : Confirmation of Computational Predictions Regarding the Effects of Pyramidalization on Alkene Ionization Energies and Electron Affinities", Note in *J. Am. Chem. Soc.* **115** 3816 (1993).
34. M. Allan, K. Asmis, C. Bulliard, E. Haselbach, P. Suppan, "Triplet-State Energy of the Photostabilizer Tinuvin P", Article *Helv. Chim. Acta* **76** 993 (1993).

Other Publications

1. K.R. Asmis, D.M. Neumark, J.M. Bowman, "Gas Phase Vibrational Spectroscopy of Strong Hydrogen Bonds", Chapter in *Physical and Chemical Aspects of Hydrogen Transfer*, edited by J. T. Hynes and H. H. Limbach; Vol. 1 of Handbook of Hydrogen Transfer, edited by R. L. Schowen (Wiley-VCH, Weinheim, Germany, 2005).
2. K. Asmis, O. Kühn, "Bausteine des Wassers unter der Laserlupe", Article in *fundiert - Das Wissenschaftsmagazin der Freien Universität Berlin* **2** 84 (2004).

G.3 List of Invited Talks

1. *"Schwingungsspektroskopische Untersuchungen an teilweise solvatisierten Ionen in der Gasphase"*, CFN-Symposium: Cluster als molekulare Nanostrukturen, September 11-16, 2005, Bad Herrenalb (Germany).
2. *"Infrared Photodissociation Spectroscopy: About Strong Hydrogen Bonds and Metal Oxide Clusters"*, 53rd American Society for Mass Spectrometry (ASMS) Conference on Mass Spectrometry, June 5-9, 2005, San Antonio, Texas (USA).
3. *"Gas Phase Infrared Spectroscopy of Strong Hydrogen Bonds: The Protonated Water Dimer and Related Systems"*, Gordon Conference on Water and Aqueous Solutions, 1-6 August 2004, Plymouth, New Hampshire (USA).
4. *"Probing Strong Hydrogen Bonds and Cold Metal Oxide Clusters with Infrared Photodissociation Spectroscopy"*, Abteilungsseminar, Technische Universität Chemnitz, 18 May 2004, Chemnitz (Germany).
5. *"Gas Phase Infrared Spectroscopy of Vanadium Oxide Cluster Ions"*, Symposium of the DFG Collaborative Research Center 546, 21-24 March 2004, Berlin-Schmöckwitz (Germany).
6. *"Probing Strong Hydrogen Bonds and Cold Metal Oxide Clusters with Infrared Photodissociation Spectroscopy"*, Chemistry Seminar, University of California, 19 February 2004, Santa Barbara, California (USA).
7. *"Probing Strong Hydrogen Bonds and Cold Metal Oxide Clusters with Infrared Photodissociation Spectroscopy"*, Chemistry Seminar, University of British Columbia, 28 January 2004, Vancouver (Canada).
8. *"Probing Strong Hydrogen Bonds and Cold Metal Oxide Clusters with Infrared Photodissociation Spectroscopy"*, Seminar Physikalische Chemie, Technische Universität München, 22 January 2004, München (Germany).
9. *"Mass-selective Infrared Spectroscopy of Hydrogen-bonded Ions in the Gas Phase"*, 15th Horizons in Hydrogen Bond Research, 15-22 September 2003, Berlin (Germany).
10. *"Vibrational Spectroscopy on Mass-selected Cluster Ions"*, KVI Seminar, University of Groningen/FOM, 15 April 2003, Groningen (The Netherlands).
11. *"Infrared Spectroscopy of Mass-selected Gas Phase Cluster Ions"*, hot topic talk, XIth International Symposium on Small Particles and Inorganic Clusters (ISSPIC 11), 9-13 September 2002, Strasbourg (France).
12. *"Infrarot Photodissoziationspektroskopie massenselektierter Clusterionen in der Gasphase"*, Hauptvortrag, AMOP-Frühjahrstagung der Deutschen Physikalischen Gesellschaft, 4-8 March 2002, Osnabrück (Germany).
13. *"IR Photodissociation Spectroscopy of Mass-Selected Gasphase Cluster Ions"*, XIIIth International Symposium on Atomic, Cluster and Surface Physics, 17-22 February 2002, Going (Austria).
14. *"Femtosecond Charge Reversal Spectroscopy: Taking a Closer Look at Molecular Vibrations"*, European Cluster Cooling Network Meeting, 19-22 August 2001, Nieuwegein (The Netherlands).
15. *"Measurement of Absolute Differential Cross Sections at 180 Degrees"*, International Symposium on Electron- and Photon-Molecule Collisions and Swarms, 22-25 July 1995, Berkeley (USA).

16. *"Selective Formation of Triplet States in the Decay of Radical Anions with Two Excited Electrons"*, Fall Meeting of the Swiss Society for Photochemistry and Photophysics, 13-14 October 1994, Fribourg (Switzerland).

G.4 Curriculum Vitae: Knut R. Asmis

PERSONAL

Address: Brunhildstr. 15 *Telephone:* +49 30 857-31824
D 10829 Berlin, Germany *Fax:* +49 30 857-31825

Office: Freie Universität Berlin *Telephone:* +49 30 838-56120
Fachbereich Physik *Fax:* +49 30 838-55567
Arnimallee 14 *e-mail:* asmis@physik.fu-berlin.de
D 14195 Berlin, Germany *web:* www.physik.fu-berlin.de/~asmis
and

Fritz-Haber-Institut *Telephone:* +49 30 8413-5735
der Max-Planck-Gesellschaft *Fax:* +49 30 8413-5603
Abteilung Molekülphysik *e-mail:* asmis@fhi-berlin.mpg.de
Faradayweg 4-6 *web:* http://www.fhi-berlin.mpg.de/mp/
D 14195 Berlin, Germany

Date of Birth: June 25, 1968 *Place of Birth:* Berlin, Germany

Citizenship: German & Swiss

EDUCATION

HABILITATION	Experimental Physics	Freie Universität Berlin, Germany	<i>submitted</i>
PH.D.	Physical Chemistry	Université de Fribourg, Switzerland	1996
DIPLOMA	Chemistry	Université de Fribourg, Switzerland	1992

PROFESSIONAL POSITIONS

1999-	Group Leader* (with Prof. L. Wöste)	Institut für Experimentalphysik, Freie Universität Berlin, Berlin, Germany.
1996-1999	Postdoctoral Researcher (with Prof. D. Neumark)	Department of Chemistry, University of California, Berkeley, U.S.A.
1993-1996	Research Assistant (with Prof. M. Allan)	Institut de Chimie Physique, Université de Fribourg, Switzerland.

AWARDS

1999-2001 Swiss National Science Foundation Advanced Researcher Scholarship.
1996-1998 Swiss National Science Foundation Young Researcher Scholarship.

TEACHING

2005 Adv. Exp. Physics Lab Course, with Prof. Kaindl, Freie Universität Berlin.
2003-2004 Atomic and Molecular Physics I, with Prof. Stehlik, Freie Universität Berlin.
2003 Seminar on Strong Hydrogen Bonds, DFG Research Training Group 788.
2002-2003 Physical Experiments for Teachers, with Prof. Vieth, Freie Universität Berlin.
1993-1996 Physical Chemistry Laboratory Course, Université de Fribourg.
1995-1996 Chemistry and Environment (with others), Université de Fribourg.

* Since July 2003 my position is financed with FHI funds as part of a collaboration between the two institutes.

STUDENT SUPERVISION

PhD Thesis (4-5 years), Freie Universität Berlin:

Gabriele Santambrogio (2002-), Mathias Brümmer (2001-), Cristina Kaposta (2000-5).

Diploma Thesis (1 year), Freie Universität Berlin:

Sara Fontanella (2004-), Oliver Gause (2003-4), Carlos Uhalte (2003-4), Gabriele Santambrogio (2001-2).

Summer Intern (6 weeks), Freie Universität Berlin:

Nadia Elghobashi (2002).

Diploma Thesis (6 months), Université de Fribourg;

Vroni Huber (1996), Dunja M. Frey (1994), Sarah El houar (1993).

EXTRACURRICULAR ACTIVITIES

2003 Organization: PhD Student-Seminars of the SFB 546.

2003 Thesis Committee, Deniz van Heijnsbergen, Universitij of Nijmegen (NL).

2002 Thesis Committee, Steffen Schuler, Freie Universität Berlin (D).

1999- Referee: CPC, JACS, JCP, JPC A, PCCP, JMS, Department of Energy, ACS.

1994-1996 Member of the Faculty Council, Université de Fribourg (CH).

OTHER ACTIVITIES

1995 Participant 4th European Summer School of Quantum Chemistry, Lund, Sweden.

1987 Mechanical Engineering Traineeship (6 months), Siemens AG, Berlin, Germany.

RESEARCH SUPPORT

1. Co-Investigator (Asmis/ Wöste) – “Structure, Stability and Reactivity of Small Vanadium Oxide Clusters in the Gas Phase”. 328'200 € Jul. 2005-Jun. 2008. Part of the Dedicated Research Center 546 “Structure, Dynamics and Reactivity in Transition Metal Oxide Aggregates”, German Research Foundation DFG.
2. Co-Investigator (Asmis/Wöste) – “Characterization in Real-time of Proton Transfer in Dihalogen-Hydride Anions in the Gas Phase”. 62'078 € Jan. 2005-Dez. 2007. Part of the Research Training Group 788 "Hydrogen Bonding and Hydrogen Transfer", German Research Foundation DFG.
3. Co-Investigator (Asmis/Rademann/Wöste) – “Structure, Stability and Reactivity of Small Vanadium Oxide Clusters in the Gas Phase”. 594'900 € Jul. 2002-Jun. 2005. Part of the Dedicated Research Center 546 “Structure, Dynamics and Reactivity in Transitionmetaloxides-Agregates”, German Research Foundation DFG.
4. Co-Investigator (Asmis/Wöste) – “Characterization in Real-time of Proton Transfer in Dihalogen-Hydride Anions in the Gas Phase”. 62'078 € Jan. 2002-Dez. 2004. Part of the Research Training Group 788 "Hydrogen Bonding and Hydrogen Transfer", German Research Foundation DFG.
5. Research Scholarship – “Characterization in Real-Time and Control of Ultrafast Chemical Processes in Mass-Selected, Neutral Molecules and Clusters”. 83'400 SFr. Jul. 1999-Jun. 2001. Swiss National Science Foundation.
6. Research Scholarship – “Anion Photoelectron Spectroscopy”. 73'900 SFr. Nov. 1996-Okt. 1998. Swiss National Science Foundation.